DEVELOPMENT OF A NUMERICAL FLUID-STRUCTURE INTERACTION METHODOLOGY TO MODEL TRANSIENT LEAKAGE PHENOMENA

Mikel Ezkurra Mayor

Mechanical and Industrial Production department

Applied Engineering PhD Program

Thesis supervisors:

Dr. Jon Ander Esnaola Ramos
Dr. Manex Martinez Agirre

Arrasate-Mondragón, July 2021

Saioari, Laiari eta Ibairi, nire bizitzaren zutabeak

Amari eta aitari, zauden lekuan zaudela...

Acknowledgement

Tesi hau egiteko aukera sortu zitzaidan, espero ez nuen momentuan, egun batetik bestera… eta hegan pasa diren urte luze hauetako abenturari ekin nion.

Eskerrik asko Mondragon Goi Eskola Politeknikoari, bere langileen kapazitaziorako planaren bidez tesi hau egiteko emandako aukeragatik, eta horretarako jarritako baliabideengatik. Neurri berean, eskerrik beroenak Ampori tesi hau aurrera eramateko egindako apustuagatik.

Bizitzako etapa honek arrasto sakona utziko du nigan, zalantzarik ez dut. Jakintza berriak, ikuspuntu anitzak, lanarekiko ardura eta jarrera, etab. ekarri dizkit, eta bide honetan lagun izan ditudanak. Horiek guztiak ere badira (bazarete) lan honen protagonista.

Hasteko bihotzez eskertu nahi ditut zuzendari eta lagun izan ditudan Jon Ander eta Manex. Ezingo nuke gidari hoberik izan. Aztarna utziko nau zuen zientziarekiko grinak, zehaztasun beharrak, ideien etorriak, soluzioak planteatzeko erraztasunak eta, bereziki, landu dugun harreman pertsonalak. Hitzak ez dira nahikoak zuengandik jaso dudan guztia eskertzeko, beraz zorretan nago…

Tesi honetako protagonista handiak balbulak izan dira, zenbat ikasi dudan! Eta zenbat aldi berean oraindik ikasteko. Lan-talde jatorra eta aberatsa izan dut inguruan. Kolaborazio lan honetan eskerrak, benetan, Ampoko Berrikuntza taldeko Leire, Arianne, Irati, Arkaitz eta Mikeli. Bestalde, unibertsitateko lankide diren Done eta Xubani, eta gurekin aritutako Unairi, bihotzez eskerrik asko. Bide honetan lagun eta sostengu izan zarete.

Saiakuntza esperimentalek ere ekarri zizkidaten buruko-minak. Laborategiko kezkak eramanerrazagoak izan ziren Larraitz eta Erikarekin, irribarre batekin eta beti laguntzeko prest. Eta ezin ahaztu gainazalen ingeniaritza pasioz bizi duten Alaitz eta Iñigo, ilusio horrekin kutsatu nautelako aholku eske joandako bakoitzean. Mila esker!

Eskerrik asko lankideei. Gertukoenak ditudan Mekanika Aplikatuaren arloko lagunei, eta Egituren Mekanika eta Diseinua ikerketa-taldekoei, tesi hau egiteko esfortzua guztiona izan delako, eta niregatik kezkatu zaretelako. Era berean, Fluidoen ikerketa-taldekoei, zuen eguneroko munduan atzerritar den honen kezkak argitzen lagundu didazuelako.

Eskertu beharrean nago baita ere denbora honetan zeharka sortu zaizkidan hainbat arazotan beraiengandik onena eman didaten Harkaitz, Angel, Maider eta beste asko.

I am sincerely grateful to Davide, who I met at the right time in the right place. I admire your continuous willingness to help. I'm lucky to have met you on this adventure.

I would also like to thank Sharon for her professional help, rigour and interest in my work. You can add one more thesis to your long list.

Tesiek izaten duten gorabeheretan lagungarri izan da egoera beretsuan izan zaretenak ondoan izatea: Unai, Mikel, Arantxa eta Peru. Azkenean esan dezakegu iritsi garela bidearen amaierara, eta esfortzuak bere saria izan duela.

Eta lan-esparrutik kanpo bidelagun izan zaituztedanak ere gogoan izan nahi zaituztet, “zeri buruzkoa zen zure tesia…” edo “zer moduz doa tesi hori…” galdetzera ausartu zaretenoi, edo galdetzeko momentua ez zela eta ni beste zerbaitetan entretenitzeko nirekin izan zaituztedan guztioi. Eskerrik asko!

Azkenik, etxekoak, gertu-gertuan izan zaituztedanak beti. Mila esker ama eta aita, honainoko bidea erakusteagatik eta nigan jarritako konfiantzagatik. Mila esker anaiarreba eta familiakideak, gaiaren inguruan behar nuenean hitz egin eta behar ez nuenean isilik egoten jakin duzuelako. Eskerrik asko Saioa, eskerrik asko Laia eta Ibai. Lan honen esfortzua ulertu eta partekatu duzuelako, eta zuentzat izan behar zen nire denboraren zati bat lan honetan dagoelako. Zuen irribarre bakoitza da nire energia.

Laburpena

Estankotasuna bermatzea ezinbesteko betekizuna da fluido bat biltegiratzea edo garraiatzea eskatzen duten aplikazioetan. Ihesak agertzeak ondorio larriak ekar ditzake, bai sistema horretan, bai haren inguruan. Badira presio eta tenperatura altuak dakartzaten aplikazio kritikoak, hain zorrotzak ez diren aplikazioetan ohikoak diren juntura polimerikoak erabiltzea ahalbidetzen ez dutenak. Kasu kritiko horietan, ezinbestekoa da metal-metal kontaktuan oinarritutako itxierak diseinatzea. Horietan, kontaktuaren geometriak eta gainazaleko akaberak nabarmen baldintzatzen dute estankotasuna.

Tesi honetan zenbakizko metodologia berri baten garapena aurkezten da, metal-metal kontaktuan oinarritutako sistemetan ihesen hasiera eta garapeneko fenomeno iragankorrak simulatzeko. Emaitza gisa, ihesen kokapena eta emaria identifikatzen dira, sistemaren egiturak eta barneko fluidoak baldintzatzen dituztenak. Horregatik, proposatutako metodologia fluido-egitura interakzioa (FSI – *Fluid Structure Interaction*) jasotzen duten eredu multifisikoetan oinarritzen da.

Ihesaren aurrerapena zehazteko, proposatutako metodologiak esperimentalki zehaztu beharreko irizpide bat behar du. Horretarako, iragazkortasuna kontaktu-presioen arabera zehazten duen prozedura bat proposatzen da. Karakterizazio hori kontaktu-presio uniformeak dituen sistema baten gainean egin da, eta ondorioztatu da posible dela barneko fluidoarekiko eta itxiera bermatzen duen indarrarekiko independentea den ihesirizpide bat definitzea.

Azkenik, garatutako zenbakizko metodologia bigarren sistema baten gainean baliozkotu da; bigarren sistema horrek, berriz, itxierako kontaktu-presio ez-uniformeak ditu. Eredu numeriko horren emaitzek esperimentalki ikusitakoarekin bat datozen ihesaren kokapena, atari-presioa eta emaria erakutsi dituzte.

Resumen

Garantizar la estanqueidad es un requerimiento indispensable en aplicaciones que exigen el almacenamiento o transporte de un fluido. La aparición de fugas puede suponer graves consecuencias, tanto en dicho sistema como en su entorno. Existen aplicaciones críticas que implican altas presiones y temperaturas, las cuales no permiten el uso de juntas poliméricas que son habituales en aplicaciones menos exigentes. En estos casos es indispensable el diseño de cierres basados en contacto metal-metal, en los que la geometría del contacto y el acabado superficial condicionan significativamente la estanqueidad.

En esta tesis se presenta el desarrollo de una nueva metodología numérica para simular fenómenos transitorios de inicio y desarrollo de fugas, en sistemas basados en contacto metal-metal. Como resultado se identifica la localización y el caudal de las fugas, que están condicionadas tanto por la parte estructural del sistema como por el fluido contenido. Por ello, la metodología propuesta se basa en modelos multifísicos que contemplan la interacción fluido-estructura (FSI – *Fluid Structure Interaction*).

Para determinar el avance de la fuga, la metodología propuesta requiere de un criterio que debe ser caracterizado experimentalmente. Para ello, se propone un procedimiento que determina la permeabilidad en función de las presiones de contacto. Esta caracterización se ha realizado sobre un sistema que presenta presiones de contacto uniformes, revelando que es posible definir un criterio de fuga independiente del fluido contenido y la fuerza que garantiza el cierre.

Finalmente, se ha validado la metodología numérica desarrollada aplicándola sobre un segundo sistema cuyas presiones de contacto no son uniformes en el cierre. Los resultados de este modelo numérico han mostrado una localización, presión umbral y caudal de fuga acordes con lo observado experimentalmente.

Abstract

In applications that require the storage or transport of a fluid, ensuring leak-tightness is essential. The emergence of leaks can have serious consequences, both for the system and its environment. There exist critical applications which involve high pressures and temperatures, which do not permit the use of polymeric seals that are common in less demanding applications. In these critical cases, it is necessary to design seals based on metal-to-metal contact, where the geometry of the contact and the surface finish have a significant influence on leak tightness.

This dissertation presents the development of a new numerical methodology to simulate transient leak initiation and development phenomena, in systems based on metal-to-metal contact. As a result, the location and flow rate of leaks are identified, which are conditioned by both the structural part of the system and the contained fluid. For this reason, the proposed methodology is based on multiphysics models that consider fluid-structure interaction (FSI).

To determine the progression of leakage, the proposed methodology requires a criterion that must be experimentally characterised. To this end, a procedure is proposed that determines permeability as a function of contact pressures. This characterisation was performed on a system that presents uniform contact pressures, revealing that it is possible to define a leakage criterion independent of the contained fluid and the sealing force.

Finally, the developed numerical methodology was validated using a second system whose contact pressures were not uniform at closure. The results of this numerical model revealed leakage location, threshold pressure and flow rate in accordance with that observed experimentally.

Declaration of originality

I hereby declare that this dissertation and the work described in it are the product of my own work and that, to the best of my knowledge, it contains no previously published material except where due acknowledgement has been made in the text as noted by citations. This PhD thesis has not been submitted for any other degree or diploma of Mondragon Unibertsitatea or other institute of higher education. The copyright of this document including data, figures, tables and text rests with the author and all the assistance received in preparing it has been acknowledged. Researchers are free to copy, distribute or transmit the thesis on the condition that they attribute it properly, that they do not use it for commercial purposes, and that they do not alter, transform or build upon it.

Signed: Mikel Ezkurra Mayor

Arrasate-Mondragón, July 2021

Table of contents

List of figures

List of tables

Nomenclature

List of symbols

Sign	Unit	Description
e	[J/kg]	Specific internal energy
E	[Pa]	Young's modulus
g	[m/s^2]	Gravitational acceleration
h	[W/m^2]	Heat flux
k_{system}	[m^4]	System global permeability
k	[m^3]	System permeability per unit length in leak direction
k_{unit}	[m^2]	Contact permeability per unit length
k_0	[m^2]	Contact permeability per unit length at null contact pressure, when $\lambda = 1$
K	[Pa]	Liquid bulk modulus
L	[m]	Length of the leakage path
ℓ	[m]	Fluid cell dimension in the circumferential direction
m	[kg]	Mass
$\mathbf{n}$	[-]	Unit normal vector
P	[Pa]	Fluid pressure
$\overline{p}$	[Pa]	Mean contact pressure
$\overline{p}_{\text{c}}$	[Pa]	Mean contact pressure at closure
q	[J]	Internal heat source
Q	[m^3/s]	Volumetric flow rate
r	[m]	Radius of the contact area
R	[J/(kg $\cdot$ K)]	Gas constant
Ra	[m]	Roughness average
t	[s]	Time
T	[K]	Temperature
u	[m]	Displacement
v	[m/s]	Velocity
V	[m^3]	Volume
V_0	[m^3]	Chamber volume
x	[m]	Position

Sign	Unit	Description
β	[-]	Shape parameter for the Weibull distribution
δ	[-]	Kronecker delta
	[-]	Scale parameter for the Weibull distribution
ε	[-]	Strain
κ	[W/(m · K)]	Thermal conductivity
λ	[Pa]	Lamé's first parameter
	[-]	Parameter to modulate the slope of Weibull distribution
η	[Pa · s]	Dynamic fluid viscosity
μ	[Pa]	Lamé's second parameter or shear modulus
	[-]	Friction coefficient
ρ	[kg/m^3]	Density
σ	[Pa]	Stress
Γ	[-]	Boundary
ν	[-]	Poisson's ratio
Ω	[-]	Domain

List of subscripts

Subscript	Description
$(\bullet)_{\mathrm{s}}$	Structure
$(\bullet)_{\mathrm{f}}$	Fluid
$(\bullet)_{\mathrm{fsi}}$	Fluid-structure interaction
$(\bullet)_{\ell}$	Liquid
$(\bullet)_{\mathrm{a}}$	Air

List of acronyms

Acronym	Description
AISI	American Iron and Steel Institute
ALE	Arbitrary Lagrangian-Eulerian
APDL	Ansys Parametric Design Language
API	American Petroleum Institute
ASME	American Society of Mechanical Engineers
CFD	Computational Fluid Dynamics
DSD/SST	Deforming-Spatial-Domain/Stabilised Space-Time

Acronym	Description
FEM	Finite Element Method
FPP	Fluid Pressure Penetration technique
FSI	Fluid-structure interaction
GUI	Graphical User Interface
HB	Brinell Hardness
HS	High Pressure Fujifilm Prescale measurement film
HHS	Super High Pressure Fujifilm Prescale measurement film
IB	Immersed Boundary methods
ISO	International Organization for Standardization
MAV	Micro Aerial Vehicle
ST-TC	Space-Time method with Topology Change
TUI	Text User Interface
UDF	User Defined Function (Ansys Fluent)
UPF	User Programmable Feature (Ansys Mechanical)

CHAPTER

1

Introduction

Contents

This chapter describes the general framework of this dissertation. It begins by establishing the background and motivation of the present work. Afterwards, work objectives are set based on the research gaps identified in the literature review, and the outline of this thesis document is described.

Leaks are identified as a major problem in several applications, which could cause potential harmful consequences in the oil and gas sector, automotive and aeronautical sectors, chemical industry, and biomechanical applications, among others.

Numerical simulations have significantly contributed to the design of engineering systems and the understanding of their behaviour. As a result of ever-increasing calculation capacity and developments in modelling, multi-physics simulations have made it possible to predict behaviours which cannot be addressed with analytical models. Fluid-structure interaction (FSI) is a particular case of multi-physics problems, which consists of modelling the mutual interaction between fluid flow and deformable structures. Applications of FSI are found in a wide range of natural and engineered fields. The main contribution of the present study is the development of a novel numerical methodology to predict leakage behaviours, which takes into account the complex interaction between fluids and solids. Thus, the prediction of the leak location and flow rate is provided, which enables the design of systems according to an admissible leakage threshold.

1.1 BACKGROUND

Leakage is the undesired escape of liquid or gas through a hole or crack. Fluid storage and transport are vital processes in several industrial applications, such as water or gas supply, cooling/heating systems or oil and gas extraction. Leakage may lead to severe consequences as it may cause natural disasters, costly breakdowns of the systems where they occur or even the loss of human life (Martinsanz, 2015). It is therefore important to understand and predict the leakage behaviour of systems to reduce the risk of such events occurring.

A traditional solution for leakage control is the use of seals or gaskets, which are usually made of polymeric materials. The main advantage of these elements is that they easily deform under pressure and adapt to surfaces as a result of their low rigidity, which prevents the passage of fluids. In addition, they are low cost. However, the temperature and pressure requirements of some applications mean that their use is not possible. Nuclear applications, subsea or underground equipment, the aviation industry, ultra-high vacuum vessels, petroleum recovery and cryogenic applications are examples where polymeric sealing is unfeasible. Therefore, it is necessary to achieve closure by means of direct metal-to-metal contact (Ràfols, 2016; Xin and Gaoliang, 2016; Shvarts and Yastrebov, 2018). Metal surfaces involve a rough surface, as a result of the machining processes used. As a consequence, surfaces in contact are imperfect and, at certain conditions, fluid can find a path leading to a leak (F. Bottiglione et al., 2009; Putignano et al., 2013; Pérez-Ràfols and Almqvist, 2018).

Flow rate through a gap depends upon a large number of factors, such as geometry, fluid properties, pressure and the interaction between the fluid and the surface in the flow path. In practice, it is hard to accurately define the geometry considering macroscopic and microscopic aspects which define the leakage channel. Uncertainties exist also for fluid and material properties due to pressure and temperature changes, particularly if a fluid phase change happens. Lastly, even if the total pressure drop throughout the leak is known, pressure changes along the flow path are hard to predict. Hence, accurate prediction of leak rate is a significant challenge (Chivers, 2002).

Many researchers have contributed to leakage prediction by both experimental (Murtagian et al., 2004; Marie and Lasseux, 2007; Zhang et al., 2019; Vlădescu et al., 2019) and analytical-numerical ways (F. Bottiglione et al., 2009; Lorenz and Persson, 2009; Pérez-Ràfols, Larsson, Van Riet, et al., 2018; Shao et al., 2019). The extreme conditions of some environments (such as subsea or underground appliances) make the prediction of leaks by experimental means unfeasible (Xin and Gaoliang, 2016). Consequently, numerical models are an indispensable tool to gain knowledge in these applications. Numerical solutions have been proposed using both structural simulations and flow simulations (also known as Computational Fluid Dynamics, CFD). The former predict leakage focusing on contact pressure loss, stress pattern or gap determination (Beghini et al., 2015; Gorash et al., 2016; Nelson et al., 2017). The latter estimate the leak flow rate after making a prediction of gap dimensions based on the load applied to the system (F. Bottiglione et al., 2009; Mondal et al., 2014; Silva and Deschamps, 2015). However,

to perform an in depth leak analysis it is necessary to take into account complex interactions between structures and fluids, which are not accounted for in such works.

A fluid flow exerts forces on the adjacent structure, which causes deformation. In the same vein, structural deformations may affect the fluid flow. This phenomenon is known as fluid-structure interaction (FSI), the mutual interaction between a fluid flow and a deforming structure. Numerical partitioned approaches solve flow and structural problems separately, and a coupling algorithm performs the interaction between the fluid and the structure. The information exchanged between domains depends on the coupling method. In cases where structural deformations are small, the fluid domain is hardly affected. Consequently, it is only necessary to transfer the fluid results to the structural solver (*one-way coupling* calculations). When the deformation of the structure significantly affects the fluid domain, in addition to the aforementioned exchange the structural solution is also transferred to the fluid solver (*two-way coupling* calculations). In general, two-way coupling solutions are more accurate, especially in cases of large deflections where the fluid domain is strongly influenced by the structural deformation. A benefit of one-way coupling simulation is significantly lower computational time (Benra et al., 2011; Hou et al., 2012; Zienkiewicz et al., 2014).

Leaks are an issue of critical concern in valve design, which are mechanical components that play a major role in most industries. Their main purpose is to allow, prevent or regulate the fluid flow, by means of a movable part which opens, closes or partially obstructs the channel. Leaks in valves can be classified as external or internal (Goharrizi and Sepehri, 2011). External leakage means that fluid is lost out of the circuit, whereas in an internal leakage fluid is displaced to another location within the circuit, due to inadequate sealing of the gap between the valve body and the moveable element. In both cases leakage affects the safe operation of the system and could lead to environmental damage and waste of resources. For this reason, an accurate prediction of the leakage behaviour of valves is vital. The principal reasons for valve failure are improper seating and the valve being stuck in either the open or closed position (McElhaney, 2000). Thus, the sealing zone is considered as critical in the valve design stage.

Numerical modelling plays an essential role in valve design. It is an indispensable tool to guarantee the integrity of valve components under extreme conditions. Structural simulations ensure the correct service of the valve components, whereas the behaviour of the fluid is verified by means of CFD flow simulations (Cavallo et al., 2005; Leutwyler and Dalton, 2008; Schmidt et al., 2009; Ahn et al., 2011; Song et al., 2014; Yang et al., 2017). In addition, there are several works in the literature which consider FSI in valve simulation. Partitioned approaches are broadly used due to the wide range of software available. Both one-way coupling approaches (Wang et al., 2009; Song et al., 2009; Beune et al., 2012; Song et al., 2014) and two-way coupling approaches (Choi et al., 2010; Gonzalez et al., 2016; Tao et al., 2018; Pan et al., 2019) are found.

As regards valve leakage modelling, it is important to calculate the transient evolution: from the absence of leakage, through its onset, and to its development and progress. Throughout this process, fluid domains that were previously isolated by the blocking element become connected. In the same way, when a valve is operated to open

or close, the fluid domains are required to connect or separate (see Figure 1.1). This presents a numerical problem that has to be solved, since two isolated watertight fluid domains cannot become a single domain. In fact, numerical methods can only work with initially connected computational domains (Beune et al., 2012).

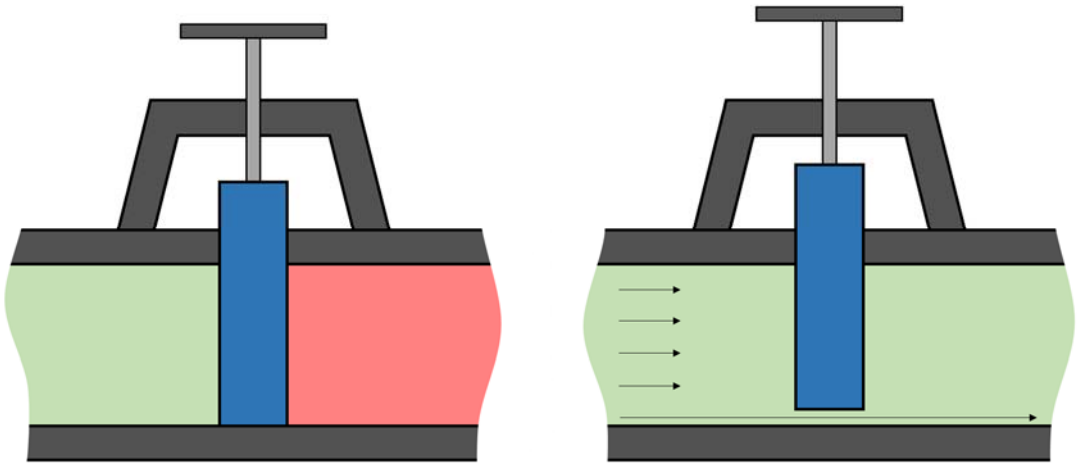

(a) (b)

Figure 1.1: (a) When the valve is closed the fluid chambers on each side are isolated, marked in green and red. (b) When the valve opens, both chambers become a single fluid domain.

Both structural and CFD solvers have their own capabilities or workarounds to address the described problem (Medvitz et al., 2007; Liu et al., 2016; Gorash et al., 2016; Anwar et al., 2016; Al-Azawy et al., 2017). In contrast, works that consider FSI broadly avoid the problem of how to connect fluid domains by linking them permanently with a channel of negligible dimensions (Beune et al., 2012; Su et al., 2014; Song et al., 2014). However, the initial conditions of the simulation do not correctly reflect the physical conditions in the absence of leaks, thus the described simulations are not able to model leakage initiation.

In summary, the following steps are required to numerically model and diagnose the transient leakage behaviour of a system: (i) addressing the problem of numerically connecting two isolated fluid domains, (ii) determining whether leakage will occur, (iii) finding the leakage location and pathway, and (iv) calculating the leak rate. First, a solution has to be proposed to model the flow between hitherto watertight fluid domains. In this regard, a criterion considering both structural and fluid conditions must be established to determine under which conditions leakage starts. Then, this criterion has to be verified locally in the locations where fluid is present. This enables the identification of the route a leak will take, which is not an obvious task. Lastly, a law needs to be established to quantify the approximate leakage flow according to geometrical, structural and fluid parameters at the time considered.

1.2 MOTIVATION

Valves are used extensively in several applications, where they play an important role in ensuring effective and safe closure. Numerical simulations are an indispensable tool in the design of these mechanical components, and in ensuring a safe and competitive product. The most accurate simulations are those that consider a two-way FSI coupling, as this means that both the fluid domain and the structural domain are updated according to the conditions of the system.

Numerical modelling of leakage presents the challenge of connecting fluid domains that were hitherto isolated. The works analysed in the literature propose a number of solutions to this problem, but none provide a transient analysis of leakage from its absence to its development. Addressing this problem contributes to the state of the art by ensuring a better understanding of leakage behaviour. In addition, it has important implications for other applications, such as the modelling of valve operations.

However, connecting isolated fluid domains is not the only issue for modelling leakage: determining the leakage location, as well as setting a leakage criterion which determines the leakage pathway and flow rate must also be considered. In terms of path determination, the spatial arrangement of a leak greatly depends on the geometry of contact, and the surface roughness (Shao et al., 2019). These factors lead to a non-uniform contact between the sealing surfaces, and consequently fluid must seek a route which is often tortuous. In addition, the loads or fluid pressure in the system may change, which can result in a regression of the leak which must also be predicted.

With respect to a leakage criterion, establishing an objective rule which ensures the absence of leaks is of utmost importance. Too strict a criterion may lead to overdimensioned devices and actuators of the valves, whereas a lack of proper definition of the criterion may not ensure safe performance.

Therefore, in this work a new methodology to predict transient leakage behaviour is developed, which is based on a two-way coupled FSI approach. The purpose is to give the most accurate prediction of the sealing behaviour of two structural elements in contact, when it is subjected to an internal fluid pressure. Furthermore, the two-way coupled simulation provides the most accurate representation possible of the system behaviour at the sealing zone, as it considers the interaction of the structural and fluid domains and the resulting changes in geometry.

The aim of the developed methodology is to enable the direct identification of leaks in a numerical model, by assessing structural and fluid conditions. In addition, an experimental procedure to predict the leakage outflow rate is proposed, regardless of the sealing force and the fluid contained in the system.

In conclusion, the key challenges addressed in the present research are:

- Develop an FSI-based numerical methodology to identify the leak location and its progression.

- Determine the evolution of leaks over time, so that their location and pathway is predicted based on the local fluid and structural conditions. It should be noted that leaks could progress or regress depending on these conditions.
- Propose an experimental methodology which results in the establishment of a leakage criterion. This criterion enables an accurate prediction of the leak onset and leakage flow rate.

1.3 RESEARCH OBJECTIVES

The main objective of this research is to develop a numerical two-way coupled FSI methodology to model transient leakage phenomena.

To this end, the following technical objectives are stated:

- Objective 1: define a numerical methodology to connect two initially isolated fluid domains.
- Objective 2: define a numerical methodology to identify the evolution of leaks between two solids in contact, so that their location and the corresponding path is determined.
- Objective 3: develop an experimental bench to characterise a leakage criterion, which determines the onset of leakage and the outflow rate as the leakage progresses.
- Objective 4: validate the developed numerical methodology and leakage criterion in a case study.

1.4 DISSERTATION OUTLINE

This thesis document has been divided into four technical chapters (chapter 2 to chapter 5) so as to achieve the aforementioned operational objectives, as shown in Figure 1.2.

Chapter 2 introduces the numerical methodology developed to connect isolated fluid domains, giving response to **Objective 1**. In this section, the main facts concerning geometry and structural and fluid model definitions are explained. The geometrical model must fulfil some requirements to permit the application of the developed methodology, and also specific subroutines have to be implemented both in structural and flow solvers so that the model behaves appropriately. Once each domain is defined, how to properly perform the two-way coupled FSI analysis is presented.

Chapter 3 describes an algorithm that complements the methodology set out in Chapter 2 to determine the leakage pathway, and hence fulfil the needs of **Objective 2**.

Chapter 4 focuses on the determination of a leakage criterion in order to address **Objective 3**. An experimental setup is designed and manufactured to identify leakage onset and progress. A methodology is explained to quantify the leakage flow rate for specific structure and fluid conditions, based on fluid pressure measurement and mechanical contact pressure simulation.

Chapter 5 meets the demands of **Objective 4** of validating the developed methodology by means of a case study. Experimental tests are carried out and a two-way coupled FSI simulation is performed using the developed leak detection methodology. Results of the simulation and experimental tests are compared and discussed to validate the predictions of the numerical model.

Finally, in **Chapter 6** the overall conclusions of the thesis are summarised and future research lines are defined.

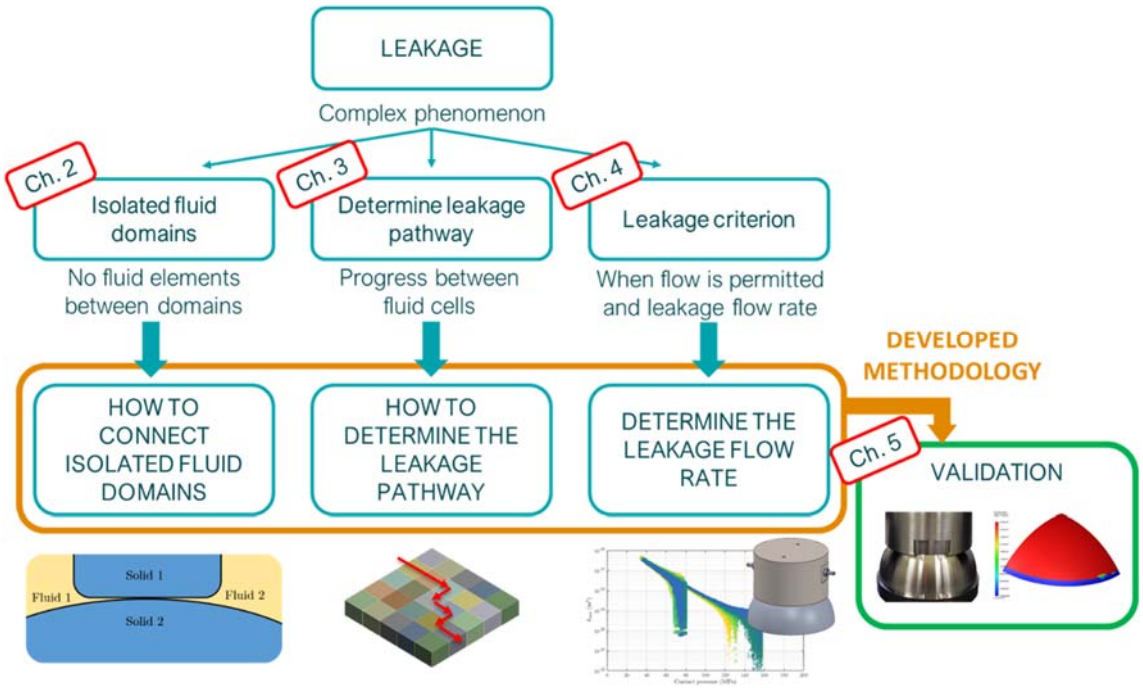

Figure 1.2: Organisation of the thesis.

CHAPTER

2

Development of a new methodology to connect isolated fluid domains

Contents

This chapter provides an overview of the methodology developed to numerically connect two fluid domains separated by solid elements. Structural and fluid parameters are considered to determine the behaviour of a fluid between two solid surfaces in contact. Fluid-structure interaction (FSI) was taken as a key aspect in the development of this methodology, and a general overview of FSI is presented. The solutions provided by other authors to address the problem of numerically connecting isolated fluid domains are also examined. None of them however, contribute to a transient modelling of that connection. Therefore, the general approach of the developed methodology is presented, which can be implemented in any multiphysics simulation solver. In the current work Ansys software was chosen, as it is a robust and widely accepted multiphysics simulation tool. In this regard, the particular aspects of the implementation in the selected software are described. Finally, the potential applications for the use of the developed methodology are presented.

2.1 FLUID-STRUCTURE INTERACTION

Fluid-structure interaction (FSI) is the mutual interaction between a deformable structure and an internal or surrounding fluid flow. The fluid exerts forces which deform the structure and at the same time the fluid adapts to the new configuration of the surrounding structure.

Fluid-structure interaction is present in several natural and engineered systems. The interactions between a tree and wind or groundwater with the soil are known examples of the former, and applications of the latter can be found in automotive and aeronautic sectors, biomechanics, constructions, etc. A selection is presented below to clarify the concept of FSI:

- Automotive sector: inflation of air bags and impact of a person on them, door seals, design of valves that restrict flow, etc. (e.g. Jaiman et al.(2012)).
- Aerodynamics: wings of an aircraft, blades of a turbo-machine, etc. (e.g. Guruswamy (2002), Takizawa et al. (2015)).
- Biomechanics: interaction of blood flow with natural or artificial heart valves and arteries, functioning of the respiratory system, etc. (e.g. Su et al. (2014), Al-Azawy et al. (2016a)).
- Constructions: design of bridges or tall buildings and their interaction with the wind (e.g. Huang et al. (2013), Kavrakov and Morgenthal (2018)).
- Offshore: platforms in the ocean and wave impact, motion of a boat, etc. (e.g. Jaiman et al. (2009)).
- Energy and distribution: liquid or gases transported in pipes and passing through valves, wind turbine design and operation, engines, etc. (e.g. (Lin Wang et al. (2016), Ferras et al. (2018)).

The complex interaction between solids and fluids may be modelled numerically. Methods which integrate the solution of different physics, such as structural and fluid behaviours, are implemented in simulation software. They enable the understanding of behaviour resulting from coupled phenomena which cannot be predicted with analytical models (Hou et al., 2012). However, not all problems involving fluids and structures require FSI modelling. Pressure vessels are subjected to the constant pressure of the contained fluid, which can be modelled as a boundary condition in a structural solver, whilst the behaviour of a fluid conducted by a pipeline does not need structural elements when modelling in a Computational Fluid Dynamics (CFD) solver. In the stated cases structural deformation does not substantially affect fluid flow, so the solution may not vary significantly if FSI is considered or not. Conversely, FSI is crucial to achieve accurate results when the interaction between the fluid and the structure affects the response of a system. Therefore, considering FSI is a must when high security is a requirement (e.g. nuclear and chemical industry) and in post-accident analysis (Tijsseling, 1996; Ferras et al., 2018). Liquid and gas distribution is one of the critical sectors because of the harm a possible failure could cause.

2.1.1 Governing equations

The solution of an FSI problem requires the formulation of a coupled problem that gives answer to the following requirements (El Hami and Radi, 2017):

1. Solving the structural problem, to describe the behaviour of the structure in terms of displacement u, strain ε and stress σ.
2. Solving the fluid problem, to describe the behaviour of the fluid in terms of pressure p and velocity v.
3. Ensuring the conditions in the fluid-structure interface, influenced by (i) the force exerted by the fluid as a boundary condition for the structural problem, and (ii) the velocity imposed by the structure as a boundary condition for the fluid problem.

Moreover, the thermal conditions must be taken into account if the temperature affects the domains under study.

The whole analysis is composed of the structural domain, Ω_s, and the fluid domain, Ω_f. The subscripts s and f respectively denote solid and fluid. Their boundaries are represented by Γ_s and Γ_f, and the fluid-structure interface is defined by $\Gamma_{fsi} = \Omega_s \cap \Omega_f$ (see Figure 2.1).

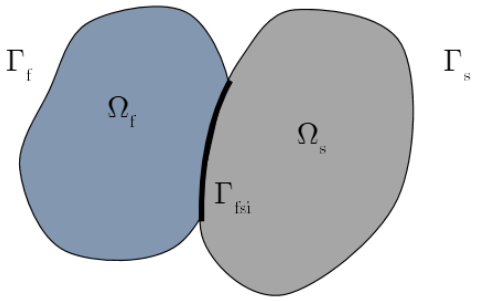

Figure 2.1: Fluid and structural domains in an FSI system.

Structural equations

The structural domain is governed in Ω_s by the equation of motion (Equation (2.1)) and linear elasticity in the material behaviour (Equation (2.2)). All subscripts (i, j, k) represent spatial dimensions:

$$\rho^s \frac{\mathrm{d}v_i^s}{\mathrm{d}t} - \frac{\partial \sigma_{ij}^s}{\partial x_j} = \rho^s g_i, \tag{2.1}$$

$$\sigma_{ij}^s = \lambda \delta_{ij} \varepsilon_{kk} + 2\mu^s \varepsilon_{ij}, \tag{2.2}$$

where:

ρ^s density of the solid.

v_i^{s} velocity components of the solid.

σ_{ij}^{s} stress tensor components of the solid.

g_i acceleration due to gravity.

λ Lamé's first parameter, $\lambda = \dfrac{E\,\upsilon}{\left(1+\nu\right)\left(1-2\,\nu\right)}$, being E Young's modulus and ν the Poisson's ratio.

μ^{s} Lamé's second parameter or shear modulus, $\mu^{\mathrm{s}} = \dfrac{E}{2\left(1+\nu\right)}$.

δ_{ij} Kronecker delta, which is 1 if $i = j$, and 0 otherwise.

ε_{ij} strain tensor components, $\varepsilon_{ij} = \dfrac{1}{2}\left(\dfrac{\partial v_i}{\partial x_j} + \dfrac{\partial v_j}{\partial x_i}\right)$.

ε_{kk} trace of strain tensor.

In the case of solving numerical problems with heat conductive solid bodies, a simple conduction equation is used:

$$\rho^{\mathrm{s}}\,\frac{\partial e^{\mathrm{s}}}{\partial t} = \frac{\partial}{\partial x_i}\left(\kappa^{\mathrm{s}}\,\frac{\partial T^{\mathrm{s}}}{\partial x_i}\right) + q_{\mathrm{int}}^{\mathrm{s}}\,, \tag{2.3}$$

where:

e^{s} specific internal energy of the solid.

κ^{s} thermal conductivity of the solid.

T^{s} temperature of the solid.

$q_{\mathrm{int}}^{\mathrm{s}}$ internal heat sources of the solid.

In thermal fluid-structure interaction problems Equation (2.3) must be considered.

Flow equations

In the fluid domain, the description of fluid flows is generally based on an Eulerian formulation. For linear incompressible viscous fluids, known as Newtonian fluids, their behaviour is governed by the following equations in Ω_{f}:

$$\rho^{\mathrm{f}}\,\frac{\mathrm{d}v_i^{\mathrm{f}}}{\mathrm{d}t} - \frac{\partial \sigma_{ij}^{\mathrm{f}}}{\partial x_j} = \rho^{\mathrm{f}}\,g_i\,, \tag{2.4}$$

$$\frac{\partial v_j^{\mathrm{f}}}{\partial x_j} = 0\,, \tag{2.5}$$

$$\sigma_{ij}^{\mathrm{f}} = \eta^{\mathrm{f}} \left(\frac{\partial v_i^{\mathrm{f}}}{\partial x_j} + \frac{\partial v_j^{\mathrm{f}}}{\partial x_i} - \frac{2}{3} \frac{\partial v_k^{\mathrm{f}}}{\partial x_k} \delta_{ij} \right) - P \, \delta_{ij} \,, \tag{2.6}$$

where:

ρ^{f} density of the fluid.

v_i^{f} velocity components of the fluid.

σ_{ij}^{f} stress tensor components of the fluid.

η^{f} fluid viscosity.

P fluid pressure.

In thermal fluid-structure interaction problems, conservation of energy must be considered:

$$\begin{aligned} \rho^{\mathrm{f}} \frac{\partial e^{\mathrm{f}}}{\partial t} + \rho^{\mathrm{f}} \frac{\partial \left(v_i^{\mathrm{f}} e^{\mathrm{f}} \right)}{\partial x_i} = \eta^{\mathrm{f}} \left[\frac{\partial v_i^{\mathrm{f}}}{\partial x_j} \left(\frac{\partial v_i^{\mathrm{f}}}{\partial x_j} + \frac{\partial v_j^{\mathrm{f}}}{\partial x_i} \right) - \frac{2}{3} \left(\frac{\partial v_i^{\mathrm{f}}}{\partial x_i} \right)^2 \right] \\ - P \frac{\partial v_i^{\mathrm{f}}}{\partial x_i} + \frac{\partial}{\partial x_i} \left(\kappa^{\mathrm{f}} \frac{\partial T^{\mathrm{f}}}{\partial x_i} \right) + q^{\mathrm{f}} \end{aligned} \tag{2.7}$$

$$h_i = -\kappa^{\mathrm{f}} \frac{\partial T^{\mathrm{f}}}{\partial x_i} \,, \tag{2.8}$$

where:

e^{f} specific internal energy of the fluid.

h_i heat flux.

T^{f} temperature of the fluid.

κ^{f} thermal conductivity of the fluid.

q^{f} heat sources of the fluid.

For a complete temperature field coupling, the energy equation should be solved both for the solid bodies and the fluid.

Boundary conditions at the interface

Two conditions are used at the interface to ensure equilibrium: the kinematic condition and the dynamic condition.

On the one hand, the kinematic condition guarantees the no-slip condition, assuming that the velocities are equal at the interface:

$$v_i^{\mathrm{s}} = v_i^{\mathrm{f}} \quad \text{at } \Gamma_{\mathrm{fsi}}\,. \tag{2.9}$$

On the other hand, the dynamic condition guarantees the mechanical equilibrium at the interface:

$$\sigma_{ij}^{\mathrm{s}}\,\mathbf{n}_{\mathrm{s}} = \sigma_{ij}^{\mathrm{f}}\,\mathbf{n}_{\mathrm{f}} \quad \text{at } \Gamma_{\mathrm{fsi}}\,, \tag{2.10}$$

where n_{s} and n_{f} are the unit normal vectors that point outwards from the solid and fluid domains.

2.1.2 Solution procedures

Many strategies have been proposed to numerically solve FSI problems. Selecting the most appropriate depends on the characteristics of the problem (Rugonyi and Bathe, 2001; Belostosky et al., 2014). These strategies can be grouped into two: the *monolithic approach* and the *partitioned approach* (Figure 2.2).

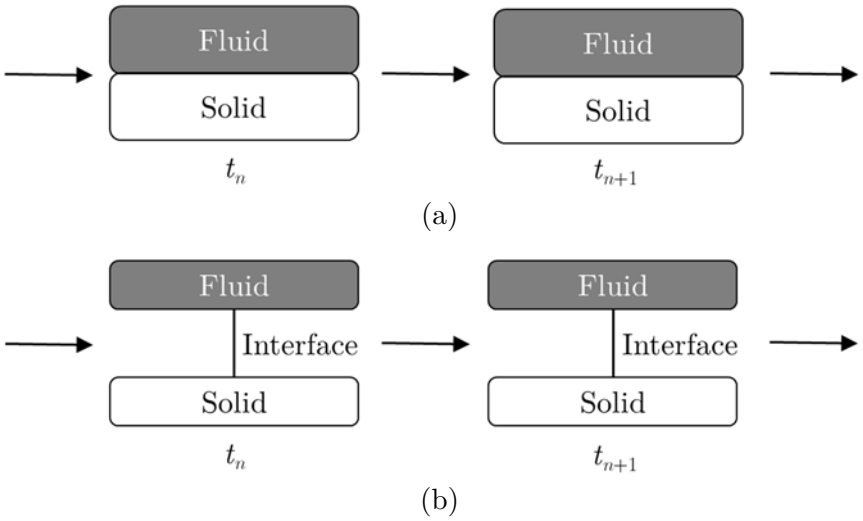

Figure 2.2: (a) Monolithic and (b) partitioned approaches (based on Hou et al. (2012)).

The monolithic approach considers the dynamics of both the fluid system and the structural system in a single set of equations which must be solved at the same time. The interface conditions are an implicit part of the problem. A specific code must be developed to solve the particular combination of physical problems and thus, higher expertise is required. The main advantage of the monolithic approach is that it is potentially more accurate. However, it is more complex to solve because it requires higher calculation resources, and cannot take advantage of off the shelf specific solvers (Hou et al., 2012; Drewczynski et al., 2012).

The partitioned approach is also referred to as *staggered* or *segregated*, and takes advantage of previously developed and tested specific solvers for structural and fluid problems. The boundary conditions are explicitly used to link fluid and solid solutions.

Each domain is considered independently, with its corresponding meshes and algorithms, so code development is required only to program the information transfer between solvers. In fact, the main challenge is to use a stable and accurate coupling algorithm to link the solutions of the two domains for each time step (Tijsseling, 1996; Wang, 2013; Garelli et al., 2016). In this regard, FSI simulations can be classified as *one-way coupled* or *two-way coupled* as shown in Figure 2.3.

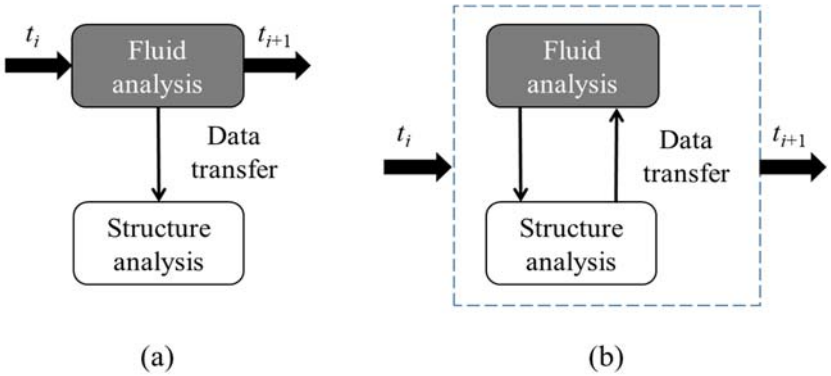

Figure 2.3: (a) One-way and (b) two-way coupled FSI approaches.

In one-way coupled simulations, it is considered that the fluid domain is hardly affected by the resulting small structural deformation. This allows CFD and structural problems to be calculated independently with unidirectional data transfer: only fluid pressure is transferred from CFD to the structural domain. In two-way coupled simulations, structural deformation due to fluid pressure affects the flow field and, therefore, fluid and structural domains must be considered simultaneously with bidirectional data transfer. Pressure is exported from CFD to structural analysis, and deformation is transferred from structural to CFD so that the geometry of the fluid domain is updated at each solution iteration, until both solutions converge (Zienkiewicz et al., 2014; El Hami and Radi, 2017).

Two-way coupled problems are further classified as weakly coupled (or explicit) and strongly coupled (or implicit) (Benra et al., 2011). In the former case, flow and structural equations are solved and corresponding data is transferred once per time step, which does not ensure a converged solution. In the latter case, multiple fluid and structural iterations and data transfers are performed within each time step to achieve a synchronised and converged solution (Figure 2.4). Caution is required in explicit calculations, since significant errors could be accumulated throughout the solution. In general, implicit solutions are recommended although the total computational cost can increase significantly.

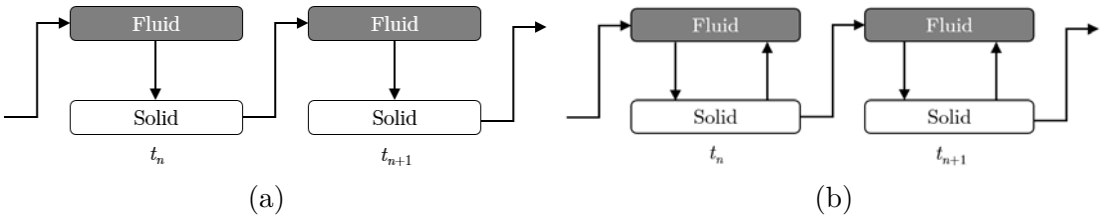

Figure 2.4: (a) Explicit and (b) implicit partitioned procedures (based on El Hami and Radi (2017)).

Considering the different solution procedures discussed in this section, it can be concluded that the monolithic approach leads to better convergence and is recommended for problems with large deformations where both domains influence each other (Ha et al., 2017). However, the partitioned approach is widely employed because optimised existing solvers can be used and coupled. In such cases, strongly coupled approaches should be used to ensure accuracy, which implies a large number of iterations per time-step, or very small time-steps, and subsequently a much higher computational cost (Rugonyi and Bathe, 2001; Vassen et al., 2011; Belostosky et al., 2014).

2.1.3 Computation of moving boundaries

Structural calculations are mainly simulated based on Lagrangian formulation. This means that the mesh is fixed to the structure and, consequently, elements deform as the structure moves. On the other hand, when simulating fluids, Eulerian formulation is usually chosen. The mesh is still and the fluid particles cross the domain (see Figure 2.5).

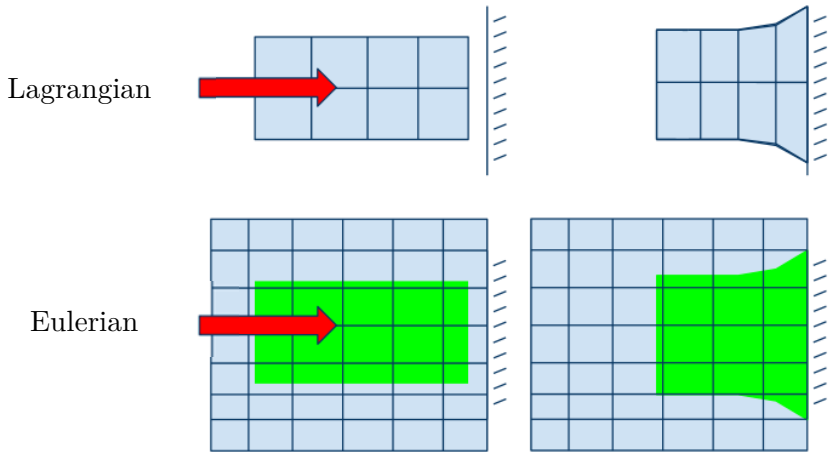

Figure 2.5: A block of material impacting a rigid wall, both in the Lagrangian and Eulerian reference frames (Ansys Inc., 2017a).

To deal with the fluid domain motion associated with structural displacements in FSI simulations, numerical methods can be classified into fixed mesh and moving mesh methods (see Figure 2.6) (Hou et al., 2012; Basting et al., 2017; El Hami and Radi, 2017; Kim and Choi, 2019):

- Fixed mesh methods (also known as non-conforming mesh methods or interface-capturing methods): a fixed fluid mesh is used regardless of the changes in the interface.
- Moving mesh methods (also known as conforming mesh methods or interface-tracking methods): the fluid mesh follows the motion of the structure to ensure that the boundary of both the fluid mesh and the structural mesh coincide.

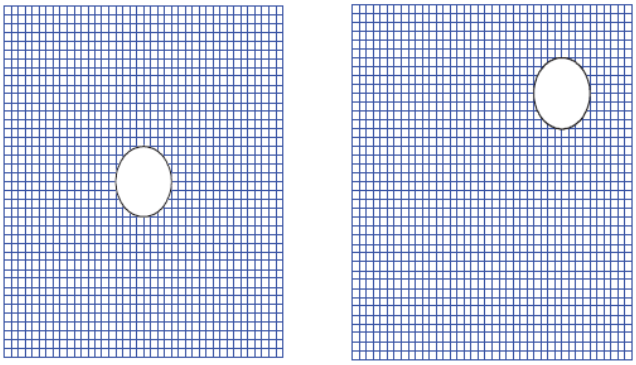

(a) Fixed mesh. Left: $t = t_1$; Right: $t = t_2$

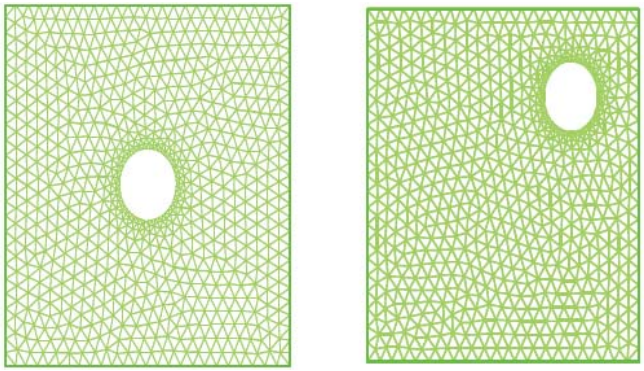

(b) Moving mesh. Left: $t = t_1$; Right: $t = t_2$

Figure 2.6: (a) Fixed and (b) moving meshes (Hou et al., 2012).

Immersed Boundary methods (IB), cut-cell methods, and level-set methods are examples of fixed mesh methods. They permit the use of Eulerian formulation for solving the fluid flow and Lagrangian formulation for calculating the structure motion (Kim and Choi, 2019).

The Arbitrary Lagrangian–Eulerian (ALE) finite element formulation (Hirt et al., 1974; Hughes et al., 1981) is the most widely used moving-mesh technique (Takizawa, Tayfun E. Tezduyar, et al., 2014). The Lagrangian formulation is used in zones with small motion, and the Eulerian in zones where the mesh is not able to follow the motion (T. Tezduyar et al., 1992). The deforming-spatial-domain/stabilized space–time (DSD/SST) method (T. Tezduyar et al., 1992; T. E. Tezduyar et al., 1992) is also a general-purpose moving-mesh technique.

In moving mesh methods it is easy to transfer the information to perform an FSI calculation in a partitioned approach, because the information exchange is directly trans-

ferred through the fluid-structure interface (El Hami and Radi, 2017). When the structure moves the fluid mesh must be updated. Fluid elements are moved and deformed, and consequently the mesh needs to be regenerated at regular intervals. This procedure entails a high computational cost, especially when small elements are used to obtain a higher resolution of what happens at the interface and in 3D problems.

ALE formulation has been the preferred method for handling moving interfaces involved in FSI modelling (Takizawa et al., 2012). However, when there is a large displacement of the structure ALE methods fail due to excessive mesh deformation (Basting et al., 2017).

2.2 CONNECTION OF ISOLATED FLUID DOMAINS IN NUMERICAL MODELS

When a leak happens, the fluid flows from a chamber where it was contained to a new location which was not accessible before. Therefore, the fluid domains that have been isolated previously become connected. In principle, it is not possible to numerically simulate the discontinuity that happens in this process, as numerical methods cannot work with initially separated domains (Beune et al., 2012). A continuous flow field is required so that information is transported in the fluid domain.

The same problem arises in valve opening and closing operations (Wu et al., 2014; Song et al., 2014), since separated upstream and downstream chambers become connected, or vice versa. Consequently, different workarounds have been found in the literature to address this problem. Some are limited to just structural simulations, others only address flow simulations, and a third and final group performs FSI models which are a combination of both.

2.2.1 Workarounds in structural simulations

In structural simulations which contain a fluid, its pressure is usually considered as a constant and uniform external boundary condition. In the cases where the fluid remains steady this model is sufficient. However, when leak and manoeuvring phenomena are considered in a structural model, a uniform pressure is not an appropriate approach. An optimum model should consider that the area where the fluid pressure is applied enlarges as the fluid penetrates through the surfaces that are in contact.

Ansys Mechanical includes the Fluid Pressure Penetration (FPP) technique (Ansys Inc., 2016b) to represent the pressure exerted by the fluid as the closure opens (see Figure 2.7) (Gorash, Dempster, W. D. Nicholls, et al., 2015; Gorash, Dempster, W. Nicholls, et al., 2015; Gorash et al., 2016; Anwar et al., 2016). The main advantage of this tool is that the area under pressure is updated as the fluid opens the contact between the surrounding surfaces. However, using FPP the value of pressure is predetermined and constant, whereas real fluid pressure changes over position and time as the structure deforms. Furthermore, the definition of FPP is not accessible from Ansys Mechanical Graphical User Interface (GUI) and it must be programmed by the user (using APDL commands).

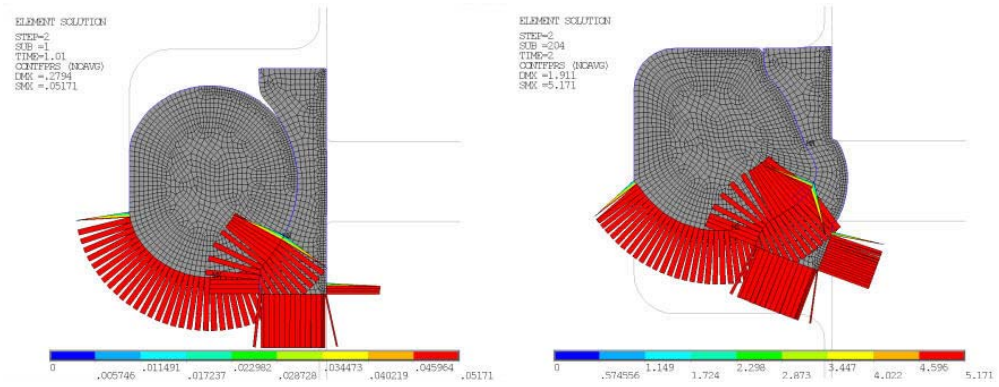

(a) (b)

Figure 2.7: Example of a sealing simulation model taking into consideration the FPP technique. Pressure is applied in a wider area in (b) than in (a) as the contact between solids disappears (Ansys Inc., 2017d).

2.2.2 Workarounds in CFD simulations

In CFD numerical models only the fluid domain is considered. The structural elements are considered as boundary conditions of the problem, which implies that solid elements are treated as completely rigid.

Some alternatives to solve the problem of how to connect isolated fluid chambers can be found in works in the biomechanical sector. When modelling the full pumping cycle of a ventricular assist device it is necessary to simulate the valve closure. Medvitz et al. (2007) conducted such simulation by dramatically increasing the fluid viscosity in a local region surrounding the valve, resulting in greatly reduced fluid velocity. Al-Azawy et al. (2016b) performed a similar study by changing fluid interface boundary conditions according to the valve behaviour. When the valve was closed, the interface boundary condition was set as a wall, and fluid flow across the interface was not permitted. Conversely, fluid flow occurred when the interface was open (see Figure 2.8).

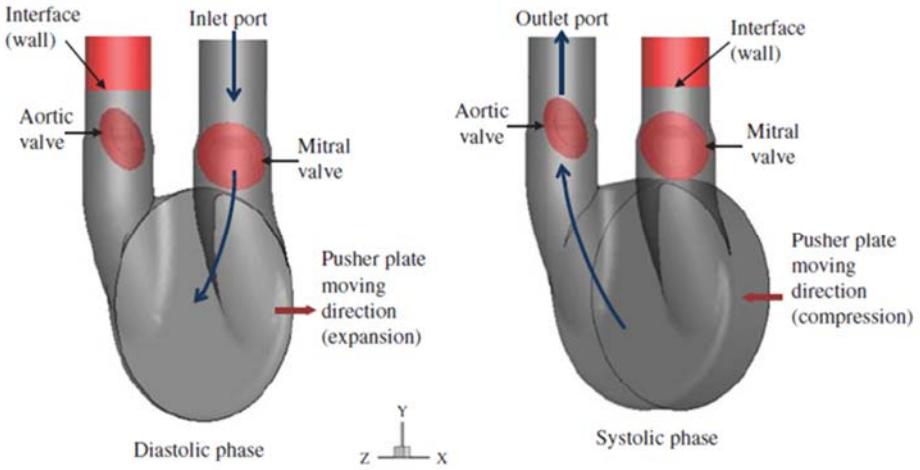

Figure 2.8: Ventricular assist device models where the wall boundary condition is used to model closed valves (Al-Azawy et al., 2016b).

In a later work Al-Azawy et al. (2017) took advantage of the overset mesh technique, also known as *Chimera*. This technique permits the creation of the mesh of individual parts independently. Thus, it is possible to create a finer mesh in the areas required by each. The mesh of the components is then overlapped with a background mesh and the connectivity between grids is automatically established. In this process, undesired fluid cells are discarded (see Figure 2.9).

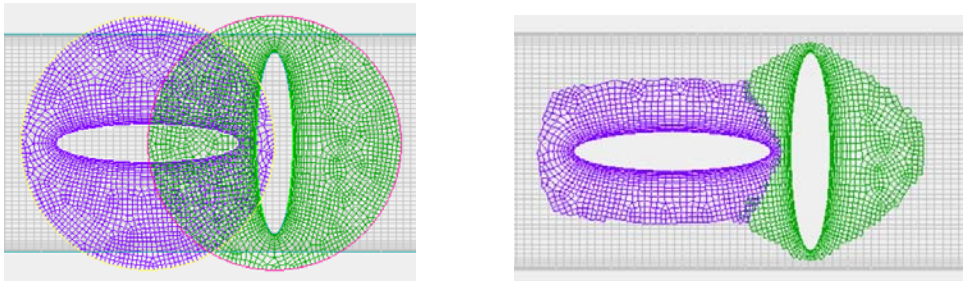

(a) (b)

Figure 2.9: (a) Background mesh and component meshes overlapped. (b) Overset mesh after mesh connectivity is performed (Ansys Inc., 2017c).

There must be a minimum number of cells between interfaces to have good mesh connection. Below that number, no connection is guaranteed and the fluid domains become disconnected (Ansys Inc., 2017c). This fact presents a way of modelling the connection/disconnection of fluid domains. Al-Azawy et al. (2017) took advantage of this technique to model a fully closed valve (see Figure 2.10).

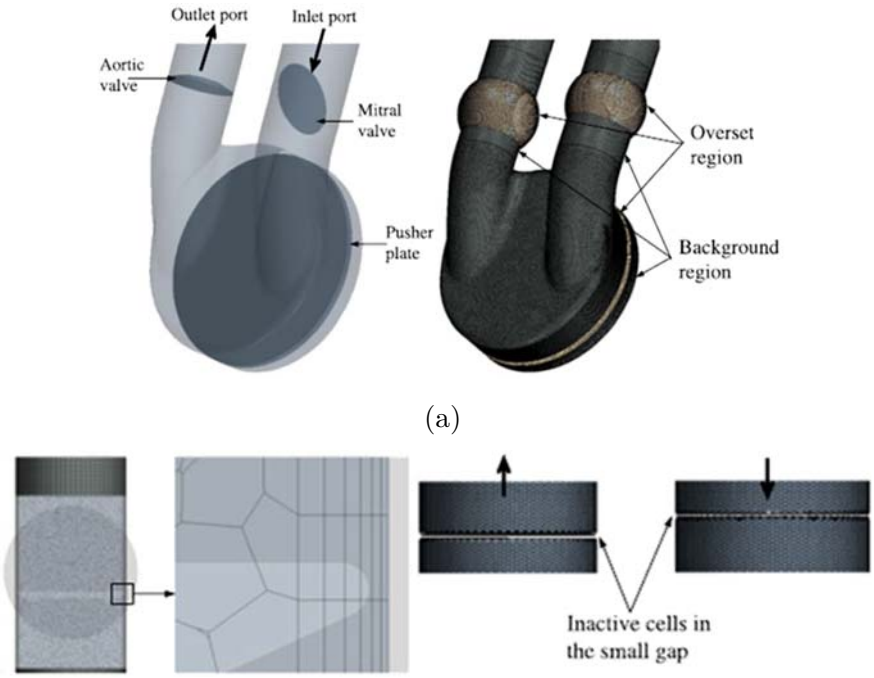

(a)

(b)

Figure 2.10: (a) Ventricular assist device model using overset and background meshes. The gap between the background and the valve can be seen in (b). If few elements remain between interfaces, two isolated fluid domains are created (based on Al-Azawy et al. (2017)).

A different workaround is presented by Liu et al. (2016) to analyse the opening and closing of a globe valve. In their numerical model mesh elements are created or eliminated as the valve core moves.

2.2.3 Workarounds in FSI simulations

The topology change that happens when structural elements come into contact and block the fluid flow presents one of the main reasons in the literature for the development of non-conforming mesh FSI methods (Hsu et al., 2015). In a work by Loon et al. (2006) based on non-conforming mesh a method was proposed to model large movements of a solid through the fluid domain, also considering contact between solids. It was applied to compute the motion of a heart valve in a pulsatile blood flow. One drawback of this method however, is that the compliance of the wall was not taken into account, which is important for the closing behaviour of the valve.

Ager et al. (2018) and Pauw et al. (2019) also presented a monolithic approach based on a fixed fluid mesh which was capable of working down to a zero gap between solid bodies. A poroelastic layer was used to include the effect of the solid asperities of the rough surfaces in the model. When elastic structures are in contact with a vanishing fluid gap in between, the influence of the surface roughness has to be considered in the computational model. Therefore, a variable porosity was included in the poroelastic medium, so that roughness influence increased as the gap reduced. Such an approach takes into account the effect of surface roughness on fluid flow in the whole contacting process, ranging from free flow situations to pure solid contact without any flow.

As regards conforming mesh techniques, an enhanced version of DSD/SST methods was developed by Takizawa et al. (2014). The Space-Time method with Topology Change (ST-TC) includes a master–slave system that maintains the connectivity of the "parent" mesh when there is contact between the moving solid surfaces. Examples of applications, among others, include fluid mechanics of heart valves, where the flow has to be completely blocked when the valve is closed (Takizawa, Tayfun E Tezduyar, et al., 2014), or the computational analysis of a micro aerial vehicle (MAV) with wing clapping, whose wings are brought into contact when they clap (Takizawa et al., 2015).

However, many works found in the literature that use moving mesh techniques (e.g., Aksenov et al. (2005), Beune et al. (2012), Wang (2013), Song et al. (2014), Su et al. (2014), Yang et al. (2017)) have approached the problem of how to connect isolated fluid domains by including a channel between them (see Figure 2.11). In all these cases the gap left between solids is considered negligible, but the conditions at which the analyses start do not represent the real situation.

In this chapter a methodology is proposed to connect isolated fluid chambers. A general approach is presented, and specific implementation is performed in commercial finite element solver. The multiphysics commercial FEM software which are most widely used in the industry use moving mesh techniques and partitioned procedures. Therefore, the developed methodology is formulated for interface-tracking methods for two-way FSI

partitioned schemes, so that the process of connecting isolated fluid chambers is simulated with the most accurate prediction.

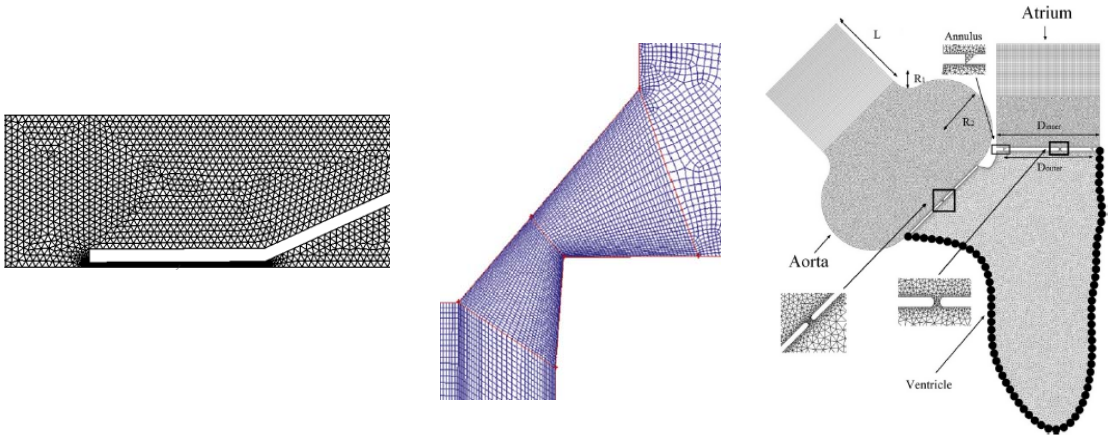

(a) (b) (c)

Figure 2.11: Examples of a channel connecting fluid chambers and a negligible gap between solids in the works of (a) Wang (2013), (b) Beune et al. (2012) and (c) Su et al. (2014).

Numerous analyses in the literature that consider the movement of solids take them as rigid bodies. Their motion is imposed or calculated by an analytical expression that gives the position depending on the force in the system (e.g., Beune et al. (2012), Song et al. (2014), Yang et al. (2017)). A key advantage of the methodology presented in this research is that the developed two-way FSI simulations consider the deformation of the solids as the fluid flows between their surfaces in contact, and the fluid flow is updated with the corresponding new boundaries.

2.3 GENERAL APPROACH TO THE METHODOLOGY TO CONNECT ISOLATED FLUID DOMAINS

The methodology developed in this research aims to connect two fluid domains that are separated by solid elements in a numerical model. This section sets out the fundamentals of this methodology, since its implementation may vary from software to software. First, the basic considerations upon which the methodology is based are described. Then, specific aspects related to geometry, structural and fluid domains and how to perform a coupled FSI analysis are explained.

2.3.1 Basic considerations

As a fundamental principle, it is not possible to numerically connect two isolated fluid domains that are totally independent. This usually occurs in systems where the pressure exerted between solid bodies prevents the fluid from entering the intermediate space. System conditions may change and allow fluid to pass between the surfaces in contact, but in a numerical model it is not possible to connect both domains because there are no fluid elements between them. In addition, fluid elements with null volume cannot be mathematically formulated.

In the present research, the connection process is made possible by defining a set of fluid cells in the pathway between the solid elements in contact. These cells remain inactive while the fluid domains are isolated. The progressive activation of these cells simulates the process of connection between domains when the conditions of the system allow it. However, fluid elements cannot be superimposed on solid elements. This implies that a gap must exist between the solid elements in contact, which cannot affect the mechanical behaviour of the system. Therefore, the solid elements are located not exactly in contact, but separated by a negligible distance which corresponds to the fluid domain size in the pathway (see Figure 2.12). In the structural model the bodies have to be considered in contact disregarding the existing gap.

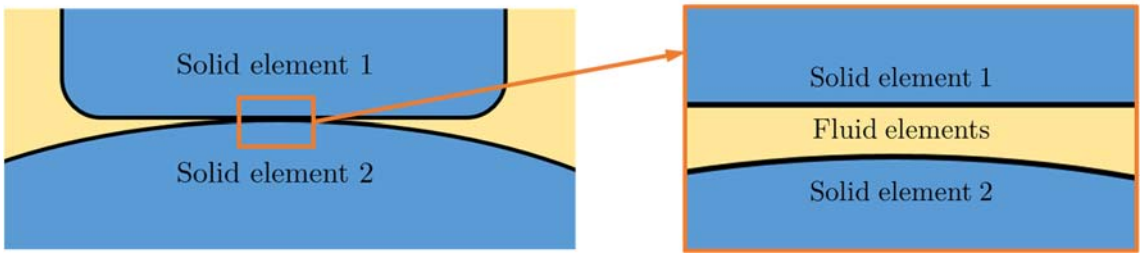

Figure 2.12: Fluid elements in the gap between the solid bodies in contact.

A criterion must be defined to determine when the fluid cells in the pathway are activated. In a real system flow happens when the pressure exerted by the fluid is sufficient to separate the structural surfaces in contact. This causes the contact pressure to decrease. When the contact pressure drops below a threshold value, separation occurs and fluid can flow. This means that in the numerical model the criterion must depend on the contact pressure from the solid domain and the fluid pressure from the fluid domain.

It is considered essential to represent the connection process as rigorously as possible. Therefore, the presented methodology is implemented in a two-way coupled FSI numerical model. As a result, the space filled by the fluid is updated when the pressure exerted by the fluid deforms the solid bodies. In the same way, fluid pressures change as the fluid occupies this space.

The following sections set out the general considerations to build the numerical model and specific aspects of structural and fluid domains.

2.3.2 Geometrical considerations

To analyse the behaviour of how the fluid flows between solid surfaces in contact, the area surrounding the pathway is of vital importance. Some specific geometrical considerations have to be taken into account in this area, whereas the rest of the model is treated as any other FEM model.

The geometrical model is comprised of the structural and the fluid domains. Creating a single model ensures a perfect match between both domains. Afterwards, fluid entities are supressed in the structural calculation, and vice versa.

As regards the fluid domain, the different chambers have to be connected by fluid elements even if they are isolated when the solid bodies that divide the chambers are in contact. As a consequence, a channel exists which connects the fluid domains on both sides. While the solid bodies remain in contact the elements in this channel will not permit any flow. The choice of the channel height is arbitrary. On the one hand, it has to be taken into account that a gap is created that separates the solids which are really in contact. This is addressed by defining appropriate contact properties in order to disregard this gap in the structural solver. On the other hand, the chosen channel height determines the initial flow rate when the fluid chambers are fully connected.

In order to study how the connection process evolves, the pathway between solids is divided into fluid cells along the direction of the flow. The number of cells depends on the required solution accuracy and the available computing resources. In addition, the surfaces of the solids that are in contact with the fluid in the pathway, are divided into sections whose dimensions correspond to those of the fluid cells. In this way the structural contact pressure exerted onto the corresponding fluid cell is captured and compared to the fluid pressure at the same location, in order to permit or not the flow through a specific fluid cell. Fluid cells and the corresponding solid surface sections in contact are given a name to easily and unambiguously identify their relative location. Similarly, the interfaces that connect fluid elements to each other are assigned a name that helps to determine which interface permits the fluid flow into a new cell.

After having defined the geometry of the whole system, just the solid geometry is considered in the structural solver, and fluid geometry in the fluid solver.

2.3.3 Structural calculation setup

The structural domain is composed of the solid bodies whose behaviour is evaluated by means of the structural solver. As has been stated before, solid bodies are separated by a negligible gap that defines the pathway between the fluid chambers. The response of the elements in contact must be the same as if no gap existed. Therefore, a contact offset is defined in the model, with a value that corresponds to the defined gap. In this way the solver considers the elements closer to each other so that they behave as if in contact.

To establish if fluid is contained in a certain fluid cell, its corresponding fluid pressure and contact pressure have to be determined. Contact pressure has to be stored at the end of each structural calculation step so that the fluid solver can retrieve this information. This is achieved by the following steps:

1. A text file is exported containing the identification of the contact elements that correspond to each named contact section in the structural solver.
2. The contact pressure solution of each named contact section is written to a text file which is made accessible to the fluid solver. A user-defined subroutine is required to write this result after each calculation step.

To achieve a two-way FSI solution the surfaces in contact have to be defined as FSI interfaces in the structural solver. In this way, the surfaces exposed to the fluid will receive the pressure exerted by the fluid.

2.3.4 Computational Fluid Dynamics calculation setup

Flow along the channel between solid bodies occurs depending on whether or not the fluid cells connecting the chambers contain fluid. The boundary conditions on the interfaces between adjacent cells are changed to determine if fluid can access the adjacent cell or not. The interface behaves as if it did not exist when fluid flow is allowed. Conversely, the interface can behave as a barrier if its boundary condition is changed, and thus prevent the fluid from crossing it.

The interfaces between the fluid cells in the pathway are initially defined as barriers if the surrounding solid elements are in contact. A subroutine is implemented in the fluid solver to control when to change the boundary conditions of the interfaces, and as a consequence, control the fluid flow. For each specific interface, the subroutine requires the following information:

1. Pressure exerted by the fluid on that interface, which is directly obtained from the fluid solver.
2. Contact pressure between the structural elements on the top and bottom of the next empty fluid cell. This information is calculated in the structural solver. The subroutine retrieves this contact pressure from the text file that is written after each structural calculation.
3. Criterion to determine whether to change the boundary condition of the interface, depending on the fluid pressure and contact pressure that have been obtained.

To achieve a two-way FSI solution, fluid cell interfaces in contact with solid elements have to be defined as coupled to the structural domain. This ensures that the nodes on these interfaces move according to the displacement calculated in the structural solver.

2.3.5 Coupled FSI analysis setup

The developed methodology is designed to be implemented using a partitioned FSI approach. This means that structural and fluid solutions are achieved independently, with their corresponding meshes and algorithms. An additional coupling algorithm is used to transfer information between the domains and ensure a simultaneous solution of structural and fluid solvers.

The calculation is divided into several time intervals, which are called *coupling steps* (see Figure 2.13). For each *coupling step*, structural and fluid solvers determine the solution of their corresponding domain. Each solver requires its own solution iterations to achieve a solution at the end of the *coupling step*. At the end of each *coupling step* solution information is exchanged between the solvers. For this purpose *data transfers*

are defined for the interfaces shared by the solid and fluid domains. Force exerted by the fluid pressure is transferred to the structural solver, and the corresponding displacement calculated in the structural solver is transferred to the fluid solver to update the system geometry. After that, convergence is checked in both structural and fluid solvers, and in the coupled solution. If no convergence is achieved, *coupling iterations* are performed, which means that further calculation and *data transfer* loops are carried out to achieve a more accurate solution in that *coupling step*. *Coupling iterations* are performed until convergence is achieved or until the established maximum number of *coupling iterations* is reached.

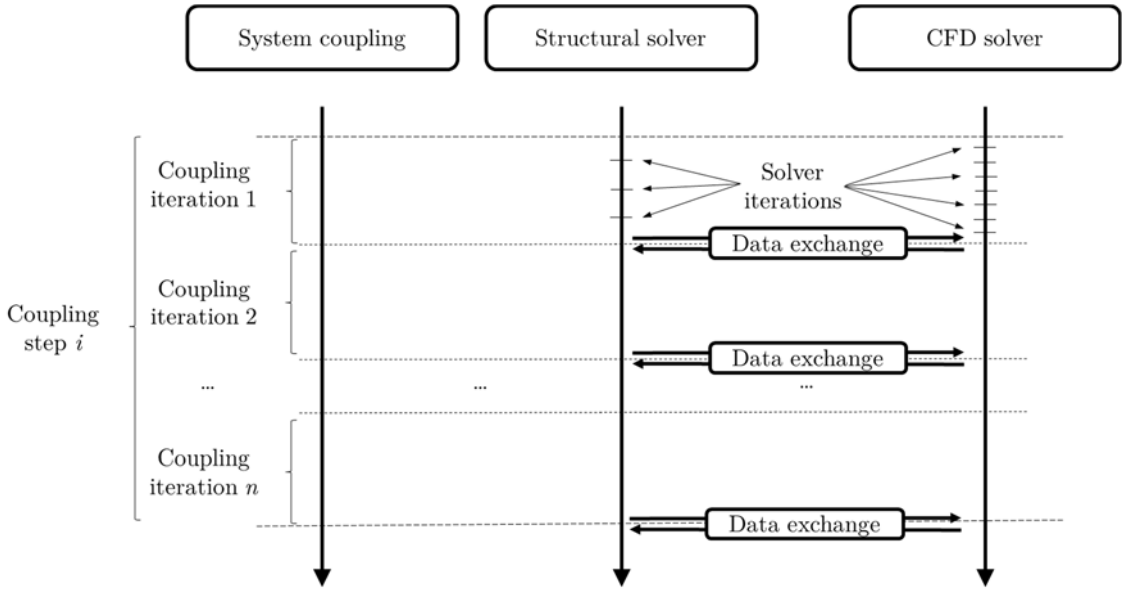

Figure 2.13: Flow chart of a coupled FSI analysis.

2.4 IMPLEMENTATION OF THE DEVELOPED METHODOLOGY IN ANSYS SOFTWARE

There are several commercial simulation programs to test a virtual prototype by means of FEM. Most of them have tools to perform multiphysics analyses in their environments, such as Ansys, COMSOL Multiphysics, Abaqus or MSC.

Ansys software[1] was chosen to develop the present work as it is a robust and widely accepted simulation tool. Its structural and fluid solvers are among the leaders in the field and are widely extended in the industry. In addition, they can easily be combined to perform FSI simulations with results as reliable as the solvers themselves.

Implementing the developed methodology in Ansys required certain adaptations which are thoroughly explained in the following sections.

[1] Ansys® Academic Research, Release 19.2

2.4.1 Introduction to Ansys software

The key Ansys products related to this work are the following (El Hami and Radi, 2017):

- Ansys Mechanical: an FEM analysis tool for structural analysis to perform static analysis, modal analysis, dynamic studies, nonlinear problems and thermal analysis.
- Ansys Fluent: Computational Fluid Dynamics (CFD) software tool to simulate fluid flows. It has a wide variety of models and tools to solve turbulence, multiphase problems, combustion, particle transport, dynamic meshes, etc. Ansys also includes CFX package to solve CFD problems.
- Ansys Meshing: automated product to obtain an appropriate mesh for FEM analyses.
- Ansys Workbench: platform that permits coupled simulations. It takes advantage of single Ansys products which can be connected in the Workbench environment (see Figure 2.14).

When different physics are involved they must be coupled to solve the global problem. The solution of each particular discipline or domain is achieved in the most appropriate package, and the multiphysics solution is performed by coupling these independent analyses. Thus, coupled problems are addressed by means of partitioned approaches.

Ansys launched Ansys AIM in 2015 as a tool where multiphysics problems can be solved within a single interface. One of its strengths is that the main processes and physics combinations are standardised. Its main drawbacks however are that only steady-state solutions can be calculated and only one-way couplings can be performed, thus rendering it unsuitable for two-way FSI simulations or achieve transient solutions. For this reason, linking Ansys Mechanical and Ansys Fluent in the Workbench environment was selected in the present work.

By using Ansys Workbench to connect structural and fluid solvers both unidirectional or one-way couplings and bidirectional or two-way couplings are possible. In one-way FSI analysis, CFD results (forces, temperatures, heat flows, heat transfer coefficients or near wall temperatures) are transferred as inputs in the structural analysis. In two-way FSI analysis, in addition to the above, the structural results (displacements, temperatures or heat flows) are also passed as loads to the CFD solver (Ansys Inc., 2016a; Ansys Inc., 2016d). The former are used when the structural domain is notably affected by the fluid flow, but not the other way around (e.g. thermal stress problems). The latter are required when both domains affect each other in a significant way (e.g. interaction between high pressure fluid and flexible structure).

The links between individual domains are easily performed in the Ansys Workbench environment using System Coupling components, which are responsible for synchronising the overall simulation and exchanging information between individual solvers.

2.4.2 Model setup

The basic structure for the two-way FSI calculation must be assembled in Ansys Workbench as shown in Figure 2.14. Both structural and fluid modules share the same geometry, as was established in section 2.3.2. The mesh of each domain is created in its corresponding module, as each has its own specific requirements. *Static Structural* or *Transient Structural* is chosen for the structural domain, depending on the calculation to be carried out. *Transient Structural* is chosen if the time scale of the loading is such that inertia or damping effects are considered to be important. In the contrary case, *Static Structural* is chosen. Even if the Fluent module is the same for both static and transient calculations, the CFD solver must be defined in accordance with the structural one.

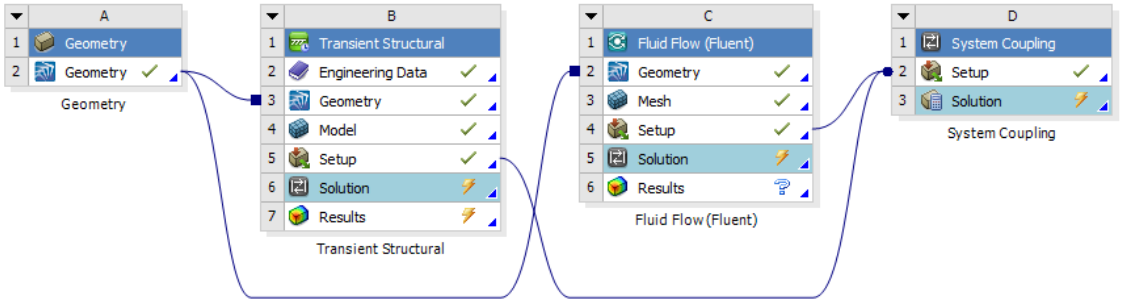

Figure 2.14: General arrangement for a two-way FSI simulation in Ansys Workbench, where the fluid chamber connection methodology is implemented.

2.4.3 Structural calculation in Ansys Mechanical

Geometry is adopted from the module that is shared with Ansys Fluent. Structural bodies are only considered and those corresponding to the fluid domain are supressed.

Correctly defining the contact between the surfaces of the solids through which the flow will pass is one of the key aspects. In a real system the surfaces remain in contact when there is no flow along the channel. However, the developed methodology requires a set of fluid cells to connect the fluid domains at each end of the channel. Therefore, a gap whose size is equal to the fluid cell height exists in the structural geometry. In order to consider the cited structural surfaces initially in contact, an offset has to be imposed.

The fluid channel created in the closure is composed of several fluid cells. The number of fluid cells depends on the accuracy with which it is necessary to evaluate the process of connection between chambers. The surfaces of the solid elements above and below each fluid cell are divided into sections whose dimensions correspond to those of the fluid cells (see Figure 2.15). Each pair of these sections are given a unique identification number, creating named contact pairs. This is essential to capture the structural contact pressure and the fluid pressure at the same location, in order to evaluate if the adjacent fluid cell contains fluid. In this regard, it is necessary to determine and register the contact pressure between each named contact pair.

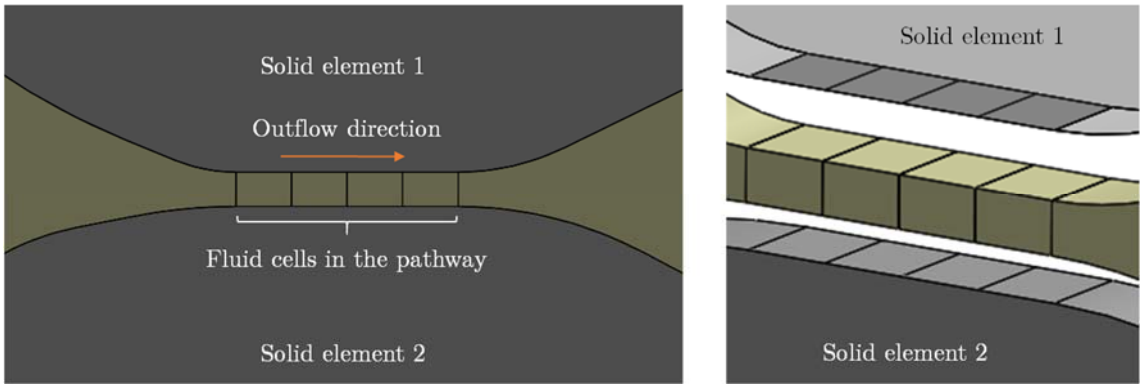

(a) (b)

Figure 2.15: (a) Fluid cells in the channel between solid elements, and (b) solid surfaces divided into sections that match the dimensions of each fluid cell.

Meshing properties are then defined, such as element type and sizing. When mesh is generated, Ansys Mechanical creates structural and contact elements in the geometry.

With respect to the boundary conditions, loads and restrictions related to the structural model are defined. In addition, the *Fluid Solid Interface* boundary condition must be assigned to regions that will receive data from the *System Coupling* module. This ensures that structural surfaces in contact with fluid receive the exerted pressure, which is the principal feature to perform a two-way coupled FSI analysis.

The specific features developed to achieve the isolated fluid chamber connection are detailed hereafter. Two different types of codes must be implemented in the Ansys Mechanical environment:

1. *Command snippets*: Ansys Mechanical uses Ansys Mechanical APDL as the finite element solver. When a solution calculation is run, an input file is sent to the Mechanical APDL solver. After the solution is complete, a result file is created, which is read by Ansys Mechanical. By using *command snippets*, additional instructions are given to the Mechanical APDL solver to perform user-specified tasks in the pre-processing, solution or post-processing phases of the analysis. APDL stands for Ansys Parametric Design Language, and *commands snippets* use this scripting language.

2. *User Programmable Features* (UPFs): users can write their own subroutines to adapt the Mechanical APDL program to their needs. In this way, a new material behaviour, a special element, a contact interfacial model, or a modified failure criterion for composites can be defined. It also permits the retrieval of information from the Mechanical APDL database (Ansys Inc., 2016c). These subroutines may be written in C, C++, or Fortran and they are then compiled and linked to the simulation.

APDL is a scripting language that may be slower to execute than compiled code. However, changing or adjusting APDL input files is much easier than modifying subroutines, as the latter requires recompiling and relinking. Hence, it should be considered whether the desired functionality can be achieved by means of APDL *command snippets*,

as this is a much easier and quicker approach than implementing UPFs (Ansys Inc., 2016c).

In the present work, Ansys Mechanical is employed to obtain the contact pressure on each fluid cell, and to export it to a text file. This information must be written at the end of each *coupling step* during the FSI calculation. The resulting file will then be accessible to the CFD solver to determine the behaviour of each fluid cell in the channel between the solid bodies. To achieve this goal, a combination of *command snippets* and a UPF are needed, which will be explained hereafter.

Three different *command snippets* are required in the Ansys Mechanical environment, all of them at the *Analysis type* level (*Transient* or *Static Structural*):

1. A *snippet* is required to ensure that results are saved in the database during solution. This is necessary to register contact pressure information after each *coupling step* calculation is performed.
2. Another *snippet* writes the contact element identification numbers for each previously named contact pair in a text file. It should be noted that each of these named contact pairs is usually composed of several contact elements.
3. The third *snippet* is responsible for linking the developed UPF into Mechanical APDL and request its execution.

With regards to the UPF, among all the types available in the program (such as user-defined elements, materials or contact behaviours) only those that allow the evaluation of results during solution were applied in the presented methodology. These permit user access at the beginning and at the end of each run solution, load step, substep, or equilibrium iteration (Ansys Inc., 2016c). A specific subroutine is defined for each of these particular cases, and they all must be written in Fortran programming language. They are activated by issuing the USRCAL command, which corresponds to the third *command snippet* mentioned earlier in this section.

In our particular case of interest, the UPF that best suits the needs for the methodology is USSFIN, which allows user access to the developed subroutine after each calculation substep. Therefore, during the coupled FSI simulation, whenever Ansys Mechanical achieves the structural solution for the *coupling step* under execution the implemented subroutine is executed. The tasks performed by the implemented subroutine are the following (see Figure 2.16):

1. Open a text file where contact pressure solutions will be written (*file 1*).
2. For every structural named contact pair that corresponds to a fluid cell:
    a. Open the text file containing the identification of its corresponding contact elements, which is created by the first *command snippet* mentioned earlier in this section.
    b. Create a vector that contains the identification of all contact elements.
    c. Open a text file where the contact pressure for the actual contact elements will be written (*file 2*).

d. Retrieve the contact pressure for each contact element from the solution database.

e. Write the contact element identification and the corresponding contact pressure (in *file 2*).

f. Compute the average contact pressure for the overall named contact pair.

g. Write the calculated average contact pressure (in *file 1*).

h. Close *file 2*.

3. Close *file 1*.

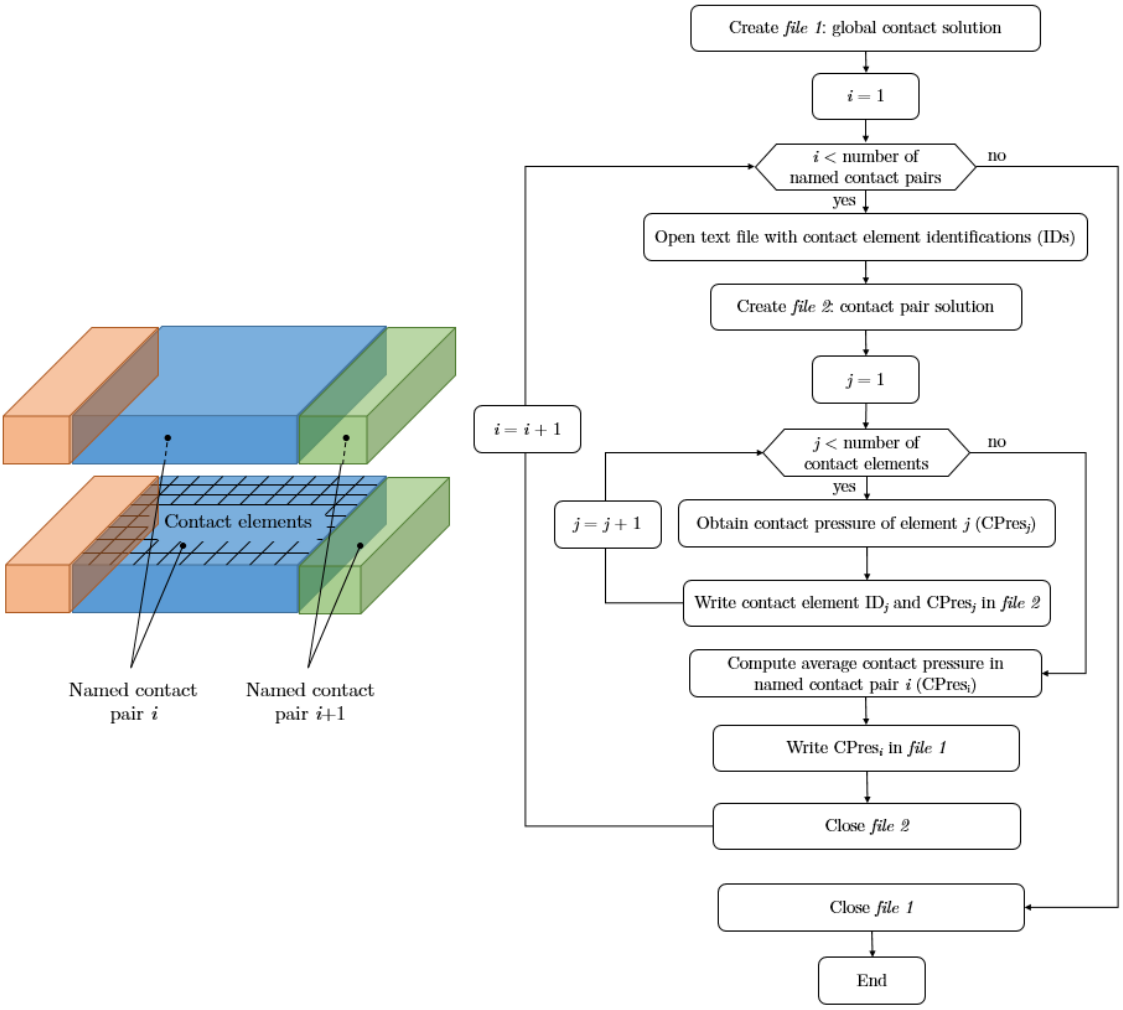

Figure 2.16: Flow chart of the developed USSFIN UPF.

Consequently, at the end of USSFIN subroutine execution the average contact pressure that corresponds to each fluid cell is stored in a text file which is shared with the CFD solver.

2.4.4 Computational Fluid Dynamics (CFD) using Ansys Fluent

As with Ansys Mechanical, geometry is adopted from the module that Ansys Fluent and Ansys Mechanical share. Structural bodies are suppressed and only the fluid domain geometry is considered.

As a first step, the analysis type must be determined as *Steady* or *Transient*. It should be noted that it must match the type of structural analysis in Ansys Mechanical to perform a coupled FSI analysis. As regards the model specifications for the computation, choosing an appropriate turbulence model is a significant issue which depends on the particular system to analyse. Then the *Cell Zone Conditions* are determined. Taking into account the foundations of the developed methodology, an independent cell zone must exist for each fluid cell in the channel. This fact ensures an interface exists between adjacent fluid cells, so that the flow along the pathway can be controlled. Whether fluid is contained in a specific fluid cell depends on the boundary conditions in those interfaces. In this regard, *wall* boundary conditions are generally used to separate fluid and solid regions. An interface defined as *wall* behaves as a barrier and does not permit the fluid to cross it. Therefore, this boundary condition is assigned to interfaces between fluid cells where fluid must stop. On the other hand, *interior* boundary conditions permit the fluid to pass through the assigned interface (see Figure 2.17). Consequently, an interface defined as *wall* which is turned into *interior* allows the fluid flow to access the next fluid cell. Conversely, when an interface between two adjacent fluid cells defined as *interior* changes to *wall*, the fluid that had been flowing through that interface is blocked at that location. Boundary condition change is controlled by a subroutine which will be explained subsequently. However, it is important to properly assign the initial behaviour of these interfaces according to the initial conditions in the model.

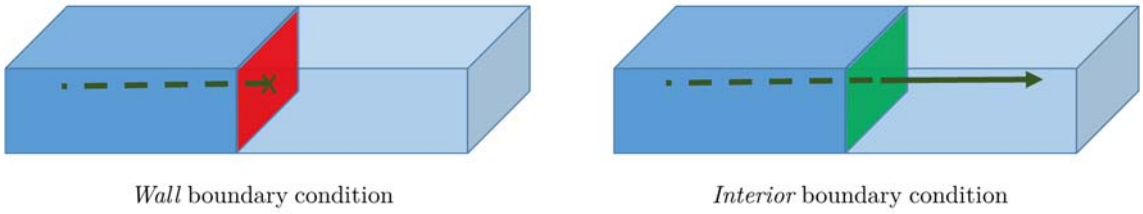

Figure 2.17: Different boundary conditions in Fluent. (a) *Wall* blocks the flow while (b) *interior* permits it.

A key step to perform two-way coupled FSI simulations is to define the fluid boundaries so that they adapt to the displacements computed in Ansys Mechanical. Therefore, the mesh on the interfaces that separate the fluid and the solid domains must be defined as *dynamic mesh* with the *System Coupling* option, in order to obtain displacements from the structural domain. In the same vein, surfaces in symmetry planes are also *dynamic meshes* which have to be defined as *deforming*, so that their mesh can be adapted in the corresponding plane to the calculated displacement.

As with Ansys Mechanical, special code has to be implemented in Ansys Fluent to analyse the behaviour of a system according to the developed methodology. In order to customize Fluent users can implement their own subroutines, called User-Defined Functions (UDFs), to enhance its standard features. Among other functionalities, special boundary conditions, customised or solution dependent material properties, new physical models and customised post-processing may be accomplished by the use of UDFs. The corresponding subroutines are written in C or C++ languages. After the UDF code is compiled, the functions contained are ready to be activated in the CFD model, and appear in drop-down lists in the dialog boxes. In addition, UDFs can be called at predetermined times during the solution process, or even on demand depending on how the functions are defined (Ansys Inc., 2017b).

In this research a key UDF was developed for application in simulations where the presented methodology is implemented. Its aim is to retrieve the contact pressure information that is stored in a text file by Ansys Mechanical. It is defined as an *on demand* UDF, so that it can be called whenever the main algorithm checks if the boundary conditions at fluid cell interfaces have to be changed. It scans the text file to save the contact pressure of a certain interface in a variable. In addition, further UDFs may be required in each particular model, such as to control inlet or outlet fluid behaviour according to a certain pattern.

Changing the boundary conditions of the interfaces between adjacent fluid cells is the most significant feature of the developed methodology. At the end of each *coupling step* a subroutine has to determine the *wall* or *interior* condition for each interface. This control cannot be achieved by means of UDFs. Changing boundary conditions must be done via the GUI (Graphical User Interface) or TUI (Text User Interface). The Fluent GUI consists of a menu bar to access the menus, a toolbar, a navigation pane, a task page, a graphics toolbar, graphics windows, and a console, which is a textual command line interface (TUI) (Ansys Inc., 2017c). Boundary conditions can be changed by navigating in the GUI to the correct command, or by referring to this action by means of the appropriate TUI command. It should be noted that boundary conditions must be checked during the solution process at the end of each *coupling step*, and that various interfaces may need to be changed simultaneously. Therefore, automating this operation is a must, and the steps to do so are set out in the following paragraphs.

TUI commands are written in a dialect of Lisp programming language, called Scheme. As the TUI is tightly integrated with the Scheme language, it can be programmed to provide user-defined functionality. When entering characters between parentheses into the TUI, the contained code is passed to Scheme to be evaluated, and the result of evaluating the expression is displayed. In addition, Scheme procedures can use Fluent TUI commands to change the desired simulation settings in a parametric manner (Ansys Inc., 2017c). To execute a Scheme algorithm, first it has to be loaded to Fluent and next, the user determines when to run the subroutines contained. The commands are executed at the specified interval of iterations or time steps during the calculation.

With all this in mind, a Scheme algorithm was developed which automates the changes in boundary conditions of fluid interfaces when required. The content of the

implemented algorithm is shown in the flow chart in Figure 2.18. The code is implemented so that at the end of each *time step* (which in coupled FSI calculations becomes a *coupling step*) the status of each fluid interface is checked.

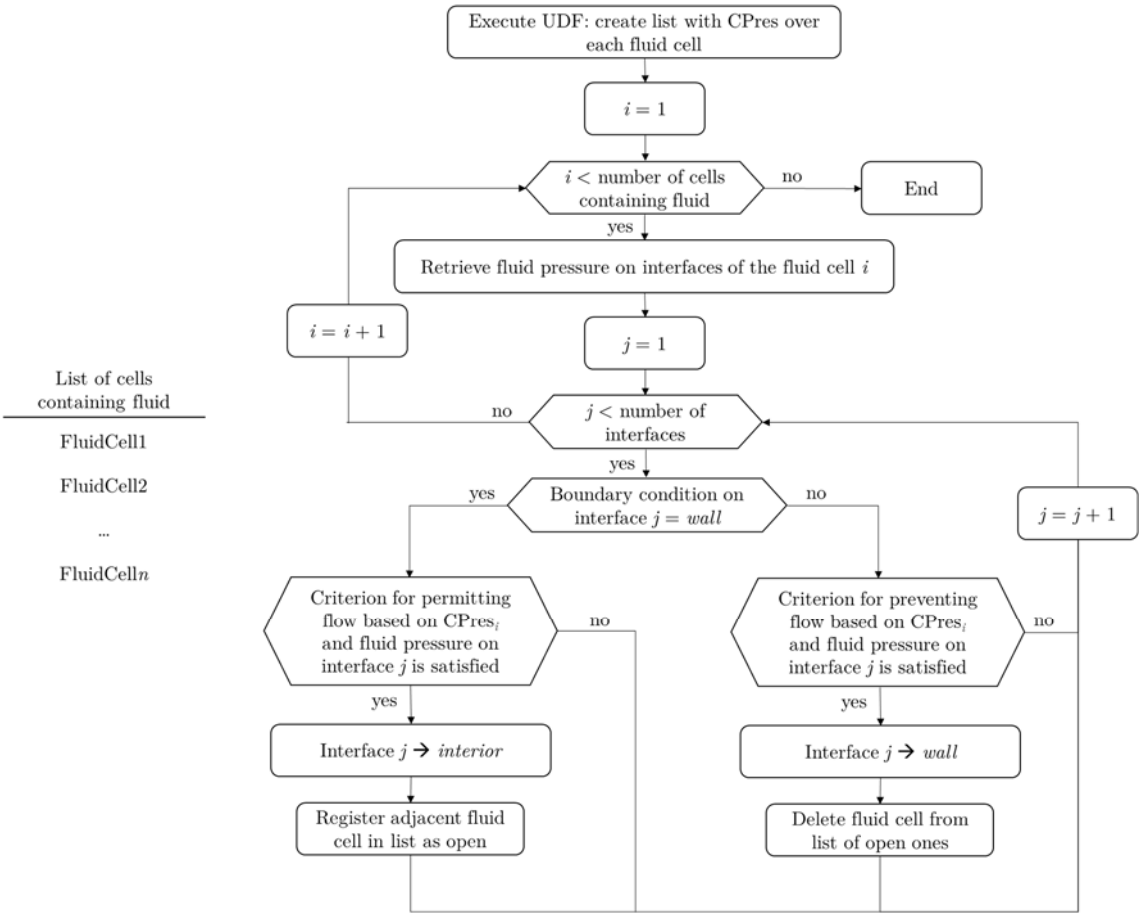

Figure 2.18: Flow chart describing the Scheme algorithm that controls the change of the boundary conditions of fluid interfaces.

Only cells that already contain fluid can give the flow access to a new cell. In addition, the opposite effect may also occur: a fluid cell containing fluid may lose this condition if the contact pressure on it increases above a limit. Therefore, the identification of the fluid cells which contain fluid at each moment must be registered in a list.

Hence, the steps that are performed by the Scheme algorithm are as follows:

1. Contact pressure on each fluid cell zone is read and stored in a list by means of the defined *on demand* UDF.
2. The interfaces of the fluid cells that contain fluid are checked.
3. Fluid pressure exerted on these surfaces are retrieved from Fluent.
4. Contact pressure and fluid pressure are compared based on the established criterion:

i. Boundary condition is changed from *wall* to *interior* if the interface was previously closed and flow is permitted from that moment on.

ii. Boundary condition is changed from *interior* to *wall* if the interface was previously open and flow is not permitted from that moment on.

iii. Boundary conditions are kept without changes if the behaviour of the interface does not need to change.

5. Fluid cells containing fluid are updated in the list.

At the beginning of its execution the Scheme algorithm retrieves the identification of the cells containing fluid in the list created for this purpose. Therefore, before running the algorithm for the first time a list of cells must already exist. The identification of the fluid cells located in the upstream fluid chamber which are adjacent to the fluid cells at the beginning of the channel must be included in this list. It is also necessary to initialise the value of the variables that are used in the algorithm. The way of making the list and variables accessible to the Scheme algorithm is by writing a *journal file*. A *journal file* contains a sequence of Ansys Fluent commands recorded as Scheme code, whose purpose is to automate a series of commands instead of entering them repeatedly in the TUI (Ansys Inc., 2017c). The *journal file* must be read before releasing the calculation. At this point, it is vital to check that the boundary conditions imposed in the fluid model and the fluid cell identifications contained in the list match.

As a result of the implemented UDF and Scheme subroutine, after each *coupling step* of the FSI simulation, Ansys Fluent updates the boundary conditions of the interfaces between fluid cell zones. This ensures that the behaviour of each interface is updated to permit or not the flow through it. The following *coupling step* is then calculated with the updated scenario for the simulation.

2.4.5 Coupled FSI analysis in Ansys Workbench

Ansys Mechanical structural solver and Ansys Fluent CFD solver are connected in the Ansys Workbench environment using the *System Coupling* component to perform the two-way coupled FSI analysis (see Figure 2.14). Consequently, the overall simulation is synchronised and information is exchanged between both solvers. The coupled environment has to be configured to perform the required calculation. As the cited solvers are linked to the *System Coupling* module, they both appear as *participants* in the calculation outline. Moreover, the interfaces defined as *Fluid Solid Interface* in the structural domain, and those marked as coupled to the structural domain with a *dynamic mesh* in the fluid domain, are transferred to the *System Coupling* setup window. This allows their connection by means of *data transfers*, which are defined by one source and one target region. *Data transfers* are able to take one variable in one direction between two participants. In a two-way coupled analysis, as data has to be transferred in both directions, source and target regions are defined for both participants. For FSI problems, one *data transfer* is defined with Ansys Fluent as the source region for the transfer of force,

whereas Ansys Mechanical works as the target region to receive it. Another *data transfer* is defined where the structural solver is the source for the transfer of incremental displacement, which is received by Ansys Fluent as the target region (Ansys Inc., 2017e). Therefore, two *data transfers* must be identified for each interface between structural and fluid cells.

Coupled FSI simulations may be defined to achieve steady or transient analyses. Steady-state solutions are achieved by coupling a *Static Structural* and a Fluent module. Transient solutions require a Transient Structural and a Fluent module. In this case, the time step of each *coupling step* is defined by the user and it is equal for both solvers. In other words, the total calculation time is divided into time increments and the considered time span for each of these increments is the same for both structural and fluid solvers.

2.5 POTENTIAL APPLICATIONS OF THE DEVELOPED METHODOLOGY

The following cases can be identified in which two isolated fluid domains become connected:

1. Deliberate connection of the domains: this is usually controlled by means of valves, devices that allow, prevent or regulate the fluid flow. When a valve opens, the connection of the fluid domains at the sides of the valve occurs (Beune et al., 2012; Wu et al., 2014; Song et al., 2014; Liu et al., 2016).
2. Unintended connection of the domains: a fluid contained in a closed volume reaches a new location in an uncontrolled way. This refers to leakage phenomena, which includes the connection of a fluid domain under control to another fluid volume, or to the open air domain.

In the present work an effective methodology to simulate and analyse both phenomena is presented. The problem to address is roughly the same in both cases, since the challenge is to determine the conditions and the behaviour of the fluid when chambers are connected. However, there is the nuance that the deliberate manoeuvres inevitably connect the fluid domains, although depending on the control implemented in the system, the connection may be slower or more abrupt. However, with regard to leakage analysis, the problem is more uncertain, since it lies in the concise analysis of whether the conditions are met for the fluid chambers to connect and lead to a leak.

This work provides an in-depth analysis of leaks to provide greater knowledge in this area.

CHAPTER

3

Methodology to determine the leakage path

Contents

In Chapter 2 a methodology was presented to numerically connect isolated fluid chambers along a channel between two solids in contact. This solution meets the requirements of planar and axisymmetric models. However, general three-dimensional systems require a solution for a closure defined in real geometries.

In this chapter a solution is presented which considers the closure as a surface between solids in contact, disregarding the height of the passage. The contribution of this chapter is the prediction of the direction the fluid takes at each moment and at each position.

The challenge is to establish whether the fluid moves forwards, sideways or backwards from any given position. This is determined by comparing the fluid pressure which results from the CFD calculation, with the contact pressures retrieved from the structural calculation, on the basis of a criterion that is experimentally established in Chapter 4.

3.1 LITERATURE REVIEW

The distribution of contact in a metal-to-metal closure determines the likelihood of leakage channel creation. Surface topography plays a crucial role in the resulting contact and thus, identifying the potential leakage channel is a challenging task.

The studies in the literature are generally limited to basic leakage path geometry, or they are focused on surfaces achieved by turning, a widely used machining process. In such surfaces, an anisotropic microgeometry is achieved characterised by a regular spiral. Hence, radial and circumferential flows may appear, depending on microgeometric imperfections and the load applied between the components in contact. The former occur with low and moderate loads, across local fluctuations of the crest height; and the latter in high load applications, when the passages on the crest disappear and flow happens along the valley of the spiral. For intermediate loads a combination of both flows takes place. In conclusion, two main flow directions are possible in turned surfaces, but it is still a challenge to predict what happens.

Predicting leakage involves several operations. Many works in the literature undertake the following three steps: (i) obtain the real topography of the surface, (ii) compute the elastoplastic behaviour of the surfaces at various scales (from roughness to component scale) to achieve the aperture between surfaces through which the fluid flows, and (iii) determine the leak rate through the calculated space.

Geoffroy and Prat (2004) considered a representative topography of a turned surface to analyse radial and circumferential flows. They developed an analytical model to analyse leakage both through radial passages and through the spiral groove, simplifying the surface as a combination of sinusoids. They showed that the leak transition from radial to circumferential was sharp, i.e. the transition occurred with a small variation of the applied load. However, the model of roughness they considered was too simple for a real sealing surface.

Robbe-Valloire and Prat (2008) considered a proper description of the surface microgeometry to be of vital importance. Therefore, they developed a model based on a statistical distribution of asperities having the same roughness level. They concluded that surface microgeometry of the sealing surface played a key role in leakage initiation and paths. However, they did not perform an estimation of leakage rate.

Nitta et al. (2013), using a laser microscope with a wide field of view identified the location of contact marks over the apparent contact area. Thus, the leakage flow in both radial and circumferential directions were recognised, and the critical contact pressure at which the radial flow disappeared was identified. In previous research (Nitta and Matsuzaki, 2010), the authors analysed sealing surfaces using 1 μm thick polymer films between the elements in contact. This method only provided contact marks, and furthermore, the film thickness may influence the contact behaviour. Laser microscope observation, however, showed clear images that led to a better understanding of the contact status.

Later Liao et al. (2015) considered a simplification of the micromorphology of radial and circumferential paths on a turned surface, and leakage models were presented for both. These results were in good agreement with the experimental tests. Using this methodology, the effects of microscopical characteristics of a turned surface in the leakage rate can be predicted.

Determining the leakage path in a turned surface requires identifying flows in the radial and circumferential directions. The following works have focused on determining the leakage path in generic contact surfaces, where the path could be considered random.

Zhang et al. (2017) presented an approach to estimate leakage channels based on a 3D finite element method (FEM) contact analysis. They first performed a macro-mechanical model of the sealing structure to achieve the contact pressure. Then they experimentally measured the surface topography, which was used in a 3D FEM model to apply the calculated contact pressures as the boundary condition. As a result, the geometries of the leak channels were obtained from the model, which enabled the calculation of the leak rate by means of CFD.

Ren et al. (2018) highlighted the importance of correct surface mating in an assembly, considering it to be more critical than the flatness of each individual surface. According to their observations, a better flatness does not always guarantee a better seal between surfaces. Therefore, they revealed the importance of modeling and characterising the surface mating quality to diagnose leakage paths. However, mating error is not directly measurable. The authors proposed a leak prediction model that estimated the most probable leakage path, as the one that required the least pressure loss when the fluid leaked along the path. This technique requires the height distribution of the surfaces to be mated, so that the gaps created in the contact can be evaluated.

Shao et al. (2019) proposed a surface-connectivity based approach to predict the leakage pathway. Connectivity is a concept from topological geometrical theory. The contact surface must be measured first, by means of a high definition metrology instrument. Next, the pecualiarities of the contact surface are represented by two leakage parameters: connectivity and correlation parameters. The authors proposed an algorithm to determine the potential leakage pathway, and the experimental tests demonstrated that the achieved results were accurate.

Given that surface topography is a vital factor in sealing performance, most of the works in the literature aim to provide information for optimising surface processing techniques, surface topographies and static seals. However, the research carried out in this thesis aims to indicate a global trend in how leakage is initiated and the most probable leakage path.

Moreover, in most of the presented works measuring the 3D surface topography is required. In mass-produced products where the absence of leakage is of vital importance, unitary and detailed surface control is usually not feasible. Therefore, the developed methodology considers an ideal flat contact between surfaces, without taking into account the micro-profile parameters. Nevertheless, the technique proposed could be extended to allow the addition of surface topography.

The presented methodology determines the most likely leakage channel by evaluating at each instant the fluid and contact pressures, which are calculated simultaneously in structural and CFD solvers. To the best of the authors' knowledge, this approach has not been presented before.

3.2 CONNECTION OF FLUID CHAMBERS VIA A RANDOM PATH

3.2.1 Basis of the methodology

In Chapter 2, the methodology developed to numerically connect isolated fluid chambers was explained. Thus far the methodology has focused on how to connect fluid chambers along the channel that links them. This solution meets the requirements of planar and axisymmetric models, however in a general context the fluid must advance in a three-dimensional space.

During the connection process in a 3D configuration, the gap created between the solids that were in contact can be considered negligible compared to the longitudinal and transversal dimensions of the closure. With this assumption the flow is considered to occur at a surface level. The challenge addressed in this chapter therefore, is to determine the direction the fluid takes from a given position, as it can progress forwards, sideways or backwards (see Figure 3.1), depending on the fluid pressure and the contact pressure between the solids where the fluid is contained.

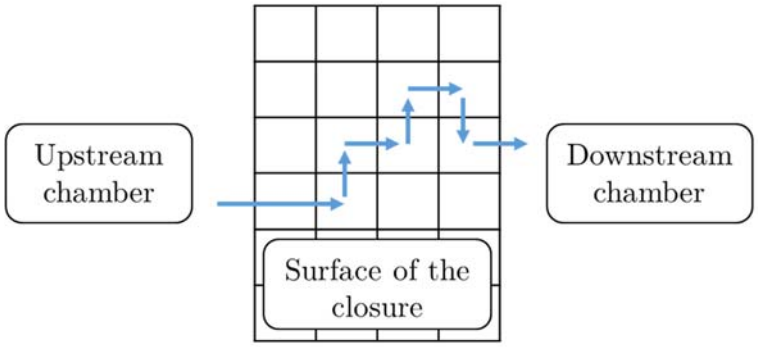

Figure 3.1: Model of a leak pathway between two fluid chambers.

To tackle the challenge of determining the leakage path, the surface of the closure is divided into a set of fluid cells arranged in rows and columns (see Figure 3.2). Each cell is identified by a number related to its position in the channel. In the same way, the interfaces that belong to each cell are named as top (T), bottom (B), front (F), left (L), right (R), and back (A), followed by the number that identifies the corresponding fluid cell (e.g. F203).

The front and rear interfaces of neighbouring cells overlap, as also happens with those to the left and right. As they all belong to a single fluid domain no interface overlapping can occur. Therefore, front and right faces are prioritised which means, for example, that the interface on the left of a certain cell becomes the one on the right of the adjacent cell (i.e. L203 becomes R204, or A403 becomes F303) (see Figure 3.3).

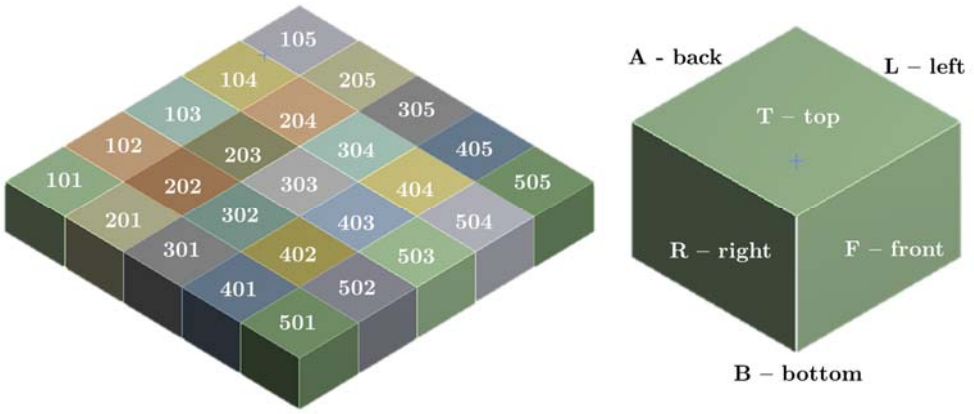

(a) (b)

Figure 3.2: (a) Fluid cells arranged in rows and columns. (b) Identification of each interface of a fluid cell.

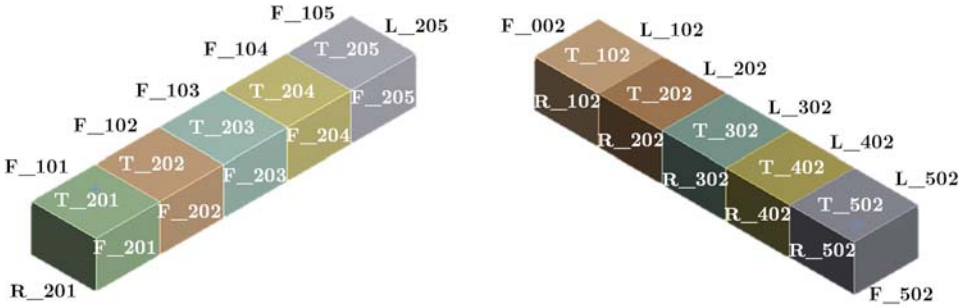

Figure 3.3: Identification of the interfaces of the fluid cells in the closure surface.

The top and bottom interfaces of these fluid cells are in contact with the solid surfaces that close the connection between fluid chambers. Hence, the fluid must advance through the front, side or rear interfaces (see Figure 3.4). To determine this path the fluid is given access to adjacent fluid cells if the defined criterion is met, as was explained in Section 2.3.2. Depending on the boundary condition defined, each interface permits the fluid to flow across it, or it behaves as a wall to block the passage.

Determining the extent of the fluid at any instant and how it evolves, requires an algorithm that (i) identifies the cells containing fluid, (ii) identifies the adjacent fluid cells, and (iii) determines the boundary condition at each interface depending on the established criterion.

3.2.2 Path determination algorithm

To determine the leakage path at a surface level the methodology presented in Chapter 2 was extended, which required changes in the Scheme algorithm developed for Ansys Fluent.

To begin with, a journal file is read where the user has previously established the number of rows and columns defined in the pathway. This structured layout helps the algorithm identify the fluid cells where the flow may advance from a certain location. As an example, the fluid cannot flow to its right or left if the fluid cell is located in the first

or last column. In addition, adjacent cells are easily identified because of their arrangement.

The identification of the boundary condition at each interface at any moment is essential. In those assigned as closed (*wall* boundary condition in Ansys Fluent), it must be verified whether the condition of giving way to the fluid is fulfilled. In the same vein, the interfaces which permit the fluid flow (*interior* boundary condition in Ansys Fluent) can change their state to block the passage. The criterion to perform these changes compares the fluid pressure exerted on the interface being checked, and the contact pressure on the adjacent fluid cell. The former is directly retrieved from the Ansys Fluent calculation, and the latter from the text file written by Ansys Mechanical.

Two lists are defined to control the leak progress. Each pair of numbers at the same position in both lists indicates the number of a cell containing fluid (*leak_cell* list) and the identification of the interface through which the fluid has had access (*leak_interface* list) (see Figure 3.4). A number is assigned to identify each interface: 1 indicates front, 2 left, 3 right and 4 rear. It should be noted that a cell number may be repeated in the *leak_cell* list as a single cell may have had access from different interfaces.

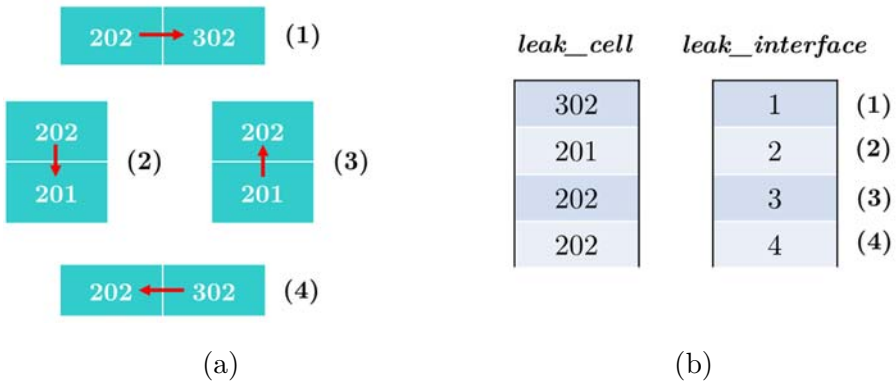

(a) (b)

Figure 3.4: (a) From a certain position fluid can advance (1) forwards, (2) to the right, (3) to the left or (4) backwards. (b) Each pair of fluid cell and interface identification is stored in a list to register the cells containing fluid and the interface the fluid goes through.

At the beginning of the execution the algorithm must read the initial state of the cells and the interfaces of the model from the lists. If the flow is assumed to be totally blocked in the upstream chamber, the lists only contain the elements at the entrance of the closure, so that in the first instant the only chance for the fluid to advance is through the front interfaces of these cells.

Then, during the calculation, the cells containing fluid at each moment are stored in the *leak_cell* list. The fluid can only advance from active fluid cells. Thus, the algorithm checks all the interfaces (front, left, right and rear) of the listed cells (see Figure 3.5). For each algorithm loop, the interfaces defined as *wall* are analysed to decide whether to keep the same boundary condition or change it to *interior*, and vice versa. After each calculation loop the interfaces in the model may have a new status, which contributes to defining the leakage path.

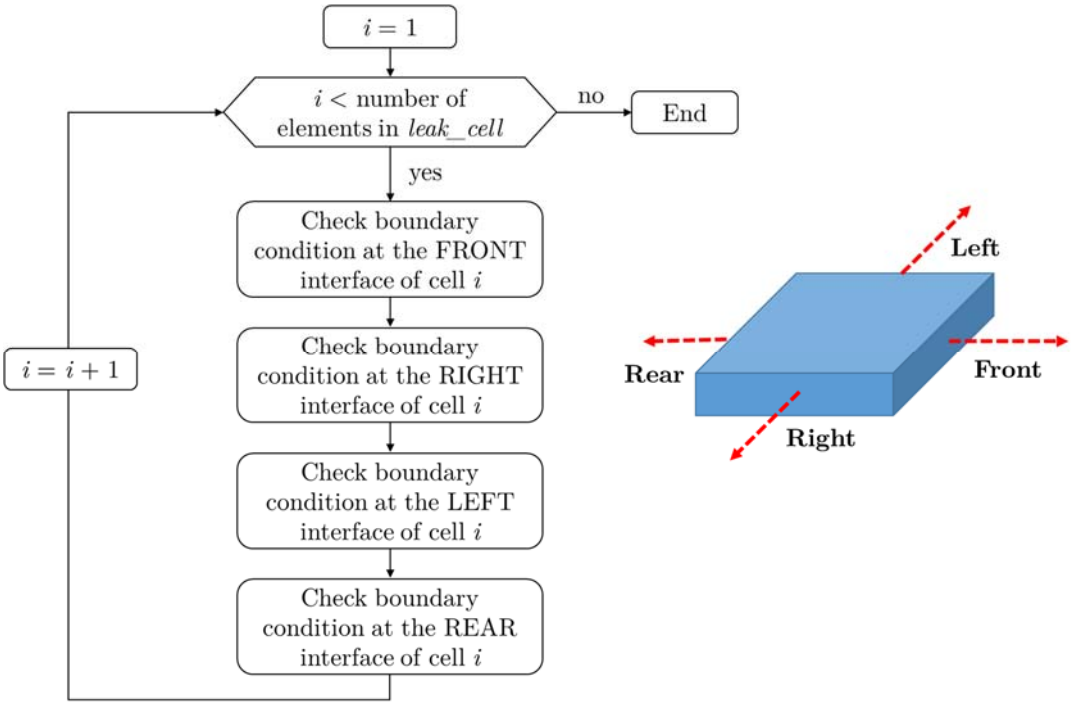

Figure 3.5: General diagram of the algorithm that determines the leakage path.

For each of the interfaces surrounding a cell, the steps to be followed are the same, as described in in Figure 3.6.

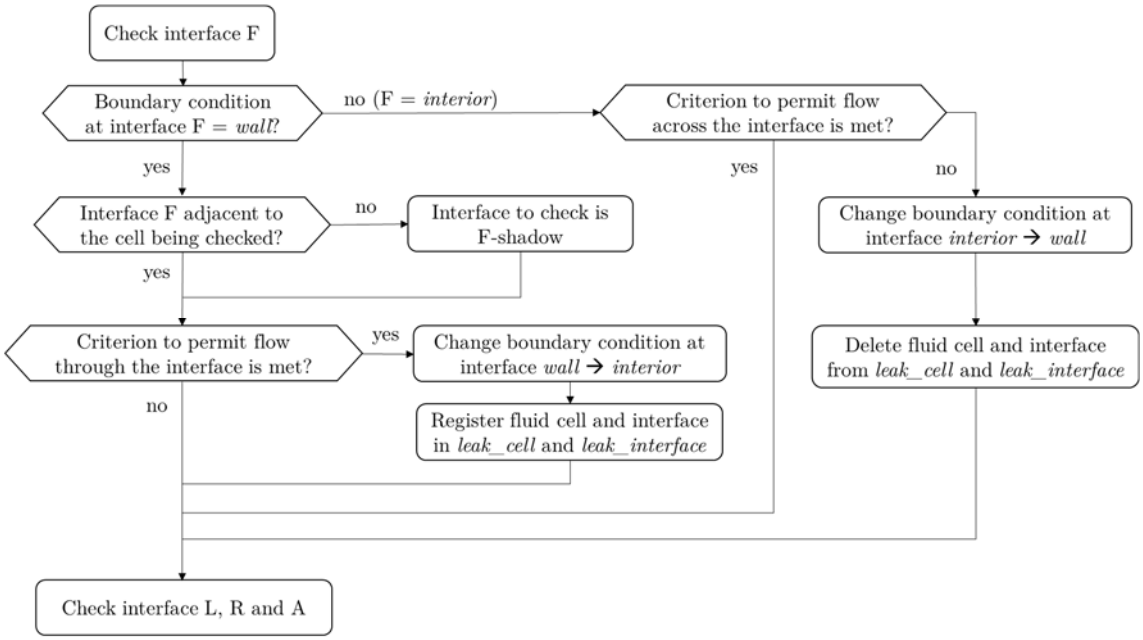

Figure 3.6: Algorithm to check if the boundary conditions at the interfaces of the fluid cell being analysed must be changed. The algorithm presented refers to the front (F) interface. The same is repeated afterwards, with the interfaces on the left (L), right (R) and rear (A).

First, the boundary condition in the analysed interface must be identified. This information is retrieved from Ansys Fluent by means of Scheme TUI commands. The analysis performed at each interface is different depending on the boundary condition being *wall* or *interior*:

(i) *Wall* interface: when two cells are separated by an interface with *wall* boundary condition Ansys Fluent automatically generates an additional *shadow* wall. For example, for a *wall* interface named *F104*, *F104-shadow* interface is created (see Figure 3.7). Ansys Fluent treats them as two interfaces that belong to different adjacent cells. Therefore, the interface that corresponds to the cell being analysed must be identified. This adjacency can be checked by a TUI command implemented in the Scheme algorithm. If the interface is not adjacent to the fluid cell under study, its *shadow* must be considered. The correct interface must be chosen so that the fluid pressure is correctly retrieved, as the pressure is null at the coupled interface.

(ii) *Interior* interface: a single interface exists between adjacent cells. There is no *shadow* interface.

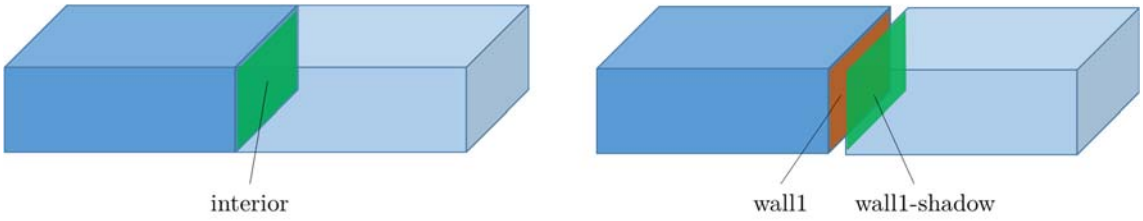

(a) (b)

Figure 3.7: (a) *Interior* type interface is a single entity between cells, and (b) *wall* interfaces are split into *wall* and its corresponding *shadow*.

The problem of identifying whether to check the *wall* or its *shadow* interface is also present when the channel is one-dimensional (see Chapter 2). However, under this circumstance it is easy to rename the interfaces to have their adjacency under control. In a structure of rows and columns this assignment can be much more complicated, so it was decided to implement the identification of the adjacent interfaces in the developed algorithm.

The fluid pressure on the identified interface is retrieved from the Ansys Fluent database and stored in a variable. As regards contact pressure, the values calculated in Ansys Mechanical are stored in a text file according to the cell arrangement. Thus, it is straight forward to identify each cell with the corresponding contact pressure value. The pressure value to check is that of the adjacent fluid cell, in the direction in which the fluid flows, if permitted. As set out in Figure 3.2 (a), the identification of the fluid cells at the sides is correlative and is a higher or lower number than the cell analysed. As for the cells at the front and rear, the identification number is increased or decreased in terms of the jump corresponding to a row.

The fluid pressure and the contact pressure are compared in the terms established by the assumed leakage criterion, which is based on experimental results and is presented in Chapter 4. Whenever a boundary condition change is performed, the *leak_cell* and the *leak_interface* lists are updated so that they contain the up-to-date information for the next algorithm loop. Cell and interface identifications of those that change to permit fluid flow are added to the registration lists. In contrast, the registers corresponding to those that switch to block the fluid flow are deleted. In the following loop of the algorithm in Figure 3.5, the *leak_cell* list includes the cells containing fluid after performing the corresponding changes in the previous iteration.

At this point, it should be highlighted that the content of the *leak_interface* list is not employed by the algorithm. As previously stated, the condition at each interface is obtained by means of TUI commands in the Scheme algorithm. However, the content of this list indicates whether a particular cell receives fluid through various interfaces. In such cases, the cell number record is duplicated with different interface identification. The interface register allows the cell to be considered as containing fluid even if one of the interfaces becomes closed.

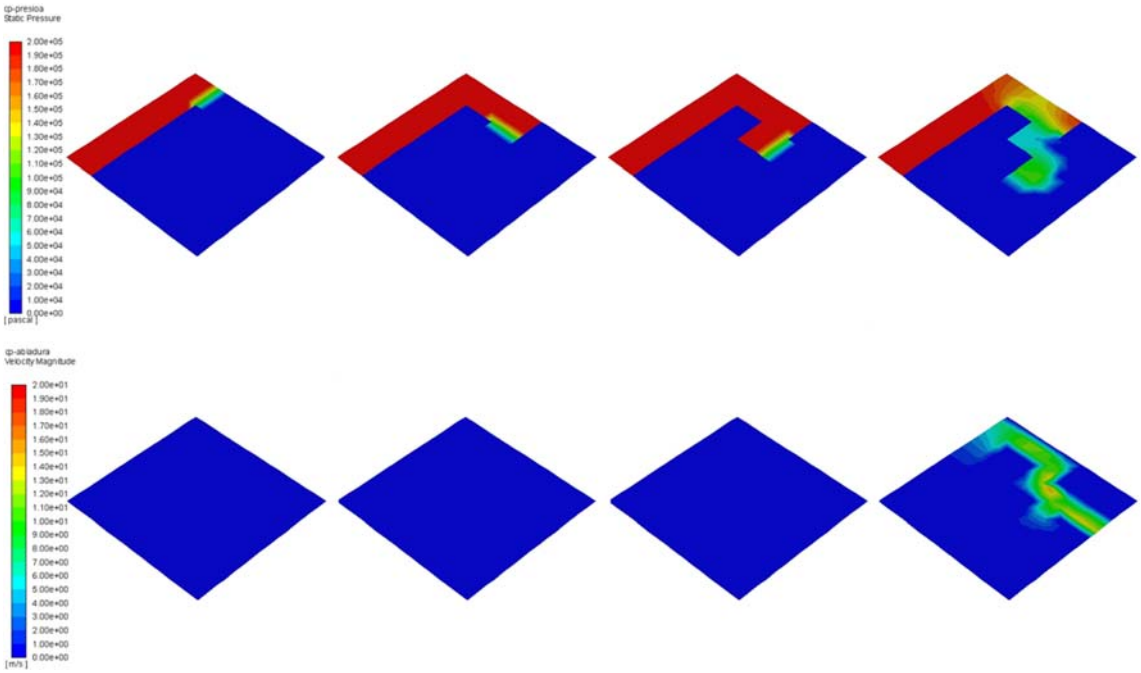

(a) (b) (c) (d)

Figure 3.8: Example of a leakage pathway determination result. From (a) to (d) different instants of the calculation are presented. The figures in the top row show the fluid pressure results. The ones in the bottom row refer to the fluid velocity, which is not manifested until upstream and downstream chambers are connected.

An example of the result achieved employing the presented algorithm is shown in Figure 3.8. The leakage path is arbitrarily established, as no leakage criterion has been defined yet. As the cells are filled with fluid their pressure equals the one in the upstream chamber. This permits the identification of the pathway the fluid is describing in the

closure area, as can be seen in the top row figures. Leakage does not happen until upstream and downstream chambers are connected. Therefore, fluid speed is not visualised in the bottom row figures before a complete connection occurs, which shows the whole leakage path.

3.3 CONCLUSIONS

The main objective of this research is to achieve the connection between isolated fluid domains in numerical models. The implementation of the methodology and algorithms described in this chapter provides a viable solution to determine a leakage path.

However, just as important as the cited methodology is the criterion that determines the conditions under which the connecting path must be opened. This criterion must take into account the conditions of both the fluid and the structural domains, namely the pressure of the fluid contained in the system, and the contact pressure that determines the closure of the passage.

Therefore, another important contribution of this research is the definition of a leakage criterion based on an experimental methodology, which is explained in the next chapter. This law is implemented together with the numerical methodology to predict leakage behaviour in FSI simulations.

CHAPTER

4

Experimental methodology to define a leakage criterion

Contents

In the previous chapters a methodology is presented to numerically determine the most probable leakage path. However, a criterion was needed to determine whether flow

advance occurs at a certain location in the closure between surfaces. In this chapter an experimental methodology is presented to set a criterion to determine leakage onset.

In this methodology, tests are performed on a testbench, comprised of two parts kept in contact with an inner chamber. A controlled force maintains the system closed and a liquid is then injected into the chamber, the pressure of which is increased by means of a hydraulic pump. The liquid pressure drop is measured and its relationship with the leakage rate through the surfaces in the closure is established. This leads to the determination of the leakage criterion that then permits the identification of the leakage onset and the prediction of the leak flow rate. This criterion considers the fluid properties, fluid pressure, system geometry and local contact pressure between the surfaces in the closure.

After the general approach of the methodology is described, the design of a testbench is presented as a case study, based on an industrial check-valve model. The leakage criterion that results from this study is valid for any different geometry of testbench with the same materials and surface finish, as is shown for validation in Chapter 5.

4.1 LITERATURE REVIEW

Several studies exist in the literature regarding leak flow rate calculation. Most of the works present theoretical approaches for the calculation, and some of them have designed experimental procedures to test their predictions. Few works are focused only on experimental studies.

This section presents experimental tests designed to gain knowledge about sealing performance, and leak initiation criteria found in the literature.

4.1.1 Leakage experimental testing

There are several factors that determine leak initiation and leak rate in metal-to-metal contact. Numerous experimental procedures are found in the literature to test how leaks are affected by different factors, such as surface roughness, channel dimensions, contact pressure, material of parts in contact or fluid contained.

Matsuzaki and Kazamaki (1988) carried out gas leak tests in metal-to-metal seals and metal gasketed seals to analyse the effect of surface roughness. Nitrogen was used and the gas leaked through the clearance between contact surfaces was measured by gas chromatography. With their experimental apparatus they evaluated the metal-to-metal sealing efficiency of contact between (i) flat and rough surfaces, and (ii) rough and rough surfaces with different interpenetrations of their asperities by controlling the cutting conditions.

Clarke et al. (1997) performed tests on specimens with cracks with controlled dimensions. A constant pressure difference was assigned to conduct water across them, and measure the resultant flow. Different leakage mechanisms were observed depending on the crack dimensions. Larger crack openings behaved as a laminar flow between parallel planes and, at smaller crack openings, the flow followed the pattern of pressure drop due to bends and changes in area. They also observed that for crack openings below a threshold value no leakage occurred.

Bagshaw et al. (2000) designed a testbench were air was blown through an idealised crack achieved by placing two blocks with the same geometry side by side. Pressure difference and flow rate were measured. Moreover, a larger second crack model was manufactured, which was placed in a wind tunnel to visualise the crossing air flow using smoke particles. CFD simulations were also carried out to compare results. The modelling and experimental work identified multiple flow regimes, as changes in the gradient of leak rate were observed.

Arghavani et al. (2003) experimentally analysed turned, milled and ground surfaces with different roughness values. They observed that surface forms, which depend on the manufacturing process, affect the contact surface and the corresponding stress levels, changing the shape, size and directions of the leakage path. They concluded that surface roughness had no effect on the leakage rate for turned and milled surfaces, and

that surface forms were the determining factor. Moreover, they established that turned surfaces provided the best sealing performance.

Murtagian et al. (2004) conducted experiments to check the effectiveness of metal-to-metal seals. An experimental setup comprised of a cone pressed against a cup was immersed in a chamber with transparent walls filled with water. This configuration presented a low sensitivity to an angular misalignment between the cited parts. Different cone radii and cup angles were manufactured to analyse the effect of contact pressure. Nitrogen gas was introduced to the space between the cup and the cone, with increasing pressure. The gas leaked from the closure formed visible bubbles, and the displaced water was measured in a pipette to determine the amount of leaked gas.

Marie and Lasseux (2007) presented an experimental setup and procedure for a precise fluid leakage measurement. Experiments were performed analysing the contact between a turned-surface plane metallic ring and a sapphire surface, which was considered as flat and non-deformable because of its properties. Moreover, the transparency of the sapphire surface allowed visualisation of the contact area. The experiments were carried out in two different contact situations: the contact surface was kept dry before starting the leakage analysis, and also was wetted and saturated with the leakage fluid. No significant differences were appreciated between the two situations.

In the work of Lorenz and Persson (2009) a testbench was designed to compare experimental leak rate of seals to their theoretical results. A rubber ring was pushed against a hard surface with a vertical glass cylinder, which was filled with water. The leak rate was measured by the change in liquid level in the cylinder. In their tests the pressure was established only by the water level.

Grine and Bouzid (2009) undertook theoretical and experimental studies of the flow of gas through gaskets. The gasket porosity was determined experimentally in terms of the number of the micro paths and the size of the voids, which were obtained from tests with helium as a reference gas. The leak rates of other gases could then be predicted. In later works (Grine and Bouzid, 2010; Grine and Bouzid, 2011) a method for predicting liquid leak based on the porosity was presented. The correlation between liquids was set to depend on the liquid dynamic viscosity, the pore size and the pressure difference across the gasket. Gas and liquid leak measurements were conducted experimentally and then compared to analytical predictions.

The effect of surface roughness in leakage performance was studied in the tests carried out by Haruyama et al. (2013). They subjected gaskets to different axial forces using flanges with three different surface roughness values. They measured the leaked helium flow, and concluded that for the same average contact pressure surface roughness caused a significant change in the system behaviour to leakage. In a previous work (Choiron et al., 2011) they compared the experimental contact width measured using pressure-sensitive paper with the width achieved by numerical simulation.

Nitta et al. (2013) analysed leaks in turned surfaces, where leaks can happen in radial and circumferential directions, in accordance with the spiral groove which results from the manufacturing process. They provided a new observation technique using a

laser microscope, to predict the leakage rates in both directions. The critical contact pressure at which the radial leakage flow stopped was determined.

Zhang et al. (2018) performed experiments on contact static seals with different materials and surface topographies, to analyse the effects of contact load, fluid pressure and apparent contact surface size on the leak rate. Cylindrical test pieces were pushed against a silicon wafer, which was considered as a smooth plane. The contact force was measured by a pressure sensor located below the wafer. A gas was inserted through a hole in the centre of the test piece, and the leakage rate was calculated by measuring the injected fluid level using a syringe. The measured leak rates were compared to their leak rate prediction model. As an interesting conclusion, they observed that for the same surface roughness, the sealing performance of turned surfaces which present spiral grooves was better than that of evenly distributed rough surfaces. In these tests the fluid properties were not taken into account, as the tests were carried out with only one unspecified gas.

Ernens et al. (2019) investigated metal-to-metal seals using an experimental setup, to measure liquid sealability. Thermal oil was used in the tests, and a circumferential line contact was achieved by pressing a seal with a round-off radius against a flat surface. The sealing limit was determined by applying fluid pressures up to 700 bar and gradually reducing the contact force. The specimen was submerged in a transparent chamber filled with glycol, so that when leakage occurred it was visually detected in the form of droplets or a foamy streak due to the density difference of the outer and inner fluids. The contact pressure distribution was measured using a pressure-sensitive film and the results were used to validate a previously developed model (Pérez-Ràfols, Larsson, Lundström, et al., 2016; Pérez-Ràfols, Larsson and Almqvist, 2016; Pérez-Ràfols, Larsson, Riet, et al., 2018; Pérez-Ràfols, Larsson, Van Riet, et al., 2018; Pérez-Ràfols and Almqvist, 2018). Their work supported conclusions observed in other works regarding surface topography. In addition they confirmed the benefits of preloading the seal to a higher contact pressure than in operating conditions, and the use of a thread compound (ensuring (i) low wear to preserve sharp topography that leads to localised high contact stress, and (ii) blocking of channels).

The sealing mechanism of metallic ball seat valves was studied by Fischer et al. (2020; 2021), as they are an essential component in almost any hydraulic system. Their aim was to observe the influence of plastic deformations, surface finish and normal force on leakage behaviour. They concluded that the surface is a vital factor that affects leakage, and that plastic deformations increase the real contact area in the closure, which reduces the outflow rate by roughly a factor of 8. Moreover, they highlighted the strong influence of contact pressure on the resulting leakage, as an error in the calculation of this parameter has a considerable impact on the result. Furthermore, the undesired accumulation of particles in the fluid has a negative effect on seal tightness.

In conclusion, the analysis of the literature presents different experimental solutions to analyse leakage. All the presented testbench designs show axisymmetry, with both in-line and surface contacts. The findings of the studies coincide in indicating the trends that meet the system parameters: in general, leakage increases with higher surface

roughness and lower contact force or pressure (Haruyama et al., 2013; Zhang et al., 2018; Ernens et al., 2019; Fischer et al., 2020; Fischer et al., 2021). Furthermore, a turned surface with its consequent spiral groove has a better sealing performance than surfaces with evenly distributed roughness (Arghavani et al., 2003; Zhang et al., 2018; Ernens et al., 2019). Different leakage mechanisms were detected in some works, resulting from a different behaviour of the flow depending on the gap size (Clarke et al., 1997; Bagshaw et al., 2000; Pérez-Ràfols and Almqvist, 2018). However, few studies have investigated how fluid properties affect sealing efficiency, as most of the works were carried out with only one fluid, either liquid or gas.

4.1.2 Determination of leakage initiation

In the literature a wide range of solutions can be found related to a criterion to determine the onset of leakage: from very simple to more complex statements, considering a different number of parameters, based on experimental results, etc.

As the most basic criterion, some researchers associate leakage initiation with the loss of contact; i. e., leakage is assumed when contact pressure becomes zero between the surfaces in contact (Calvert et al., 2002; Kawamura et al., 2003; Abid, 2005; Beghini et al., 2015). Some others compare the fluid pressure with the contact pressure on the contact surface, and when the former exceeds the latter in some area the creation of a leakage is understood to occur (Ahn et al., 2011; Liu et al., 2014; Shvarts and Yastrebov, 2018).

Tian et al. (2019) also set leakage criteria based on contact pressure. They analysed the effect of temperature and materials on the sealing performance in reactor pressure vessels. As cited in their work, the safe sealing contact pressure can be expressed in terms of the contained fluid pressure, by considering a coefficient that depends on the gasket, in accordance with ASME VII-2 Section 4.16 “flange connector design guidelines”.

Nitta et al (2013) performed contact surface observations with a laser microscope and leakage tests in gaskets between surfaces with a groove as a result of a turning process. They concluded that a critical contact pressure value of 30 MPa could be set, at which radial flow vanished and only circumferential flow remained. Predicted values were slightly higher than experimental ones, due to the influence of stress concentrations. Nitrogen gas was used in their leakage tests. Fluids with a higher viscosity may not leak even with a lower contact pressure, but no research was carried out in this regard. In addition, they did not determine the critical contact pressure to fully block leakage paths.

A sealability criterion was proposed by Murtagian et al. (2004) based on the product between contact pressure and seal length in the direction of the leak. The critical value of this result was determined by the contained gas pressure. An exponent was assigned to the contact pressure to weight the contribution of both contact pressure and seal length, as pressure peaks in a smaller length could be more effective than lower pressure in a wider length, or vice versa.

Wei et al. (2016) studied the sealing performance of mechanical connectors for subsea oil-gas pipelines and developed the calculation for the critical mean contact pressure. They also established a minimum value equal to the Brinell hardness (HB) of the

softest material to ensure an appropriate sealing performance, in accordance with the work by Robbe-Valloire and Prat (2008). In a later paper by the same authors (Wang et al., 2018), they referred to the works by Bucher (1988) and Liquan Wang et al. (2016) to establish a new sealing criterion. They concluded that correct sealing performance was achieved when a contact width over 1.6 mm and a contact pressure over the double of the yield strength of the contacting materials was ensured. Specific solutions for subsea pipeline connectors were designed in their works.

There are many works in the literature (F. Bottiglione et al., 2009; Lorenz and Persson, 2009; F Bottiglione et al., 2009) that have analysed the leak rate of seals based on percolation theory (Stauffer and Aharony, 1994) and contact mechanics theory. In accordance with the former, the contact surface is divided into identical squares; the smaller the size of the squares the larger their number. Each square is set to be in contact or not with the mating surface. If only one square is taken into account in the contact surface, an apparent full contact is assumed (which is the nominal contact area). However, as more squares are considered, in some of them the contact is lost due to surface roughness (resulting in an apparent area which is smaller than the nominal contact area). At a high enough number of squares a path of non-contacting squares can be identified connecting the two ends of the sealing area, which indicates that a leakage path has been created. The largest size of the squares in which a channel is first observed determines the narrowest width along the channel.

The observed critical square dimension is related to a relative contact area (apparent contact area/nominal contact area), and depends on the surface roughness, the applied loads and the mechanical properties of the elements in contact. Such a relative contact area and the critical square dimension were calculated by the abovementioned authors by employing contact mechanics theories. In addition, such theories were used to determine the separation of surfaces in the critical path section, which permitted an estimation of the leakage rate.

Pérez-Ràfols, Larsson and Almqvist (2016), Pérez-Ràfols and Almqvist (2018), and Ernens et al. (2019) employed the concept of permeability to evaluate seal performance, which allowed the prediction of the leakage rate not only depending on the contact pressure, but also considering surface topography, coatings or the use of sealants. They identified three flow regimes through the gap between two bodies, as the pressure applied to close the gap increases (Figure 4.1): (i) free flow regime, (ii) channelled flow regime, and (iii) constriction flow regime. They stated that there is no available functional form to determine the permeability of the former regime. However, an exponential and potential behaviour was assigned to the remaining two regimes. Since leak rate is proportional to permeability, their work was focused on analysing the variations of this variable. However, the effect of different fluids was not observed in their works.

In summary, most works set the leakage initiation criterion on the basis of a minimum contact pressure. These are based on both theoretical concepts and experimental observations. Nevertheless, it is not possible to establish a universal contact pressure value that guarantees the absence of leakage, since the materials in contact, their surface finish, the pressure of the fluid contained and the properties of the fluid influence

this value. Pérez-Ràfols, Larsson, and Almqvist (2016) employed the permeability concept to take into account more parameters involved in the system. However, no results were shown comparing how the threshold contact pressure value changes depending on the fluid contained in the system.

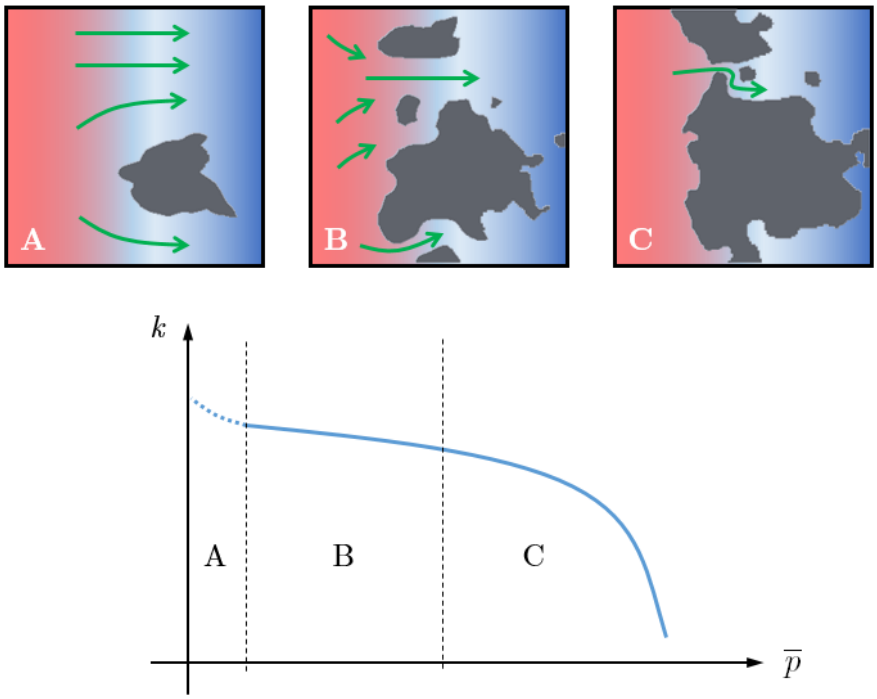

Figure 4.1: Flow regimes through the gap between two bodies, as the mean contact pressure between the surfaces increases: (A) free flow regime, (B) channelled flow regime, and (C) constriction flow regime. Grey areas represent the surfaces in contact, and the fluid is represented from red to blue indicating the pressure drop. The higher the contact pressure, the higher the surface in contact (based on Pérez-Ràfols and Almqvist (2018)).

4.2 METHODOLOGY TO EXPERIMENTALLY CHARACTERISE A LEAKAGE CRITERION

The basis of a methodology to numerically connect two isolated fluid domains was presented in Chapter 2, and this was extended to a three-dimensional geometry in Chapter 3. Using this methodology, a leakage pathway can be identified based on the local fluid pressure and contact pressure between the structural surfaces in contact. However, to complete the methodology, a criterion must be established to determine whether fluid flow is permitted according to each local condition. In this chapter an experimental methodology is presented to determine a leakage criterion, so as to implement it in an FSI numerical model.

4.2.1 Basis of the methodology

A leakage criterion is defined as a result of the tests carried out on a bench, comprised of two parts in contact under a controlled preload. An internal chamber exists,

in which a fluid is introduced at increasing pressure, until it leaks through the surfaces in contact. The developed methodology sets out how to define a leakage criterion valid for a generic system, based on the measurements of preload and fluid pressure in the testbench. Figure 4.2 presents the steps of the methodology.

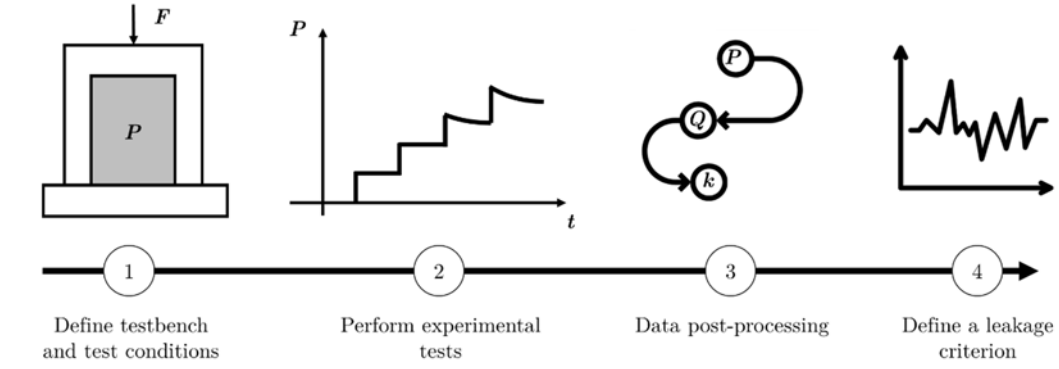

1. Define testbench and test conditions

Test parameters: - Preload range
- Fluids to be tested: viscosity range
- Fluid pressure range

2. Perform experimental tests

Output: fluid pressure time signal

3. Data post-processing

4. Define a leakage criterion

Leakage initiation criterion, valid for a system with:
(i) the considered material pair in contact,
(ii) the considered surface finish,
(iii) under a preload within the defined range,
(iv) containing a fluid whose viscosity is within the defined range,
(v) under a fluid pressure within the defined range.

Figure 4.2: Methodology to define a leakage criterion.

Once the specific design and size of the testbench is defined, the test conditions and parameters have to be established, i.e. the fluids to be tested, and the preload and pressure levels. The tests essentially involve maintaining a constant closing load on the system, and the behaviour of the system at different pressure levels is analysed. For each applied pressure, the pressure drop is recorded over time. The data processing allows the establishment of a relationship between pressure levels and leakage flow rate, the analysis of which leads to the establishment of a leakage criterion. This criterion makes it possible to predict the leakage behaviour of a system at different pressure values.

The fluids analysed in the present work may include both liquids and gases. In the transition from the absence of leaks to their onset, leaks occur along channels of a very small size. Gases in such channels can achieve very high velocities which can lead to choked flow. This behaviour makes the analysis more difficult than that of liquids. Moreover, as regards leakage in a system containing liquid, a small leak is enough to

induce a considerable pressure drop. Conversely, if gas is contained in the same system a significant amount of gas must escape to reach the same pressure loss. Consequently, as pressure measurement is appropriate to identify leakage in systems containing liquids, the described methodology to experimentally set a leakage criterion is developed to work only with systems containing liquids.

In each test, the balance between the force that acts to keep the parts in contact and the pressure of the contained fluid determines whether leakage occurs or not. The higher the external force, the higher the inner pressure required to open a pathway for a leak. Furthermore, the fluid pressure needed to cause leakage under a certain external force will depend on the design of the testbench. In addition, for the same structure under the same conditions, a fluid with a low viscosity is more prone to leak.

Therefore, fluid pressure and preload are not enough to establish a leakage criterion for any system, since their values that lead to leakage depend on the geometry of the system, the materials used, the surface finish, and the properties of the fluid contained.

The materials chosen for the components and the surface finish of the contact surfaces, are considered intrinsic to the system under analysis. Hence, the described methodology must achieve a prediction of leaks in any system with the selected materials and surface finish, and the parameters employed must be within the range defined in Step 1 (see Figure 4.2).

The research performed in this thesis demonstrates that a universal leakage criterion can be set in terms of (i) contact pressure and (ii) permeability. The former provides the response of the structural components under the exerted forces, and the latter establishes the sealing effectiveness of the system in accordance with the contained liquid.

The achieved criterion is then applied to numerical models to determine leakage paths with the methodology presented in Chapters 2 and 3, so as to control whether fluid flow is permitted through the structural elements in contact, and determine the leakage flow rate.

The following sections describe the details of the steps shown in Figure 4.2, which are required to set a leakage criterion with the described experimental methodology.

4.2.2 Step 1: Definition of the test parameters

The test plan includes defining the following:

a) Preload range: the closure performance is ensured by an external force that keeps the structural components in contact. Such a force is maintained constant throughout the test, so that the fluid pressure is the only factor that influences the contact pressure that maintains closure. The values of the preload are determined in accordance with the application where leakage analysis is required. The resulting leakage criterion is independent of the applied preload, but a minimum of three preloads is proposed to ensure result repeatability.

b) Liquids to test: liquid viscosity is a key factor to establish if leak occurs, as it measures its own resistance to flow. Two liquids contained under the same conditions show a greater or lesser tendency to leak depending on their viscosity. Therefore, a minimum of two fluids ranging from the minimum to maximum viscosities of interest should be tested. In this way the viscosity range is established, and the leakage behaviour of any liquid within this range can be calculated with the established criterion.

c) Fluid pressure range: the pressure exerted on the liquid contained in the testbench is increased until the pressure can no longer be incremented. The higher the system preload and fluid viscosity, the higher the pressure that can be achieved in the tests. It is necessary to estimate the maximum test pressure to ensure that the pump required for the tests is appropriate. A structural numerical model can help to do so (as explained in Section 4.3.1).

A number of test repetitions must be established for each set of equal conditions, to ensure the repeatability and reliability of the results.

4.2.3 Step 2: Perform the experimental tests

The experimental tests involve the application of a constant preload on the system, and a controlled pressure on the fluid contained. The existence of leaks results in a pressure drop in the chamber. Thus, the pressure signal is recorded after applying a known pressure value. As illustrated in Figure 4.3, at low pressures leakage is non-existent or negligible, so the pressure remains constant. At higher pressures, conversely, a sharper pressure drop is observed, which is related to a higher leakage. Therefore, to achieve a good characterisation of leakage behaviour the applied pressure increments are higher at lower pressures ($\Delta P_1 > \Delta P_2$).

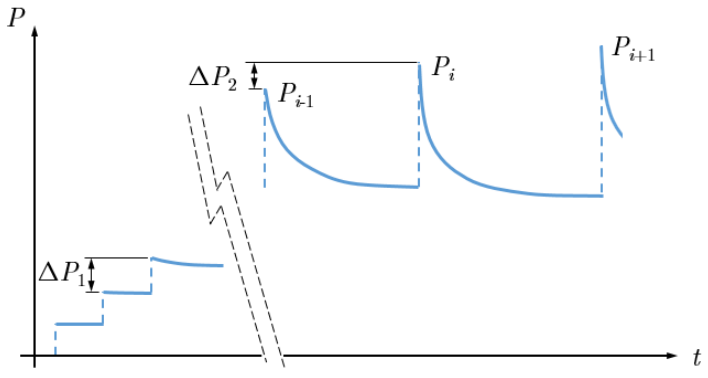

Figure 4.3: Application of controlled pressure values and subsequent pressure drop.

To carry out the experimental tests in accordance with the developed plan, the steps shown in Figure 4.4 must be followed.

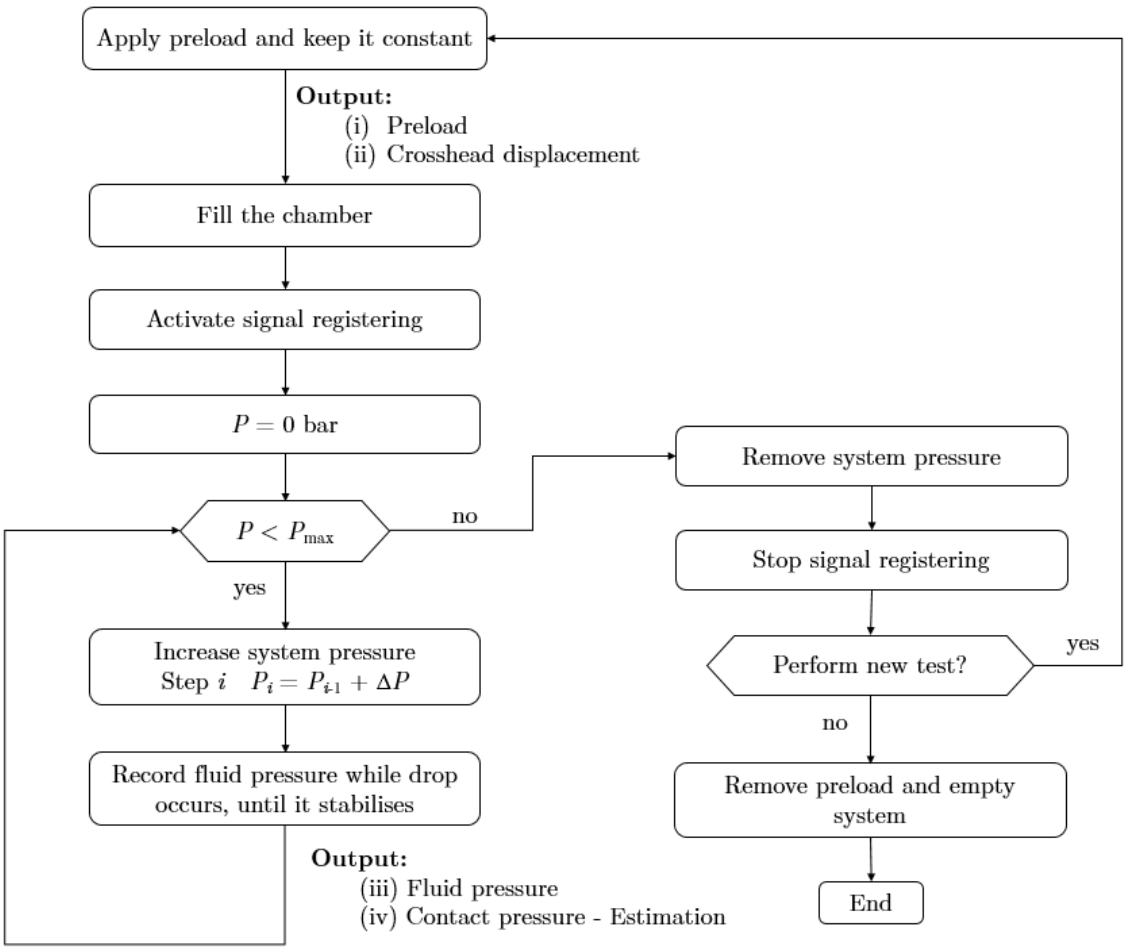

Figure 4.4: Steps to carry out the experimental tests.

The details of each step are the following:

1. Apply the corresponding preload between components and keep it constant.
2. Fill the testbench chamber with the chosen liquid using the pump. It is vital to ensure the absence of air in the chamber, due to the difference in compressibility of the air and the liquid. Having a volume of air in the chamber distorts the pressure value, as its volume increases (leading to a pressure decrease) when liquid leaks. Therefore, the chamber outlet must be open until all the air is released. Once the chamber is full and the absence of air is guaranteed, the chamber outlet is closed.
3. Activate signal recording: (i) preload exerted on the components, (ii) crosshead displacement, and (iii) pressure in the chamber.
4. The study of the behaviour of the system under pressure begins at this step. The following steps are repeated until the maximum test pressure is achieved:
    a. Open the chamber inlet.
    b. Using the pump, apply a pressure increment.

c. When the desired pressure is achieved in the chamber close the inlet, so that any potential leak occurs only between the surfaces of the elements in contact.

d. Preserve system conditions and measure the fluid pressure as it decreases, until pressure is stabilised at a lower value where no leak occurs (see Figure 4.3).

5. When maximum pressure is achieved and after the pressure is stabilised, remove the pressure by opening both chamber apertures. The chamber is still full of fluid but with no pressure.

6. Stop signal recording and save the acquired data.

7. If new tests must be carried out with the same liquid, return to Step 1. Otherwise, remove the preload and separate the elements in contact to empty the chamber.

To change the liquid to be tested, after removing the liquid from the chamber and the piping all the components must be cleaned.

4.2.4 Step 3: Data post-processing

Preload and fluid pressure signals are registered during the tests using an acquisition system. A constant preload is imposed throughout the tests, so this signal is used just for validation requirements. Conversely, pressure signals must be processed to achieve a leakage criterion in terms of contact pressure and permeability (see Figure 4.5).

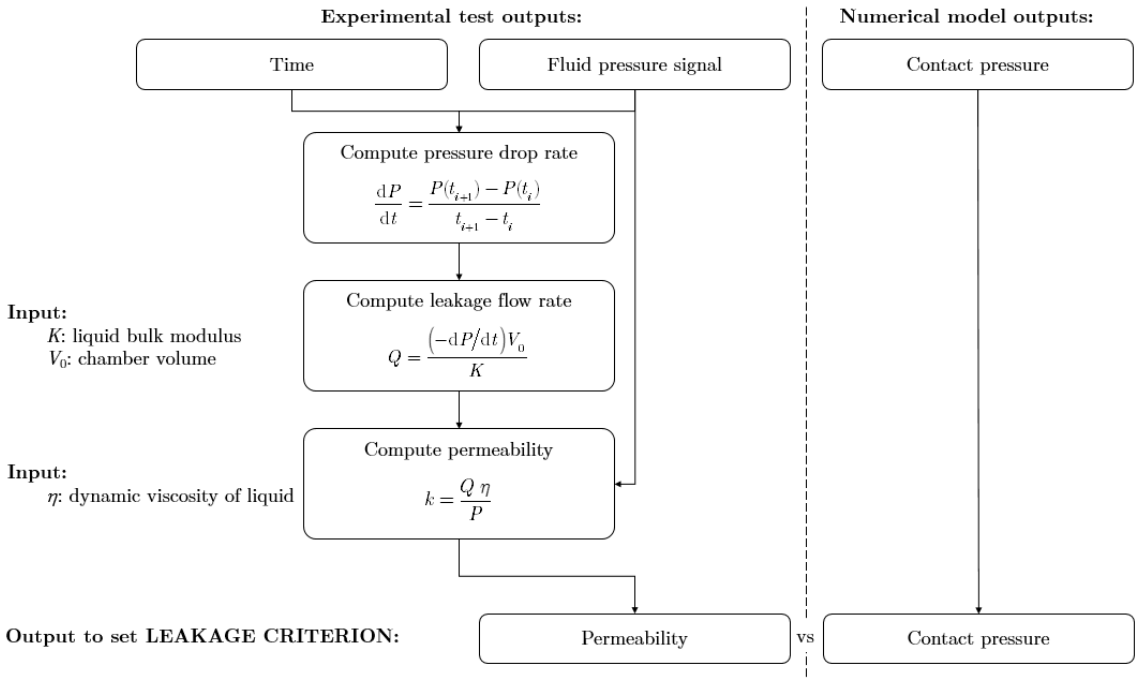

Figure 4.5: Steps to carry out the data post-processing and achieve a leakage criterion.

Contact pressure measures the force on the contact surfaces per area unit. It was selected as a key parameter because it takes into account the system preload and the inner fluid pressure value, and determines the resultant load distribution in accordance with geometrical factors and stiffness. Thus, a criterion based on contact pressure ensures its applicability to smaller or larger systems, with geometrical variations that may change the local stiffness.

The main limitation of this approach, however, is that it is not possible to experimentally measure the contact pressure at each location along the perimeter of contact. Although there are devices to do so, they require the insertion of an external element between the contact surfaces, which affects the conditions of the system (both in contact pressure and in leakage performance).

This problem is addressed by using an axisymmetric testbench, which means that the geometry and the properties of the system are equal at any location around an axis. This provides a uniform force distribution along the whole perimeter, as well as an equal probability of leakage. In such a configuration, contact pressure can be calculated by means of analytical expressions or numerical models, for each combination of preload and fluid pressure.

As regards permeability (also known as contact transmissivity), this is defined as a key parameter to assess sealing effectiveness, and has precedent in the literature (Marie and Lasseux, 2007; Pérez-Ràfols, Larsson and Almqvist, 2016). According to Darcy's law, in the absence of gravitational forces, considering a single phase, incompressible and laminar flow of a Newtonian fluid, if the contact is a homogeneously permeable medium along its length, the volumetric flow rate Q is written in terms of the system permeability k_{system}, the dynamic viscosity of the fluid η, and the pressure drop along the leakage path ∇P:

$$Q = -\frac{k_{\text{system}}}{\eta}\nabla P\,, \tag{4.1}$$

where the minus sign indicates that the flow occurs in the direction of pressure decrease. This system permeability is inherently related to an area through which occurs, and can be defined as:

$$k_{\text{system}} = \frac{Q\,\eta}{P\,/\,L}\,, \tag{4.2}$$

where L refers to the length of the leakage path, which is directly related to the contact width of the structural elements in contact. In the systems analysed this distance is kept constant, which permits to disregard it in the permeability definition. In this sense, the system permeability considered in the present research is described as:

$$k = \frac{k_{\text{system}}}{L} = \frac{Q\,\eta}{P}\,. \tag{4.3}$$

As the system permeability k defines the relationship between the outlet volumetric flow rate, the dynamic viscosity of the fluid, and the gauge pressure in the chamber P, it can be compared with the value achieved with different configurations and fluids.

However, to quantify the system permeability the flow rate of the leaks is required. A very low flow rate is expected at the initiation stage, which requires very precise measuring devices. To overcome this problem, the outlet volumetric flow rate is calculated based on the pressure drop measurement over time. This can be determined by use of the liquid bulk modulus K, which is a property that describes the compressibility of liquids: the ratio of pressure change to a variation in volume.

$$K = -V\frac{\mathrm{d}P}{\mathrm{d}V} \tag{4.4}$$

The bulk modulus determines the fluid volume decrease when a certain pressure is applied. Assuming as a hypothesis that the fluid volume inside the chamber V does not change, any volume variation that occurs under applied pressure must result in a leak. Thus, the outlet volumetric flow rate can be calculated as:

$$Q = \frac{\mathrm{d}V}{\mathrm{d}t} = -\frac{V}{K}\frac{\mathrm{d}P}{\mathrm{d}t}, \tag{4.5}$$

where $\mathrm{d}P/\mathrm{d}t$ refers to the instantaneous pressure variation rate, which can be obtained from the pressure signal in Step 2 (see Figure 4.4) as the change in pressure per time unit:

$$\frac{\mathrm{d}P}{\mathrm{d}t} = \frac{P(t_{i+1}) - P(t_i)}{t_{i+1} - t_i}. \tag{4.6}$$

A positive value of $\mathrm{d}P/\mathrm{d}t$ indicates a pressure increment in the system, which only happens during the short time that pressure is exerted by the pump. Conversely, a negative value of $\mathrm{d}P/\mathrm{d}t$ involves pressure loss due to the existence of leakage. Therefore, the leakage criterion is based on the segments of the pressure signal where drop occurs.

The permeability achieved by Equation (4.2) refers to the whole system, as it is calculated based on the total leakage in Equation (4.5). The axisymmetric condition of the testbench permits an even distribution of the outlet flow throughout the perimeter, so as to compute the permeability per unit length:

$$k_{\mathrm{unit}} = Q_{\mathrm{unit}}\frac{\eta}{P} = \frac{Q}{\ell_{\mathrm{contact}}}\frac{\eta}{P}, \tag{4.7}$$

where ℓ_{contact} is the total length of contact.

Taking the above into consideration, a leakage criterion can be set in terms of permeability and contact pressure, as a result of the tests carried out in a bench. The permeability achieved for a given contact pressure is applicable to any different system

whose parameters are defined within the range specified for the performed tests. The achieved criterion is based on the measurement of the fluid pressure and the applied preload to maintain the sealing, which means that the bench must have sensors to measure the cited parameters.

4.2.5 Step 4: Determination of the leakage criterion

Based on the proposed methodology to determine a leakage criterion, a threshold that defines the progression or regression of the fluid can be set in terms of either the variables that define it:

1. Contact pressure: a threshold value can be determined which defines leakage onset. This may be a fixed value (as in the works of Calvert et al. (2002), Kawamura et al. (2003), Abid (2005), Nitta et al. (2013), Beghini et al. (2015)), or a relationship between the local values of contact pressure and fluid pressure (as in the works of Ahn et al. (2011), Liu et al. (2014), Shvarts and Yastrebov (2018)). The algorithm checks for cells whose contact pressure is less than the threshold.
2. Permeability: an allowable leak flow rate value is set which limits the permissible flow rate through a single fluid cell. Thus, the fluid viscosity and its pressure value determine a threshold permeability, above which the total flow exceeds the admissible. The established leakage criterion determines which contact pressure leads to this permeability threshold. Cells with a lower contact pressure allow fluid flow across them.

The latter approach may be feasible in cases with uniform contact pressure profiles, which result in uniform leakage around the perimeter. In these cases the leakage flow rate in each cell is evenly distributed. However, in cases with non-uniform contact pressure distribution, a relationship should be applied to establish the allowable leakage at each cell, which is in principle unknown. Therefore, in this work it is proposed to use a criterion that establishes a minimum contact pressure to determine the fluid progress.

The purpose of opening or not the fluid cells to permit flow is to visualise where and when the onset of leakage occurs. In addition, the established leakage criterion can also provide a prediction of the leakage flow rate. To this end, the flow rate through each section of the system is calculated from the permeability per unit length assigned to it, based on the contact pressure to which it is subjected. From Equation (4.7):

$$Q_{\text{cell}} = k_{\text{unit}} \ell_{\text{cell}} \frac{P}{\eta}, \tag{4.8}$$

where ℓ_{cell} is the length of the fluid cell in the circumferential direction. The total leak flow rate of the system Q_{system} is the result of the sum of all the cell contributions. If an admissible total leakage Q_{adm} is defined, the local contact pressures must ensure that the sum of all contributions does not exceed that limit:

$$Q_{\text{system}} = \sum Q_{\text{cell}} < Q_{\text{adm}}. \tag{4.9}$$

4.3 EXPERIMENTAL CHARACTERISATION OF A LEAKAGE CRITERION

In accordance with the developed methodology, a testbench was designed to set a leakage criterion to determine leakage onset and leak flow rate in numerical models. The design is based on an industrial valve model, where the closure is achieved by the contact between a cylindrical component and a sphere. The closure is performed by a cone-to-ball contact, accomplished by bevelling the edge of the inner cylinder.

By following the procedure presented in Section 4.2, a leakage criterion was set with the results obtained after performing the tests required by the methodology. This criterion is valid for different system configurations, as long as the pair of materials tested with their surface finish is maintained, and it is independent of the preload and the properties of the contained fluid.

In the following sections, (i) the design of the testbench, (ii) the equipment and resources required to carry out the tests, (iii) the parameters defined for the tests, and (iv) the achieved results are presented.

4.3.1 Design of the testbench

The designed testbench is a simplified model of a check-valve, a device that allows flow in one direction but prevents backflow in a piping system. In such a system, the fluid flow is contained by a device which is pushed against a metallic seat. The pressure of the fluid opens the valve, while reverse flow closes it.

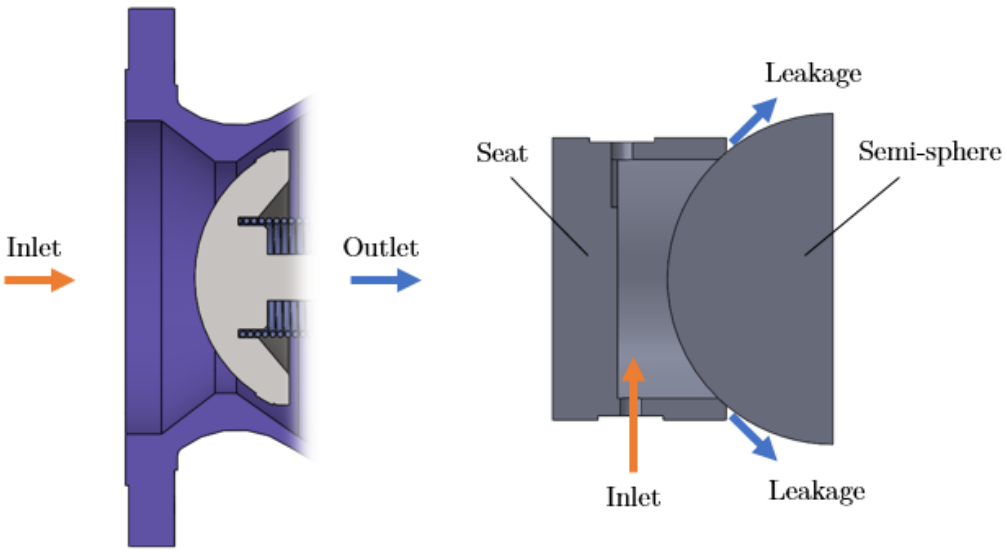

(a) (b)

Figure 4.6: (a) Axial flow check-valve and (b) simplified model of the testbench design.

The design of the proposed bench is based on an axial flow check-valve, where the closure is accomplished by a spherical surface against a tapered metallic seat (see Figure 4.6 (a)). In such valves a spring is used to control the closing load and, consequently, the pressure at which fluid flows. The testbench imitated the closure of the described system, and was comprised of a cylindrical seat against a semi-sphere (see Figure 4.6 (b)). A universal test machine was used to keep the elements in contact and control the closing load. The pressure of the liquid contained in the chamber between the components was manually controlled according to the test requirements.

The diameter of the semi-sphere was set to 6". As regards the seat, the dimensions of the inner chamber were 110 mm in diameter and 50 mm in height. The outer cylinder was 130 mm in diameter, with a height of 80 mm. Details of the testbench are presented in Appendix A. AISI 304 was chosen for both the seat and semi-sphere, which mechanical properties are shown in Table 4.1.

Table 4.1: Material properties for AISI 304.

	AISI 304
Density	7850 kg/m^3
Young's modulus	200 GPa
Poisson's ratio	0.3
Yield strength	190 MPa

It should be noted that structural simulations were carried out to choose the correct dimensions for the presented components. As an approximation, the loss of contact pressure between components as the fluid pressure in the chamber increased, was considered to be a rough indicator of leakage initiation. The purpose of the simulations was to ensure that leakage happened in the range where the parameters of the equipment and measuring devices could be controlled.

A manual pump was used to fill the inner chamber with fluid, and to increase the pressure until leakage occurred between the surfaces in contact. Therefore, the inner chamber required two external apertures: one through which the fluid entered the chamber, and another to release the air during the filling process.

The axisymmetric design of the testbench ensured a uniform contact between the seat and the semi-sphere along the whole perimeter. A three-dimensional numerical model confirmed that the geometric details which make the real system not fully axisymmetric had no significant influence on the homogeneous distribution of the contact pressures.

The semi-sphere and the seat were manufactured by turning. The area where the seat and the semi-sphere come into contact is of vital importance, as the surface finishing of these surfaces affects leak initiation. Therefore, the contact surfaces were ground to achieve a surface finish of $Ra = 0.4$ μm in the semi-sphere and $Ra = 0.8$ μm in the seat.

4.3.2 Equipment and resources

Instron 4206 universal test machine was used to apply the required closing force between the designed parts. This equipment allows force control or position control tests. The former provides a constant force throughout the test and the latter keeps the crosshead of the machine in a constant position, adjusting the force exerted for that purpose. The tests in this research were carried out in force control. By doing so, the loss of contact pressure between seat and semi-sphere was only attributable to the increase in pressure inside the chamber.

The load cell installed in the test machine admitted a maximum force of 10 tonnes, with an error of 0.12 %. The position control was achieved with an error lower than 0.15 %. An overview of the testbench during the tests can be observed in Figure 4.7.

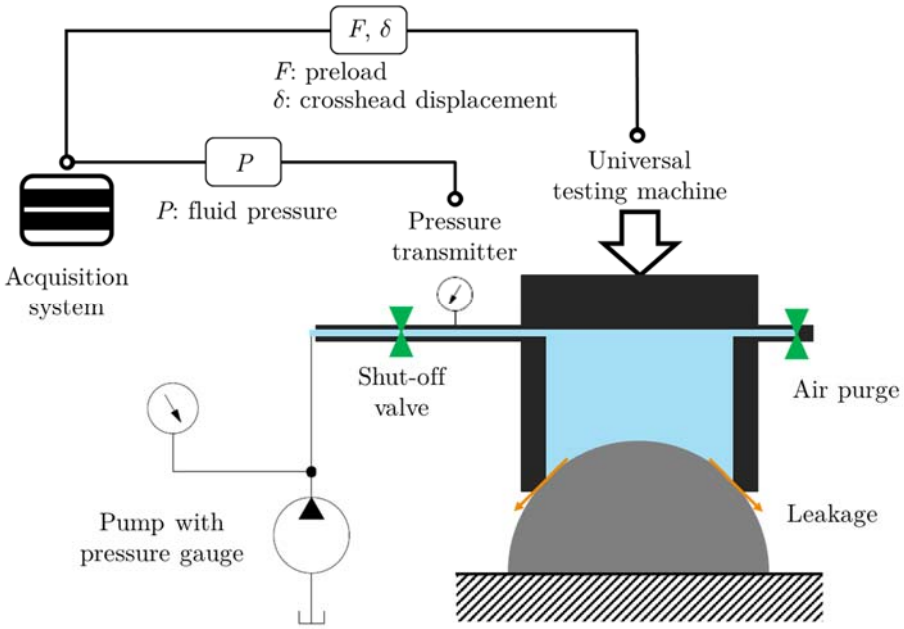

Figure 4.7: Configuration of the experimental tests.

A Rothemberger TP25 hand pump was used to fill the seat cavity and to apply pressure. It included a pressure gauge, and the maximum pressure that could be achieved was 30 bar. The piping between the pump and the seat was assembled by means of rigid elements and connections.

An Aplisens PCE-28 pressure transmitter was installed to monitor the fluid pressure contained in the system, with a maximum pressure of 50 bar and 0.2 % accuracy.

A shut-off valve was located in the piping directed to the chamber inlet, before the pressure transmitter. After regulating the pressure in the chamber by the pump this valve was closed, to ensure that any pressure loss was attributable to leaks through the closure. Another shut-off valve was used in the outlet to permit the air purge.

Figure 4.8 shows an overview of the devices involved in the experimental tests.

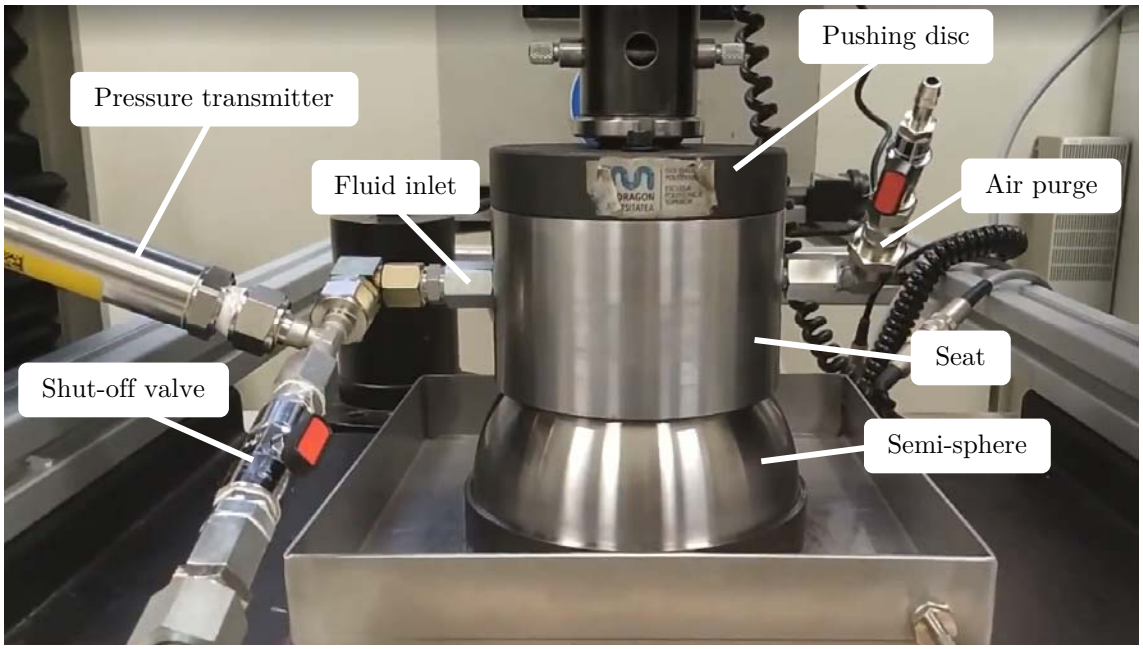

Figure 4.8: Testbench installed in the universal test machine.

A National Instruments NI-9219 universal analog input module and Signal Express software were used to register the signals proceeding from the devices: (i) applied preload, (ii) crosshead displacement of the Instron test machine, and (iii) pressure obtained from the Aplisens pressure transmitter. For each magnitude two measurements were recorded every second.

This data was processed to set a leakage criterion, as described in Section 4.2.4.

4.3.3 Parameters to perform the tests

The tests were planned by setting the parameters described in Section 4.2.2: (i) preload between seat and semi-sphere, (ii) fluids to test, and (iii) fluid pressure range.

1. Preload:

Preliminary tests were conducted to adjust the preload level of the test machine, to ensure leaks with the pressure level achievable by the pump (30 bar). A small preload can cause leaks with hardly any pressure applied, while an excessively large preload prevents the presence of measurable leaks and may cause permanent deformations in the components.

Therefore, a minimum and maximum preload had to be established. The former was set to a value of 20,000 N, which led to leak onset at a threshold pressure appreciably greater than zero. The latter was set to 30,000 N to guarantee that leakage was initiated with inner pressure below 30 bar, for the liquids under consideration. In the preload range indicated, tests were carried out considering 5 load levels, as indicated in Table 4.2.

To ensure test repeatability it was important to ensure identical contact conditions regardless of the applied load. Therefore, a preload of 40,000 N was applied prior

to adjusting the preload to the test value. This load increase guaranteed a better settlement between the surfaces in contact, as was observed by Ernens et al. (2019).

Table 4.2: Preloads considered to perform the experimental tests.

Preload 1	20,000 N
Preload 2	22,500 N
Preload 3	25,000 N
Preload 4	27,500 N
Preload 5	30,000 N

2. Tested fluids:

To measure the effect of viscosity on the leakage behaviour, two available liquids with highly differing properties were chosen to carry out the tests: water and Nuto H46 oil[2] (an anti-wear hydraulic oil used in industrial and mobile service applications). Their properties are shown in Table 4.3.

Table 4.3: Properties of the fluids employed in the tests.

	Water	**Nuto H46 oil**
Density	0.998 kg/l	0.876 kg/l
Dynamic viscosity	1×10^{-3} Pa · s	8.32×10^{-2} Pa · s
Bulk modulus	2.2×10^{9} Pa	1.72×10^{9} Pa

3. Pressure range:

Before testing with a particular preload, the system was subjected to a rapid increase in pressure until leakage was visually identified. This allowed an estimation of the maximum admissible pressure for each pair of preload and liquid. Once the maximum pressure was identified, the pressure increments were adjusted as the pressure level approached the maximum value (from $\Delta P_1 \approx 2$ bar to $\Delta P_2 \approx 0.5$ bar when the pressure was close to the upper limit, as illustrated in Figure 4.3). This provided an accurate insight of the leakage behaviour after leakage onset occurred.

The system was brought back to zero pressure and the pressurisation procedure was carried out according to the established increments. When maximum pressure was achieved and after stabilising the pressure as a result of the pressure drop, the system pressure was again increased directly to that maximum value two or three times. This was done to analyse the influence of the filling rate, or the achieved maximum pressure at each pumping step.

For each preload four repetitions were carried out to ensure the repeatability of the results.

[2] https://www.global.mobil.com/en/lubricants/products/products/nuto-h-46

4.3.4 Results

As a result of each test a file containing the following data was obtained: (i) preload applied to the components, (ii) crosshead displacement of the Instron test machine, and (iii) pressure in the chamber obtained from the Aplisens pressure transmitter. In addition, notes and visual media were collected as a register of the visual inspection. As the tests were carried out with force control, the register of the applied preload showed a constant force throughout the measurement. The crosshead displacement, on the other hand, indicated a shift consistent with the pressure applied. In other words, the crosshead rose as the pressure on the system was increased. These parameters were used as an indicator of the correct behaviour of the testbench, but were not directly employed to determine the leakage criterion.

In accordance with the procedure outlined in Section 4.2.4, the permeability per unit length and the contact pressure were computed to set a leakage criterion, and the data processing was carried out using Matlab software[3].

1. Calculation of the permeability per unit length:

The permeability was determined based on the measured liquid pressure signal. Figure 4.9 sets out an example of the results achieved in one of the tests. Figure 4.9 (a) refers to the pressure signal and Figure 4.9 (b) to the position of the testing machine crosshead, both plotted over time. As shown in the figure, pressure was gradually increased during the test until maximum pressure was achieved. It can be observed that the fluid pressure behaved differently depending on the pressure reached when pumping. Up to a certain value, there was no significant pressure loss after pumping (from point A to B). However, as higher pressure was reached during pumping, a greater pressure drop occurred. As regards displacements, the crosshead rose from the reference position identified in the testing machine as higher pressure was applied in the chamber. A higher pressure involved a higher resultant vertical force and, as the force exerted by the machine remained constant, that resulted in an upward displacement of the seat. The pressure drop subsequent to the application of pressure led to a progressive decrease of the measured position.

[3] MATLAB, 2017. version 9.2.0 (R2017a), Natick, Massachusetts: The MathWorks Inc.

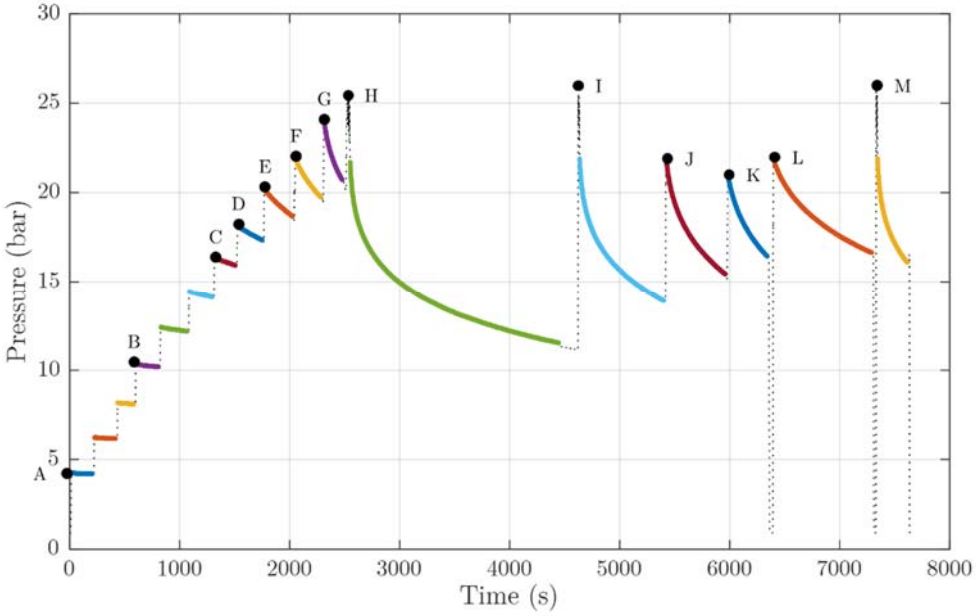

(a)

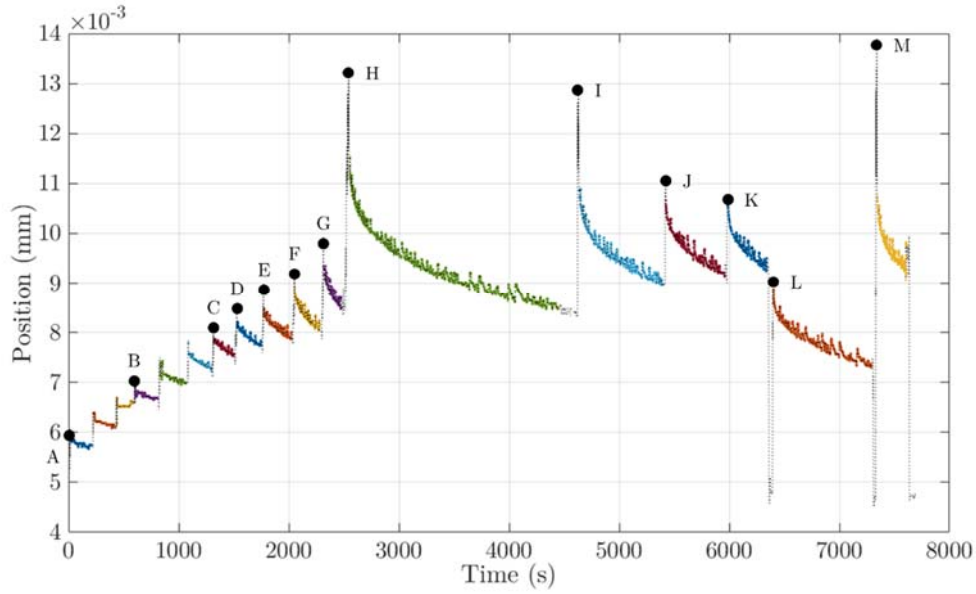

(b)

Figure 4.9: Result of an experimental test which shows (a) pressure and (b) crosshead position over time.

By combining the presented parameters, a pressure drop rate versus pressure graph can be computed, as shown in Figure 4.10 (b). In this plot the pressure loss rate remained null until a threshold pressure value was reached. If an admissible leak flow rate Q_{adm} is defined in accordance with Equation (4.9), the pressure drop rate that results from the relationship in Equation (4.5) establishes the pressure threshold value required to not exceed the stated leakage.

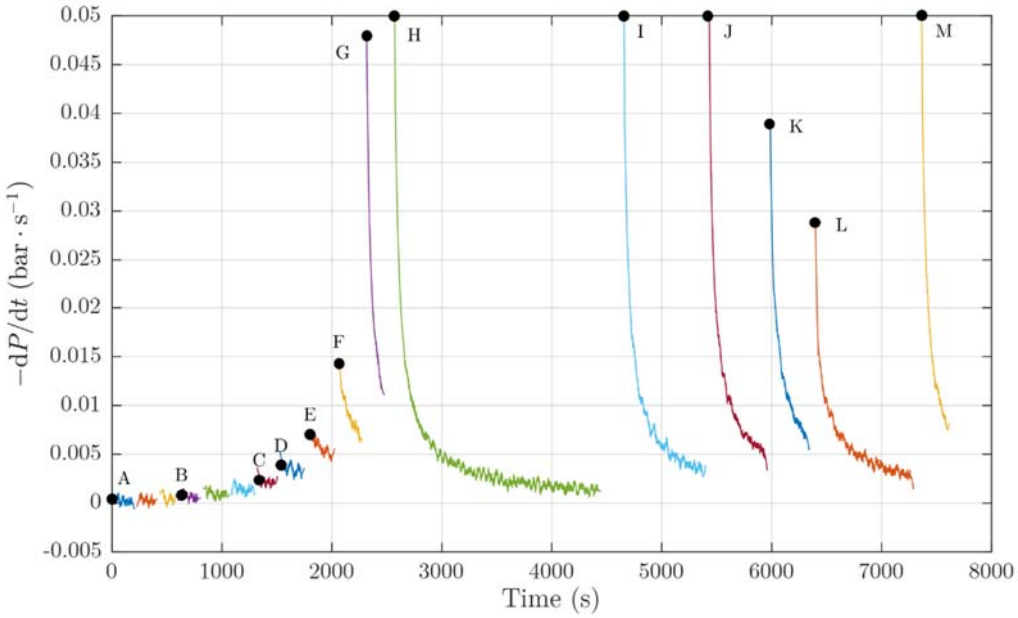

(a)

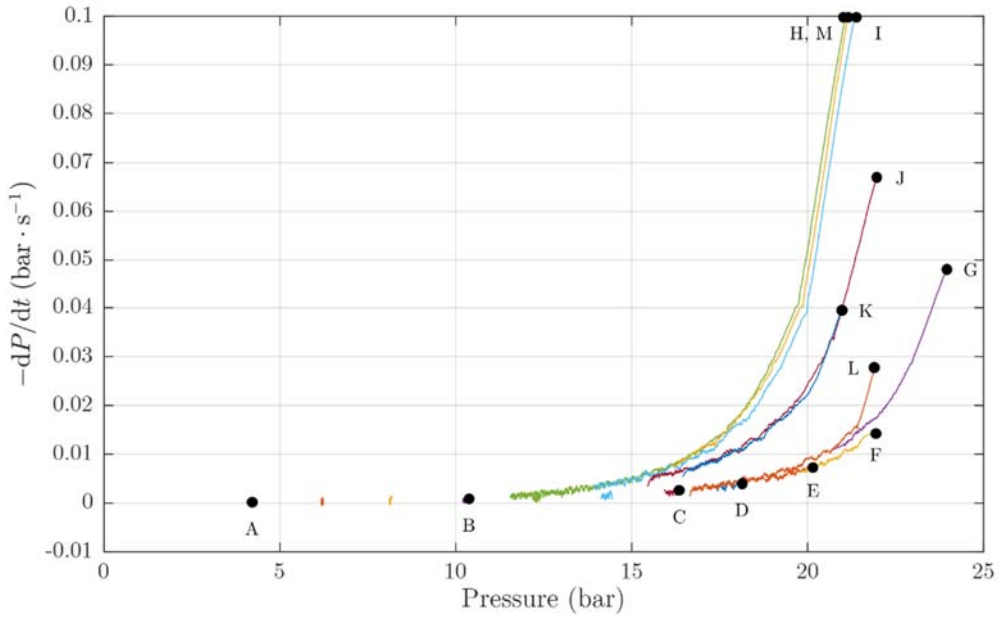

(b)

Figure 4.10: Result of an experimental test which shows the pressure drop rate (a) over time, and (b) versus system pressure.

It can be observed in Figure 4.10 (b) that above a certain pressure value the pressure drop rate curves provide a range of responses, resulting in different values for the same liquid pressure. When the liquid pressure was gradually increased starting from a null value, the pressure drop rate initially described the curves shown at the bottom of the graph (points A to F). As the pressure exceeded a certain value (points G, J, K, L), the pressure drop curves showed an incremental jump above the preceding curve. The

discharge curves at the top are those achieved when the system was brought to its maximum pressure (points H, I, M).

The described behaviour is inherent to the chosen system, conditioned by the geometry of the contact on a semi-spherical surface. Depending on the resultant force on the seat, the position and angle of the contact changes, and the seating occurs on a different diameter of the semi-sphere. Changes in position can be analysed in Figure 4.9 (b), where it can be seen that there is no direct pressure-position relationship. The large difference in position between points G and H is particularly noteworthy, and results from a pressure jump equivalent to the previous points (from F to G, for example). It can be deducted that the seat subsequently rested on a new position, as observed in the positions plotted throughout the pressure drop from H to I. In this step, pressure values lower than C and D were achieved, but with a higher seat position. Additionally, points J and K were at a higher position than G, even though their pressure was lower. Of particular interest is also point L which, with a pressure equivalent to J and K, presented a much lower position. These differences confirm that the behaviour of the system is not equal in loading and unloading, as observed by other authors in their systems (Pérez-Ràfols, Larsson, Van Riet, et al., 2018). In fact, point L was measured after unloading the pressure inside the chamber (Figure 4.9 (a)). For this reason, the position of the seat and discharge curve at point L in Figure 4.10 (b) was more similar to point F than to point J. However, point M which was also obtained after a total discharge of the internal pressure, presented a position equivalent to all measurements at maximum pressure (points H and I), and the same pressure drop curve. Therefore, it can be affirmed that the curves of maximum pressure and, thus, maximum pressure drop presented a repetitive behaviour.

Thus, it can be concluded that the phenomenon described above regarding different seatings for given internal pressure values has a significant influence on leakage and pressure loss. This is discussed in detail in later sections.

In order to describe the system leakage behaviour a single answer must be set for each input pressure. Therefore, only the pressure loss rate curves at the top of the plot (i.e. the discharge curves corresponding to what happened after subjecting the system to its maximum pressure) were considered for each test. This decision was taken to ensure the most conservative criterion possible, since these curves correspond to the highest leakage flow for a given pressure. All the results presented hereafter refer only to the described curves.

The results of pressure loss rate versus pressure for different system preloads and liquids are shown in Figure 4.11. It can be observed that the higher the preload the higher the pressure required to achieve leaks, both for water and oil.

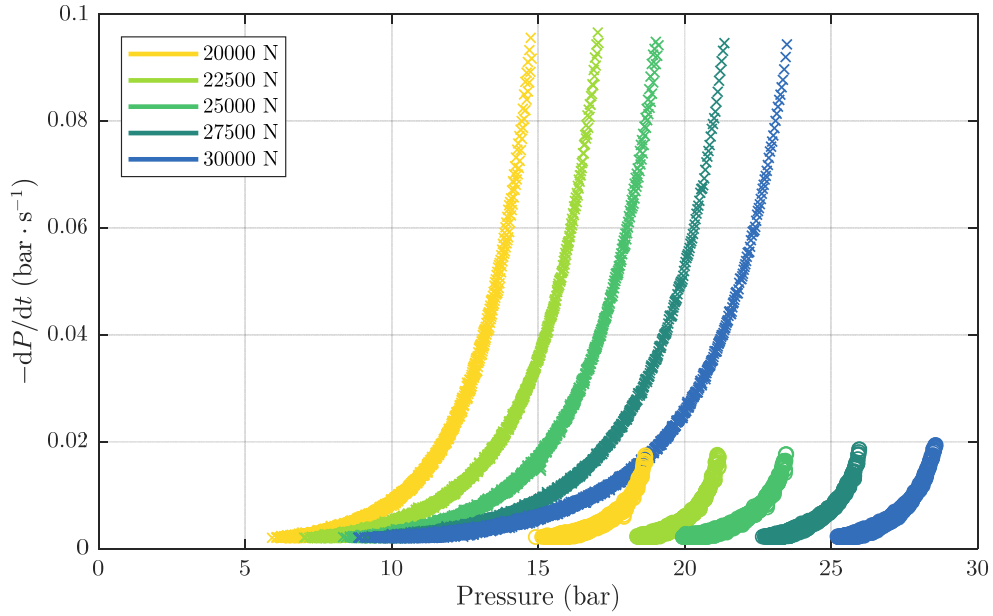

Figure 4.11: Pressure loss rate versus liquid pressure at different preloads. 'x' indicates results achieved with water, and 'o' results with Nuto H46 oil.

If results at a certain preload are analysed, it can be concluded that leakage starts at higher pressure values when oil is contained in the chamber. This is because the higher viscosity of the oil restricts the flow of liquid though the leakage channels that appear between the surfaces in contact. Moreover, a sharper pressure drop occurs in the tests carried out with oil.

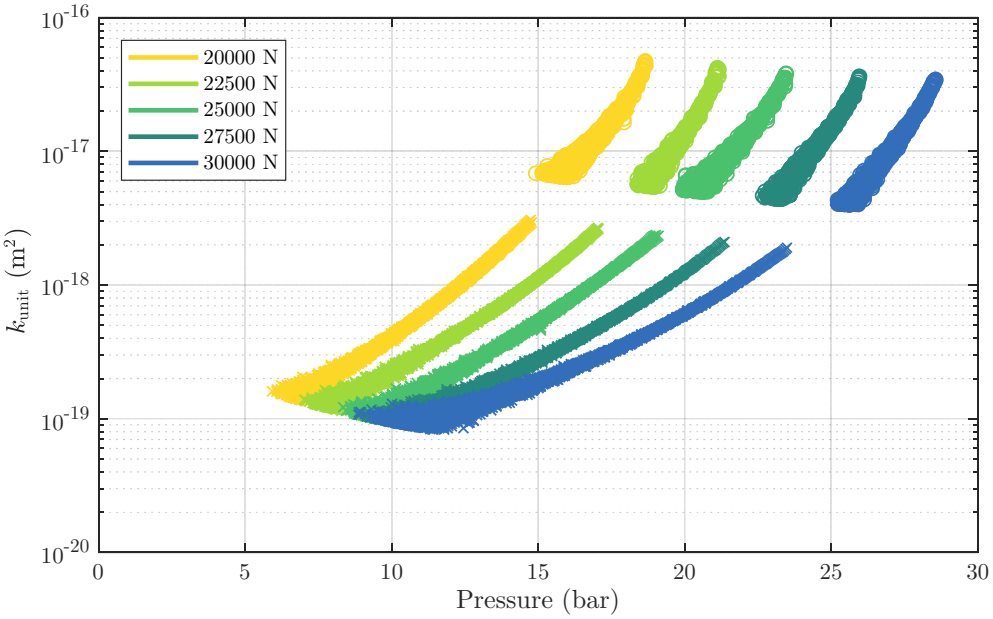

Figure 4.12: Permeability versus liquid pressure at different preloads. 'x' indicates results achieved with water, and 'o' results with Nuto H46 oil.

Consequently, if a leakage criterion is set based on an admissible leakage rate, the threshold pressure depends on the applied preload and the liquid contained. The variation associated with the liquid properties disappears when considering the permeability per unit length, as indicated in Section 4.2.4. Figure 4.12 shows that water and oil results present the same trend for each preload.

To confirm the cited assumption and validate the relationship between pressure drop rate and leakage flow rate given by Equation (4.5), specific tests were designed and conducted. The testbench was kept at a constant preload and pressure, and required the application of pressure when necessary to compensate for losses due to leakage. After 10 minutes of testing, the released liquid was collected with absorbent paper. The difference in the mass of the paper before and after this absorption indicated the amount of liquid leaked. Each test was repeated three times. In addition, a theoretical total outflow mass was calculated based on Equation (4.5). For each pressure drop interval in the signal, the mean pressure loss rate was calculated, which was multiplied by the duration of this interval to compute its contribution to the total outflow mass. After the total leaked mass was calculated, it was compared to the experimental results, as shown in Figure 4.13. Although a higher dispersion was observed at higher pressure values, a good correlation was found in all cases, which validates the process established to calculate the leakage flow rate based on the measurement of the pressure of the liquid.

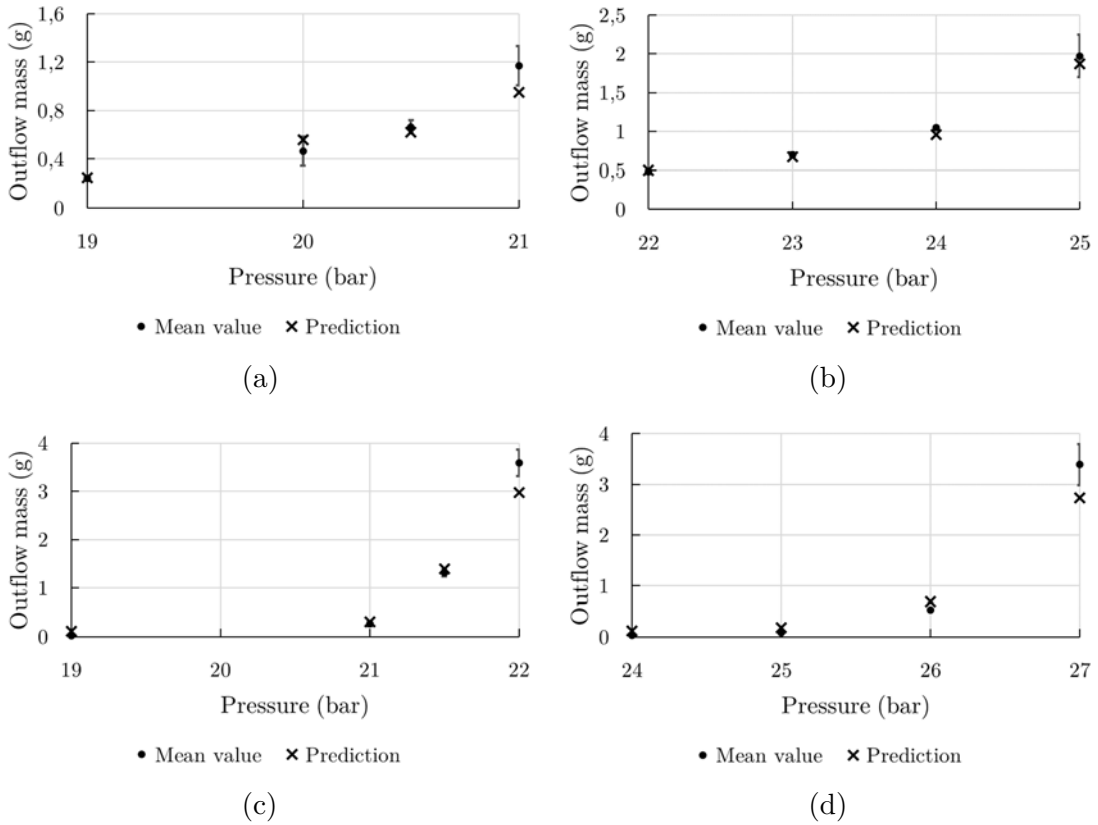

Figure 4.13: Comparison of the measured and calculated outflow liquid mass. Water was used with a 22,500 N preload in (a) and 27,500 N in (b). Nuto H46 oil was used with a 22,500 N preload in (c) and 27,500 N in (d).

2. Calculation of the contact pressure:

The sealing of the developed testbench is performed by means of a cone-to-ball contact. In such cases, and if perfectly smooth surfaces are considered, a Hertzian distribution of the contact pressure occurs around the contact edge. The width of the contact area is related to the stiffness of the components (Johnson, 1985).

It was not possible to experimentally measure the contact pressure in the experimental tests and, to the best knowledge of the authors, no analytical expression has been described for the cone-to-sphere elastic contact considering the friction force. Therefore, numerical simulation was considered the best solution to achieve an estimation of contact pressure distribution. A structural model was defined to obtain contact pressure values depending on the applied external preload and inner pressure.

The contact of the case study occurred in a very narrow width. Characterising this contact required a numerical model with a very small element size to capture the resulting contact pressures in detail. Assigning a mesh size of this order to a three-dimensional model involves an excessively large number of elements which dramatically increases the computational time, resulting in a not practical model for analysis. However, the axisymmetry of the testbench allowed the modelling of its behaviour by means of a two-dimensional axisymmetric model. This type of surface modelling is representative of all the sections around the axis of revolution, since the model conditions are reproduced in the same way in all these sections. A two-dimensional axisymmetric model allows the use of sufficiently small elements, which guarantees the optimum result in terms of contact pressures (Figure 4.14 (a)).

AISI 304 material properties were assigned to both the seat and semi-sphere (Table 4.1). A frictional contact condition was established between them, with a friction coefficient of 0.2, commonly found in metal-to-metal contacts. A predominantly quadrilateral shaped mesh was used. As regards boundary conditions, fixed support was assigned to the bottom surface, and the system preload was applied as a constant remote force consistent with the chosen value in Table 4.2.

Once the model was created, a mesh sensitivity analysis was carried out to determine the optimum element size to ensure the accuracy of the results. The influence of the element size in the contact zone was analysed, assuming a growth factor of 1.1 and a maximum mesh size of 2 mm in zones sufficiently far. A preload of 25,000 N was assigned to the model, and no pressure was applied in the chamber. An element size of 0.5 mm was initially chosen, and the achieved contact pressures were compared to those with progressively smaller elements. It can be observed in Figure 4.14 (b) that convergent results were achieved for a mesh size below 0.1 mm. An element size of 0.05 mm was chosen for the numerical models, since the calculation time was acceptable and in order to achieve a higher accuracy.

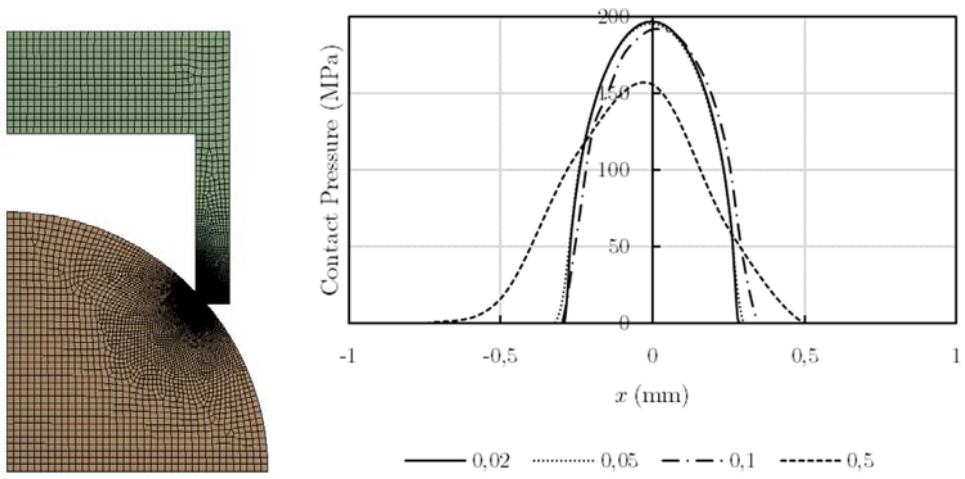

(a) (b)

Figure 4.14: (a) Two-dimensional axisymmetric model used to calculate contact pressures. (b) Contact pressures achieved for different mesh sizes in the contact zone.

Returning to the establishment of the relationship between contact pressures and inner fluid pressure for each preload, fluid pressure was added to the internal surfaces of the described two-dimensional axisymmetric model. Pressure values ranging from 0 to 31 bar (in the case of the higher preload) were assigned, with 0.2 bar intervals.

The results determine the distribution of the contact pressure across the width of the contact zone. However, a single value is needed to determine the leakage criterion in terms of permeability and contact pressure. Therefore, the peak contact pressure value was assigned to establish the relationship between fluid pressure and contact pressure. The results achieved are set out in Figure 4.15.

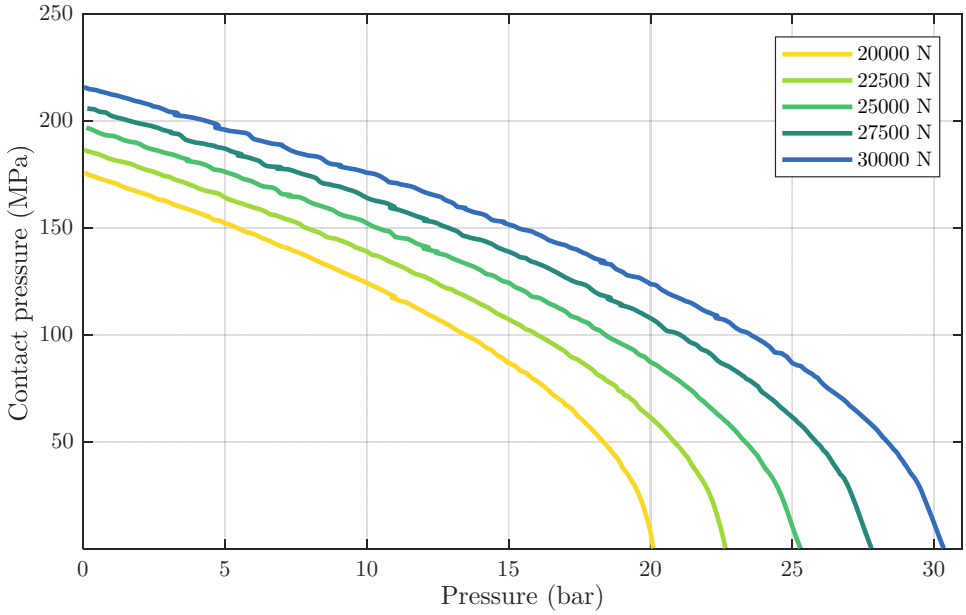

Figure 4.15: Contact pressures achieved for different preloads and pressures.

As the preload was kept constant (tests were carried out with force control), contact pressure decreased from its maximum value (with null inner pressure) to zero. The same contact pressure decrease pattern is observed regardless of the preload value. In addition, at each preload the contact pressure drop is more pronounced above a certain pressure value.

In order to validate the achieved results, Fujifilm Prescale measurement film[4] was used. It is a sheet-type material to measure contact pressure, with a thickness of 90 to 110 μm. Micro-capsules are embedded in the film, which are broken when pressure is applied. The colour forming material contained in these micro-capsules causes the appearance of red patches on the film, which shows the pressure distribution. In addition, the colour density changes in accordance with the pressure level, and different grades of films are available depending on the pressure range to be measured (from 0.2 to 300 MPa).

The Fujifilm Prescale grade was chosen according to the value determined by the simulations. For a 27,500 N preload a maximum contact pressure of 206 MPa was obtained, with a contact width close to 0.6 mm (Figure 4.16 (a)). For this reason, High Pressure (HS) and Super High Pressure (HHS) mono-sheet type films were chosen, whose pressure ranges are between 50 and 130 MPa, and between 130 and 300 MPa respectively (Figure 4.16 (b)). The film was located along the perimeter of contact between the seat and the semi-sphere. The test could only be performed without inner pressure, as the contact pressure decreases when internal pressure is increased, and the footprint on the film only records the maximum contact pressure reached. After subjecting the system to the same preload as that of the simulations, the HS film showed an intensively red coloured area (Figure 4.16 (c)), whereas the HHS film showed barely noticeable red marks (Figure 4.16 (d)).

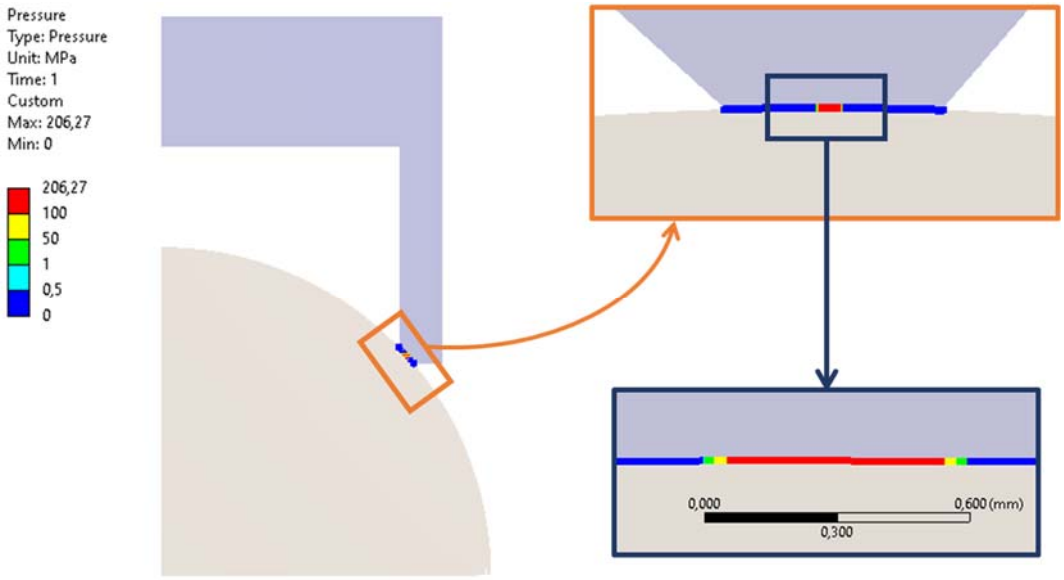

(a)

[4] https://www.fujifilm.eu/eu/products/industrial-products/prescale

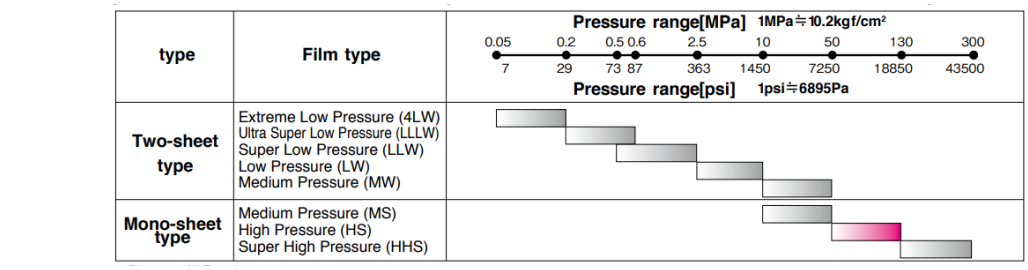

(b)

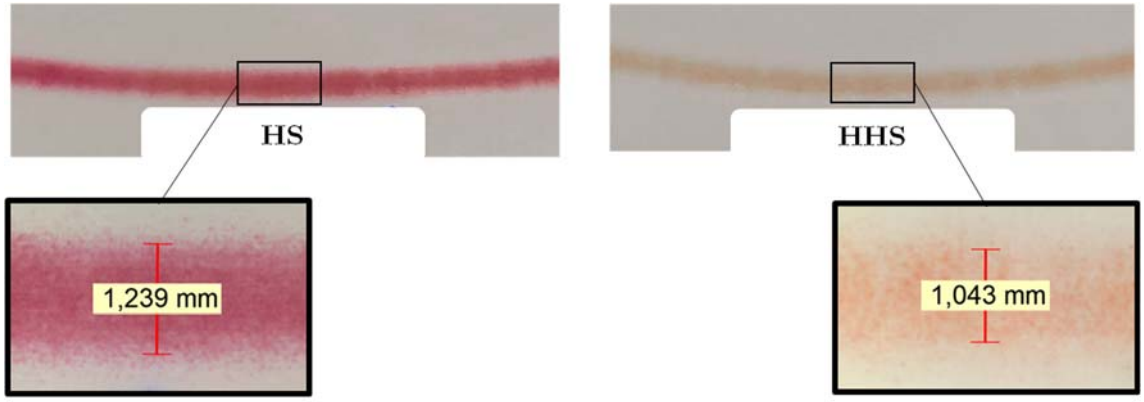

(c) (d)

Figure 4.16: Comparison of the contact pressure with a 27,500 N preload. (a) Result of the numerical model. (b) Range of the measured contact pressure corresponding to the films[5]. (c) Footprint on the tested HS Fujifilm Prescale sheet. (d) Footprint on the tested HHS Fujifilm Prescale sheet.

Contact pressure measurement with Fujifilm Prescale Measurement Film does not result in accurate quantitative results. Rather, it allows a range of contact pressures and contact width to be identified. In the particular case of this application, the measurement with High Pressure film (HS) showed a red saturation, which means that the pressure reached was beyond the range of 130 MPa corresponding to that film. However, the measurement with the Super High Pressure film (HHS) was slightly coloured, so it can be established that the measured pressure was well in accordance with that estimated by the numerical model. Additionally, the width of the footprint was measured using a macroscope LEICA DSM 1000 with a result of over 1 mm in both cases (Figure 4.16 (c) and (d)). This width was significantly greater than that achieved in the simulations. A wider contact may be attributable to the fact that the surfaces are not perfectly smooth, as is the case of the numerical model. Nevertheless, there is a relationship between the contact pressure value and the contact width, as the resultant force must balance the applied preload. In other words, it is not possible to reach the same pressure level as the simulation and have a larger contact width.

Additionally, a topographical measurement was performed to characterise the contact under analysis, by using a SensoFar S-NEOX optical profilometer (Wight light Interferometry 20xDI). The surfaces of the seat and semi-sphere were analysed before

[5] https://www.fujifilm.eu/eu/products/industrial-products/prescale

and after testing. In both components, the grooves resulting from the manufacturing process were easily observed. The contact area was identified in the confocal images (Figure 4.17), the width of which could be established at around 0.6 mm as predicted by the simulations. However, in terms of surface height the differences were practically imperceptible, leading to the conclusion that no plastic deformation occurred during the tests.

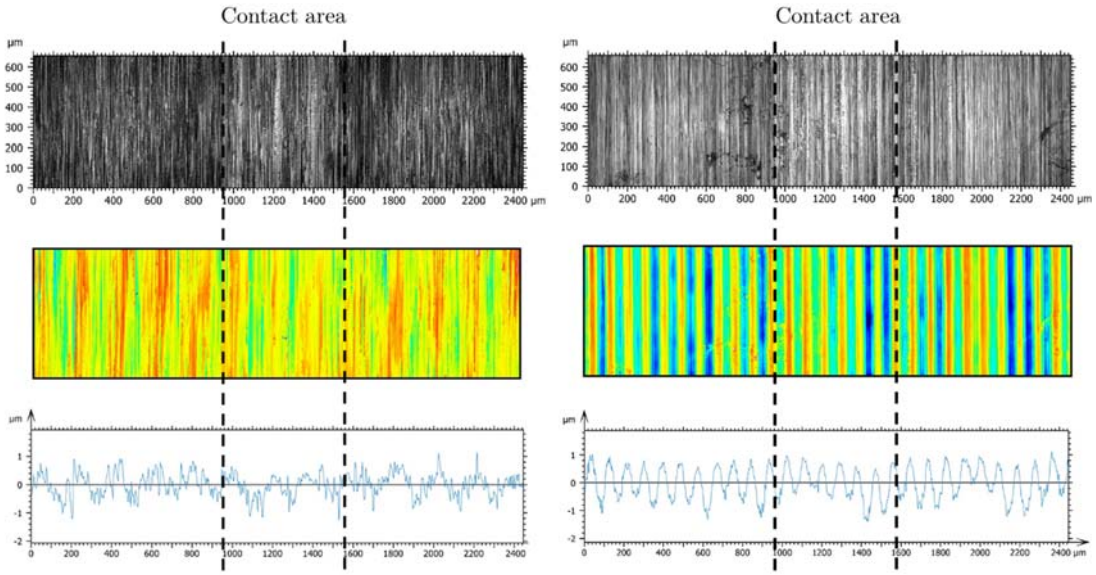

Figure 4.17: Results of the topographical measurements on the contact surface of (a) the seat and (b) the semi-sphere, after performing the tests.

In summary, the qualitative character of the measurements with Fujifilm Prescale together with the observations in the optical profilometer validated the results of the simulations, in terms of contact pressure level and contact width.

3. Determination of the leakage criterion:

After performing the corresponding calculations, permeability per unit length versus maximum contact pressure was plotted. The plot from the tests carried out in this research is shown in Figure 4.18, which presents the results for both liquids, and the chosen five preloads.

The result is shown in a graph with a logarithmic scale. The graph shows the same trend for all the tests, regardless of the fluid and preload, which confirms the hypothesis in Section 4.2.4. The results of the tests undertaken with water are related to higher contact pressures than those with oil, as water leakage starts at lower pressure values. Conversely, results with oil show lower contact pressure values, as the pressure of water never reaches such high values because of its lower viscosity.

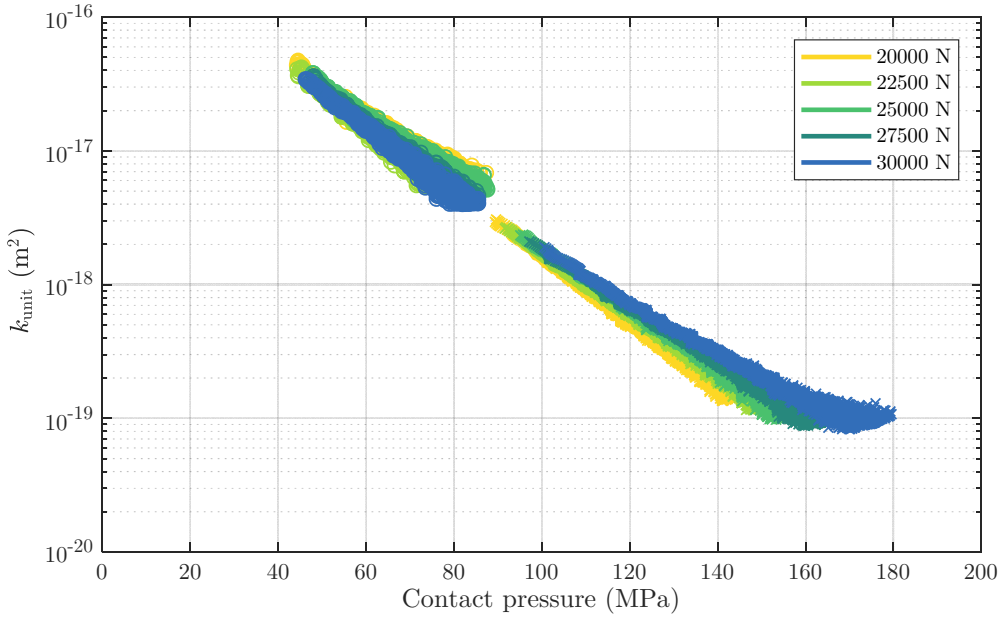

Figure 4.18: Permeability per unit length versus maximum contact pressure plot. "x" refers to test results with water, and "o" to Nuto H46 oil test results.

As observed in Figure 4.18, the permeability per unit length showed a linear trend with a negative slope with respect to contact pressure. This behaviour was also observed by Pérez-Ràfols and Almqvist (2018), which they described as a channelled flow regime (Figure 4.1). This indicates that the permeability reduces as contact pressure increases. In fact, a higher contact pressure ensures a lower leak rate between the surfaces in contact. The permeability (and hence the leak rate) increases as contact pressure decreases, and these values grow in a logarithmic scale. Therefore, it is of vital importance to properly capture the system behaviour at lower contact pressure values.

4.4 DISCUSSION

In the proposed methodology, a relationship is established between contact pressure and permeability. The source data corresponds to experimental results obtained from leakage tests on an axisymmetric bench.

The plot in Figure 4.11 shows consistent results as regards leak behaviour with different preloads and liquids. As expected, leakage onset occurs at higher pressures as the preload and/or liquid viscosity is higher. Therefore, at this step the results are both system and fluid dependant.

To remove fluid dependency, the permeability concept was introduced as can be observed in Figure 4.12. This graph shows that for a given preload the results for water and oil show the same behaviour, which permits the establishment of a law regardless of the fluid used. However, at this step the results are still system dependant.

The system geometry inherently conditions the results concerning the leakage behaviour. When contact pressure is used as a variable, a local assessment is made at each point where leakage occurs, so that the result becomes independent of the system

under analysis. For this reason, the results at this point are also independent of the preload and overlap, presenting a unified trend (Figure 4.18).

The law described was obtained on the basis of certain assumptions that required a decision to reach a result. However, it is necessary to perform an analysis of the factors that most influence the result, and how they affect the final outcome (presented in the following section).

4.4.1 Analysis of the factors that affect the leakage criterion

The leakage law achieved as a result of the presented methodology is defined in terms of (i) the system permeability, and (ii) the contact pressure between the structural elements. An accurate estimation of both these variables is affected by several factors.

- **Sensitivity of the permeability:**

The calculation of permeability involves the outflow rate, the liquid viscosity and the fluid pressure, in accordance with Equation (4.2). The former is the factor which entails more uncertainties, as it is calculated based on the bulk modulus of the liquid, the volume inside the seat, and the pressure drop throughout the test (see Equation (4.5)). Nevertheless, the bulk modulus is known and not expected to change during the tests. Additionally, fluid pressure is achieved by means of the pressure transmitter with a high degree of accuracy, and the pressure drop is deducted from this measurement by simple mathematical operations (see Equation (4.6)).

Therefore, a factor that was identified as crucial for the calculation of the permeability was the volume employed to compute the leakage rate (see Equation (4.5)). The developed methodology predicts the leak flow rate under the hypothesis that the whole inner cavity of the seat and the ducts are filled with liquid. However, some air bubbles may remain trapped in the circuit, and this may have an influence on the results.

Liquid is considered practically incompressible, so that a loss of pressure hardly changes its volume. However, the compressibility of air is much higher, which causes the volume that it occupies to increase when a pressure drop occurs. This means that the pressure loss values, on which the calculated flow rates depend, may not be entirely accurate.

Assuming the hypothesis that the liquid volume inside the cavity does not change, the outflow rate was determined by Equation (4.5). Nevertheless, in the case that there are any air bubbles the chamber volume V_0 can be expressed as:

$$V_0 = V_\ell + V_\mathrm{a}\,, \tag{4.10}$$

where V_ℓ refers to the liquid volume and V_a to the air volume. In consequence, the liquid volume variation over time is defined by:

$$\frac{\mathrm{d}\,V_\ell}{\mathrm{d}t} = \frac{\mathrm{d}\,V_0}{\mathrm{d}t} - \frac{\mathrm{d}\,V_\mathrm{a}}{\mathrm{d}t}\,. \tag{4.11}$$

The first term refers to the variation of the chamber volume, where V_0 remains constant. The second term is related to the volume variation of the air bubbles. In accordance with the ideal gas law:

$$V_{\mathrm{a}} = \frac{m\mathrm{R}T}{P}, \tag{4.12}$$

where m, T and P are, respectively, the mass, temperature and the absolute pressure of the air contained, and R is the gas constant for air. As both air and liquid are contained in the same chamber, their pressure is the same. In addition, it can be assumed both fluids are in thermal equilibrium, and as long as there is no air leakage, its mass remains constant. Therefore, the variation of air volume is expressed as follows:

$$\frac{\mathrm{d}V_{\mathrm{a}}}{\mathrm{d}t} = -\frac{m\mathrm{R}T}{P^2}\frac{\mathrm{d}P}{\mathrm{d}t}. \tag{4.13}$$

Taking into account all these considerations, the liquid volume variation can be established as:

$$\frac{\mathrm{d}V_{\ell}}{\mathrm{d}t} = \frac{m\mathrm{R}T}{P^2}\frac{\mathrm{d}P}{\mathrm{d}t}. \tag{4.14}$$

On the other hand, it can be determined that the described liquid volume change has two sources: (i) a pressure variation in the chamber taking into account the compressibility of the liquid, and (ii) leakage. Using the definition given by Equation (4.4):

$$\frac{\mathrm{d}V_{\ell}}{\mathrm{d}t} = \left(\frac{\mathrm{d}V_{\ell}}{\mathrm{d}t}\right)_{\text{air compresibility}} + \left(\frac{\mathrm{d}V_{\ell}}{\mathrm{d}t}\right)_{\text{leakage}} = -\left(\frac{V_{\ell}}{K}\frac{\mathrm{d}P}{\mathrm{d}t} + Q\right). \tag{4.15}$$

By equalling Equation (4.14) and Equation (4.15), the leak rate can be computed as:

$$Q = -\left(\frac{V_0 - V_{\mathrm{a}}}{K} + \frac{m\mathrm{R}T}{P^2}\right)\frac{\mathrm{d}P}{\mathrm{d}t}, \tag{4.16}$$

where the first term was used to calculate Q in Equation (4.5). However, a second term is added to account for the air contained in the liquid chamber. The negative sign indicates that a pressure loss ($\mathrm{d}P/\mathrm{d}t < 0$) leads to a leak ($Q > 0$). As a consequence, the outlet flow computed in Equation (4.16) considers the effect of an air volume inside the chamber, which results in a higher leakage rate in comparison to the previously calculated by Equation (4.5).

In summary, having air in the system is a source of error in the analysis if the post-processing is carried out without considering this aspect. The relationship in Equation (4.16) presents a more accurate method to compute the leakage flow rate, leading to a higher result than that calculated previously. This affects both the experimental

results and those predicted by the developed methodology. Therefore, the resulting permeability of the axisymmetric bench is also higher, as it is proportional to the leakage flow rate. In any case, and being aware that any air volume has an impact on the experimental measurements, special care was taken in the arrangement of the piping and other devices, so that no air accumulation could occur. This aspect was also taken into account in the design of the seat, so that air could easily be expelled when filling the chamber with fluid.

- **Sensitivity of the contact pressure:**

As stated in the work by Fischer et al. (2021), the calculated outflow rate is extremely sensitive to the contact pressure, and any error in this value has an impact on the achieved prediction. The contact pressure in the present study could not be experimentally measured, so the results of numerical models were necessary to determine a contact pressure value for each fluid pressure in the system cavity. However, it was verified that several factors affect the contact pressure values specified for each case, among which the following can be highlighted:

  - Factors related to numerical modelling.
  - The cone-to-sphere contact geometry.
  - The surface roughness and friction coefficient.

A numerical solution is always an approximation of a real result. Appropriate boundary conditions and mesh parameters are crucial to achieve reliable results. In the case of contact configurations such as the one under consideration (contact on an edge), an abrupt contact pressure value change occurs in a very short contact width. The contact pressure value is null at the edges of the contact and a peak value is given with a Hertzian distribution, as the numerical model assumes perfectly smooth surfaces. A very small element size is required to numerically capture this effect. Otherwise, the achieved results are not representative of either the maximum value or the distribution shape. The mesh sensitivity analysis provided the optimum element size for the two-dimensional axisymmetric model. In addition, different parameters of the contact definition were checked to achieve the most accurate results.

An aspect with a decisive influence on the contact pressure is the geometrical configuration of the testbench. As explained in Section 4.3.1, the design of the bench was based on an axial flow check-valve, in which the cylindrical seat is placed on the semi-sphere. When applying the compressive load and internal pressure, the diameter of the seat in contact with the semi-sphere expands and comes to rest progressively lower on the surface of the semi-sphere (Figure 4.19). The position at which the seat rests on the semi-sphere is thus of vital importance when quantifying the contact pressure. On the one hand, the lower the new contact occurs, the greater the perimeter of interaction becomes. This implies a lower contact pressure for a given preload. On the other hand, the contact angle also changes, as a lower contact position corresponds to a lower contact angle. Hence, the horizontal component of the reaction force grows, leading to a higher resultant reaction, which implies a higher contact pressure. Nevertheless, the following

parameters oppose a change in the contact position under the applied force: (i) the circumferential stiffness of the seat, (ii) the friction force in the contact area, and (iii) a possible locking of the seat on the semi-sphere at a certain position.

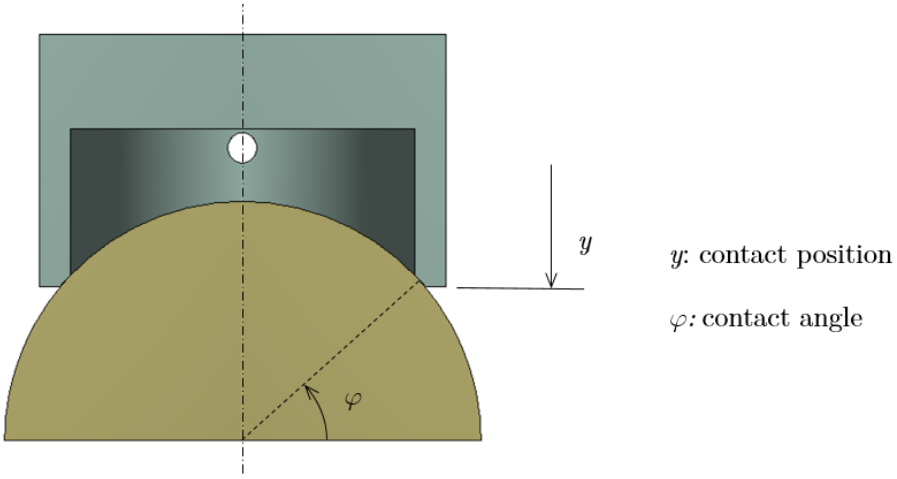

Figure 4.19: Contact position of the seat and the semi-sphere, and the corresponding contact angle.

The seat circumferential stiffness is directly related to its material and geometry, and is therefore implicitly considered in the numerical model. However, the friction coefficient between the components is an independent variable which has a direct impact on the friction force. Therefore, the effect of the friction coefficient is examined in the following lines.

Simulations with different coefficients of friction were carried out, namely 0, 0.1, 0.2 and 0.4, for all preloads. The results of the relationship between fluid pressure and contact pressure are shown in Figure 4.20, where only the data for 20,000 N and 30,000 N preloads are shown for clearness.

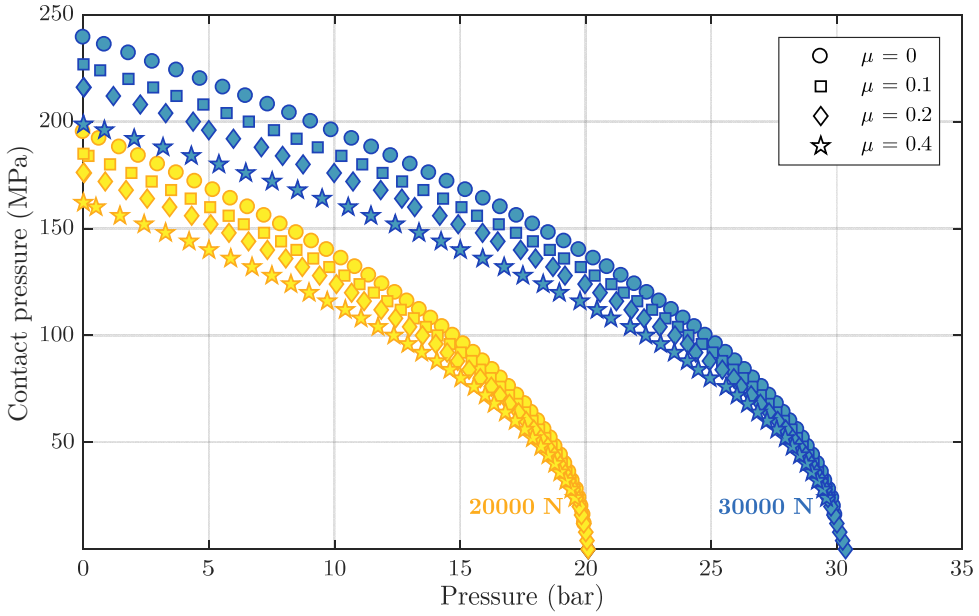

Figure 4.20: Relationship between contact pressure and liquid pressure using different friction coefficients, with a preload of 20,000 N and 30,000 N.

The figure shows the same trend at all preload values. As the coefficient of friction increases, the contact pressure that corresponds to a given fluid pressure is lower. In addition, all the results that correspond to a given preload converge at the same point of maximum liquid pressure. This finding is to be expected, as it indicates that at the moment of contact separation the equilibrium between the imposed preload and the resultant force of the internal pressure must be fulfilled.

The differences between the results with the considered friction coefficients are larger at lower fluid pressures. However, the highest liquid pressures are those which lead to a higher leakage rate. Thus, the corresponding contact pressures greatly affect the results. Perceivable differences are also observed in this range in Figure 4.20, hence it is critical to determine the appropriate relationship between contact pressure and liquid pressure.

This relationship directly affects the leakage law to be determined. Regardless of the coefficient of friction considered, it was observed that this law can be adjusted to a linear behaviour for the relationship between permeability per unit length and contact pressure on a semi-logarithmic scale. Figure 4.21 illustrates the results with different friction coefficients with a preload of 30,000 N.

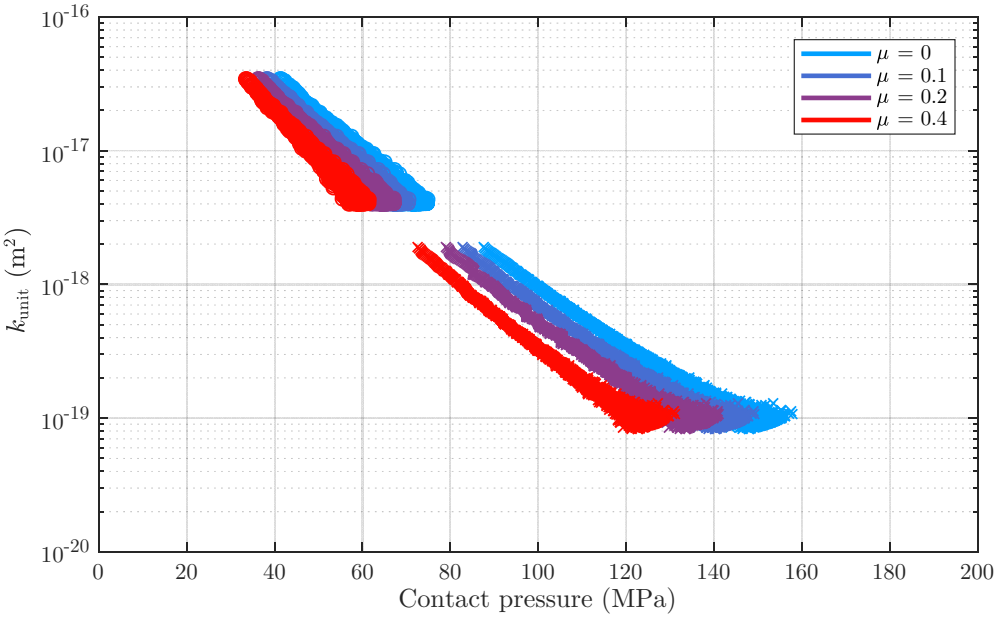

Figure 4.21: Permeability per unit length versus contact pressure for different friction coefficients, with a preload of 30,000 N.

The figure shows that a higher coefficient of friction corresponds to a steeper slope of the relationship between permeability and contact pressure. In addition, the intersection with the vertical axis is the same for all the curves. Null contact pressure means that the contact between the structural elements no longer exists. The force equilibrium in this situation does not depend on the coefficient of friction, hence all the curves must converge at the same permeability point.

No measurement of the coefficient of friction between the seat and the semi-sphere was carried out. For this reason, the displacements of the upper carriage of the testing machine in the experimental tests were compared to the results in the numerical models, using different friction coefficients. The results are shown in Figure 4.22.

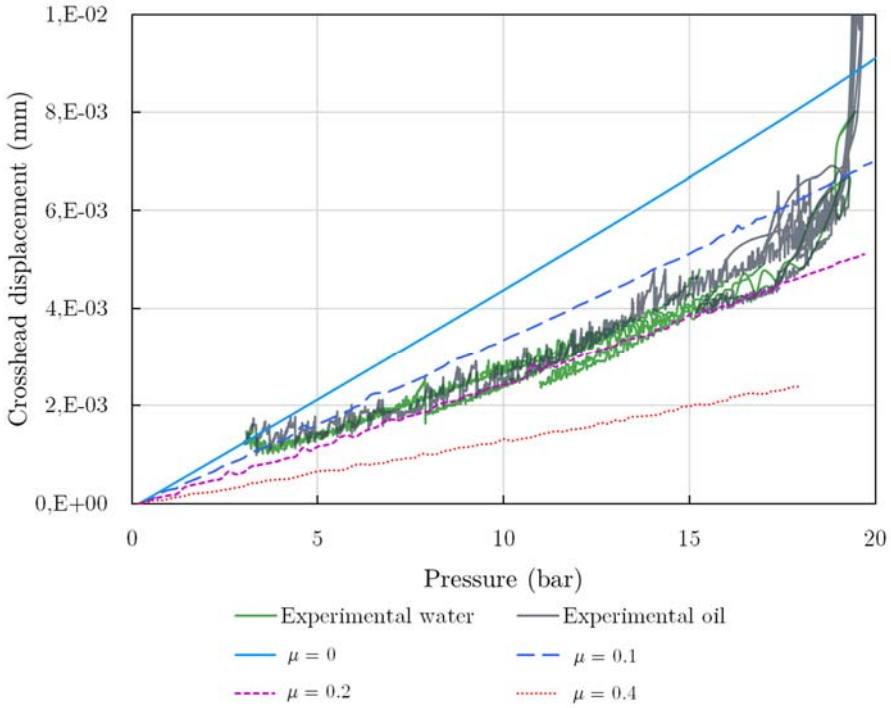

Figure 4.22: Experimental vertical displacement of the universal testing machine, compared to the simulation results for different frictional coefficients.

The plots show the vertical displacement of the testing machine crosshead as the liquid pressure increased. The dashed lines in the figure correspond to the behaviour predicted by the simulations. As higher friction coefficients are considered, the slope of the answer is lower. The curve that best fits the experimental results is that of the coefficient of friction 0.2. Furthermore, coefficients of friction between 0.1 and 0.2 are the most commonly observed in metal-to-metal contact, and for this reason a coefficient of friction of 0.2 was chosen.

Another factor that affects the vertical position of the contact is that the seat may become locked on the semi-sphere. This can be attributed to the system geometry, as the inner cavity of the seat adopts different shapes depending on the inner fluid pressure. When the seat is pushed against the semi-sphere with a given preload and null internal pressure, the lower area of the seat expands due to the contact pressure until it reaches the equilibrium position. From this position, when the pressure in the inner chamber is increased, the sides of the seat bulge and the angle at which the conical surface contacts the spherical surface changes (Figure 4.23). As the inner pressure is progressively reduced, a position may be reached where the inner diameter attempts to return to its initial dimension, but the geometrical configuration of the contact at that instant, together with the frictional force, obliges it to maintain this position. This would involve higher contact pressures than those corresponding to this configuration.

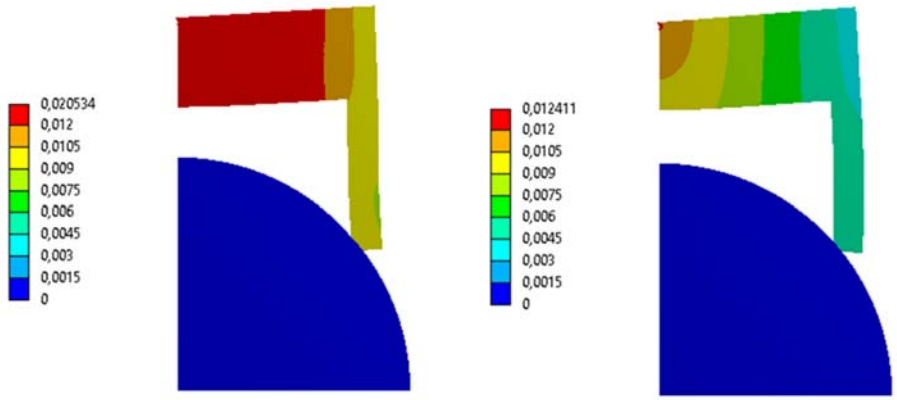

(a) (b)

Figure 4.23: Vertical displacement and geometrical configuration of the contact between the seat and the semi-sphere for 20,000 N preload, (a) with null internal pressure, and (b) 20 bar pressure. Displacements are magnified for a better understanding.

In fact, during the performance of some tests a distinctive noise could be heard when the chamber was depressurised in the experimental tests, which could be an indicator of the seat being locked against the semi-sphere.

As already described, the peak value of the Hertzian distribution is used to set the contact pressure that corresponds to each fluid pressure (Figure 4.15). This means that when computing the permeability, the total pressure drop and the resulting leak occurs on the contact edge. However, the pressure difference inside and outside the chamber is the result of a progressive drop in pressure across the contact width. Each of these incremental drops in pressure contribute to the permeability of the system at this location. When simplifying the contact to a single edge, the total pressure difference is assigned to a single position, and the pressure drop occurs abruptly.

As the developed methodology should take into account the pressure drop all along the leakage pathway, the peak contact pressure value may not be the most representative to calculate the permeability. In fact, the mean contact pressure value may be used instead. This considers a contact pressure value evenly distributed in the contact-width, which applies the same resultant force. This condition is achieved by applying a reduction factor of $\pi/4$ to the peak contact pressure value, which affects the slope of the permeability per unit length in Figure 4.18, but not its intersection with the vertical axis.

In addition, the surface finish which is not accounted for in the numerical model also affects the contact pressure. The simulation considers a perfectly flat and smooth conical surface against a smooth spherical surface. Under this assumption, a Hertz-like contact pressure distribution is achieved. This is a good approximation if the surface roughness amplitude is very small. However, as surface asperities become larger and they deform under the applied force, the nominal contact region is larger than that predicted by the Hertz theory. In this case, the pressure distribution follows a Gaussian pattern (Fischer et al., 2020). The peak contact pressure value in the latter distribution is smaller as the pressure is distributed over a larger contact area. Furthermore, local plasticity or wear of the surface could change the geometry of the contact, and contribute to this type

of contact distribution. Nevertheless, the measurements in the optical profilometer (Figure 4.17) confirmed that the effects of roughness and local plasticities are negligible in the application under analysis.

In summary, the use of numerical simulations was unavoidable to be able to determine the contact pressures for this research. However, these models are not able to reliably represent all the phenomena that occur in the cone-to-sphere elastic contact. In addition, the achieved results must be adapted to the needs of the methodology, which considers the leakage pressure drop concentrated on the edge of the contact.

4.4.2 Definition of the definitive leakage criterion

Several parameters affect the definition of the leakage law that was stated in terms of permeability and contact pressure, which is established in a semi-logarithmic scale. Having analysed how these parameters affect the permeability, the relationship between contact pressure and liquid pressure was adjusted to determine the leakage criterion for the system under analysis. This adjustment was made under the following assumptions:

- The coefficient of friction was set to 0.2. It is a commonly observed value between the metals used in this application. In addition, the position of the crosshead measured in the testing machine was in good agreement with that calculated in the simulations when using a friction coefficient of 0.2 (Figure 4.22).
- To work with the mean contact pressure values, a factor of $\pi/4$ was applied to the previously calculated peak contact pressure values. This reduction is needed to account for the leakage happening across a contact width, and not only concentrated on a contact edge.

Taking these assumptions into consideration, the relationship between fluid pressure and mean contact pressure for the preloads considered is shown in Figure 4.24. The previously achieved results considering the maximum contact pressure are also presented.

Based on this latter relationship, the leakage law that establishes the permeability per length unit values versus the mean contact pressures is illustrated in Figure 4.25. These results are shifted to the left with respect to the results in Figure 4.18, due to the reduction in the value of contact pressure caused by the correction factor applied.

This plot presents a good alignment of all experimental data on a line, for all preloads and both liquids used. The relationship set out by this plot allows the assignment of a permeability value to each area of any system that is different from that used for characterisation. This new system must be based on the same configuration, using the same materials and surface finishes, but with geometric variations in size or shape. After identifying the contact pressure at each location, the corresponding permeability per unit length can be assigned. Based on the contained fluid viscosity, a prediction of the flow rate can be calculated for this new system. To do so, the viscosity should be in the range defined by the liquids tested on the axisymmetric bench.

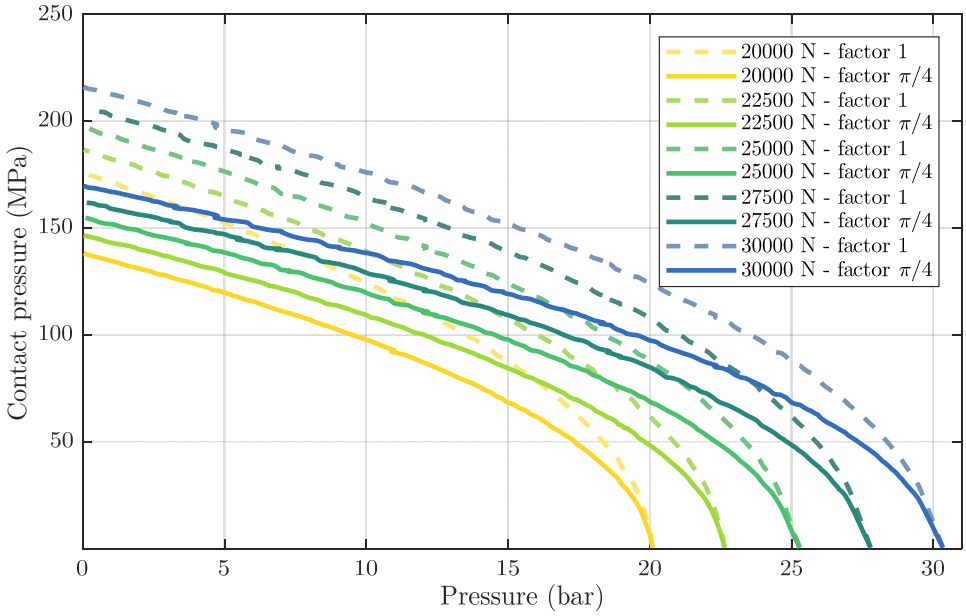

Figure 4.24: Relationship between fluid pressure and contact pressure for all the considered preloads. Continuous lines refer to mean contact pressure results after applying $\pi/4$ correction factor, and dashed lines to maximum contact pressure results.

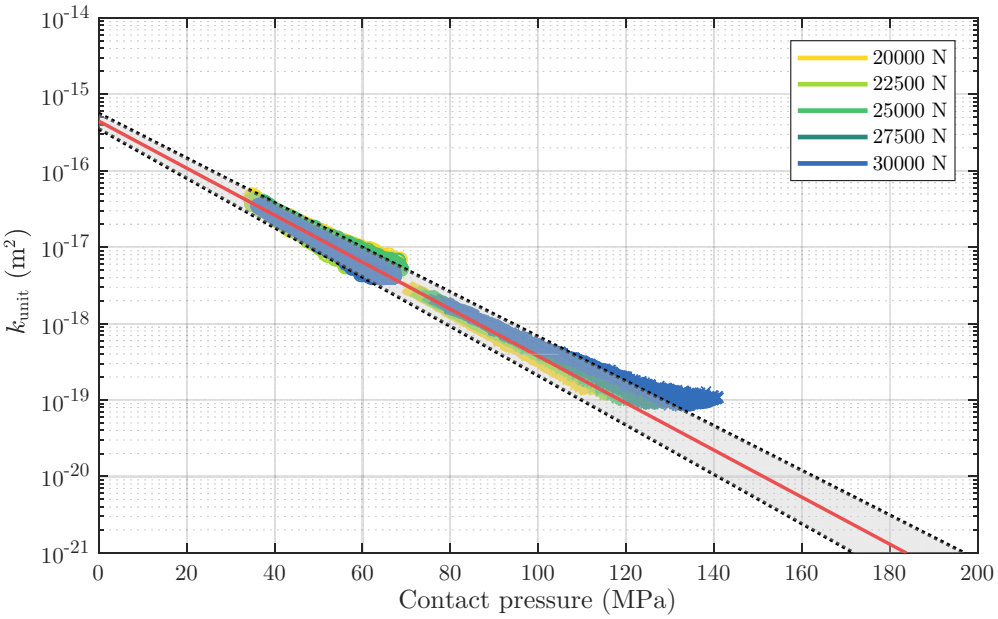

Figure 4.25: Permeability per unit length versus mean contact pressure, defining the leakage criterion. "x" refers to test results with water, and "o" to Nuto H46 oil test results.

Figure 4.25 presents a central line indicating the general trend of the results. Bands are also added sideways surrounding all the points shown on the graph. This enables the identification of the sensitivity of the calculations with respect to the identified central line. Based on this linear relationship, it is possible to quantify the leakage flow rate of any liquid employing the corresponding contact pressure pattern, in the terms

indicated before. A leakage initiation threshold can also be determined by establishing an admissible leakage rate.

In this dissertation, the leakage onset threshold is defined in terms of a minimum contact pressure, as described in Section 4.2.5. The progression of the fluid along the pathway occurs when the contact pressure decreases below this threshold value, and regression occurs in the reverse case. This behaviour belongs to the constriction flow regime (Figure 4.1), which is not shown in Figure 4.25 for a better understanding. In fact, the channelled flow regime is shown in the cited figure, which is characterised by a linear trend. The response of the system at its highest contact pressures is visible if the applied filter is reduced (Figure 4.26).

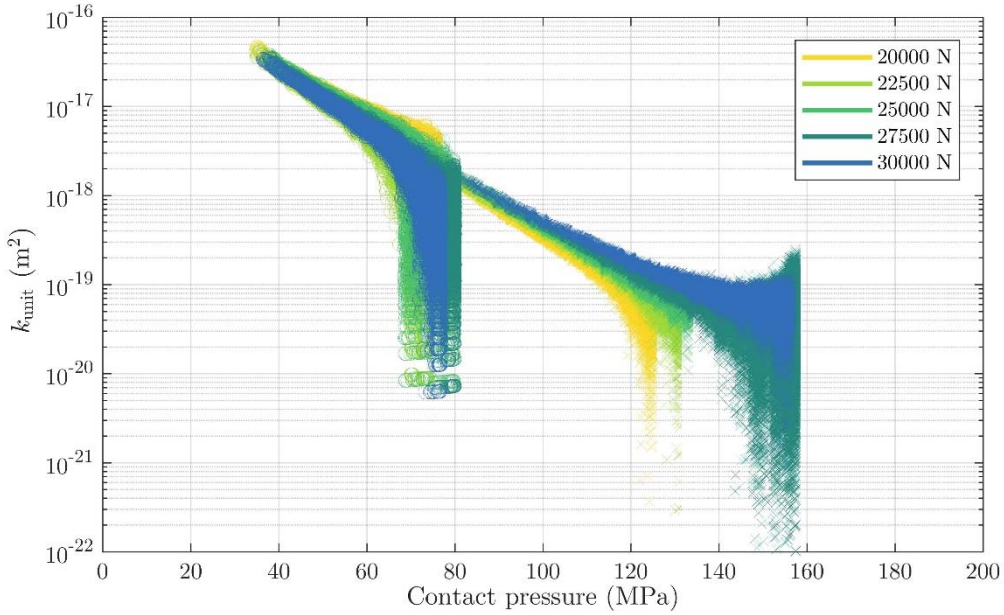

Figure 4.26: Permeability per unit length versus contact pressure, showing both channelled and constriction flow regimes. “x” refers to test results with water, and “o” to Nuto H46 oil test results.

It can be noted that the permeability decreases sharply at a certain value of contact pressure, which is different for each fluid. In the case of oil, this trend overlaps for all the preloads around 70 - 80 MPa, a limit that can be established as the onset/closure of oil leakage. In the case of water, a more dispersed behaviour is observed as a function of the preload, between 122 and 160 MPa. This is directly related to the geometry of the bench, as described in the contact pressure analysis.

The advantage of assuming a threshold contact pressure is that this approach considers an effective sealing above this value, which adjusts the leakage flow rate prediction. The disadvantage, however, is that this threshold is dependent on the fluid used. In the present work, this threshold was defined for the two fluids employed. Testing with a larger number of liquids may provide a relationship between this limit and the properties of the fluid.

In this sense, the linear trend presented for the channelled flow regime lacks the characterisation of the nonlinear region related to the onset and/or closure of the leakage (i.e. the constriction flow regime). Furthermore, the permeability is also not linear at low contact pressures as reported in the literature, when the free flow regime occurs (Figure 4.1). Pérez-Ràfols and Almqvist (2018) ignored the free flow regime, and they represented it as an extension of the linear trend in the channelled flow regime. Hence, they employed two different functions to characterise the channelled and constriction flow regimens. This required that the coefficients identified from experimental tests had to satisfy continuity and differentiability conditions.

To address the presented problem, a single function based on the Weibull distribution is proposed to characterise the whole permeability data, as it is deemed to be more versatile. The proposed function is based on the cumulative distribution function for the Weibull distribution, which is commonly used in statistics and probability theory (Weibull, 1939). It sets the relationship between the normalised contact pressure (defined as the ratio between the mean contact pressure $\overline{p}$ and the contact pressure at closure $\overline{p}_{\mathrm{c}}$) and permeability, such as:

$$\frac{\overline{p}}{\overline{p}_{\mathrm{c}}} = 1 - \frac{1}{\lambda} \mathrm{e}^{-\left(\frac{\log\left(k_{\mathrm{unit}}/k_0\right)}{\delta}\right)^{\beta}}, \tag{4.17}$$

where k_{unit} is the permeability per unit length, k_0 is the permeability per unit length at null contact pressure when $\lambda = 1$, δ is the scale parameter and β is the shape parameter. To avoid abrupt permeability changes when approximating to null contact pressure values, the authors propose adding an extra parameter λ to modulate the slope of the function without varying the closure contact pressure value. Although this region has not been characterised with the presented experimental tests, the case study presented in Chapter 5 could shed light on what form it may take.

From Equation (4.17), the permeability is derived resulting in

$$\log\left(k\right) = \log\left(k_0\right) - \delta \ln\left[\lambda\left(1 - \frac{\overline{p}}{\overline{p}_{\mathrm{c}}}\right)\right]^{1/\beta}. \tag{4.18}$$

The main advantage of the suggested function is that it characterises the three flow regimes with a single set of parameters. However, as with the solutions proposed by other authors, the parameters must be identified for each fluid as the contact pressure value at closure varies depending on the fluid being analysed. In any case, a single function presents two main advantages. On the one hand, it facilitates the identification of the coefficients from the experimental data, and on the other hand, it makes its integration into the developed numerical leakage algorithm easier.

In Figure 4.27 the proposed function is fitted to the experimental data using different λ values.

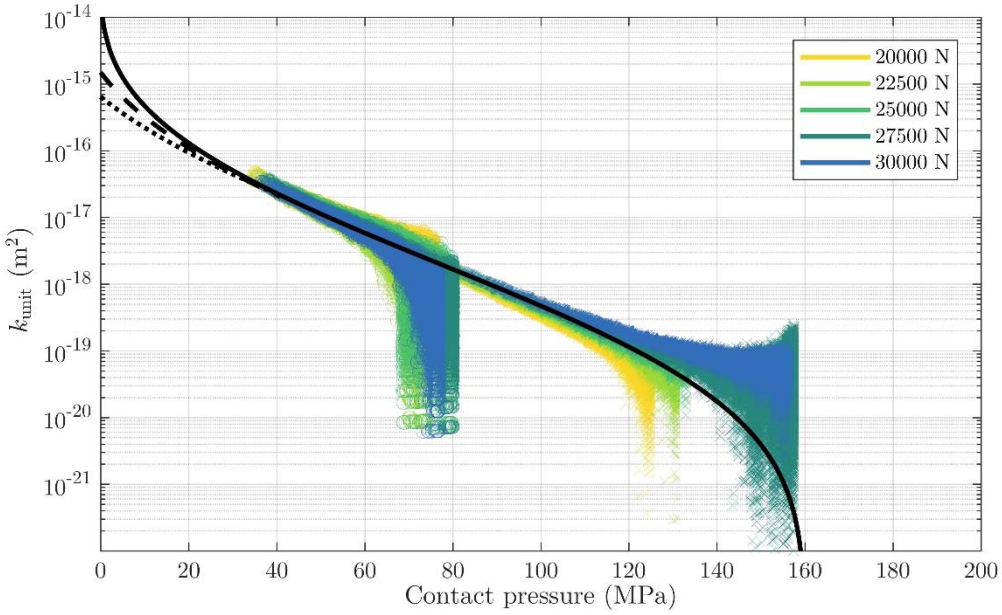

Figure 4.27: Permeability per unit length versus contact pressure, fitted by the proposed function based on Weibull distribution, using different λ values.

It can be concluded that the extra parameter λ suggested in this dissertation presents a clear advantage: a single function that characterises both the channelled and constriction flow regimes, can also describe different behaviours in the free flow regime. Therefore, the proposed function was considered to characterise the permeability function of the whole range, taking into account that different values of contact pressure at closure must be established for each of the fluids tested.

With the employed experimental setup, no information related to the free flow regime was obtained at low contact pressure values. Therefore, the appropriateness of the fitting at low contact pressures (< 35 MPa) cannot be assessed, but further discussion is provided in Chapter 5.

In Figure 4.29 the functions fitted to the contact pressure at closure for water and oil are shown. As was presented for the linear trend in Figure 4.25, the fittings to both the lower and upper limits are presented, to account for the dispersion of the experimental data.

As can be observed, the fitting of the free flow regime is represented with dashed lines because of the lack of experimental data. The coefficients that define the presented fitting curves are shown in Table 4.4.

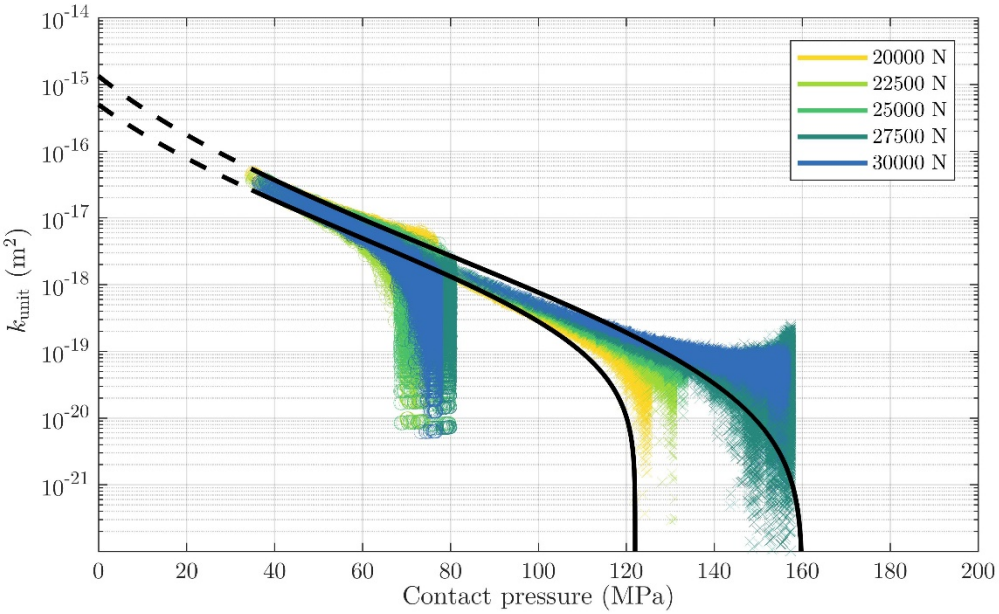

(a)

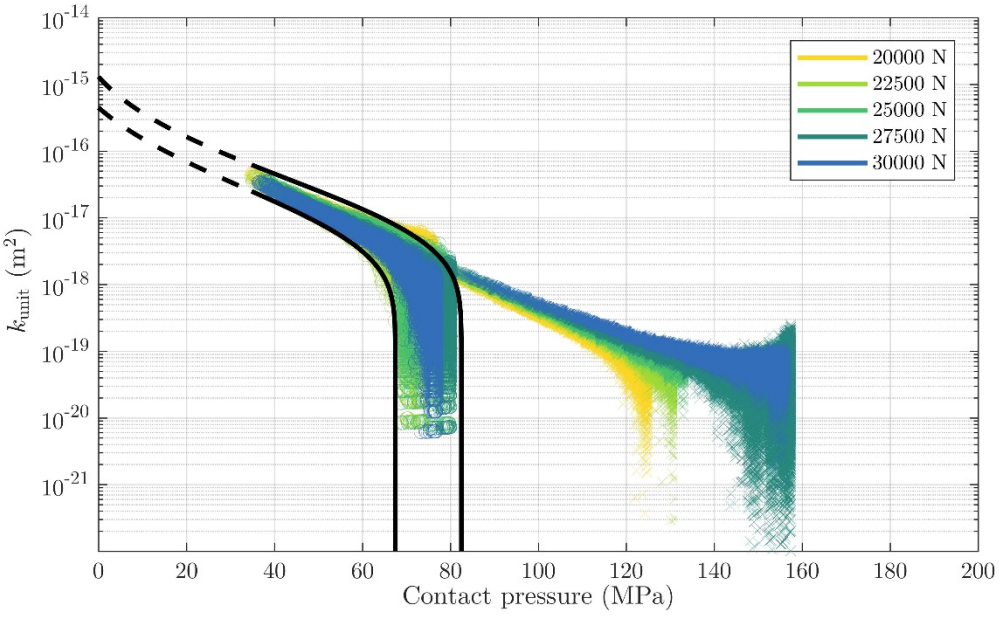

(b)

Figure 4.28: Proposed leakage criteria to cover the lower and upper limits of the experimental data, for the case of (a) water and (b) oil.

Table 4.4: Coefficients of the lower and upper fitting curves of the leakage criterion.

	Water		**Nuto H46 oil**	
	Lower curve	**Upper curve**	**Lower curve**	**Upper curve**
β	10	8	6	6
δ	16.8	16.8	6	6
λ	0.79	0.83	0.85	0.91
$\log(k_0)$ (m^2)	-1.475	-2.295	-11.51	-11.38
$\overline{p}_c$ (MPa)	122	160	67.5	82.5

The contact pressures in the testbench used for the characterisation of the leakage criterion were calculated in a two-dimensional axisymmetric numerical model, which is very efficient in terms of accuracy and computational time. However, any variation of the bench geometry may result in a system that does not fulfil the axisymmetry condition. In that case, the use of a three-dimensional model becomes a must.

As stated before, the computational time dramatically increases in three-dimensional models as the element size is decreased. Finding a balance between accurate enough contact pressures and admissible calculation time is necessary, especially if the model is subsequently used to predict leakage behaviour in an FSI environment by means of the developed methodology.

As the leakage criterion was determined based on contact pressures calculated with two-dimensional models, its application on three-dimensional models had to be validated. Therefore, the methodology to predict the leakage behaviour was applied to a three-dimensional model of the axisymmetric bench used in the characterisation phase. As the same geometry was used both to set the leakage criterion and predict leakage, an accurate prediction should be expected.

4.4.3 Application of the leakage criterion to predict the flow rate in the three-dimensional axisymmetric bench

A three-dimensional numerical model of the bench used to characterise the leakage criterion was created, to calculate the contact pressure distribution with different inner fluid pressures and compare the results with those achieved in the two-dimensional model. The aim was to assess if the leakage criterion established in Section 4.4.2 was valid to predict leakage, when using the contact pressures obtained from three-dimensional models.

Taking advantage of the symmetry of the analysed system, only a quarter of the structure was modelled (see Figure 4.29 (a)). AISI 304 was employed in both seat and semi-sphere (Table 4.1), and a frictional contact condition was established between them with a friction coefficient of 0.2, in coherence with the two-dimensional model.

As regards the elements size, it was a key aspect of this three-dimensional model. Accurate contact pressure results requires small sizes, whereas if the mesh size is too small the resulting calculation time becomes excessively long. This aspect was even more critical since this three-dimensional model was subsequently going to be used in a multiphysics FSI environment, which required even more computational resources.

The results of the mesh sensitivity analysis performed for the two-dimensional model shown in Figure 4.14 (b), indicated that a 0.1 mm mesh size ensured an accurate representation of the contact pressures. For the sake of accuracy, a 0.05 mm size was chosen for the two-dimensional model, but for the three-dimensional model it was decided to be 0.1 mm in order to reduce the computational time. A global size of 4 mm was assigned for the outermost regions of the model.

A predominantly hexahedral shaped mesh was used, combined with tetrahedral elements. As regards boundary conditions, fixed support was assigned to the bottom

surface, and the system preload was applied to the seat top surface as a constant remote force, consistent with the chosen value in Table 4.2. Symmetry conditions were added to the corresponding surfaces. Finally, a ramped pressure was assigned to the surfaces inside the chamber, with values ranging from 0 to 31 bar (in the case of the higher preload), with 0.5 bar intervals.

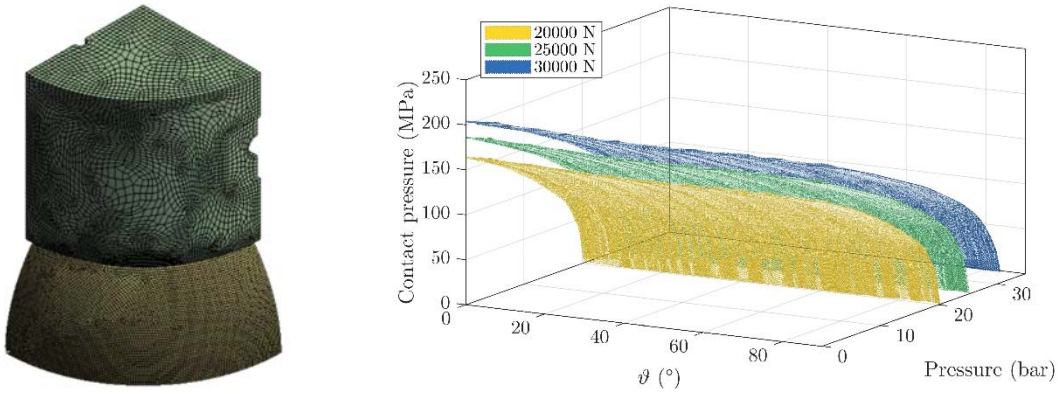

(a) (b)

Figure 4.29: (a) Three-dimensional model used to calculate the maximum contact pressures. (b) Results achieved along the contact perimeter, for different preloads and fluid pressures.

The contact pressure results of this model also presented a Hertzian distribution in the contact width. To achieve a single contact pressure value at each circumferential position, the peak contact pressure value was chosen. These results are set out in Figure 4.29 (b). As expected, no significant variation of the contact pressure occurred along the perimeter (angular position spanning from 0° to 90°). As fluid pressure increased, a contact pressure drop with the same pattern as in the two-dimensional model was observed.

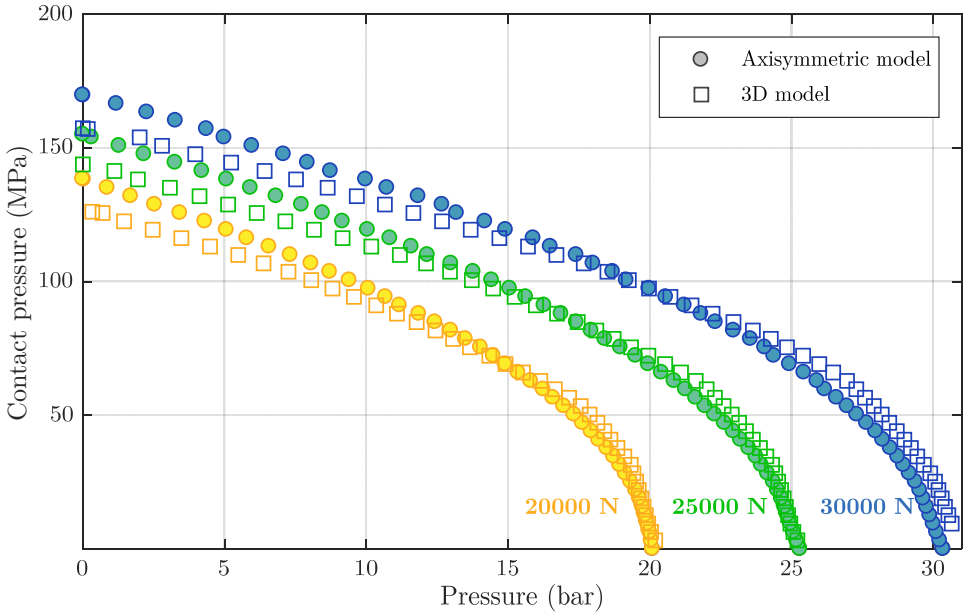

Figure 4.30: Comparison of the relationship between mean contact pressure and fluid pressure using two and three-dimensional models.

The comparison of the results for the two and three-dimensional models is presented in Figure 4.30, with preloads of 20,000 N, 25,000 N and 30,000 N. Deviations between the results provided by the axisymmetric and three-dimensional models exist, although both converge to the same pressure value when the contact pressure becomes null. As previously explained, this was expected since the balance of forces must happen when the contact is completely removed. It is therefore concluded that there are differences between the results of the two models, but a sufficiently small mesh in both models should converge to the same result. However, the limited calculation time requires this difference to be assumed.

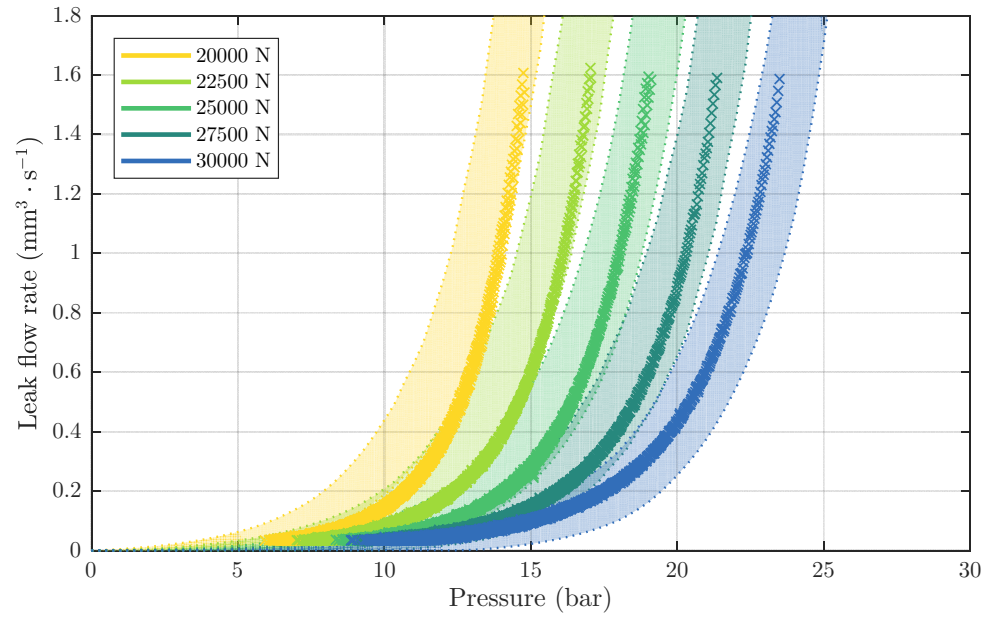

(a)

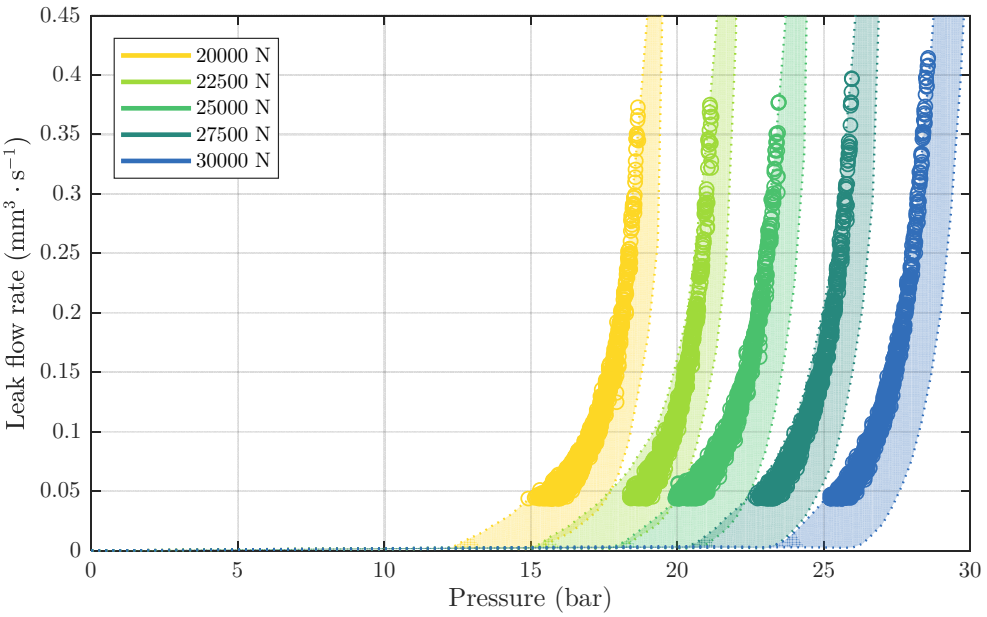

(b)

Figure 4.31: Prediction of the leakage flow rate in the axisymmetric bench in the case of (a) water and (b) Nuto H46 oil, in comparison to the experimental results.

Once the pattern of contact pressures belonging to the three-dimensional model was obtained, it was possible to predict the leakage flow rate of the system under study for each value of internal pressure. To this end, the system was virtually divided into a number of sections along the perimeter, and the mean contact pressure value was assigned to each. Based on the leakage criterion in Figure 4.28, a permeability value per unit length was assigned to each section, which permitted the calculation of its corresponding leakage flow rate (Equation (4.8)), and that of the total system (Equation (4.9)). The leakage flow rate predictions obtained for water and Nuto H46 oil are shown in Figure 4.31. The predicted results are presented as a shaded coloured area between the lower and upper prediction using the corresponding curves.

It can be seen that a good correlation between experimental results and numerical predictions was achieved. Therefore, it can be affirmed that the proposed leakage criterion is appropriate to apply to systems with geometrical variations with respect to the original bench, which require a three-dimensional simulation to obtain their contact pressure pattern. In this regard, in Chapter 5 the validation of the developed methodology is performed, using a new bench geometry which included a slot in the cylindrical seat. The aim of this slot was to weaken the seat, and to obtain a case study with non-uniform contact pressure distribution. The predicted leakage flow rate was then compared to the experimental results.

CHAPTER

5

Validation of the developed methodology

Contents

The objective of the methodology developed in this thesis is to predict leakage transient initiation and progress in the contact area between two elements. The numerical model in which this methodology is based, and the experimental tests to determine the leakage criterion are described in the previous chapters.

In this chapter the methodology is applied to a case study, which is a variant of the testbench presented in Chapter 4. A slot was manufactured in the cylindrical seat to force the leakage to occur through this weakened area. First, the experimental tests carried out with this new testbench are described. The validation is then performed in two ways: based on only structural numerical models, and using two-way FSI numerical models. The former provides a first approach to the experimental results, using models

that are simpler and more efficient to validate the results. FSI models, conversely, require more calculation time but lead to more accurate outcomes.

For each case, the construction of the numerical model and how the developed methodology was implemented is explained. Finally, the results are presented and compared. The validity of the methodology is confirmed and guidelines are discussed to improve the results.

5.1 DETERMINATION OF THE CASE STUDY

In Chapters 2 and 3 a numerical methodology was presented to predict transient leakage behaviour in a system where fluid was contained between two elements in contact. In Chapter 4 an experimental procedure was described to set a criterion to determine the start and progress of leakage. In addition, a testbench was constructed based on an industrial check-valve model, comprised of a cylindrical seat and a semi-sphere. A leakage criterion was set, valid for any geometry of testbench with the same materials and surface finish.

To validate the numerical methodology of Chapters 2 and 3, and the leakage criterion set in Chapter 4, a case study was defined to compare the results obtained from the developed model with experimental results. The model chosen for the validation was a variant of the testbench presented in Chapter 4 (Figure 5.1 (a)). This new model (Figure 5.1 (b)) had a slot cut in the external surface of the cylindrical seat, to force the leakage to occur through this weakened location. The dimensions were: height 10 mm, 40° angle and wall thickness 4 mm, in the area where the slot was located. Details of this new testbench are presented in Appendix A.

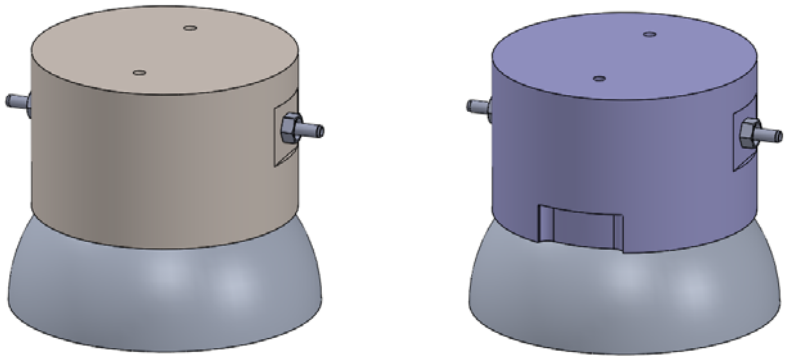

(a) (b)

Figure 5.1: (a) Virtual model of the testbench employed to determine the leakage criterion, and (b) variant of the model used to validate the developed methodology.

The contact surface between the cylindrical seats and the semi-sphere was identical in both designs: the slot did not invade the contact surface, and the manufacturing processes used in both cases were the same. However, the existence of the slot caused an unequal contact pressure pattern, attributable to the difference in stiffness along the perimeter. The area with the lowest contact pressure was the most prone to the onset of leakage.

The described case study was used in the following two approaches: (i) to create a numerical model where the developed procedure was implemented, and (ii) to setup a testbench based on the design shown in Figure 5.1 (b), and perform experimental tests. The details and results for each approach are presented in the following sections.

5.2 EXPERIMENTAL TESTS IN THE VALIDATION BENCH

To validate the results of the numerical model a testbench was manufactured based on the case study under analysis (Figure 5.1 (b)). The materials, manufacturing processes and surface finish were those used to obtain the testbench presented in the methodology to determine the leakage criterion (Figure 5.1 (a)).

5.2.1 Test procedure

The tests with the slotted seat were performed under the same terms as the tests to determine the leakage criterion, described in Section 4.3.3 (see Figure 5.2). The same five preload values were used, ranging from 20,000 N to 30,000 N, as presented in Table 4.2. The tests were carried out both with water and Nuto H46 oil.

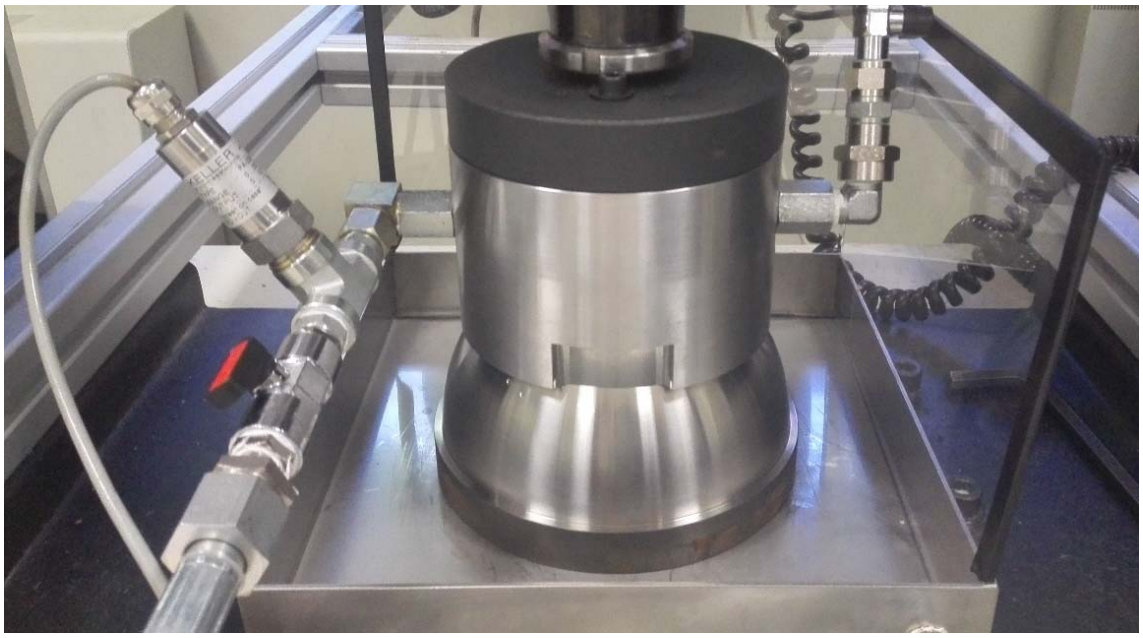

Figure 5.2: Slotted seat testbench in the universal testing machine.

5.2.2 Experimental results and post-processing

As described in Section 4.2.4, the leak flow rate was calculated from the pressure signals registered in the tests. As happened with the non-slotted bench, different pressure drop rate values were achieved for a given liquid pressure, which leads to a range of responses instead of a single value (Section 4.3.3). In each test only the pressure drop rate curves at the top of the plot were considered. As they correspond to the highest leakage flow for a given pressure, this ensures the most conservative criterion. All the results presented hereafter refer only to the cited curves.

The leakage flow rate was calculated based on Equation (4.8), which is presented in Figure 5.3 for all the tested preloads, and for both tested liquids. In all the cases, the leak flow rate was negligible until a threshold pressure value was achieved, which was higher as the preload value increases. This indicates a better sealing performance is obtained when a higher preload is applied.

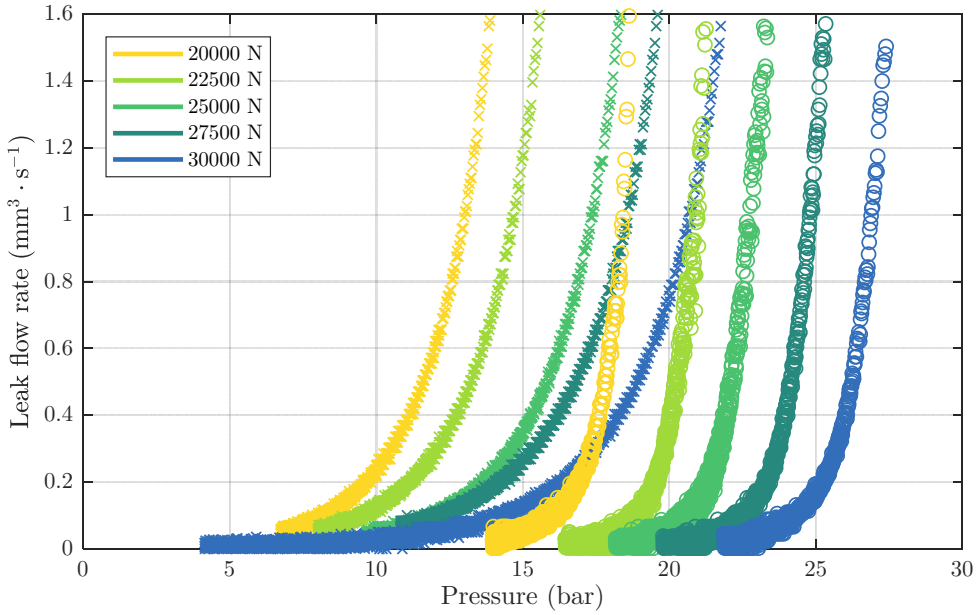

Figure 5.3: Leak flow rate in the validation model with different preloads. "x" refers to test results with water, and "o" to Nuto H46 oil test results.

For each of the preloads, leakage started at a higher liquid pressure in the case of oil. This is attributable to its higher viscosity, i.e. for leakage to occur, a lower contact pressure between structural elements is required, which is achieved when a higher fluid pressure is applied.

A particular attribute of the slotted testbench is that leakage begins from two points at the sides of the slot. This can be clearly observed in the water tests (Figure 5.4 (a)), and also in the Nuto H46 oil tests (Figure 5.4 (b)). In the latter case, leakage starting from both sides is not so marked. As oil has a high viscosity, the leaked portion remains in the contact area between the seat and the semi-sphere, and dripping starts when a sufficient amount of oil escapes.

(a) (b)

Figure 5.4: Liquid dripping in (a) water tests and (b) Nuto H46 oil tests.

The comparison of the flow rate between the slotted and non-slotted testbench is set out in Figure 5.5 for the tests using water and Nuto H46 oil tests. The results for only three preloads are presented for clearness. It can be observed that leakage occurred earlier in the testbench with a slot, which demonstrates that the slot represents a weakened area that contributes to an earlier onset of the leakage.

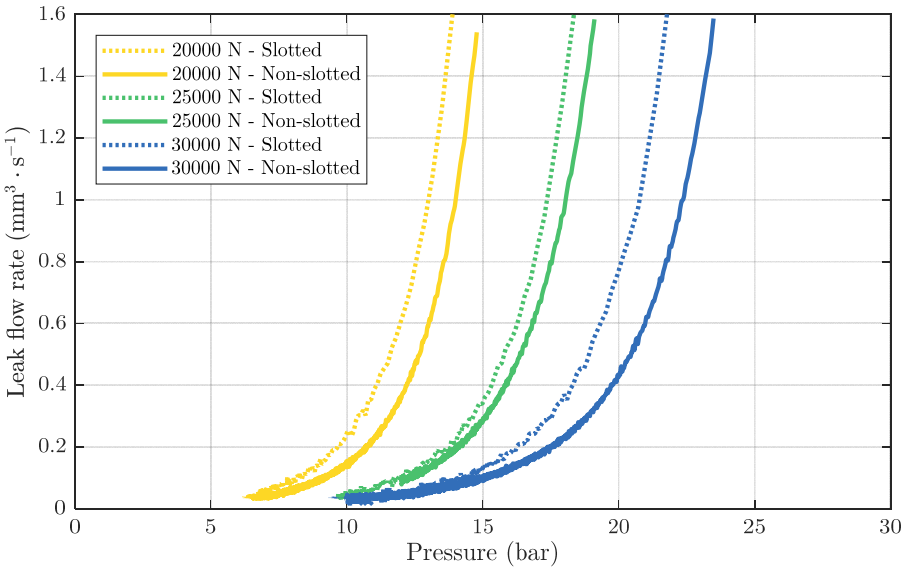

(a)

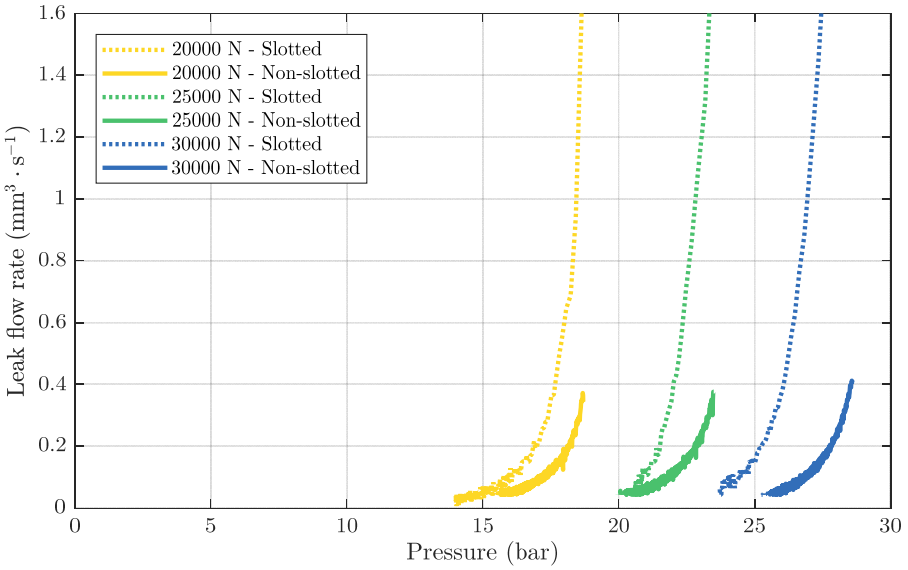

(b)

Figure 5.5: Experimental leak flow rate results with (a) water and (b) Nuto H46 oil, in the slotted and non-slotted systems, at increasing preloads.

These experimental results have to be validated with the numerical models developed in this research. The objective is to model the observed leakage behaviour in two-way numerical FSI models that provide an accurate result. However, these models

involve a high computing cost, which can be overcome with simpler but less accurate models.

Therefore, the validation of the leakage law established in Chapter 4 is first validated based on only structural models. The contact pressure distribution achieved does not take into account the fluid pressure between the solid elements as leakage evolves. However, it can be sufficient to identify the zones most prone to leakage where the contact pressure is the minimum. A first prediction of the leakage flow rate is accomplished with these models.

The implementation of the methodology to visualise the position and path of leaks, in accordance with the contributions in Chapter 2 and 3, is then carried out in an FSI model. These contributions cannot be implemented in only structural models, because the fluid domain is not modelled in this case. In addition, the FSI model considers the interaction between the fluid and the solids that the structural model lacks, and hence the results of contact pressure and leakage flow rate prediction are more accurate. A comparison of the results with both approaches is presented at the end of the chapter.

5.3 VALIDATION OF THE DEVELOPED METHODOLOGY USING STRUCTURAL MODELS

Structural numerical models permit the validation of the established leakage criterion in an agile way. In fact, the calculation of the leakage rate based on permeability determined by this criterion only requires a pattern of contact pressures in the closure zone, as shown in Figure 5.6. Structural models provide this result without considering the evolution of the leakage in the system, since the fluid pressure is established as a boundary condition on the surfaces in contact with the fluid, which do not change throughout the calculation. However, this first approximation may be sufficient in cases where this phenomenon does not involve large variations in the contact pressure profile, and provides more rapid results because the calculation of an FSI model is always more time consuming.

The flow rate prediction based on the leakage criterion stated in Section 4.3.4 requires the steps set out in Figure 5.6.

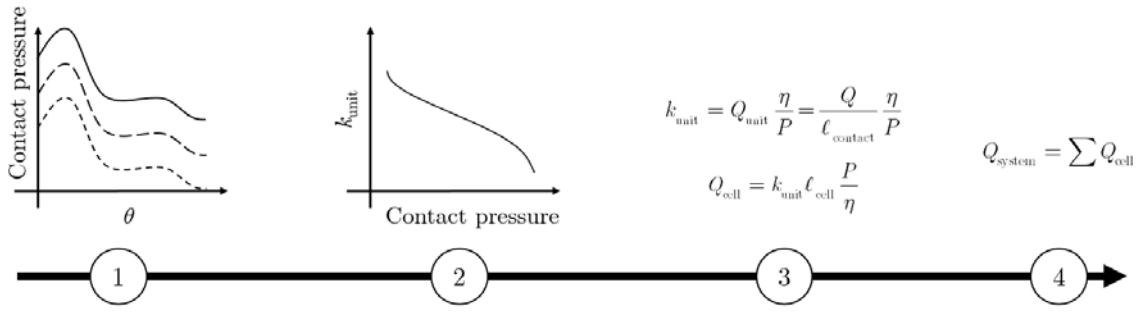

Figure 5.6: Flowchart to calculate the system leak flow rate using the stated leakage criterion.

The detail of the four steps is as follows:

1. The contact pressure distribution along the contact perimeter must be determined. These results depend on the pressure inside the cylindrical seat: the higher the pressure, the lower the contact pressure. Therefore, a total outflow leakage rate value is achieved for each pressure value.
2. A permeability per unit length value k_{unit} is assigned to each contact section (a user-determined section of the contact perimeter), in accordance to its contact pressure value, based on the leakage criterion established from the characterisation of the non-slotted axisymmetric bench.
3. The contribution to the total outlet flow rate in each section Q_{cell} is calculated based on the permeability definition in Equation (4.8). The result is dependent on the liquid contained, the work-pressure and the length of the considered section in the circumferential direction.
4. The total leakage flow rate of the system Q_{system} is calculated by adding all the individual contributions along the perimeter, as set in Equation (4.9).

The application of these steps in a structural numerical model for the slotted testbench is presented in the following sections.

5.3.1 Definition of the structural model of the slotted bench

A numerical model was used to achieve the contact pressure distribution for different fluid pressures at each preload. As the slot causes a non-uniform contact around the axis, it was necessary that the model was three-dimensional. The model was defined in accordance with the guidelines described for the non-slotted three-dimensional model set out in Section 4.4.3. To save calculation time only half of the structure was modelled, due to the symmetry condition with respect to the vertical median plane (see Figure 5.7 (a)).

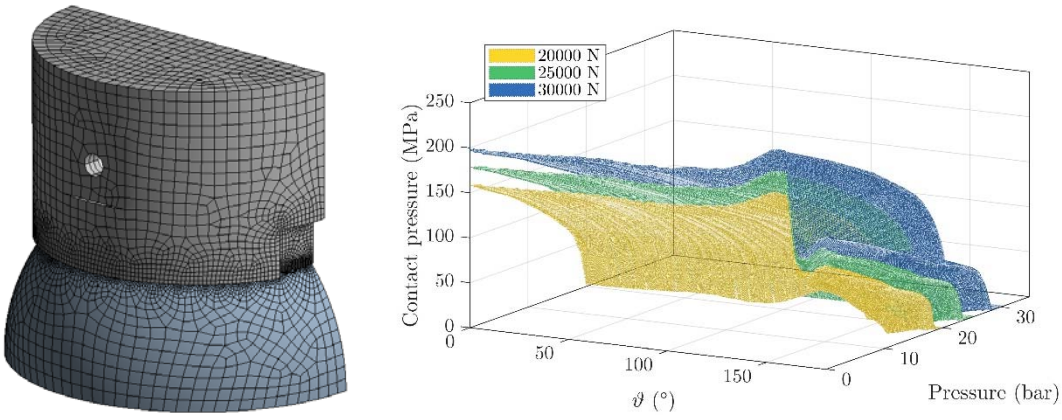

(a) (b)

Figure 5.7: (a) Three-dimensional model to calculate contact pressures in the validation model. (b) Results achieved along the contact perimeter, for different preloads and pressures.

AISI 304 was assigned to the seat and the semi-sphere (Table 4.1), and a frictional contact with a friction coefficient of 0.2 was established between them. The mesh parameters and supports were set the same as for the structural model used in the non-slotted model described in Section 4.4.3. Pressure was assigned to the surfaces inside the chamber, which increased from 0 with 0.5 bar intervals, up to the value where the components lost contact.

The contact pressure output was computed in the whole contact area between the seat and the semi-sphere. To achieve a single contact pressure value at each circumferential position, the peak contact pressure was chosen from all the nodes at different radial positions. The resulting contact pressure values are set out in Figure 5.7 (b), where only the results of half of the model are plotted for a better visualisation. The response surfaces follow the same pattern for all the preloads.

The contact pressure results showed a uniform pressure distribution in the perimeter section away from the slotted area. In the area around the slot, the pressure initially rose followed by a sharp fall to reach the minimum contact pressure value. It then increased slightly as it reached the centre of the slot. Therefore, the minimum contact pressure for the validation geometry occurred at each side of the slot. This phenomenon justifies the way in which the start of leakage was observed in both water and oil tests, as shown in Figure 5.4.

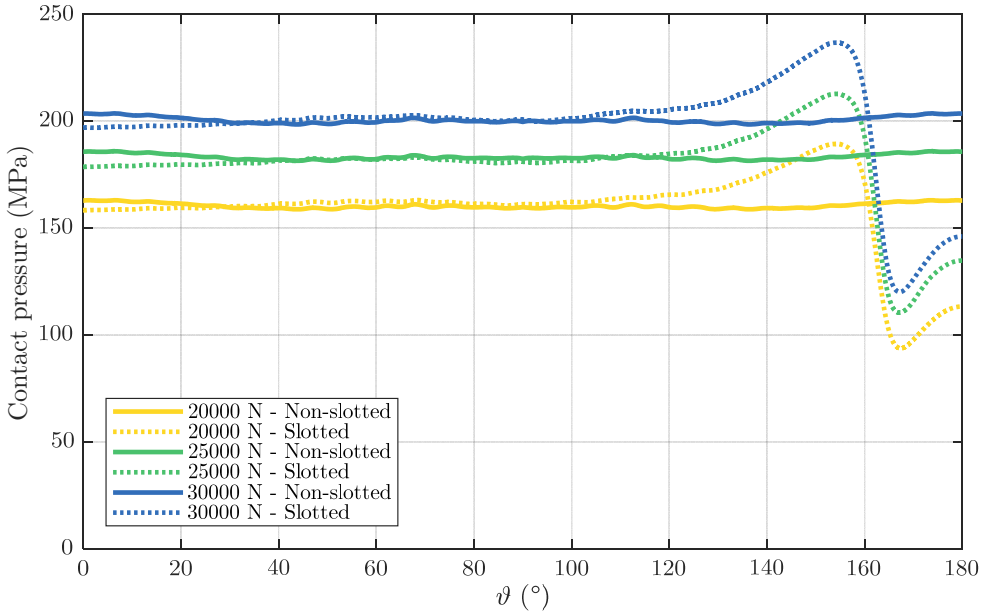

Figure 5.8: Contact pressure comparison between the non-slotted system and slotted system, for null liquid pressure. For clearness, only three preloads and the results of only half a model are shown.

If the contact pressure distribution of the slotted system is compared to the non-slotted, similar pressure values are observed away from the slot (Figure 5.8). Near the slot, higher contact pressure values can be seen that could compensate the effect of the lowest values in the slot. However, it should be noted that the relationship between contact pressure and permeability was established on a logarithmic scale. Hence, the area

of the slot is the most critical as regards leakage prediction, and this results in a higher leakage flow rate in the slotted bench.

5.3.2 Leak flow rate results

The procedure set out in Figure 5.6 was then used to calculate the leakage flow rate in the slotted validation model. The result band achieved using the leakage criterion in Figure 4.28 is presented in Figure 5.9 for water and oil.

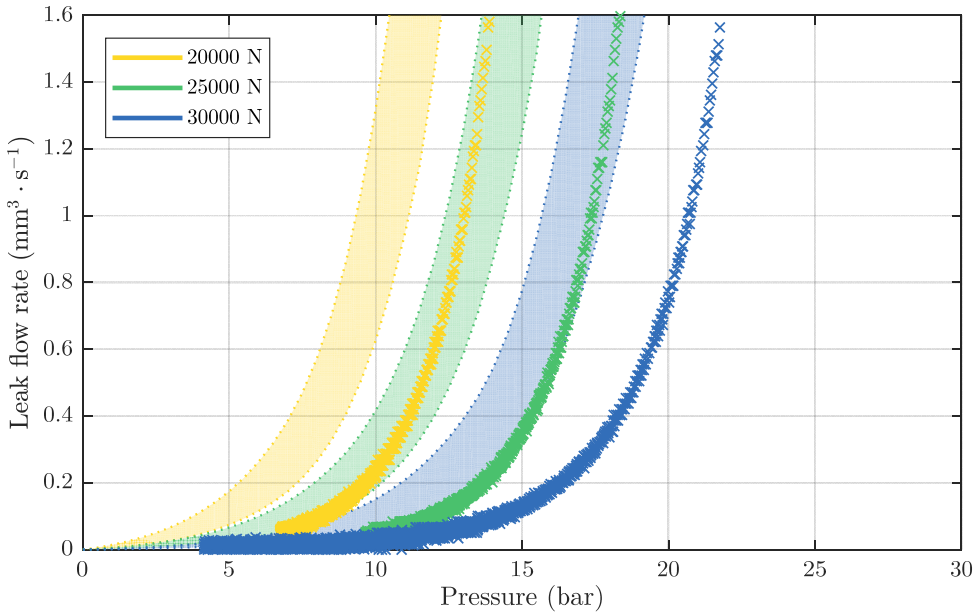

(a)

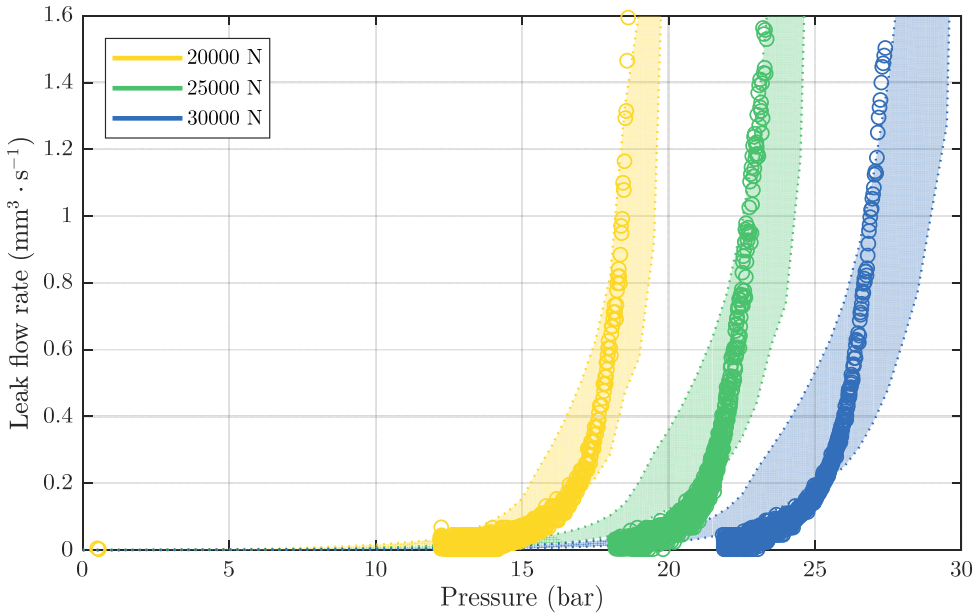

(b)

Figure 5.9: Prediction of the leakage flow rate in the slotted bench in the case of (a) water and (b) Nuto H46 oil, in comparison to the experimental results. For clearness, the results for only three preloads are shown.

A good correlation between experimental and predicted values is observed for the oil case, but not for the water. The leak flow rate trend with respect to pressure is well characterised in the case of water, and in terms of quantification the prediction is more accurate in the case of oil.

5.3.3 Discussion

The leakage flow rate predictions for the non-slotted system in Figure 5.9, were within the uncertainty range represented by the shaded area for the case of oil, but the results present an overestimation in the case of water. This result is acceptable from the point of view of designing systems that comply with a maximum leakage limit: systems would be designed with a safety margin, as they contemplate a higher leakage than that actually manifested.

As highlighted in previous analyses, one of the most influential factors in leakage flow prediction is the contact pressure. The factors that contribute to uncertainty in this parameter have an impact on the final result: the calculated peak pressure value, the real contact width, the real surface area of the seat in contact with the fluid pressure, etc.

However, a more accurate prediction of leakage flow rates could be achieved by reconsidering the leakage criterion in terms of what was presented in Figure 4.10 (b). The analysis of the pressure loading process of the system indicates that pressurisations up to a value produced discharges following the lowest curve presented in that graph (points C to G). As the pressure inside the chamber increased, the discharge curves relating the pressure drop to the fluid pressure became higher. At the limit, the pressure drop from the maximum pressurisation of the chamber was always repeated with the same curve at the top (point H, I and M). The curves obtained at maximum pressure are those used throughout the work presented thus far, on the basis that they are those with the highest leakage rate and, therefore, the highest permeability. This justifies that the prediction obtained in Figure 5.9 overestimates the experimental result.

For a comprehensive approach to establishing the leakage criterion, instead of using only the upper pressure drop curve as a function of pressure, all the curves recorded throughout the loading process can be taken into account. The analysis of the relationship between permeability and contact pressure of the non-slotted testbench is presented in Figure 5.10, where different assumptions are presented.

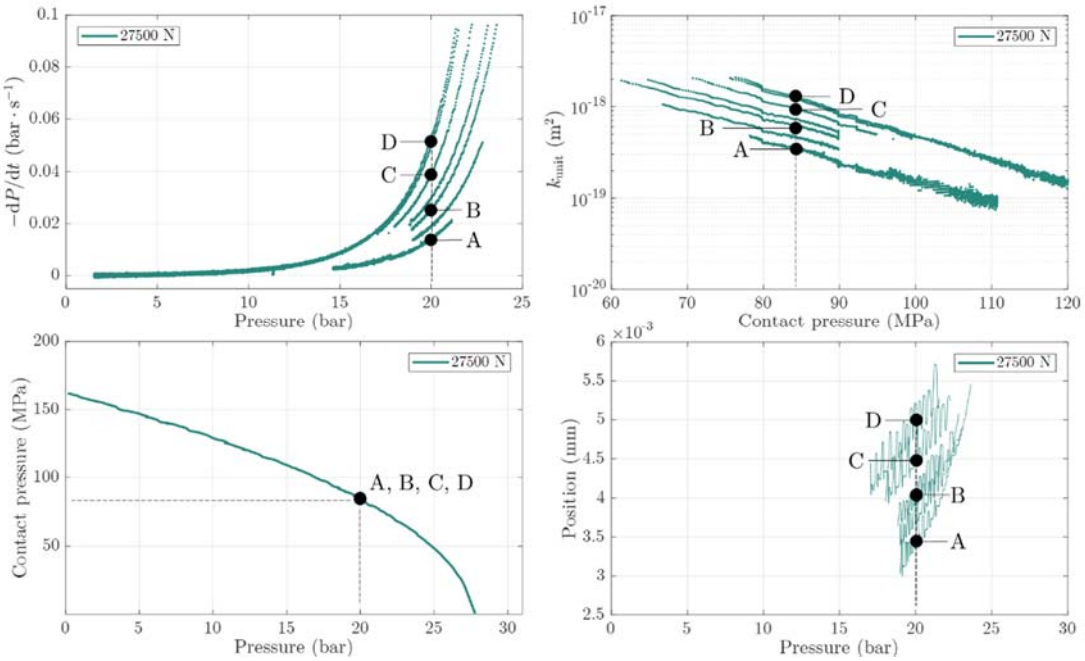

(a)

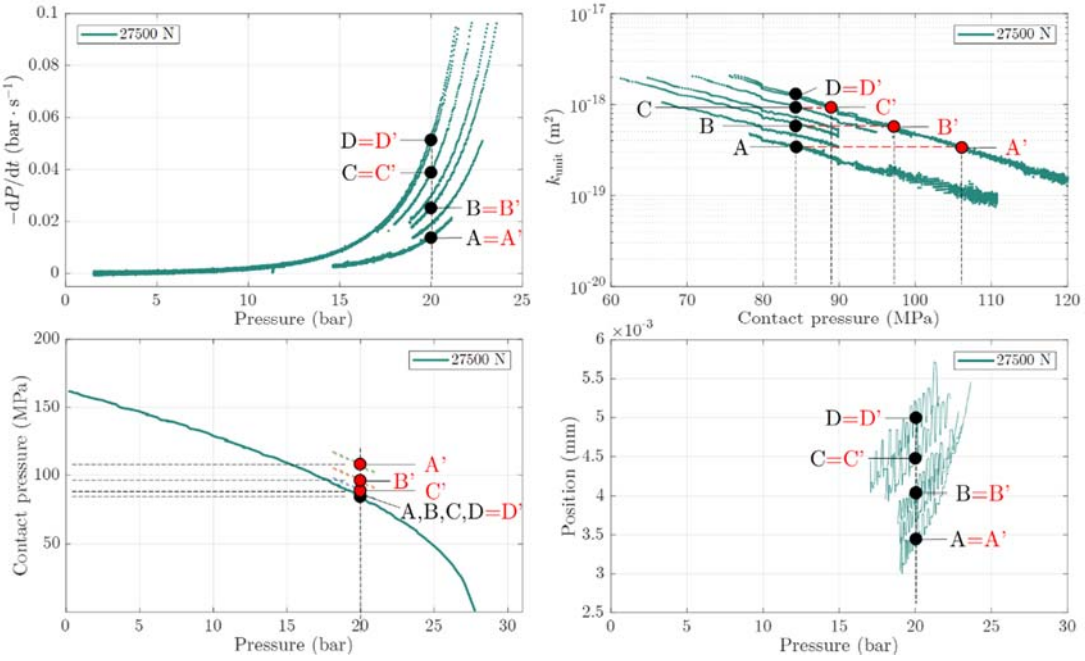

(b)

Figure 5.10: Analysis of the relationship between permeability and contact pressure under different assumptions: (a) there is a single relationship between contact pressure and fluid pressure, and (b) these relationship changes depending on the seat position. The results refer to the water test in the non-slotted bench with 27500 N preload.

Thus far, the hypothesis presented in Figure 5.10 (a) was assumed: the relationship between contact pressure and fluid pressure is univocal. In fact, this relationship was obtained by linear-static numerical simulations, which involve such univocal behaviour. This results in having different pressure drops (points A, B, C, D) for the same

fluid pressure, i.e. different pressure drops for a given contact pressure. This is because the seat rests at different positions having the same fluid pressure, as was observed in Figure 4.9 (b). As the permeability is directly related to the pressure drop (Equation (4.5) and Equation (4.7)), the system presents different permeability values for the same contact pressure (points A to D). This is incompatible with the assertion that each contact pressure value corresponds to a single permeability value.

Nevertheless, this increase in permeability is not real, as explained in Figure 5.10 (b). To begin with, it is assumed that for a given value of fluid pressure different pressure drops occur, as a consequence of the different seatings of the system described thus far. The contact pressure must inevitably vary as a result of different seat positions for the same pressure, since the interaction between the contact surfaces cannot be the same. A higher position must correspond to a lower contact pressure, which involves a non-univocal relationship between contact pressure and fluid pressure (points A', B', C' and D'). As the permeability of each point is equal to that estimated for case (a), the position of these points on the permeability relationship must be as presented in case (b). This confirms that the relationship between contact pressure and permeability is unique, and what actually changes is the relationship between the pressure and the contact pressure.

In summary, if the hypothesis that there is a single permeability value for a given contact pressure is assumed, there is a contradiction as long as a leakage criterion is used to determine the maximum leak flow rate and another for the minimum. The main problem is that there is not an unambiguous relationship between fluid pressure and contact pressure in the testbench used for characterisation, as has already been pointed out. Linear-static numerical models do not provide a representation of the actual behaviour of this system. It can thus be suggested that if the real relationship between fluid pressure and contact pressure is determined for all the cases under study, a single leakage law can correctly predict the leakage of the system.

In this regard, the relationship between fluid pressure and contact pressure should be adapted to take into account the real behaviour of the system. However, it is not possible to represent such behaviour with static-linear models, as already mentioned. To address this problem, an option is to offset the leakage criterion proposed in Figure 4.28, so as to consider an uncertainty threshold for the contact pressure. This offset, though, is not constant, and it should decrease with increasing fluid pressure. As an alternative, it is proposed to plot all the "fictitious" permeability curves obtained from hypothesis (a) in Figure 5.10, and to define the upper and lower bounds of the leakage criterion so that they embrace all the resulting data (Figure 5.11). Therefore, the upper fitting curves for water and oil remain unchanged and are defined by the coefficients in Table 4.4. As regards the new lower criteria that give rise to the minimum leak flow rate prediction, their coefficients are presented in Table 5.1. Consequently, the real leakage rate should be limited to within the two criteria described.

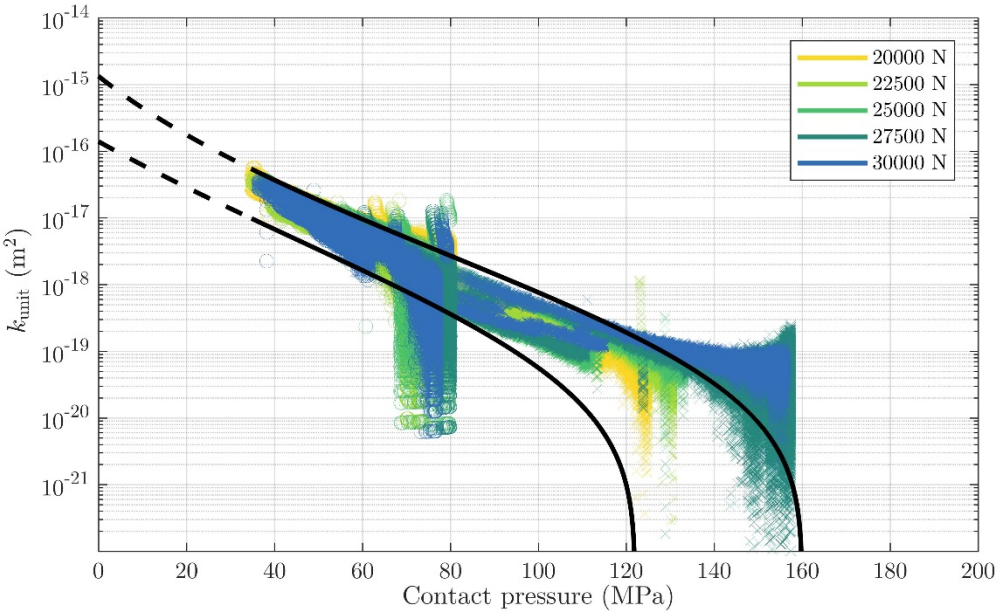

(a)

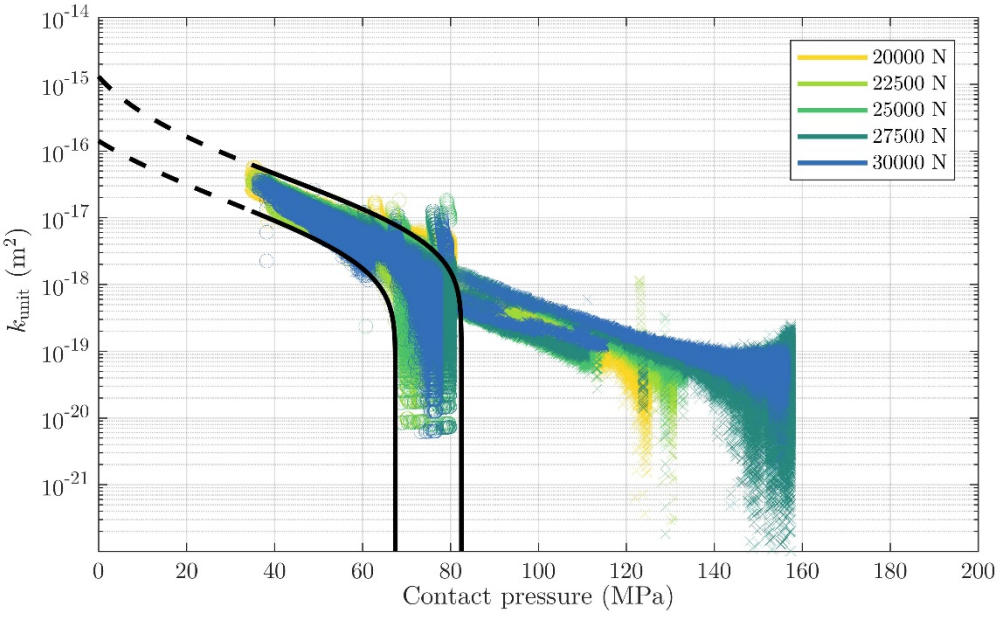

(b)

Figure 5.11: Proposed leakage criteria to account for the maximum and minimum permeabilities in the case of (a) water, and (b) Nuto H46 oil.

Table 5.1: Coefficients of the new lower fitting curve that defines the leakage criterion.

	Water Lower curve	**Nuto H46 oil Lower curve**
β	16	6
δ	36	6
λ	0.625	0.78
$\log(k_0)$ (m^2)	17.825	-11.73
$\overline{p}_c$ (MPa)	122	67.5

The leak flow rate predictions that correspond to the described leakage criteria are shown in Figure 5.12, where the coloured band presents the maximum and minimum bounds of the prediction. As can be observed, the experimental measurements lie between the two indicated predictions for water and oil.

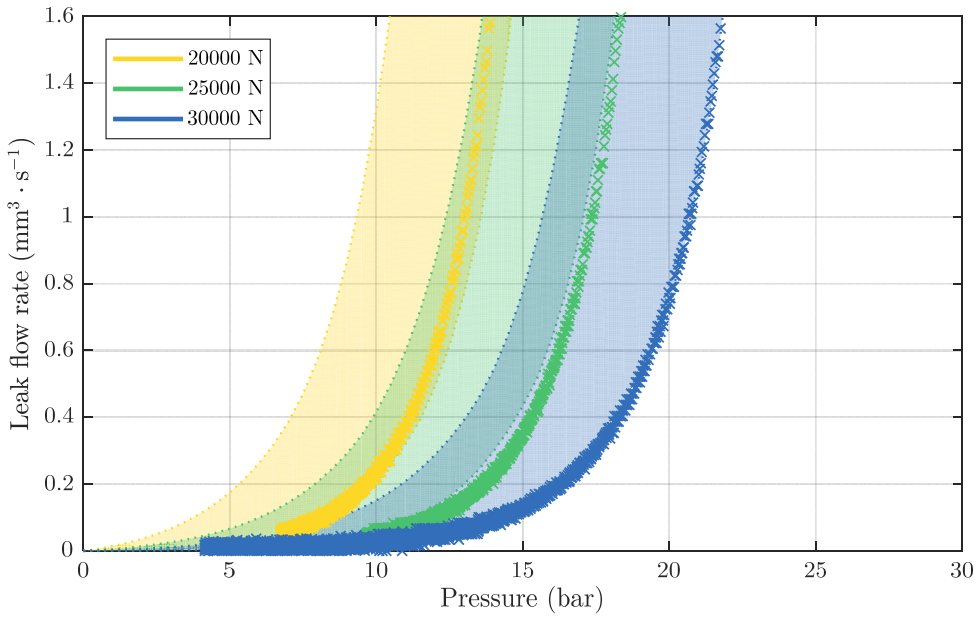

(a)

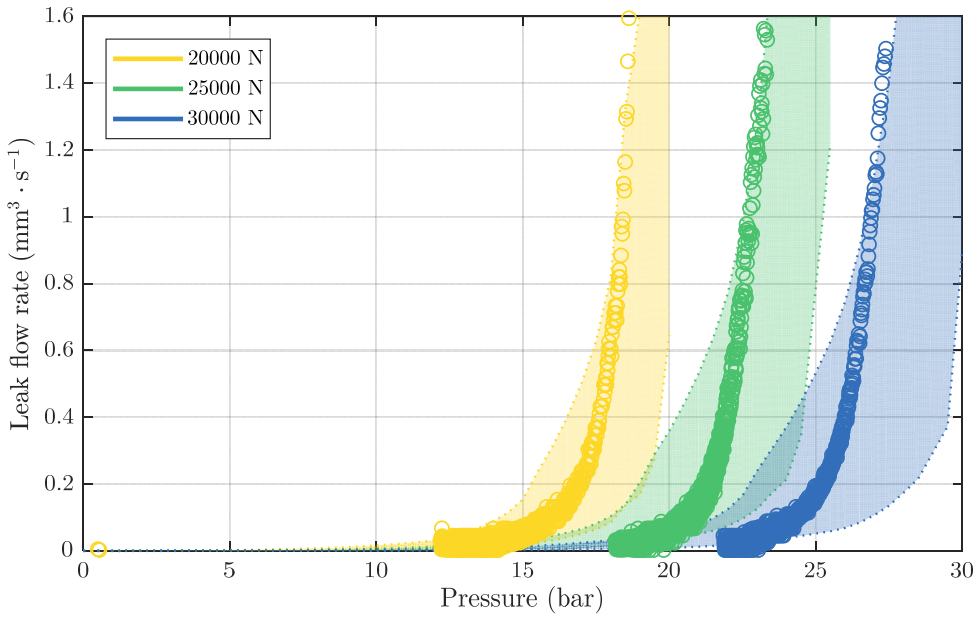

(b)

Figure 5.12: Bands representing the maximum and minimum predictions of the leakage flow rate in the slotted bench in the case of (a) water and (b) Nuto H46 oil, in comparison to the experimental results. For clearness, the results for only three preloads are shown.

In the case of water, the real result is closer to the minimum prediction, and the opposite happens with oil. The explanation for this is related to the differences in behaviour for the slotted and non-slotted testbenches. Leaks start at lower liquid pressure values in the slotted system in comparison to the non-slotted. Therefore, the fluid pressure thresholds which involve a significant increase of contact position are not reached in the case of the water, preventing the rise in permeability described in Figure 5.10. Consequently, the system presents a response curve close to the bottom boundary (curve A in Figure 5.10). In contrast, the described pressure thresholds are exceeded in the case of oil, as higher pressures are required to achieve leakage due to its higher viscosity. In this case, the abrupt change of the crosshead position occurs, shifting the response curve close to the upper boundary that corresponds to curve D in Figure 5.10.

This effect is what justifies the overestimation shown by the upper leakage criterion in Figure 5.9. In the case of water, the position of the seat always remains low, leading to the observed large overestimation. As regards oil, low seat positions are maintained for low pressures, related to lower leak flow rates than those estimated. Above a certain pressure value, a jump in the seat position occurs with a consequent increase in permeability, which brings the experimental results closer to the prediction.

5.4 VALIDATION OF THE DEVELOPED METHODOLOGY USING TWO-WAY FSI MODELS

A numerical simulation which only considers the structural model provides a preliminary insight into the benefits of the developed methodology. This approach only enables the validation of the leakage flow rate prediction based on a contact pressure pattern. Although this does not take into account fluid-structure interaction, can be a good approximation in applications where this phenomenon does not have much impact.

However, the most accurate result of contact pressures is obtained with a two-way FSI model, which may lead to a closer leakage rate prediction. Moreover, the aim of this research is also to provide a visualisation of the location and path of leakage, which can only be achieved in a coupled calculation.

A two-way coupled FSI model was developed based on the presented numerical methodology, and the established leakage criterion was implemented therein. The major limitation of this approach is the computational time required, as the fluid and structure domains must be solved simultaneously and a result that converges and satisfies both domains must be achieved. This limits the size of the elements to be used, which has a direct impact on the accurate determination of the contact pressures. In order to compare the results of the two proposals described, a model defined in the same terms was used in both cases. The validation was limited to the highest preload of 30,000 N with the two tested fluids, which was considered sufficient to validate the contributions of the developed methodology that were not tested with the previous approach.

5.4.1 Geometrical model

The geometrical model included two physical domains: (i) the fluid domain, which corresponds to the liquid inside the seat chamber, and (ii) the structural domain, which includes the semi-sphere and the slotted cylindrical seat (Figure 5.13). Both domains were generated in a single geometrical file, to ensure the best fit of both systems (i.e. the geometry of both domains had to match). To reduce the number of elements, and thereby calculation time, only half of the system was modelled. To this end, the system was divided along the vertical median plane of symmetry (i.e. the slot was divided into two). Afterwards, the structural domain was suppressed in the CFD simulation, and the fluid domain was suppressed in the structural simulation.

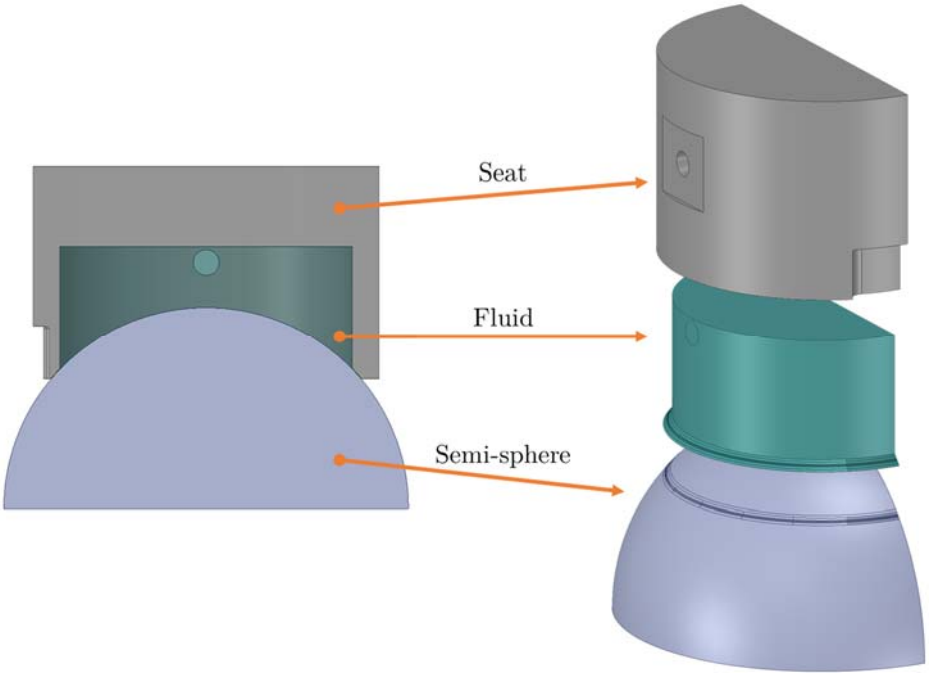

Figure 5.13: The geometrical model is comprised of (i) the fluid domain, and (ii) the structural domain (seat and semi-sphere).

The model geometry was created in accordance with the guidelines cited in Section 2.3.2. To detect leakage, a fluid domain must exist between the surfaces in contact, and this domain has to be divided into cells. The accuracy of the identification of the leakage phenomenon depends on the cell size, i.e. a smaller size delivers more accurate results. When leakage occurs, fluid is contained in these cells and a leakage path can be observed. In this work, an extension of the fluid domain with a height of 0.1 mm was created between the structural elements (Figure 5.14).

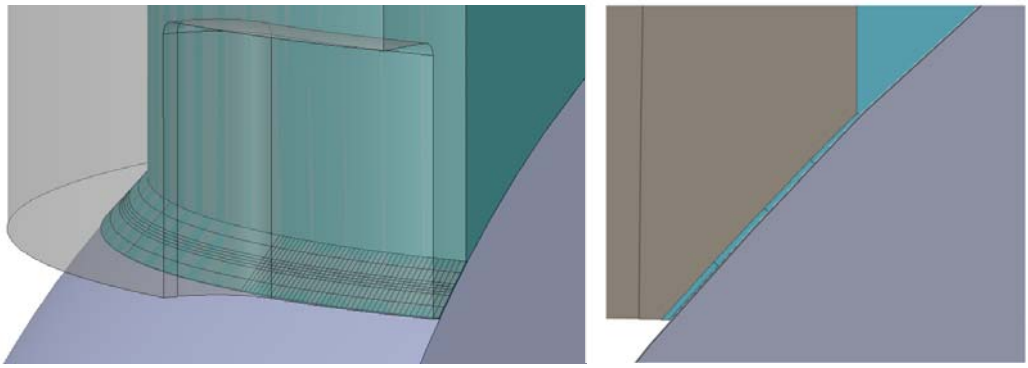

(a) (b)

Figure 5.14: (a) Detailed view and (b) cross section of the geometrical model, where fluid cells are shown between the elements in contact.

As the slot created in the seat involved a weakened section, the leakage observation was focused on that area, and therefore smaller fluid cells were located there. Leakage can happen in two directions: radial and circumferential. In the radial direction, the most critical area was that located around the contact edge between the seat and the semi-sphere. A contact width below 1 mm was predicted according to preliminary simulations (see Figure 4.16). Therefore, 4 divisions with a 0.25 mm width were created around the contact edge (Figure 5.15).

As regards the circumferential direction, the slot spanned 40°, and a geometrical division was marked every 0.5°. Therefore, 40 divisions were created in the slot area in the half model. By doing so, an approximated size of 0.5 × 0.25 × 0.1 mm was achieved in the most critical fluid cells, those surrounding the contact edge (Figure 5.15).

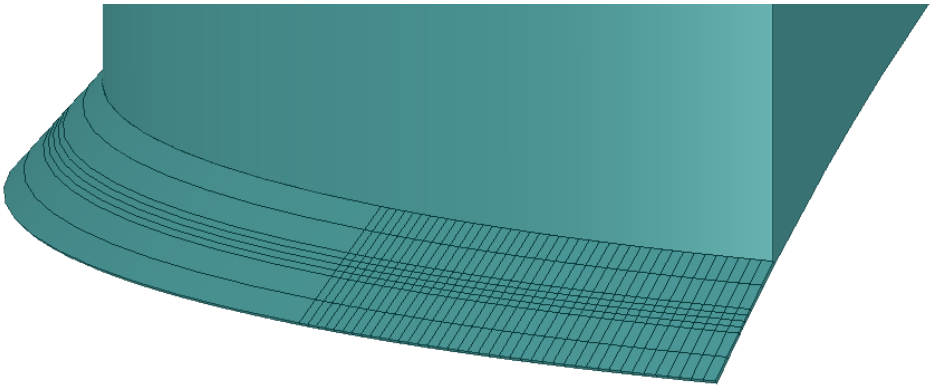

Figure 5.15: Fluid domain extension in the pathway between seat and semi-sphere, in the slot area. Small fluid cells were created to better identify leakage.

The surfaces in the contact area of the structural domain must coincide with those in the fluid. This allows the identification of the contact pressure between the components and the fluid pressure contained within in the same location. The developed algorithm determines the presence of fluid in a given cell considering these two parameters.

Therefore, the contact surfaces between the seat and the semi-sphere were divided into a structured grid. Small rectangular surfaces which matched the size of the fluid cells were created (Figure 5.16).

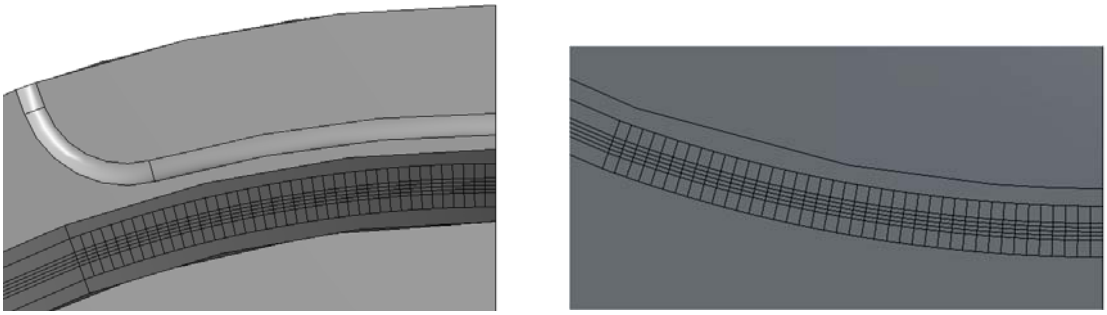

(a) (b)

Figure 5.16: Contact area between (a) the seat, and (b) the semi-sphere, divided into rectangular surfaces which match the fluid cells.

To establish the relationship between contact pressure and fluid pressure, the location of each fluid cell and its corresponding upper and lower structural surfaces had to be determined. A correlative number was assigned to each row the fluid had to cross in the radial direction, and also to each cell in the circumferential direction. Thus, fluid cells in the first row had an identification from 101 to 141, those in row two from 201 to 241, etc. (Figure 5.17).

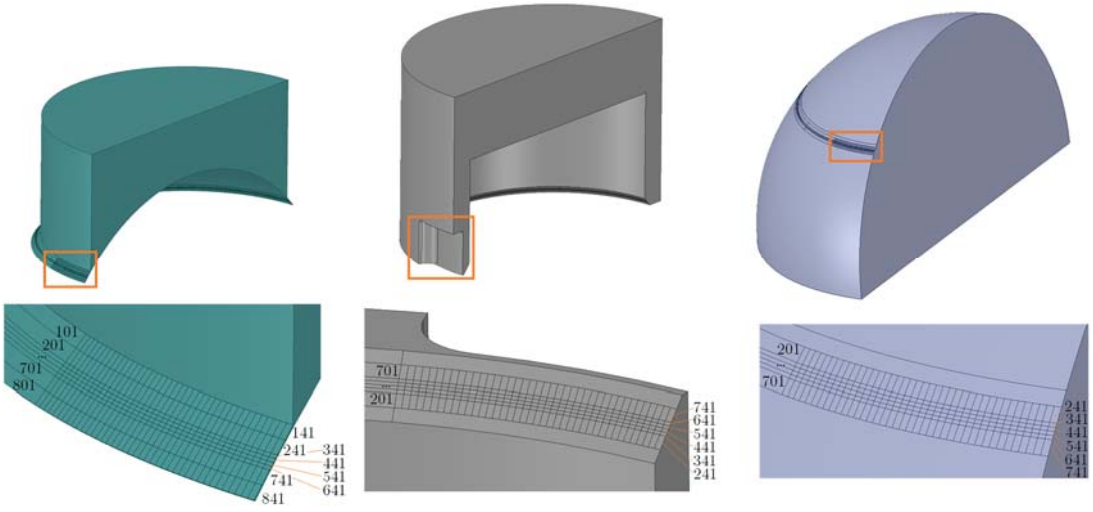

(a) (b) (c)

Figure 5.17: Identification of (a) fluid cells and their corresponding (b) upper and (c) lower surfaces.

5.4.2 Structural calculation setup

Only the structural domain was considered to proceed with the structural calculation, and AISI 304 material properties were assigned to both parts (see Table 4.1). The key features regarding this model are set out in Section 2.4.3.

A frictional contact was established between the conical surface of the seat and the whole surface of the semi-sphere, with a friction coefficient of 0.2. A contact offset of 0.1 mm was assigned. This was to ensure that the seat and the semi-sphere behave as if in real contact, even if a geometric gap existed to contain the fluid cells.

A predominantly hexahedral shaped mesh was used. The mesh size was assigned based on the model used for the non-slotted system, so that the contact pressure results were achieved with the same accuracy in both models. Hence, a general element size of 5 mm was set for the model, and the size of the elements in the smallest surfaces of the contact area was adjusted to hold 8 elements of roughly 0.1 mm, as shown in Figure 5.18. A total of 849,780 elements and 2,905,314 nodes were defined.

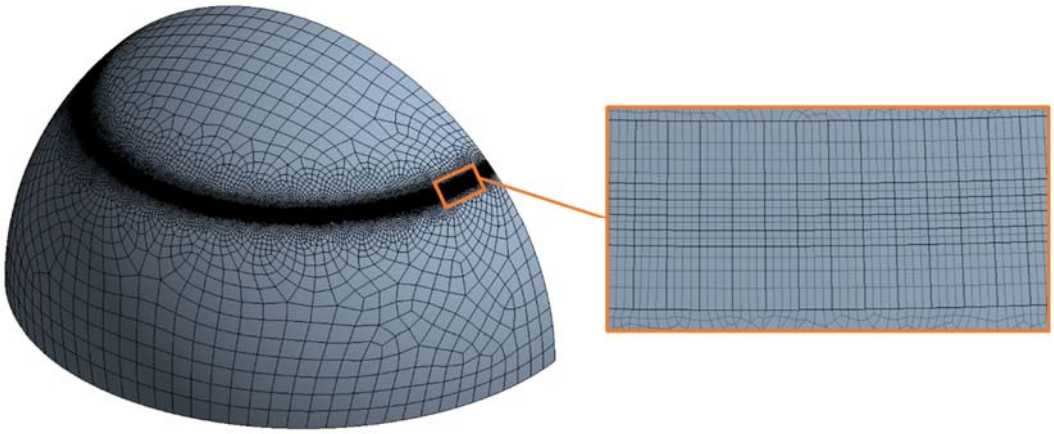

Figure 5.18: (a) Mesh employed in the model, and (b) mesh detail in the contact area.

As regards boundary conditions, the base of the semi-sphere was fixed and a symmetric boundary condition was assigned to the median surfaces. Radial and circumferential displacements were blocked in a slice created on the top of the cylindrical surface of the seat. The force values established for the validation models were the same as the ones determined in Section 4.3.3. As only half of the system was modelled, half of the force was applied to the surface on the top of the seat. In addition, to achieve a two-way FSI solution, the surfaces in contact with the fluid had to be defined as FSI interfaces in the structural solver. In this way, the surfaces exposed to the fluid were subjected to the pressure exerted by the fluid.

To model increasing pressure inside the chamber of the structure a transient analysis is required by the CFD solver. Hence, as the structural analysis must be in accordance with the fluid analysis to perform a two-way coupled simulation, the structural analysis must be defined as transient.

The FSI solution requires time-consuming calculations since the fluid and structural domains have to be solved simultaneously. To reduce computation time, it is possible to start the coupled calculation from a pressure value close to the leakage threshold. There are two options for this: (i) initialise the fluid domain at this pressure value, which forces the calculation of the equilibrium situation of the structural domain in the first coupling step, or (ii) define an initial steady-state coupling step of the coupled system when subjected to an internal constant pressure. This solution is used as the initial state

for the successive transient steps, in which the pressure is progressively increased in the fluid model until leakage occurs. From the two proposals, the solution of initialising the calculation at a given pressure is simpler if the model does not have convergence problems in the first coupling step of the calculation.

After setting up the model, the developed algorithms had to be implemented, which involved adapting them to the case study in terms of the number of rows and cells defined in the leakage area.

As a result of the implemented procedures, the following outcomes were achieved:

1. A text file per surface in the contact area, containing the identification of the contact elements therein.
2. A text file with the values of contact pressure between each pair of surfaces in the contact area. Each of these values corresponded to a fluid cell contained between surfaces. The contact pressure results were retrieved after each calculation step, and shared with the CFD solver.

5.4.3 CFD calculation setup

The fluid domain was retrieved from the system geometry, and the structural domain was suppressed to work in the fluid solver. The key aspects to set up the CFD model are explained in Section 2.4.4.

Each cell defined in the geometry is recognised as a cell zone in the CFD solver. This ensures the existence of an interface between cells, which identifies leakage when the algorithm allows fluid to pass from one cell to another. In accordance with the identification number used in the structural model, each fluid cell was assigned a correlative number according to its row and position (from 101 to 141 in the first row, from 201 to 241 in the second, etc.). In addition, the interfaces of each fluid cell in the leakage area were identified with their corresponding cell number and a suffix related to their location (e.g. 134_f was the front interface of cell 134, 241_r was the right interface of cell 241, etc.).

As regards fluid flow, the most critical zone in the model was the fluid extension between solid surfaces, because leakage was expected in this area of 0.1 mm height. Therefore, the smallest elements were located in this zone. After performing a mesh sensitivity analysis, the height was divided to contain two elements to better capture the flow, and a further two elements were created to cover the surface. Hence, 4 elements were located in each fluid cell. For the rest of the model, a growth rate of 1.2 was set, as well as a general element size of 3 mm. A total of 96,209 elements and 42,797 nodes were defined. The resulting mesh is shown in Figure 5.19. Laminar flow was assigned to the model, as turbulence is not expected in this application.

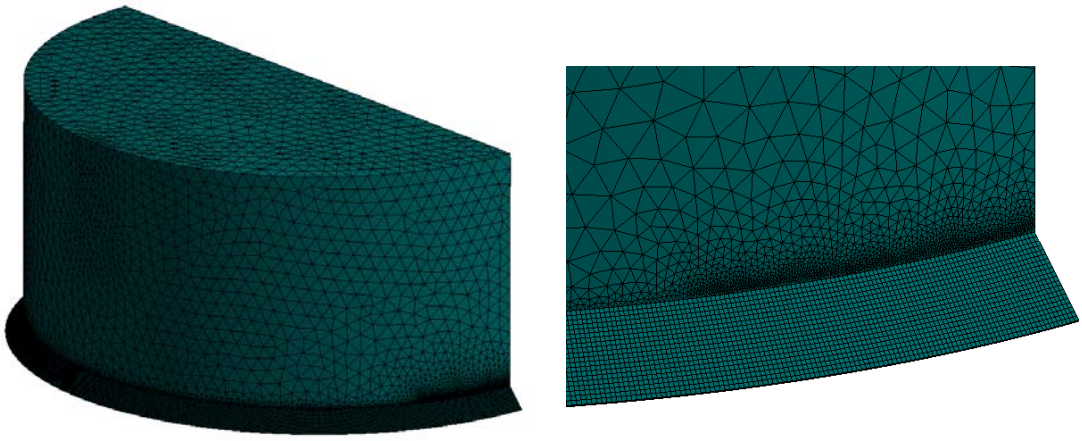

(a) (b)

Figure 5.19: (a) Mesh of the fluid domain, and (b) detail of the mesh in the leakage area.

To analyse the effect of fluid properties on leakage behaviour, water and Nuto H46 oil properties were assigned to the fluid cells in separate simulations. The data for both cases is listed in Table 4.3.

The fluid domain was initialised to null fluid pressure to obtain the behaviour of the system throughout the whole pressure loading process. A greater pressure increase was applied in the initial steps, which was reduced when getting closer to the leakage threshold. This threshold was determined based on preliminary structural calculations for each preload value.

The abovementioned pressure was assigned to the circular inlet surface (Figure 5.15), and a symmetry condition was set to the median plane. This implies that another inlet surface exists in the other half of the model, which is not the case, but as the inlet is pressure-driven there is no impact on the system behaviour.

The surfaces at the end of the fluid extension were defined as outlets. The fluid reaches the outlet only when a leakage path connects the inlet to the outlet. Otherwise, the fluid remains blocked inside the fluid chamber. The rest of the fluid surfaces (i.e. the ones on the top, side and bottom of the fluid chamber, and the ones on the top and bottom of the extension) were defined as walls.

As regards the interfaces between fluid cells, those initially allowing flow across them were assigned an *interior* boundary condition, and those blocking the flow a *wall* condition, as required by the developed algorithm. During the calculation, the algorithm changes these conditions as a result of the calculated contact and fluid pressure.

It is important to assign the correct boundary conditions to such interfaces in accordance with their initial behaviour. As stated in the structural simulation setup, contact was expected between the elements in the four rows surrounding the edge in contact between the seat and the semi-sphere. To model the fluid blocked at the entrance of these rows, all the fluid interfaces up to this region were defined as *interior*, and those

in the rows surrounding the contact as *wall*. The interfaces from the end of these rows to the outlet remained as *interior* boundaries, as no contact exists in this area to prevent leakage.

To enable a two-way coupled FSI analysis, it was necessary to assign a *System Coupling* type dynamic mesh to the interfaces between the fluid and the structure. Thus, the fluid pressure in these interfaces was transferred to the structural model, and the subsequent structural displacement was reflected in the fluid model. A *Deforming* type dynamic mesh was assigned to the symmetry plane, to permit the in-plane movement of the nodes as a consequence of the structural deformations.

The procedures developed in this research were implemented in the CFD solver (see Section 3.2.2) to analyse the behaviour of the system under the assigned pressure:

1. The variables used in the algorithm to determine the leakage path and to monitor the state of the fluid interfaces were initialised, by reading a journal file. The initial interface boundaries were defined according to those assigned in the model.

2. A Scheme algorithm was executed at the end of each coupling step, at which point a criterion was needed to determine whether the interface behaviours were kept or changed. As stated in Section 4.4.2, this threshold value can be defined within a range, thus values close to the maximum were established in both cases: 160 MPa for water, and 75 MPa for oil. The contact pressure corresponding to each fluid cell was read from the text file obtained as an output in the structural solver. If the value in a cell changed with respect to this threshold, the boundary condition in the interface changed. In that case, the fluid pressure value was kept in the subsequent coupling step, until a permanent situation was reached for that pressure value. If no condition was changed, fluid pressure was increased. Moreover, the leakage criterion in Figure 4.25 was implemented in the model. To compute the leak flow rate, the cell permeability was calculated based on its contact pressure, and the fluid pressure was retrieved from the CFD database. The total outflow was obtained as the sum of the flow rates in all cells.

5.4.4 Coupled FSI simulation setup

To perform the two-way coupled FSI simulation of the validation model, a System Coupling component was used in Ansys Workbench to link the structural and CFD solvers.

Fluid-structure interaction exists on all the surfaces where the liquid and the structure are in contact, which include the areas inside the chamber and those in the fluid domain extension between the structural elements (Figure 5.20). Therefore, each of these surfaces was assigned to a *Data Transfer*, which permitted the exchange of results between solvers (i.e. fluid pressure from CFD to structural solver, and displacements the other way around).

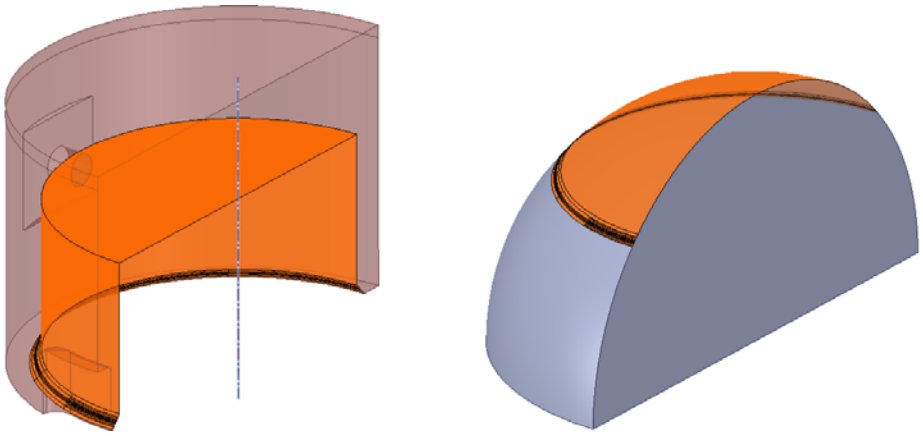

Figure 5.20: Data transfers were created in all the structural surfaces in contact with liquid.

The analysis type was set to transient, to observe the behaviour of the system as the pressure increased. This required that the structural and CFD simulations were also defined as transient.

A step size of 0.5 seconds was set for the coupled simulations, which involved a step of the same size for the solvers. A minimum of 1 and a maximum of 5 coupling iterations were established to perform the calculation.

5.4.5 Results of the two-way coupled model

The simulation of leakage behaviour in the slotted system, both in the case of water and oil, was successfully achieved and visualised. This phenomenon can be appreciated by analysing the fluid surface in contact with the semi-sphere. The existence of the leakage was confirmed by analysing the following:

1. Fluid pressure: as the leakage path was closed, the fluid pressure rose uniformly, because the fluid was contained in a closed volume. When leakage happened, a local pressure loss occurred, which can be observed in the colour map in Figure 5.21 (a).

2. Fluid velocity: as long as there was no leak, the fluid velocity remained null at all points. However, when leakage happened, a change in velocity was observed where the leak was located (Figure 5.21 (b)).

To analyse the evolution of the leak, fluid pressure was further increased beyond the onset of leakage. Once the condition of any of the interfaces changed, the fluid pressure was kept constant in the next step, to determine if the same pressure value was able to keep the leak progressing. However, as the pressure increments were small, instabilities occurred which caused some interfaces to keep opening and closing at the same pressure value. To solve this problem, the pressure was increased after a number of repetitions at the same pressure value.

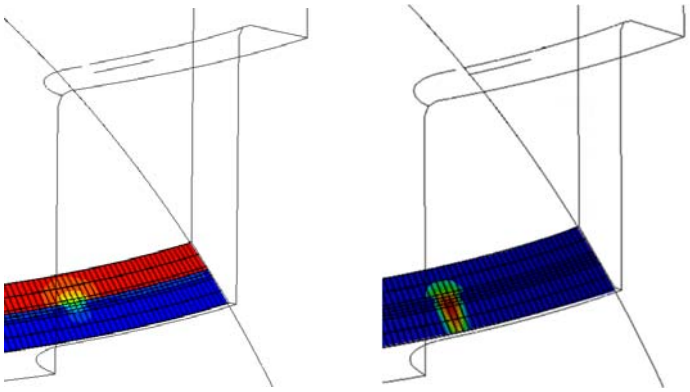

(a) (b)

Figure 5.21: (a) Pressure and (b) velocity results shown on the surface of the semi-sphere when leakage occurs.

The two-way FSI simulations were performed the same way for water and oil. A preload of 30,000 N was considered in both cases. The properties of the liquid and the contact pressure threshold were changed between simulations: 160 MPa for water and 75 MPa for oil, as stated in Section 5.4.3. As expected, leakage onset occurred earlier for water because the assigned threshold value was achieved with lower fluid pressure. In this case, the contact pressure at the whole slot area was below the threshold with null fluid pressure, thus the leakage channel spanned the whole slot. However, the corresponding permeability was so low that the leakage flow rate was still negligible. In the case of oil, the initiation of leakage was observed as from 10 bar.

Figure 5.22 shows the progression of the leakage in the contact zone for water and oil, which is represented by colouring the cells in the area in which the leakage algorithm was implemented. Bearing in mind that only half of the system was modelled, the leak started at each side of the symmetry plane of the slot as experimentally observed (Figure 5.4). At each pressure increment, fluid cells were progressively added to the leakage pathway. Those in red were the first to permit the outlet flow, and then the green and blue cells also contributed to the leakage, describing a wider leakage pathway.

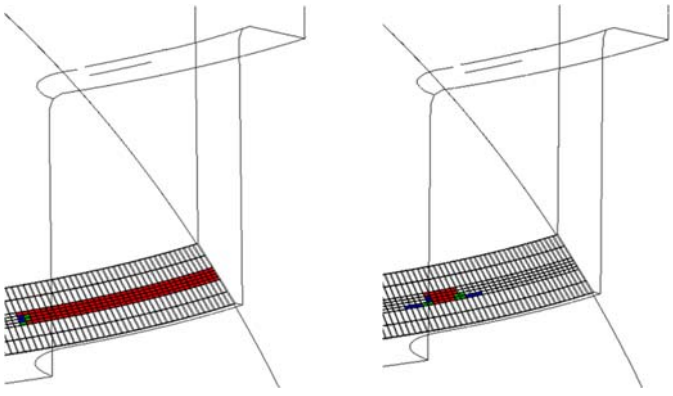

(a) (b)

Figure 5.22: Fluid cells showing the path of leakage for the case of (a) water, and (b) Nuto H46 oil. Red cells show the initial pathway, which occurs from null fluid pressure in the case of water, and from 10 bar in the case of oil. These pathways then extend to green and blue cells at each pressure increment.

To compute the leak flow rate throughout the calculation, the contact pressure distribution was needed. This was retrieved from the structural solver solution of the coupled simulation. A key contribution of these two-way FSI models is that the effect of the fluid pressure in the pathway is taken into account as leakage occurs. Figure 5.23 presents the comparison of the contact pressure distribution along the perimeter for only the structural models (Section 5.3.1), and the water and oil FSI solutions.

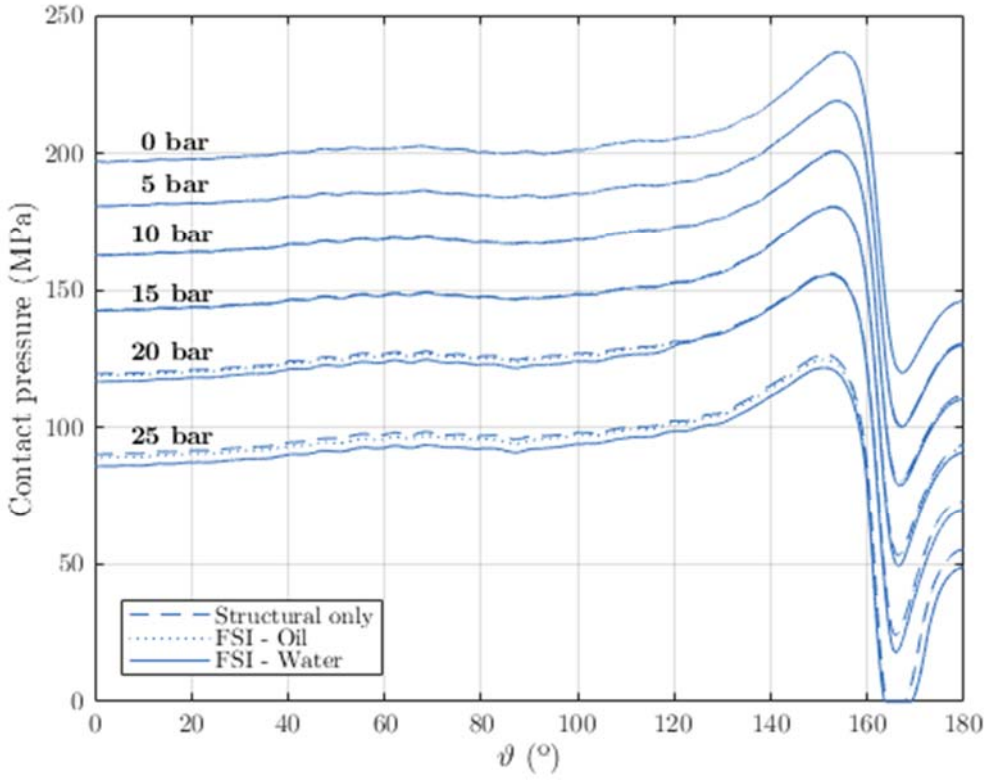

Figure 5.23: Contact pressure along the perimeter with a 30,000 N preload, at different fluid pressures. Results for only the structural model and FSI solutions are presented.

It can be observed that as fluid pressure is increased, the deviation between the presented solutions is more significant. The contact pressures decrease more in the case of water, as penetration into the leakage zone occurs at lower pressures, and pressure is exerted on a wider surface for a given fluid pressure. The differences between only the structural model and the FSI calculation with oil do not differ much. A more detailed analysis of the contact pressures in the slot area (Figure 5.24) shows that deviations occur from the beginning in the case of water, and from 10 bar in the case of oil, both coinciding with the onset of leakage described above. Once the leakage covers the complete slot area at about 20 bar in the case of oil, the contact pressures in this zone overlap for both fluids.

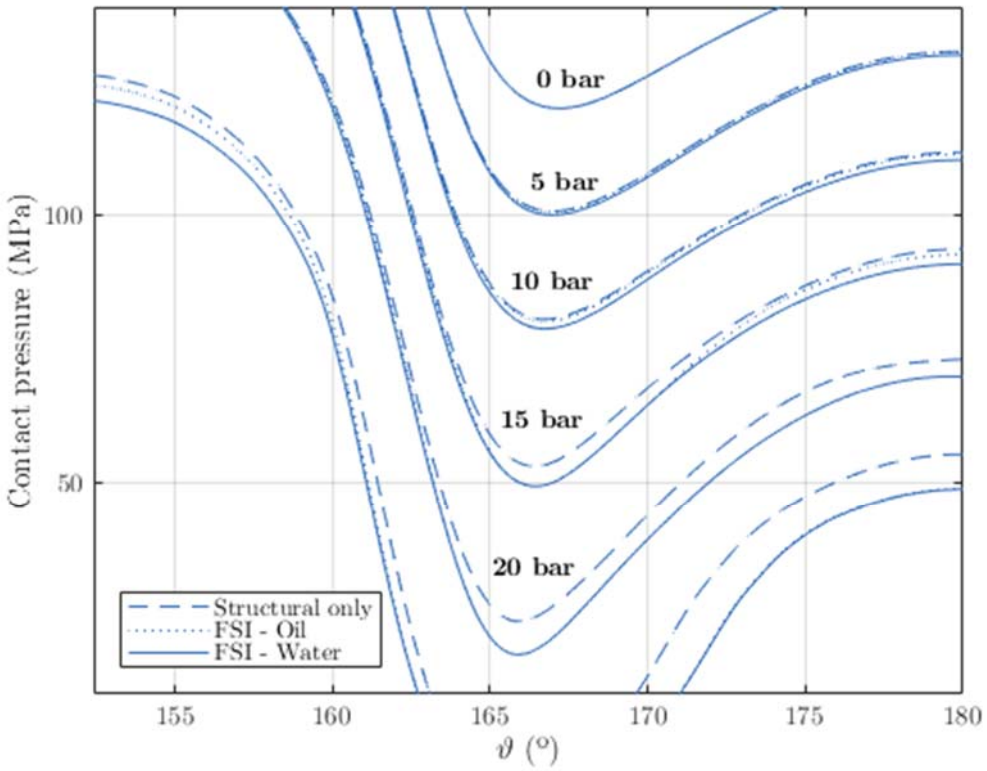

Figure 5.24: Detailed view of the contact pressure in the slot zone with a 30,000 N preload, at different fluid pressures. Results for only the structural model and FSI solutions are presented.

The leak flow rate prediction that results from the presented contact pressure distribution in the FSI simulations is shown in Figure 5.25, where it is compared to the result with only the structural model. The predictions are higher in the case of FSI for both water and oil cases, as the contact pressures are lower. The relative error between the leakage flow rates calculated with the different approaches are also presented for each case.

The results show that in the case of water the prediction of the FSI model is higher from the beginning, because it takes into account that the fluid penetrates the contact zone from null pressure. The relative error of the prediction with respect to only the structural model reaches 45 %, just before the complete separation of the structural parts. The different slopes of the error curve correspond to the progressive opening of groups of cells at the perimeter of the closure.

In the case of oil, the deviation between the two models is null up to 10 bar, when cells start to open in the slot area. From 20 bar pressure onwards, the whole slot area and some other elements in the perimeter start to open, which makes the relative error curve steeper. The maximum error reaches 60 % and then a drop happens. This is because the contact pressure in the slot area of the structural model decreases to zero, so that the resulting leakage flow rate becomes equivalent to that of the FSI model, reducing the difference observed up to this point.

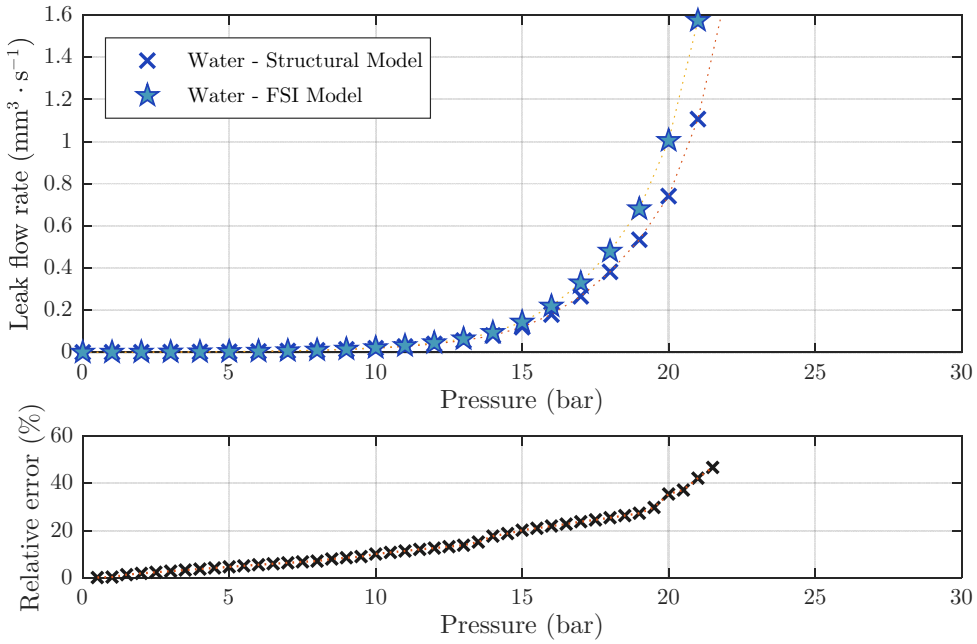

(a)

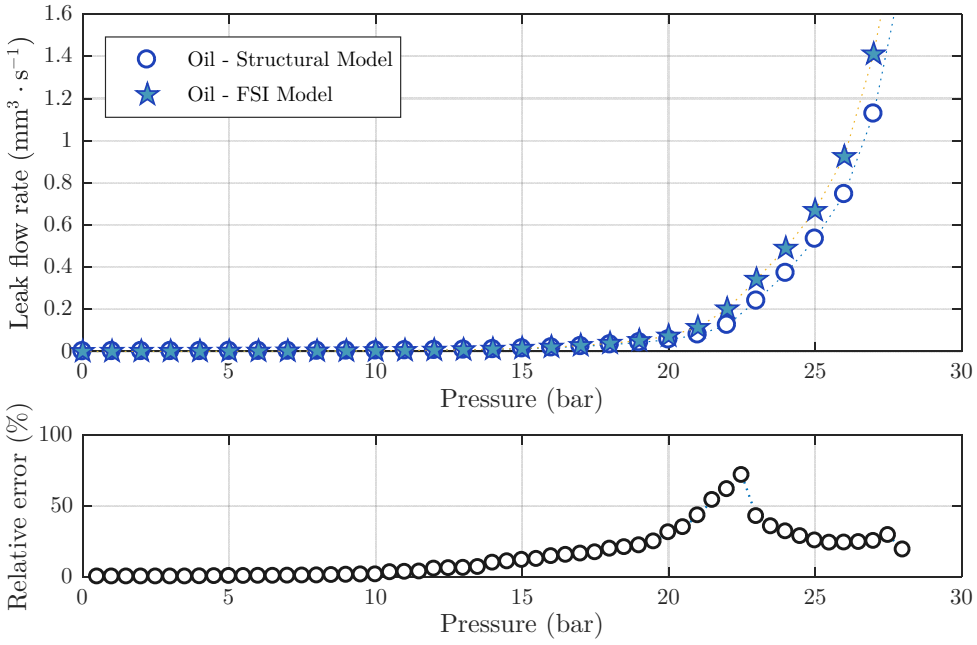

(b)

Figure 5.25: Prediction of the leakage flow rate in the slotted bench in the case of (a) water, and (b) Nuto H46 oil with a preload of 30,000 N. The solutions achieved with FSI and only structural models are compared, and the relative error is presented.

If numerical models could calculate the leakage process until the complete separation of the seat and semi-sphere, the relative error between the prediction of only the structural model and the FSI would be null, as an equal value of maximum leakage flow rate would be obtained in both cases. Figure 5.26 shows the comparison between the relative errors in the outflow rate prediction of the oil and water, between FSI and only structural models.

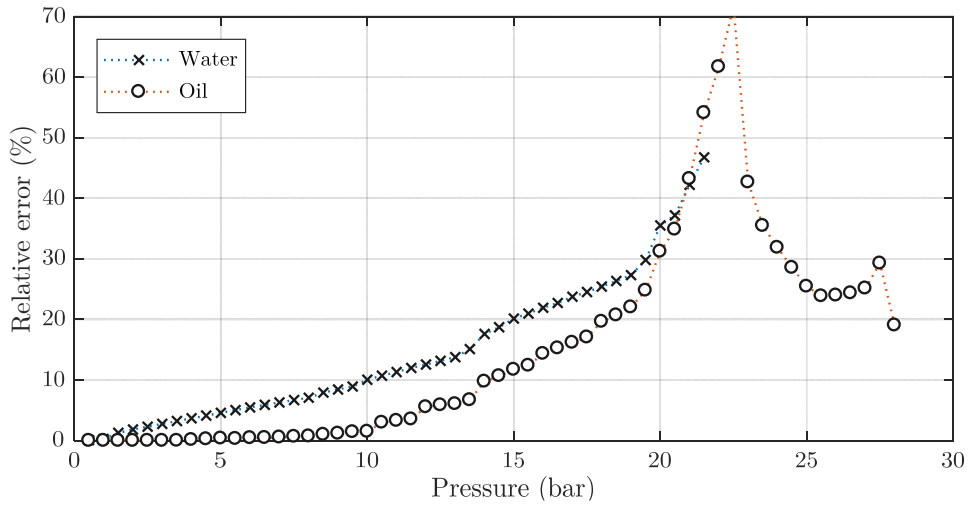

Figure 5.26: Comparison of the relative error in the prediction of the leakage flow rate, using FSI or only structural models. Results refer to the slotted bench in the case of water and Nuto H46 oil, with a preload of 30,000 N.

It can be observed that the difference in prediction is larger for the case of water, except in a small range. Furthermore, in the case of water the deviation occurs from the initial instant. Hence, it can be concluded that the use of FSI models for leakage prediction is more important in the case of lower viscosity fluids, because leakage starts at lower fluid pressures. In this sense, if the contained fluid is a gas this aspect becomes particularly important, and the use of FSI simulations is essential to achieve an accurate result.

Finally, it is important to note that the leakage rate computed by the flow solver cannot be taken into consideration. In fact, this result is calculated as a function of the fluid properties, the pressure drop and the geometry of the leakage channel. The developed model actually determines the dimension of the leakage channel in the circumferential direction, but the height at the instant of leakage corresponds to the arbitrarily chosen height of the fluid cells in the channel between the structural elements. Therefore, the leak flow rate that corresponds to a channel of that height is greater than what occurs through the real gap of the leak. As a solution, the fluid cells at the outlet could be identified as porous media, whose properties would then be controlled by algorithms to regulate their permeability in accordance with the leakage criterion established in this dissertation.

5.5 DISCUSSION

The methodology developed in this research enabled the simulation of a leakage condition through two metallic bodies in contact. The criterion controlling the fluid flow across the fluid cell interfaces was determined from experimental tests.

The validation of the methodology developed in this dissertation was performed using (i) only structural numerical models, and (ii) two-way coupled FSI models. The

latter is the only numerical solution in which the algorithm for finding the leakage pathway can be implemented, as it requires the results of both the fluid and structural domains. In this regard, a visual representation of the leakage was obtained, which was located consistent with the experimental results (Figure 5.4). FSI models were employed for water and oil analysis, with a preload of 30,000 N. The threshold contact pressure value for leakage initiation was specific for each liquid. When contact pressures lower than the threshold were identified, the model permitted leakage flow across the corresponding cells, which happened at null pressure with water, and at 10 bar pressure in the case of oil.

By means of the leakage criterion defined in this work, the leak flow rate can be predicted based on the contact pressure distribution along the perimeter. To this end, using only structural models is a solution which is less time consuming than FSI simulations. The achieved results are shown in Figure 5.12, which demonstrate the validity of the methodology developed to obtain a good prediction.

Nevertheless, only structural models do not take into account either the complex pressure distribution in the fluid chamber or the effect of fluid pressure between the solid elements in the closure as leakage evolves. In fact, this is one of the main strengths of the two-way coupled FSI models, which provide a more accurate result in terms of contact pressure. The differences in the distribution of the contact pressures for the different models are shown in Figure 5.23, where a different result can be seen depending on the liquid for the FSI results. The lower the viscosity, the earlier the leakage occurs and therefore, the lower the contact pressure in that area.

As a consequence of the observed differences in contact pressure patterns, the leakage rate prediction also differs depending on the model used. The leakage flow rate prediction of the FSI model is also more reliable, due to its higher accuracy. The difference in this estimation for the two employed models is shown in Figure 5.25.

Although the prediction is more accurate in the case of FSI coupled models, the minor deviations observed do not justify the use of such a complex model in the validation system under analysis. The two-way coupled FSI model requires simultaneous solution of the fluid and structural domains, which involves a high computational cost. The calculated solution must ensure convergence of results not only in each domain, but also in the exchanged variables (i.e. fluid pressure and displacements), which requires a greater number of iterations than resolving only one of the domains. The need for extensive resources is not justified if the output achieved with simpler models provides an equivalent result. The reason this happens in the case study of this dissertation is that the closure area in which the fluid-structure interaction occurs due to leakage is small.

Nevertheless, the strengths of the developed numerical methodology become apparent in applications where the fluid leakage expands over large surfaces. This is the case, for example, in flange joints, where large contact surfaces are closed by bolts. A high-pressure leakage can cause non-negligible resultant forces and therefore, the methodology developed is a key to accurately predict the behaviour of such systems.

Another important issue that was not considered in the present research is the potential application of the developed methodology to thermal problems. The two-way coupled FSI models in this work only exchange the pressure exerted by the fluid, and the displacement of the structure between the CFD and structural solver. However, FSI models can also be used to accurately model the convective heat exchange between the fluid and the structure. This makes it possible to determine the evolution over time of the resultant non-uniform contact pressure distribution, due to thermal expansion. In applications involving thermal loads, these parameters can be transferred in the leakage area, for a more realistic analysis of the system conditions.

CHAPTER

6

Conclusions

Contents

This investigation aims to numerically connect isolated fluid chambers, and to analyse under which conditions fluid travels from one to the other. The focus of this reasearch has been to determine when and how leakage occurs through the contact between metallic elements, and to give a prediction of the leakage flow rate.

A methodology was developed and implemented in FSI simulations, taking into account the interaction between the fluid and the structure, to achieve an accurate and complete representation of leakage phenomenon.

The law that determines the leakage behaviour in terms of permeability and contact pressure was established based on experimental results. The tests were performed using a testbench that represented a simplified industrial valve. A variation of this bench was then used to assess the validity of the proposed leakage model.

This chapter presents the general conclusions and future directions of this doctoral thesis.

6.1 CONCLUDING REMARKS

The principal aim of the present research is to develop a numerical methodology to connect isolated fluid chambers considering two-way fluid-structure interaction coupling, which was used to model leaks between elements in contact.

The topic of interest was focused on studying leakage through metal-to-metal contacts in industrial valve systems. The models and testbenches designed during this research were therefore based on a simplified axial flow check-valve. This system was comprised of a metallic cylindrical seat in contact with a metallic semi-sphere. The inner chamber of the seat was designed to contain pressurised fluid, the sealing of which was achieved by maintaining a force between the two components. The principal challenges to address were the following:

- Define a numerical methodology to connect isolated fluid chambers.
- Define a numerical methodology to identify the leakage path.
- Define a criterion to determine leakage initiation and leak flow rate, based on experimental tests.
- Implement the resulting algorithms in two-way coupled FSI simulations.

As a first step, a numerical methodology was developed to connect two initially watertight fluid chambers. In numerical models, two separated fluid domains cannot be subsequently connected if no fluid elements exist between them. To address this problem, fluid cells were defined in the pathway between the two fluid domains, the number of which was determined by the number of steps required to transition from one chamber to the other. The behaviour of the interfaces between those cells was changed using an algorithm, to determine whether fluid flow was permitted across them. Fluid cells of insignificant height were placed in the contact zone of the structural elements, creating an artificial separation between them. While no fluid was contained in these cells, the structural elements behaved as if in contact. When fluid was contained in the cells of the passage, contact pressure between the bodies decreased due to fluid pressure.

After defining the basis of the numerical methodology to connect fluid chambers, further development was required to determine the most probable leakage path. As the geometry of the domain in which leakage occurred was influenced by the insignificant height of the fluid channel between the structural elements in contact, the fluid could only move between cells in a planar motion: forwards, backwards or sideways. One further consideration to take into account was that a cell containing fluid could switch to the opposite state. To determine the leakage path, an algorithm was defined that relied on two registers: one that stored the cells containing fluid, and another that recorded the interfaces that allowed fluid flow between cells. The algorithm checks the cells containing fluid to: (i) identify whether closed interfaces become open, and (ii) verify whether open interfaces still meet the condition to remain unchanged. When an interface opens, fluid enters a new cell and thus it is added to the record of cells containing fluid. Conversely,

if an open interface becomes closed, the adjacent cell must be removed from the corresponding register, unless it maintains the condition of containing fluid through another interface. When a set of fluid cells allows the connection between the inlet and the outlet, a leakage path is defined. The fluid pressure value when this connection occurs defines the leakage onset threshold.

The methodology and algorithms described thus far provide the basic framework to identify leakage in a numerical model. However, it was necessary to define a criterion to determine the condition under which the boundary condition of the interfaces between fluid cells changes from closed to open, or vice versa. This criterion had to take into account the conditions in both the structural and fluid domains at the location where the leak progress was evaluated. The key parameters identified to carry out this assessment were (i) the fluid pressure and fluid properties, from the fluid perspective, and (ii) the contact pressure exerted on the cell adjacent to the interface being assessed, from the structural perspective.

A methodology was proposed, based on experimental testing, to determine a leakage criterion that was later implemented in the numerical FSI models. A testbench was designed and manufactured, which comprised of an axisymmetric cylindrical seat and a semi-sphere, both made of stainless steel. The bench was tested using a universal testing machine, which provided the necessary force to maintain the sealing of the inner chamber of the seat. This force was kept constant while the pressure of the fluid inside the seat was increased using a manual pump. Water and Nuto H46 oil were used as fluids in the experiments. The fluid pressure was registered throughout the tests using a pressure transmitter, to identify any positive or negative variation. Indeed, the developed methodology establishes a relationship between the leakage initiation and the pressure drop rate. To this end, outlet flow was described based on the pressure drop rate employing the bulk modulus of the liquid used in the tests. This relationship was successfully validated by complementary experimental tests.

The purpose of the current task was to define a leakage onset criterion valid for any fluid and closing force, and to determine the corresponding leakage flow rate. Variations in geometry, both in size and geometric details, were allowed provided that the sealing contact area remained unchanged, and the same materials and surface finishes as in the reference testbench were used. The definition of this law had to be set in non-specific terms to be considered universal, i.e., the terms should not be associated with the specific parameters used in the tests. From the structural point of view, the key factor was to define the leakage law as a function of the contact pressure, in order to disregard the force value and specific dimensions of the system. As regards the fluid, the relationship was established on the basis of the permeability of the system, which contemplates in a single term the outflow, the fluid pressure and the viscosity of the fluid.

The empirical findings of this study present the same trend in the results with different loads and fluids in a wide range of the contact pressure. All the resulting measurements in a semi-logarithmic plot that established the relationship between permeability and contact pressure could be considered to lie along a line with a negative slope. The contact pressure values were identified as crucial to properly identify these lines, so that

a single behaviour was achieved independently of the applied preload and the liquid tested. As it was not possible to experimentally measure the contact pressure it was necessary to obtain it from numerical simulations.

A preliminary proposal for a leakage criterion was made on the basis of the linear trend described above, with the advantage of being independent of the fluid. However, it lacked information on the behaviour at both low and high contact pressures. In this sense, it was not possible to define the threshold contact pressure at which an effective seal occurred. This behaviour was indeed observable in the measurements at higher contact pressures, but it showed a fluid-dependent result.

To enhance the definition of the leakage criterion, this work presents a new proposal based on a Weibull distribution, which provides the definition of the leakage behaviour over the whole range of contact pressures. A correct adjustment of the required parameters permits the representation of the response of the system with different fluids.

As a contribution of this research, a prediction of the leakage outflow rate was enabled based on the permeability at each location in the perimeter of the contact. Each of these permeability values was assigned based on the leakage criterion, in accordance with the contact pressure calculated in the structural model. The prediction of the leak flow rate was then made for a second bench, which varied from the reference testbench with a slot that spanned 40° in its perimeter. The experimental and predicted results presented good agreement.

The outcomes of the developed methodology were implemented in two-way FSI simulations, which means that the deformation of the solids due to the fluid pressure were calculated, and the fluid flow was updated in accordance with the changes in the structural domain. Structural and fluid solvers were set as required by their respective specifications, and coupled calculations were carried out using Ansys software. The main steps of the calculation were:

- The structural solver performed a coupling step calculation, taking into consideration the fluid pressure on the fluid interaction surfaces. The resulting contact pressure on the fluid cells was exported to a text file.
- The fluid solver updated the geometry of the fluid domain to consider the structural displacements, and performed a coupling step calculation.
- The *System Coupling* module checked the convergence of both solvers, and the pressure and displacement data interchanged. In the case of convergence, the calculation proceeded to the next step; otherwise, the coupling step calculation was repeated in both solvers.
- The algorithm in the fluid solver checked the status of the interfaces between fluid cells in the leakage zone. The contact pressures calculated in the structural solver, and the fluid pressures and fluid properties from the fluid solver were taken into account. The boundary condition at each interface was assigned as dictated by the leakage criterion experimentally established.

The fluid pressure in the seat chamber of the FSI model was progressively increased to determine the leak initiation threshold. Simulations were performed using water and Nuto H46 oil as liquid.

The results of the validation simulations revealed that the developed methodology effectively predicts leakage phenomena. The progress of the leak was clearly observable attending at the fluid cells in the pathway: (i) they acquired the pressure value in the chamber as leakage developed, and (ii) when the leak reached the outlet, the flow velocity was reported in them.

The experimental tests performed to establish the leakage criterion were repeated using the slotted bench, and the results achieved were compared for the purpose of validating the numerical models. A minimum and maximum boundary of the leak flow rate prediction was determined in the basis of the behaviours observed during the characterisation of the axisymmetric testbench. It was concluded that the developed methodology enables a correct definition of this band. Furthermore, the use of FSI coupled simulations was found to be more relevant when modelling the leakage behaviour of low viscosity fluids, as their effect on the structure occurs from lower pressures.

The scope of this study was limited in terms of the fluid employed. Experimental quantification of leakage was based on the pressure loss rate measured by the pressure transmitter. Such a loss of pressure is easily detectable regardless of how small the leakage is in the case of liquid. However, in the case of gas a significantly higher leakage must happen to reach the same pressure loss. Consequently, this research only considered liquids contained in the seat chamber.

As regards the developed algorithms, they proved to be able to predict and show the leakage progress. The fluid pressure was gradually increased at each step, and a possible change of condition was checked at the interfaces between the fluid cells. If any change occurred, the pressure was not increased in the subsequent step, in order to verify the evolution of the whole system under this condition.

The design of the testbenches themselves resulted in one of the most relevant sources of uncertainty, which had impact on the results. This research focused on developing knowledge concerning industrial valves, and therefore the system under study was based on sealing geometries used in this sector. Specifically, the analysed sealing involved a cone-to-sphere contact between a seat and a semi-sphere. It was observed that this system does not exhibit one-to-one correspondence between fluid pressure and contact pressure. This is because the seating occurs at different contact diameters on the semi-sphere. Depending on the applied pressure sequence, the seating position shows a hysteretic behaviour which is not predictable by the numerical models used. The changes in position affected the contact pressures in the leakage area and therefore, had an impact on the measured leakage flow rate. In addition, the friction coefficient determined the relative movement between the components. A sensitivity study of this parameter confirmed its strong influence on the results of the numerical model. An alternative bench design could address both, changes in contact position, and excessive influence of the

coefficient of friction. Therefore, further research should be undertaken with a revised bench design.

In summary, this research presents a good numerical-experimental correlation for leakage modelling. The methodology is applicable to other geometry, and the leakage criterion described is extendable to further systems based on that used for characterisation. It is however essential that the materials of the characterised components, the configuration of the sealing zone, and the surface finish of the contact zone are preserved. Furthermore, different leakage criterions are proposed. Fitting a linear trend permits a fluid-independent characterisation of leakage, but only reliable in a specific contact pressure range. Additionally, the proposed model based on a Weibull distribution allows the characterisation of fluid permeability for the whole contact pressure range including the onset and/or closure, but being fluid-specific.

6.2 RECOMMENDATIONS FOR FUTURE WORK

Having analysed the outcomes of this research, some insights can be provided for future investigations.

To begin with, research is underway to carry out further validation on a new system, under the indicated constraints, but with larger dimensions. This is to reflect the behaviour of real components in industrial valve applications.

Nevertheless, some identified problems are inherent to the geometry of the system used for the numerical and experimental work. For the sake of generating knowledge in industrial valves, the design of the bench was inspired by a simplified valve geometry. The cone-to-sphere contact influences the value of contact pressures, as it does not present one-to-one correspondence between fluid pressure and contact pressure. Furthermore, the friction coefficient affects the relative movement between the seat and the semi-sphere. Hence, a new design should be considered with a flat-on-flat contact, so as to minimise this effect.

Another significant aspect refers to the fluids employed in the investigations. Only liquids were used which ensured a considerable pressure loss regardless of how small the leakage was. In the case of using gases, a major outflow would be needed to perceive a leak based on the developed methodology. A natural progression of this work is to adapt this methodology to gas leakage. One possible solution is to reduce the volume of gas contained in the cavity to the minimum by means of some kind of insert. Thus, in the case of leakage the resulting pressure loss would be more pronounced, making it easier to trace the leakage with the proposed methodology.

Finally, a further improvement of the developed algorithms could make a significant contribution to the proposed coupled two-way FSI models. The current models are capable of predicting the leakage initiation threshold, and the algorithm calculates the corresponding leak flow rate. However, this latter results is not equal to that provided by the CFD solver. Once the leak occurs, the outflow rate depends on the dimensions of the geometry of the fluid cells. In particular, the height of the fluid cells at the start of the leakage corresponds to the height that was assigned when the geometry was created.

However, this height should be equivalent to the space generated between the solids that were in contact, and that have just been separated due to the fluid pressure. The improvement proposed would be to assign a porous property to the fluid cells in the leakage zone, so that the value of their porosity is calculated as a function of the permeability determined by the leakage criterion. In this way, the outflow rate provided as a result of the CFD calculation would be equivalent to the experimental results.

6.3 SCIENTIFIC CONTRIBUTIONS

Ezkurra, M.; Esnaola, J.A.; Martinez-Agirre, M.; Etxeberria, U.; Lertxundi, U.; Colomo, L.; Begiristain, M. and Zurutuza, I., 2018. Analysis of One-Way and Two-Way FSI Approaches to Characterise the Flow Regime and the Mechanical Behaviour during Closing Manoeuvring Operation of a Butterfly Valve. *International Journal of Mechanical, Aerospace, Industrial, Mechatronic and Manufacturing Engineering*, 12(4), pp.313–319.

Telleria, X.; Ugarte, D.; Esnaola, J.A.; Ezkurra, M. and Colomo, L., 2019. Automation of Simulation Based Design Validation and Reporting of a Valve Family. *Procedia CIRP*, Volume 84, pp. 986-991, ISSN 2212-8271.

Souto-Canteli, I.; Penalba, M.; Martinez-Agirre, M.; Ezkurra, M.; Esnaola, J.A.; Llavori, I. and Aizpurua, J.I., 2021. Towards a high-fidelity simulation environment for structural integrity assessment of floating wind energy platforms. *Developments in Renewable Energies Offshore*, Guedes Soares, London, ISBN 978-0-367-68131-9.

Appendix

APPENDIX

A

Details of the testbenches

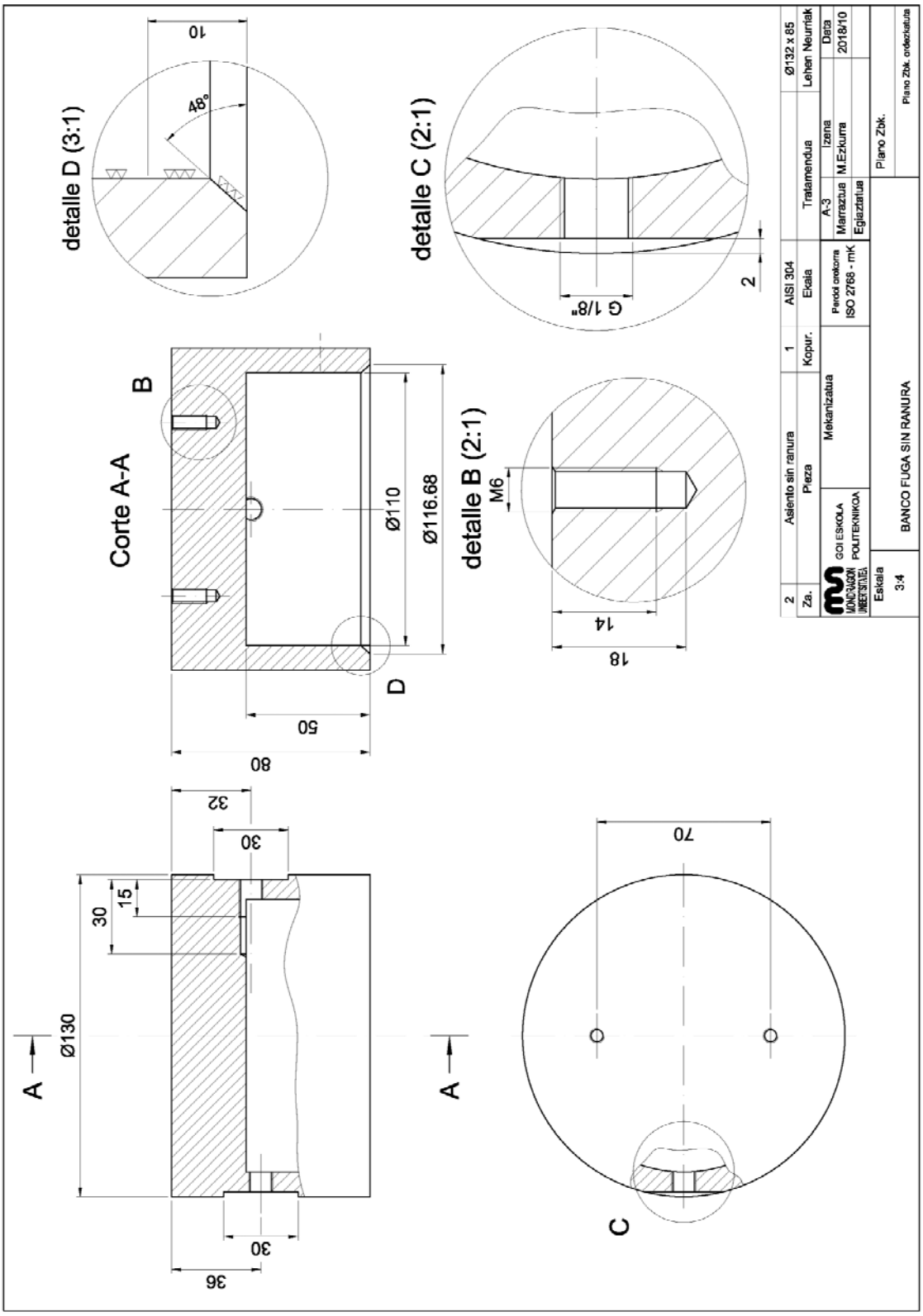

Figure A.1: Detailed drawing of the axisymmetric non-slotted seat.

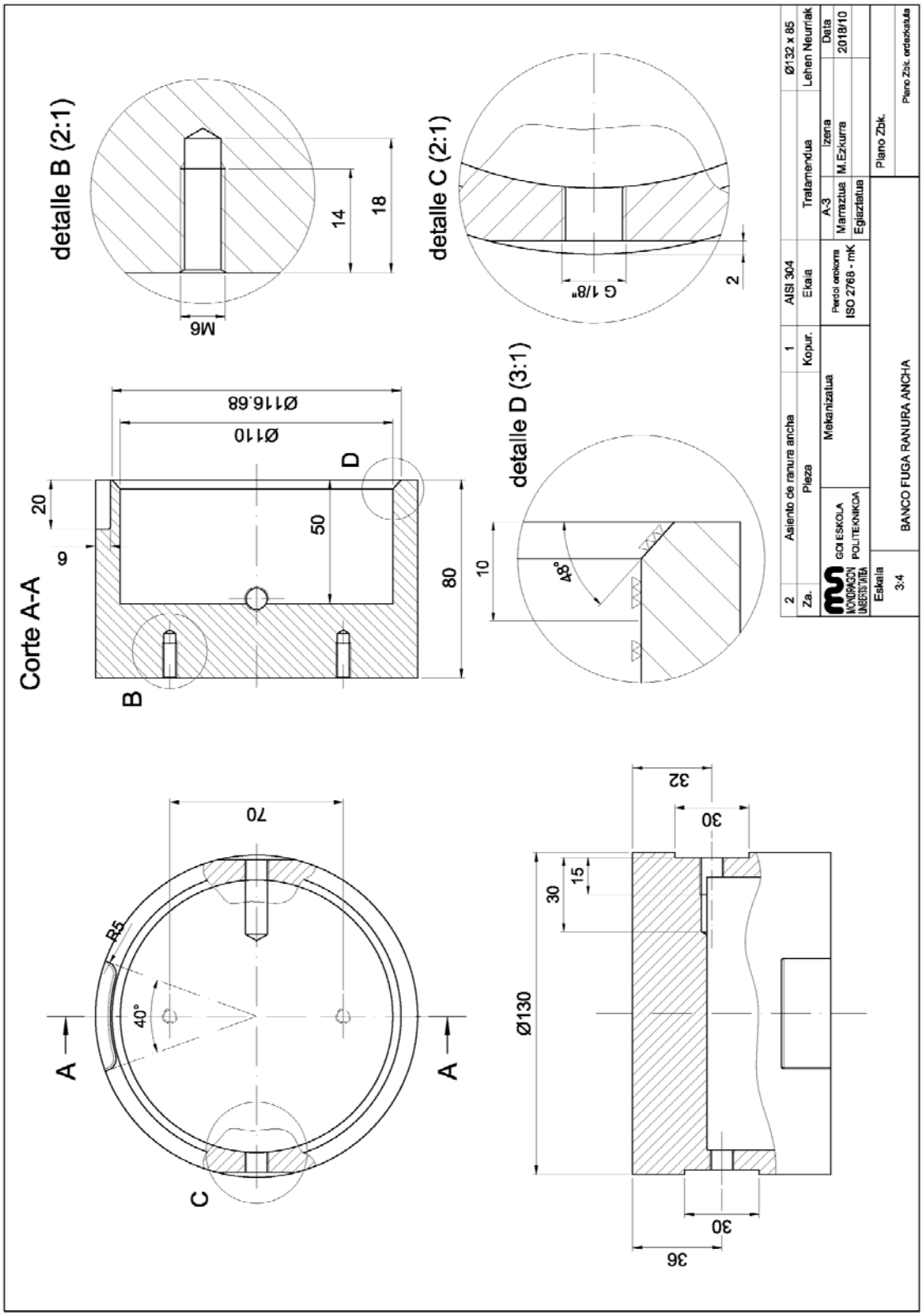

Figure A.2: Detailed drawing of the slotted seat.

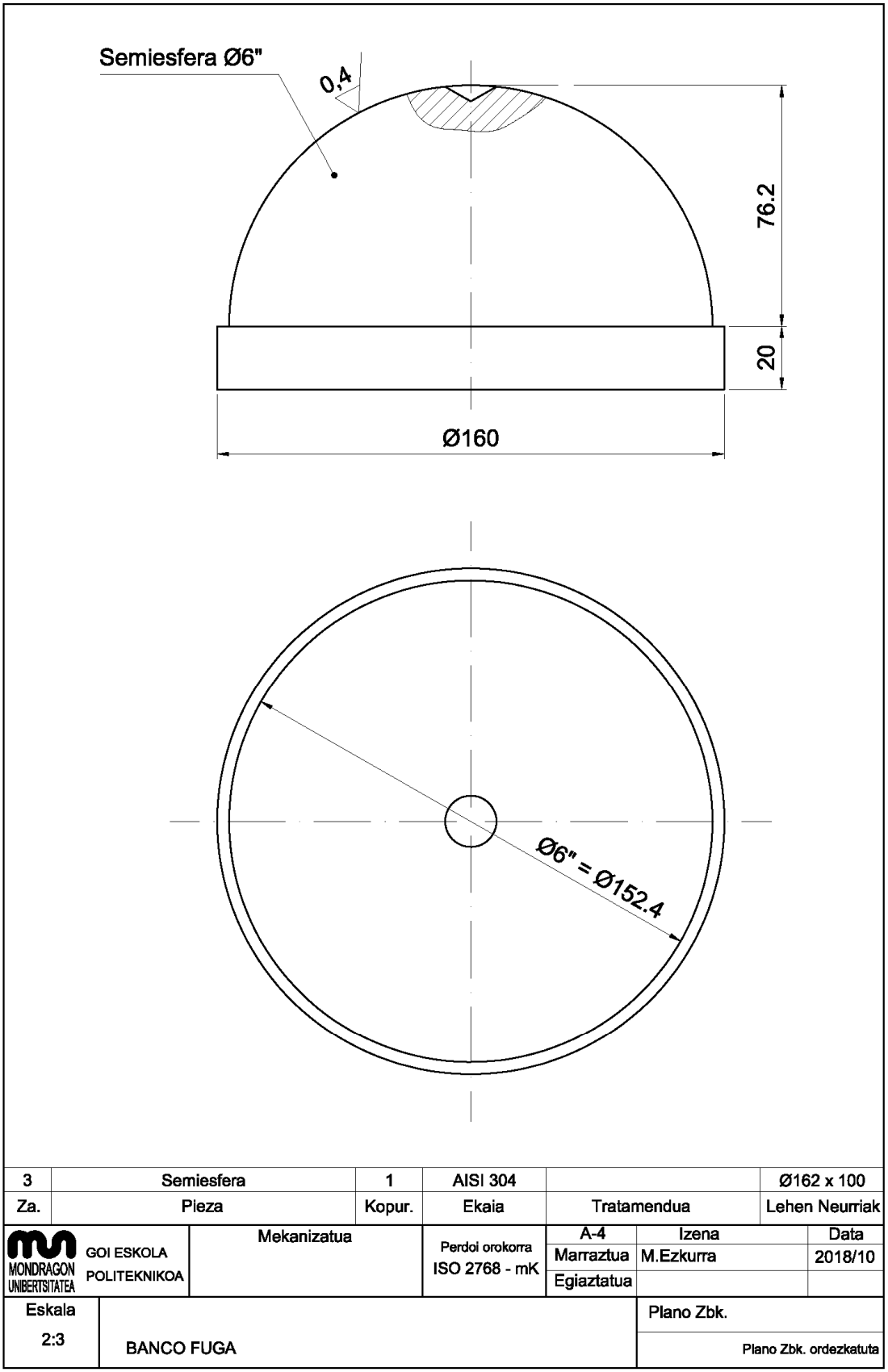

Figure A.3: Detailed drawing of the semi-sphere.

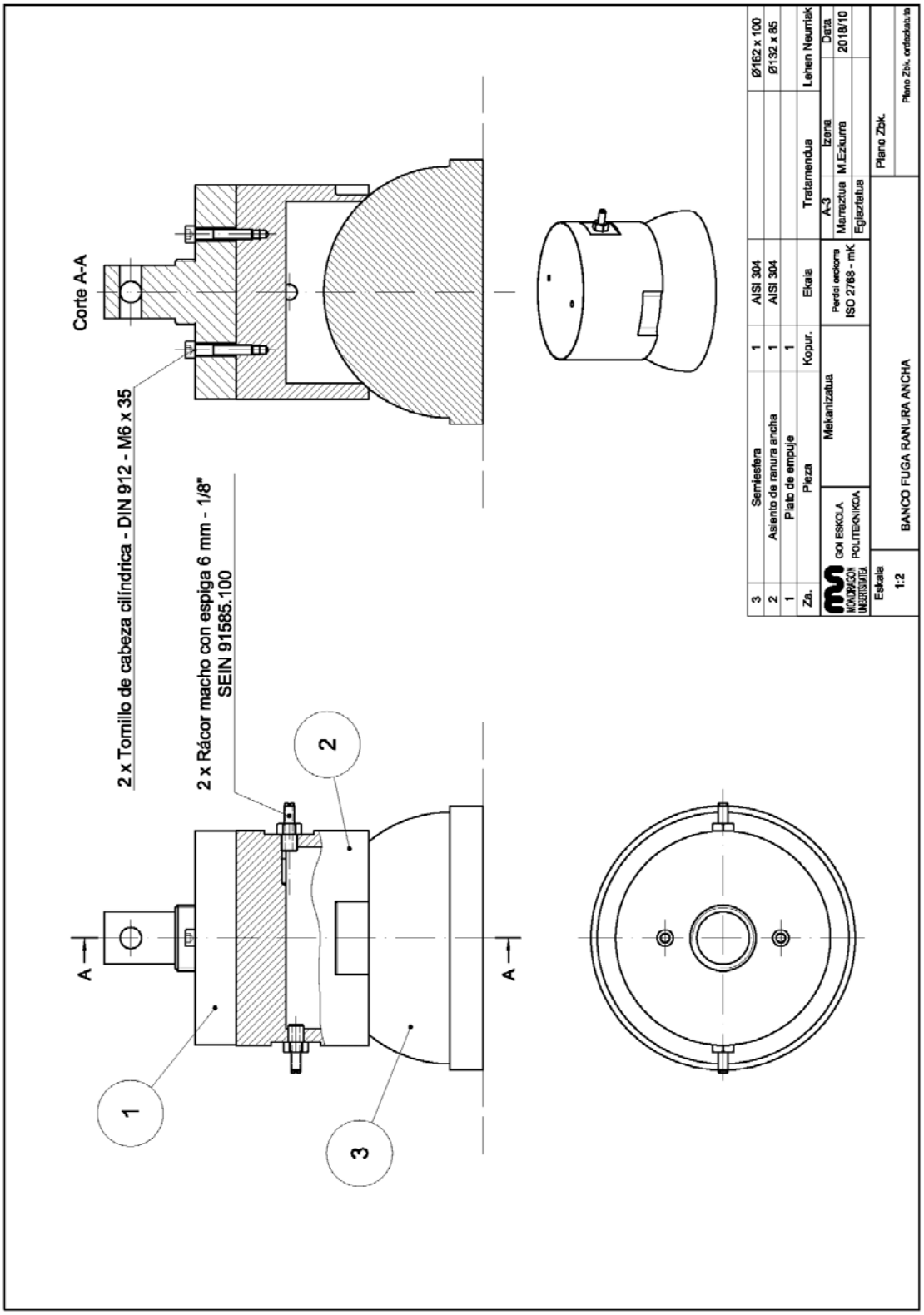

Figure A.4: Assembly drawing of the testbench.

References

Abid, M., 2005. Determination of safe operating conditions for non-gasketed flange joint under combined internal pressure and temperature. *International Journal of Mechanics and Materials in Design*, 2(1-2), pp.129–140.

Ager, C., Schott, B., Vuong, A.-T., Popp, A. and Wall, W.A., 2018. A consistent approach for fluid-structure-contact interaction based on a porous flow model for rough surface contact. *arXiv preprint arXiv:1809.04004*.

Ahn, J.T., Lee, K.C., Lee, K.H. and Han, S.H., 2011. Investigation of the mechanical behavior of a flexible solid metal seal for a cryogenic butterfly valve. *Journal of mechanical science and technology*, 25(9), p.2393.

Aksenov, A., Iliine, K., Luniewski, T., McArthy, T., Popielas, F. and Ramkumar, R., 2005. Oil Leakage Through a Valve Stem Seal. In *Proc. Abaqus User Conference*.

Al-Azawy, M.G., Turan, A. and Revell, A., 2016a. An Overset Mesh Approach for Valve Closure: An LVAD Application. In *Proceedings of the 9th International Joint Conference on Biomedical Engineering Systems and Technologies (BIOSTEC 2016)*.

Al-Azawy, M.G., Turan, A. and Revell, A., 2016b. Assessment of turbulence models for pulsatile flow inside a heart pump. *Computer methods in biomechanics and biomedical engineering*, 19(3), pp.271–285.

Al-Azawy, M.G., Turan, A. and Revell, A., 2017. Investigating the impact of non-Newtonian blood models within a heart pump. *International Journal for Numerical Methods in Biomedical Engineering*, 33(1).

Ansys Inc., 2017a. *Help System, ANSYS Explicit Dynamics Analysis Guide, Release 18.1.*

Ansys Inc., 2017b. *Help System, ANSYS Fluent Customization Manual, Release 18.1.*

Ansys Inc., 2016a. *Help System, ANSYS Fluent in ANSYS Workbench User's Guide, Release 17.1.*

Ansys Inc., 2017c. *Help System, ANSYS Fluent User's Guide, Release 18.1.*

Ansys Inc., 2016b. *Help System, ANSYS Mechanical APDL Contact Technology Guide, Release 17.2.*

Ansys Inc., 2016c. *Help System, ANSYS Mechanical APDL Programmer's Reference, Release 17.2.*

Ansys Inc., 2017d. *Help System, ANSYS Mechanical APDL Technology Demonstration Guide, Release 18.1.*

Ansys Inc., 2016d. *Help System, ANSYS Mechanical User's Guide, Release 17.0.*

Ansys Inc., 2017e. *Help System, System Coupling User's Guide, Release 18.0.*

Anwar, A.A., Gorash, Y. and Dempster, W., 2016. Application of Multi-scale Approaches to the Investigation of Sealing Surface Deformation for the Improvement of Leak Tightness in Pressure Relief Valves. In *Advanced Methods of Continuum Mechanics for Materials and Structures*. Springer.

Arghavani, J., Derenne, M. and Marchand, L., 2003. Effect of surface characteristics on compressive stress and leakage rate in gasketed flanged joints. *The International Journal of Advanced Manufacturing Technology*, 21(10-11), pp.713–732.

Bagshaw, N.M., Beck, S.B.M. and Yates, J.R., 2000. Identification of fluid flow regimes in narrow cracks. *Proceedings of the Institution of Mechanical Engineers, Part C: Journal of Mechanical Engineering Science*, 214(8), pp.1099–1106.

Basting, S., Quaini, A., Čanić, S. and Glowinski, R., 2017. Extended ALE Method for fluid–structure interaction problems with large structural displacements. *Journal of Computational Physics*, 331, pp.312–336.

Beghini, M., Bertini, L., Santus, C., Guglielmo, A. and Mariotti, G., 2015. Partially open crack model for leakage pressure analysis of bolted metal-to-metal flange. *Engineering Fracture Mechanics*, 144(Supplement C), pp.16–31.

Belostosky, A.M., Akimov, P.A., Kaytukov, T.B., Afanasyeva, I.N., Usmanov, A.R., Scherbina, S.V. and Vershinin, V.V., 2014. About Finite Element Analysis of Fluid – Structure Interaction Problems. *Procedia Engineering*, 91, pp.37–42.

Benra, F.-K., Dohmen, H.J., Pei, J., Schuster, S. and Wan, B., 2011. A comparison of one-way and two-way coupling methods for numerical analysis of fluid-structure interactions. *Journal of Applied Mathematics*, 2011.

Beune, A., Kuerten, J. and Heumen, M. van, 2012. CFD analysis with fluid–structure interaction of opening high-pressure safety valves. *Computers & Fluids*, 64, pp.108–116.

Bottiglione, F., Carbone, G., Mangialardi, L. and Mantriota, G., 2009. Leakage mechanism in flat seals. *Journal of Applied Physics*, 106(10), p.104902.

Bottiglione, F., Carbone, G. and Mantriota, G., 2009. Fluid leakage in seals: An approach based on percolation theory. *Tribology International*, 42(5), pp.731–737.

Bucher, H.H., 1988. *Industrial sealing technology*, 1st ed. ed 1st ed. ed, Chemical Industry Press, Beijing, China.

Calvert, C., Tirovic, M. and Stolarski, T., 2002. Design and development of an elastomer-based pneumatic seal using finite element analysis. *Proceedings of the Institution of Mechanical Engineers, Part J: Journal of Engineering Tribology*, 216(3), pp.127–138.

Cavallo, P.A., Hosangadi, A. and Ahuja, V., 2005. Transient simulations of valve motion in cryogenic systems. *Proceedings of 35th AIAA Fluid Dynamics Conference and Exhibit*, p.2005.

Chivers, T., 2002. The influence of surface roughness on fluid flow through cracks. *Fatigue & Fracture of Engineering Materials & Structures*, 25(11), pp.1095–1102.

Choi, Y., Lee, J., Jeong, W. and Kim, I.-G., 2010. Dynamic behavior of valve system in linear compressor based on fluid-structure interaction. *Journal of mechanical science and technology*, 24(7), pp.1371–1377.

Choiron, M.A., Haruyama, S. and Kaminishi, K., 2011. Simulation and experimentation on the contact width of new metal gasket for asbestos substitution. *International Journal of Aerospace and Mechanical Engineering*, 5(4), pp.283–287.

Clarke, L.V., Bainbridge, H., Beck, S.B.M. and Yates, J.R., 1997. Measurement of fluid flow rates through cracks. *International Journal of Pressure Vessels and Piping*, 71(1), pp.71–75.

Drewczynski, M., Solinski, M. and Rzadkowski, R., 2012. A comparison of two load transferring methods in an unsteady one-way fluid-structure interaction analysis. In *Proceedings of the ASME Turbo Expo*. Copenhagen, Denmark.

El Hami, A. and Radi, B., 2017. *Fluid-Structure Interactions and Uncertainties: Ansys and Fluent Tools*, John Wiley & Sons.

Ernens, D., Peréz-Ràfols, F., Hoecke, D.V., Roijmans, R.F., Riet, E.J. van, Voorde, J.V., Almqvist, A., Rooij, M.B. de, Roggeband, S.M., Haaften, W.M.V. and others, 2019. On the Sealability of Metal-to-Metal Seals with Application to Premium Casing Connections. In *SPE/IADC International Drilling Conference and Exhibition*. Society of Petroleum Engineers.

Ferras, D., Manso, P., Schleiss, A. and Covas, D., 2018. One-dimensional fluid–structure interaction models in pressurized fluid-filled pipes: a review. *Applied Sciences*, 8(10), p.1844.

Fischer, F., Murrenhoff, H. and Schmitz, K., 2021. Influence of normal force in metallic sealing. *Engineering Reports*, p.e12399.

Fischer, F., Schmitz, K., Tiwari, A. and Persson, B., 2020. Fluid leakage in metallic seals. *arXiv preprint arXiv:2007.13576*.

Garelli, L., Schauer, M., Rodriguez, G.R., Langer, S.C. and Storti, M.A., 2016. Evaluation of a coupling interface for solving fluid–structure interaction problems. *European Journal of Mechanics - B/Fluids*, 58, pp.117–126.

Geoffroy, S. and Prat, M., 2004. On the leak through a spiral-groove metallic static ring gasket. *Transactions-American Society of Mechanical Engineers, Journal of Fluids Engineering*, 126(1), pp.48–54.

Goharrizi, A.Y. and Sepehri, N., 2011. A wavelet-based approach for external leakage detection and isolation from internal leakage in valve-controlled hydraulic actuators. *IEEE Transactions on Industrial Electronics*, 58(9), pp.4374–4384.

Gonzalez, I., Lehmkuhl, O., Naseri, A., Rigola, J. and Oliva, A., 2016. Fluid-structure interaction of a reed type valve. In P. University, ed. *International Compressor Engineering Conference*.

Gorash, Y., Dempster, W., Nicholls, W. and Hamilton, R., 2015. Modelling of metal-to-metal seals in a pressure relief valve using advanced FE-analysis. In J. T. M. de Hosson, M. Hadfield, and C. A. Brebbia, eds. *Surface Effects and Contact Mechanics including Tribology XII*. WIT Transactions on Engineering Sciences. WIT Press.

Gorash, Y., Dempster, W., Nicholls, W.D. and Hamilton, R., 2015. Fluid pressure penetration for advanced FEA of metal-to-metal seals. *Proceedings in Applied Mathematics and Mechanics, PAMM*, 15(1), pp.197–198.

Gorash, Y., Dempster, W., Nicholls, W.D., Hamilton, R. and Anwar, A.A., 2016. Study of mechanical aspects of leak tightness in a pressure relief valve using advanced FE-analysis. *Journal of Loss Prevention in the Process Industries*, 43, pp.61–74.

Grine, L. and Bouzid, A.-H., 2009. Correlation of gaseous mass leak rates through micro and nano-porous gaskets. In *ASME 2009 Pressure Vessels and Piping Conference*. American Society of Mechanical Engineers Digital Collection.

Grine, L. and Bouzid, A.-H., 2010. Liquid leak predictions in micro and nano-porous gaskets. In *ASME 2010 Pressure Vessels and Piping Division/K-PVP Conference*. American Society of Mechanical Engineers Digital Collection.

Grine, L. and Bouzid, A.-H., 2011. Liquid leak predictions in micro-and nanoporous gaskets. *Journal of pressure vessel technology*, 133(5).

Guruswamy, G.P., 2002. A review of numerical fluids/structures interface methods for computations using high-fidelity equations. *Computers & structures*, 80(1), pp.31–41.

Ha, S.T., Ngo, L.C., Saeed, M., Jeon, B.J. and Choi, H., 2017. A comparative study between partitioned and monolithic methods for the problems with 3D fluid-structure interaction of blood vessels. *Journal of Mechanical Science and Technology*, 31(1), pp.281–287.

Haruyama, S., Nurhadiyanto, D., Choiron, M.A. and Kaminishi, K., 2013. Influence of surface roughness on leakage of new metal gasket. *International Journal of Pressure Vessels and Piping*, 111, pp.146–154.

Hirt, C.W., Amsden, A.A. and Cook, J., 1974. An arbitrary Lagrangian-Eulerian computing method for all flow speeds. *Journal of computational physics*, 14(3), pp.227–253.

Hou, G., Wang, J. and Layton, A., 2012. Numerical methods for fluid-structure interaction—a review. *Communications in Computational Physics*, 12(02), pp.337–377.

Hsu, M.-C., Kamensky, D., Xu, F., Kiendl, J., Wang, C., Wu, M.C., Mineroff, J., Reali, A., Bazilevs, Y. and Sacks, M.S., 2015. Dynamic and fluid–structure interaction simulations of bioprosthetic heart valves using parametric design with T-splines and Fung-type material models. *Computational mechanics*, 55(6), pp.1211–1225.

Huang, S., Li, R. and Li, Q., 2013. Numerical simulation on fluid-structure interaction of wind around super-tall building at high reynolds number conditions. *Struct. Eng. Mech*, 46(2), pp.197–212.

Hughes, T.J., Liu, W.K. and Zimmermann, T.K., 1981. Lagrangian-Eulerian finite element formulation for incompressible viscous flows. *Computer methods in applied mechanics and engineering*, 29(3), pp.329–349.

Jaiman, R., Thomas, H. and Shakib, F., 2012. Direct-Coupled Fluid-Structure Interaction for Automotive Applications, SAE Technical Paper.

Jaiman, R.K., Shakib, F., Oakley, O.H. and Constantinides, Y., 2009. Fully coupled fluid-structure interaction for offshore applications. In *ASME 2009 28th International Conference on Ocean, Offshore and Arctic Engineering*. American Society of Mechanical Engineers.

Johnson, K.., 1985. *Contact mechanics*, Cambridge University Press.

Kavrakov, I. and Morgenthal, G., 2018. A synergistic study of a CFD and semi-analytical models for aeroelastic analysis of bridges in turbulent wind conditions. *Journal of Fluids and Structures*, 82, pp.59–85.

Kawamura, H., Sawa, T. and Yoneno, M., 2003. FEM stress analysis and sealing performance improvement of box-shaped bolted flanged joints using silicone sealant under internal pressure and thermal conduction conditions. *Journal of Adhesion Science and Technology*, 17(8), pp.1109–1125.

Kim, W. and Choi, H., 2019. Immersed boundary methods for fluid-structure interaction: A review. *International Journal of Heat and Fluid Flow*.

Leutwyler, Z. and Dalton, C., 2008. A CFD study of the flow field, resultant force, and aerodynamic torque on a symmetric disk butterfly valve in a compressible fluid. *Journal of Pressure Vessel Technology*, 130(2), p.021302.

Liao, C., Xu, X., Fang, H., Wang, H. and Man, M., 2015. A leakage model of metallic static seals based on micromorphology characteristics of turning flange surface. *Industrial Lubrication and Tribology*.

Liu, B., Wang, J., Qian, J., Chen, F. and Jin, Z., 2016. Dynamic response analysis of pilot control globe valve focusing on opening and closing time of pilot valve. *Journal of Physics: Conference Series*, 745(3), p.032046.

Liu, Q., Wang, Z., Lou, Y. and Suo, Z., 2014. Elastic leak of a seal. *Extreme Mechanics Letters*, 1, pp.54–61.

Loon, R. van, Anderson, P.D. and Vosse, F.N. van de, 2006. A fluid–structure interaction method with solid-rigid contact for heart valve dynamics. *Journal of computational physics*, 217(2), pp.806–823.

Lorenz, B. and Persson, B., 2009. Leak rate of seals: Comparison of theory with experiment. *EPL (Europhysics Letters)*, 86(4), p.44006.

Marie, C. and Lasseux, D., 2007. Experimental leak-rate measurement through a static metal seal. *Journal of fluids engineering*, 129(6), pp.799–805.

Martinsanz, G.P., 2015. Sensors for Fluid Leak Detection. *Sensors*, 15(2), pp.3830–3833.

Matsuzaki, Y. and Kazamaki, T., 1988. Effect of surface roughness on compressive stress of static seals. *JSME international journal. Ser. 3, Vibration, control engineering, engineering for industry*, 31(1), pp.99–106.

McElhaney, K.L., 2000. An analysis of check valve performance characteristics based on valve design. *Nuclear Engineering and Design*, 197(1), pp.169–182.

Medvitz, R.B., Kreider, J.W., Manning, K.B., Fontaine, A.A., Deutsch, S. and Paterson, E.G., 2007. Development and validation of a computational fluid dynamics methodology for simulation of pulsatile left ventricular assist devices. *ASAIO journal*, 53(2), pp.122–131.

Mondal, M.K., Manna, N.K. and Saha, R., 2014. Study of leakage flow through a spool valve under blocked-actuator port condition—Simulation and experiment. *Proceedings of the Institution of Mechanical Engineers, Part C: Journal of Mechanical Engineering Science*, 228(8), pp.1405–1417.

Murtagian, G., Fanelli, V., Villasante, J., Johnson, D. and Ernst, H., 2004. Sealability of stationary metal-to-metal seals. *Journal of Tribology*, 126(3), pp.591–596.

Nelson, N.R., Prasad, N.S. and Sekhar, A., 2017. Studies on joint strength and sealing behavior of single and twin-gasketed flange joints. *Proceedings of the Institution of Mechanical Engineers, Part E: Journal of Process Mechanical Engineering*, 232(4), pp.480–492.

Nitta, I. and Matsuzaki, Y., 2010. Experimental study of the performance of static seals based on measurements of real contact area using thin polycarbonate films. *Journal of Tribology*, 132(2).

Nitta, I., Matsuzaki, Y., Tsukiyama, Y., Horita, M. and Sakamoto, S., 2013. Thorough observation of real contact area of copper gaskets using a laser microscope with a wide field of view. *Journal of Tribology*, 135(4), p.041103.

Pan, X., Yang, S., Shi, Y. and Liu, Y., 2019. Investigation on the Dynamic Characteristics of Port Valves in a Diaphragm Pump for Exhaust Gas Treatment System by FSI Modeling. *IEEE Access*, 7, pp.57238–57250.

Pauw, J.D., Veggi, L., Haidn, O.J., Wagner, C., Thümmel, T., Rixen, D.J., Ager, C., Wirtz, A., Popp, A., Wall, W.A. and others, 2019. An academic approach to the multidisciplinary development of liquid-oxygen turbopumps for space applications. *CEAS Space Journal*, 11(2), pp.193–203.

Pérez-Ràfols, F. and Almqvist, A., 2018. An Enhanced Stochastic Two-Scale Model for Metal-to-Metal Seals. *Lubricants*, 6(4), p.87.

Pérez-Ràfols, F., Larsson, R. and Almqvist, A., 2016. Modelling of leakage on metal-to-metal seals. *Tribology International*, 94, pp.421–427.

Pérez-Ràfols, F., Larsson, R., Lundström, S., Wall, P. and Almqvist, A., 2016. A stochastic two-scale model for pressure-driven flow between rough surfaces. In *Proc. R. Soc. A*. The Royal Society.

Pérez-Ràfols, F., Larsson, R., Riet, E.J. van and Almqvist, A., 2018. On the flow through plastically deformed surfaces under unloading: A spectral approach. *Proceedings of the Institution of Mechanical Engineers, Part C: Journal of Mechanical Engineering Science*, 232(5), pp.908–918.

Pérez-Ràfols, F., Larsson, R., Van Riet, E.J. and Almqvist, A., 2018. On the loading and unloading of metal-to-metal seals: A two-scale stochastic approach. *Proceedings*

of the Institution of Mechanical Engineers, Part J: Journal of Engineering Tribology, 232(12), pp.1525–1537.

Putignano, C., Afferrante, L., Carbone, G. and Demelio, G.P., 2013. A multiscale analysis of elastic contacts and percolation threshold for numerically generated and real rough surfaces. *Tribology International*, 64, pp.148–154.

Ràfols, F.P., 2016. Modelling and numerical analysis of leakage through metal-to-metal seals. Luleå tekniska universitet.

Ren, J., Park, C. and Wang, H., 2018. Stochastic modeling and diagnosis of leak areas for surface assembly. *Journal of Manufacturing Science and Engineering*, 140(4).

Robbe-Valloire, F. and Prat, M., 2008. A model for face-turned surface microgeometry: Application to the analysis of metallic static seals. *Wear*, 264(11-12), pp.980–989.

Rugonyi, S. and Bathe, K., 2001. On finite element analysis of fluid flows fully coupled with structural interactions. *CMES - Computer Modeling in Engineering and Sciences*, 2(2), pp.195–212.

Schmidt, J., Peschel, W. and Beune, A., 2009. Experimental and theoretical studies on high pressure safety valves: sizing and design supported by numerical calculations (CFD). *Chemical engineering & technology*, 32(2), pp.252–262.

Shao, Y., Yin, Y., Du, S. and Xi, L., 2019. A Surface Connectivity-Based Approach for Leakage Channel Prediction in Static Sealing Interface. *Journal of Tribology*, 141(6), p.062201.

Shvarts, A.G. and Yastrebov, V.A., 2018. Fluid flow across a wavy channel brought in contact. *Tribology International*, 126, pp.116–126.

Silva, L.R. and Deschamps, C.J., 2015. Modeling of gas leakage through compressor valves. *International Journal of Refrigeration*, 53, pp.195–205.

Song, X., Cui, L., Cao, M., Cao, W., Park, Y. and Dempster, W.M., 2014. A CFD analysis of the dynamics of a direct-operated safety relief valve mounted on a pressure vessel. *Energy Conversion and Management*, 81, pp.407–419.

Song, X., Wang, L. and Park, Y., 2009. Analysis and optimization of a butterfly valve disc. *Proceedings of the Institution of Mechanical Engineers, Part E: Journal of Process Mechanical Engineering*, 223(2), pp.81–89.

Stauffer, D. and Aharony, A., 1994. *Introduction To Percolation Theory*, CRC Press.

Su, B., Zhong, L., Wang, X.-K., Zhang, J.-M., Tan, R.S., Allen, J.C., Tan, S.K., Kim, S. and Leo, H.L., 2014. Numerical simulation of patient-specific left ventricular

model with both mitral and aortic valves by FSI approach. *Computer Methods and Programs in Biomedicine*, 113(2), pp.474–482.

Takizawa, K., Bazilevs, Y. and Tezduyar, T.E., 2012. Space–Time and ALE-VMS Techniques for Patient-Specific Cardiovascular Fluid–Structure Interaction Modeling. *Archives of Computational Methods in Engineering*, 19(2), pp.171–225.

Takizawa, K., Tezduyar, T.E. and Buscher, A., 2015. Space–time computational analysis of MAV flapping-wing aerodynamics with wing clapping. *Computational Mechanics*, 55(6), pp.1131–1141.

Takizawa, K., Tezduyar, T.E., Buscher, A. and Asada, S., 2014. Space–time fluid mechanics computation of heart valve models. *Computational Mechanics*, 54(4), pp.973–986.

Takizawa, K., Tezduyar, T.E., Buscher, A. and Asada, S., 2014. Space–time interface-tracking with topology change (ST-TC). *Computational Mechanics*, 54(4), pp.955–971.

Tao, W., Guo, Y., He, Z. and Peng, X., 2018. Investigation on the delayed closure of the suction valve in the refrigerator compressor by FSI modeling. *International Journal of Refrigeration*, 91, pp.111–121.

Tezduyar, T., Behr, M. and Liou, J., 1992. A new strategy for finite element computations involving moving boundaries and interfaces–the DSD/ST procedure: I. The concept and the preliminary numerical tests. *Computer Methods in Applied Mechanics and Engineering*, 94(3), pp.339–351.

Tezduyar, T.E., Behr, M., Mittal, S. and Liou, J., 1992. A new strategy for finite element computations involving moving boundaries and interfaces—the deforming-spatial-domain/space-time procedure: II. Computation of free-surface flows, two-liquid flows, and flows with drifting cylinders. *Computer methods in applied mechanics and engineering*, 94(3), pp.353–371.

Tian, J., Feng, H., Yang, Y., Liang, J., Kuang, Y. and Zhang, H., 2019. Influence of Material Parameters and Thermal Parameters on Sealing Performance of Reactor Pressure Vessel Under Heat Focusing Effect. *Journal of Pressure Vessel Technology*, 141(4).

Tijsseling, A., 1996. Fluid-structure interaction in liquid-filled pipe systems: a review. *Journal of Fluids and Structures*, 10(2), pp.109–146.

Vassen, J.-M., DeVincenzo, P., Hirsch, C. and Leonard, B., 2011. Strong coupling algorithm to solve fluid-structure-interaction problems with a staggered approach. In *7th European Symposium on Aerothermodynamics*.

Vlădescu, S.-C., Putignano, C., Marx, N., Keppens, T., Reddyhoff, T. and Dini, D., 2019. The Percolation of Liquid Through a Compliant Seal—An Experimental and Theoretical Study. *Journal of Fluids Engineering*, 141(3), p.031101.

Wang, J., 2013. *Fluid Structure Interaction of a Duckbill Valve*, PhD thesis, McMaster University.

Wang, L., Quant, R. and Kolios, A., 2016. Fluid structure interaction modelling of horizontal-axis wind turbine blades based on CFD and FEA. *Journal of Wind Engineering and Industrial Aerodynamics*, 158, pp.11–25.

Wang, L., Song, X. and Park, Y., 2009. The improvement of large butterfly valve by using numerical analysis method. In *Proceedings of the 6th WSEAS International Conference on Fluid Mechanics*.

Wang, L., Wei, Z., Guan, Y., Li, S. and others, 2016. A novel subsea pipeline connection method and experimental study. In *The 26th International Ocean and Polar Engineering Conference*. International Society of Offshore and Polar Engineers.

Wang, L.-Q., Wei, Z.-L., Yao, S.-M., Guan, Y. and Li, S.-K., 2018. Sealing performance and optimization of a subsea pipeline mechanical connector. *Chinese Journal of Mechanical Engineering*, 31(1), pp.1–14.

Wei, Z., Wang, L., Guan, Y., Yao, S. and Li, S., 2016. Static metal sealing mechanism of a subsea pipeline mechanical connector. *Advances in Mechanical Engineering*, 8(7), p.1687814016654821.

Weibull, W., 1939. *A Statistical Theory of the Strength of Materials*, Generalstabens litografiska anstalts förlag.

Wu, L., Xiao, J., Chen, H., Li, J., Jiang, S. and Wang, T., 2014. A Three-Dimensional Computational Analysis of One-Way Fluid-Structure Coupling in Main Steam Isolation Valve. *Nuclear Technology*, 188(1), pp.78–82.

Xin, L. and Gaoliang, P., 2016. Research on leakage prediction calculation method for static seal ring in underground equipments. *Journal of Mechanical Science and Technology*, 30(6), pp.2635–2641.

Yang, L., Wang, Z., Dempster, W., Yu, X. and Tu, S.-T., 2017. Experiments and transient simulation on spring-loaded pressure relief valve under high temperature and high pressure steam conditions. *Journal of Loss Prevention in the Process Industries*, 45, pp.133–146.

Zhang, F., Liu, J., Ding, X. and Wang, R., 2019. Experimental and finite element analyses of contact behaviors between non-transparent rough surfaces. *Journal of the Mechanics and Physics of Solids*, 126, pp.87–100.

Zhang, F., Liu, J., Ding, X. and Yang, Z., 2017. An approach to calculate leak channels and leak rates between metallic sealing surfaces. *Journal of Tribology*, 139(1).

Zhang, Q., Chen, X., Huang, Y. and Zhang, X., 2018. An Experimental Study of the Leakage Mechanism in Static Seals. *Applied Sciences*, 8(8), p.1404.

Zienkiewicz, O.C., Taylor, R.L. and P., N., 2014. *The Finite Element Method for Fluid Dynamics, Seventh Edition*, 7th ed 7th ed, Butterworth-Heinemann.